STRUCTURAL INFLUENCES ON REDUCTION POTENTIAL, ELECTRON TRANSFER AND STABILITY IN CYTOCHROME C

By

Terence Pui-Kwan Lo

B.Sc., The University of British Columbia, 1988

A THESIS SUBMITTED IN PARTIAL FULFILLMENT OF

THE REQUIREMENTS FOR THE DEGREE OF

DOCTOR OF PHILOSOPHY

in

THE FACULTY OF GRADUATE STUDIES

THE DEPARTMENT OF BIOCHEMISTRY AND MOLECULAR BIOLOGY

We accept this thesis as conforming

to the required standard

THE UNIVERSITY OF BRITISH COLUMBIA

April 1995

In presenting this thesis in partial fulfilment of the requirements for an advanced degree at the University of British Columbia, I agree that the Library shall make it freely available for reference and study. I further agree that permission for extensive copying of this thesis for scholarly purposes may be granted by the head of my department or by his or her representatives. It is understood that copying or publication of this thesis for financial gain shall not be allowed without my written permission.

The Department of Biochemistry and Molecular Biology

The University of British Columbia

2146 Health Sciences Mall

Vancouver, British Columbia

V6T 1Z3

Date: ___April 26, 1995___

Abstract

The work described in this thesis was directed toward understanding the contributions of Phe82, Leu85 and associated residues to the structure and function of cytochrome c. One focus of these studies concerned the roles of these residues at the interactive face formed during electron transfer reactions involving cytochrome c and its redox partners. Phe82 was found to make an important contribution to this process, while the adjacent Leu85 does not have a significant impact. However, both residues indirectly affect complex formation by influencing the placement of the side chain of Arg13. In related studies, Leu85 was found to contribute to the formation of the heme binding pocket as a participant in a cluster of conserved leucine residues. This leucine cluster, as well as an adjacent internal hydrophobic cavity, were shown to provide a measure of conformational flexibility when mutations are made in cytochrome c and may facilitate the structural transition of this protein between oxidation states. It was also determined that replacement of Leu94, which is also a member of this leucine cluster, did not alter the helix-helix interactions of the N- and C-terminal helices of cytochrome c as had been suggested by earlier studies. Also apparent from further studies was the important functional role played by Phe82 in the regulation of heme reduction potential which could be attributed to its contribution to the nonpolar environment of the heme pocket. Related to this, it was found that the effects of polar groups on reduction potential were mitigated when these groups were shielded from the heme macrocycle by intervening heme substituents. An additional factor in the regulation of reduction potential was characterized as part of the study of Phe82 and distal residues involved in interactions with heme propionate A. Here it was shown that the mechanisms by which Arg38 and Asn52 influence reduction potential differ from that of Phe82. Furthermore, for Arg38 and Asn52, these effects overlap and synergistic effects are observed when they are replaced in concert. In contrast, the structural implications of either single or

multiple substitutions at Arg38, Asn52 and Phe82 were determined to be independent as was the impact on structural stability as a whole. Overall it is clear from these studies that Phe82, Leu85, and likely many other residues in cytochrome c, have multiple structural and functional roles and that the interplay between the roles of these residues are correspondingly complex and difficult to predict.

Table of Contents

List of Tables

List of Figures

xiv

List of Abbreviations

B .... isotropic thermal factor

C_m .... concentration at midpoint of unfolding transition

DTT .... dithiothreitol

E_m .... midpoint reduction potential

Gdn-HCl .... guanidine hydrochloride

MW .... molecular weight

NMR .... nuclear magnetic resonance

V_m .... volume per unit mass

a, b, c .... crystallographic unit cell axes, or axis lengths

d .... distance

Δd .... average positional deviation

e.u. .... entropy units; 1 e.u. $= 1$ cal mol^{-1} K^{-1}

r.m.s. .... room mean square

α, β, γ .... crystallographic unit cell angles; also, Eulerian angles in molec-
ular replacement rotation function

μ .... ionic strength

ϕ, Ω .... rotational axes which define in part the orientation of the crystal
in the diffraction experiment

Å .... Angstrom (0.1 nm)

The conventions of the IUPAC-IUB Combined Commissions on Biochemical Nomenclature are followed for both three letter and one letter abbreviations for amino acids [*J. Biol. Chem.*

241, 527–533 (1966); *J. Biol. Chem.* **243**, 3557–3559 (1968)]; and for designating atoms and describing the conformational torsion angles of the polypeptide chain [*J. Biol. Chem.* **245**, 6489–6497 (1970)]. Designations for atoms of the protoheme IX group are according to the Brookhaven National Laboratory Protein Data Bank (Bernstein *et al.*, 1977; see also Figure 1.2).

The amino acid numbering scheme used for the yeast iso-1 cytochrome *c* mutant structures described in this thesis is based on an alignment with the sequences of vertebrate cytochromes *c* (Table 1.1). The N-terminal residue is numbered -5 and the C-terminal residue is numbered 103.

Acknowledgments

Finally, I would like to thank all of my friends who supported me during these six years; you know who you are. It's been fun. Twenty-eight years on my way ...

Chapter 1

Introduction

1.1 Eukaryotic Cytochromes c

Eukaryotic cytochromes c have been a major focus of studies to elucidate the structural factors responsible for controlling biological electron transfer and as such, these small soluble proteins (MW $\sim$13,000 daltons) have been extensively examined (for reviews of this work see Timkovich, 1979; Mathews, 1985; Moore & Pettigrew, 1990; Brayer & Murphy, 1994). Each of these proteins contains a heme functional group which is covalently attached to the polypeptide chain through two thioether linkages to cysteine side chains (Figure 1.1). These two cysteine residues are located within a Cys-X-Y-Cys-His sequence which is characteristic of c-type cytochromes. The histidine side chain in this sequence and that of an additional methionine residue act as the two axial ligands to the iron atom of the heme prosthetic group (Figure 1.1). It is this heme moiety (Figure 1.2) which bestows upon cytochrome c the ability to mediate the transfer of electrons between proteins through the reversible cycling of this group between the ferric [Fe(III)] and ferrous [Fe(II)] states.

Cytochrome c is located within the intermembrane space of mitochondria where it functions primarily as an electron shuttle in the respiratory electron transport chain by accepting electrons from the cytochrome c reductase (bc_1) complex and donating these to the cytochrome c oxidase (aa_3) complex (Pettigrew & Moore, 1987). The soluble nature of cytochrome c allows it to diffuse between these two complexes, both of which are multi-subunit integral membrane proteins. In addition to this primary function, cytochrome c also plays a role in several other electron transfer pathways (Pettigrew & Moore, 1987). In animal systems, cytochrome c serves as an acceptor of electrons from both cytochrome b_5 (Ito 1980a,b; Lederer et al., 1983) and
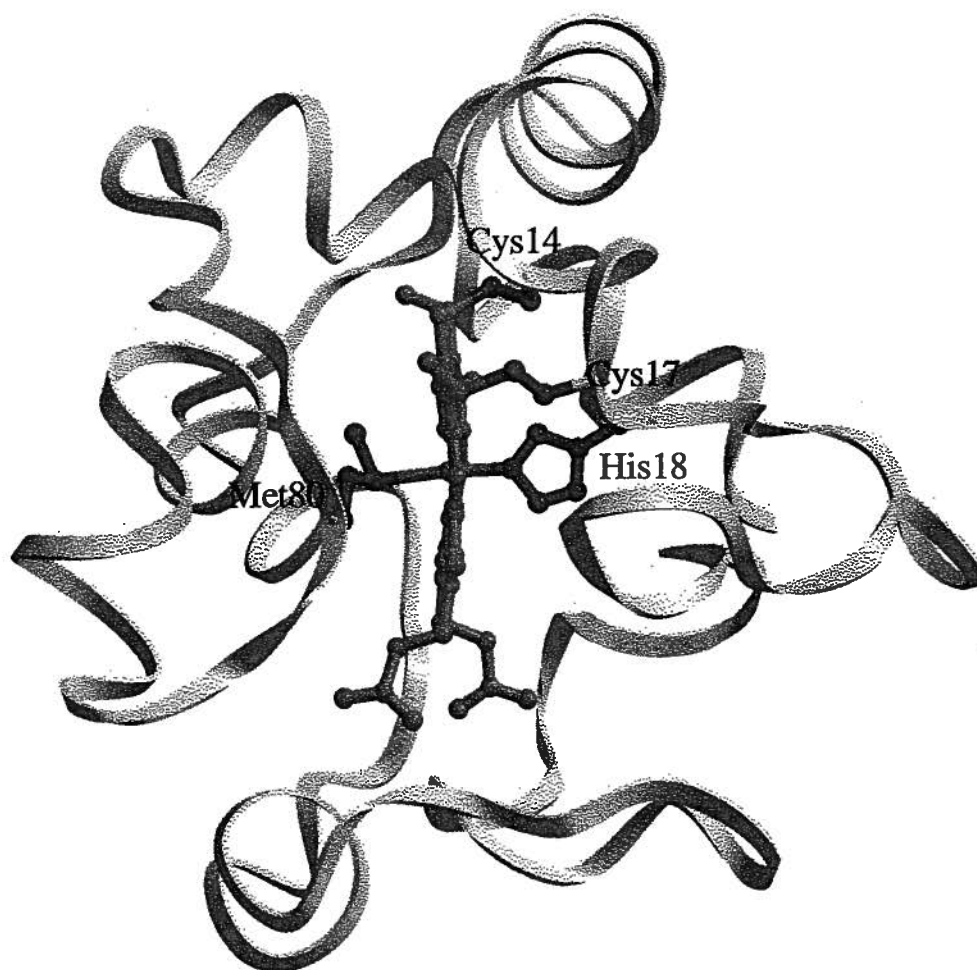
Figure 1.1: A ribbon representation of the polypeptide fold of yeast iso-1 cytochrome *c*. A ball-and-stick representation is used to show the heme group as well as the two thioether linkages to Cys14 and Cys17 and the two axial heme ligands to His18 and Met80.
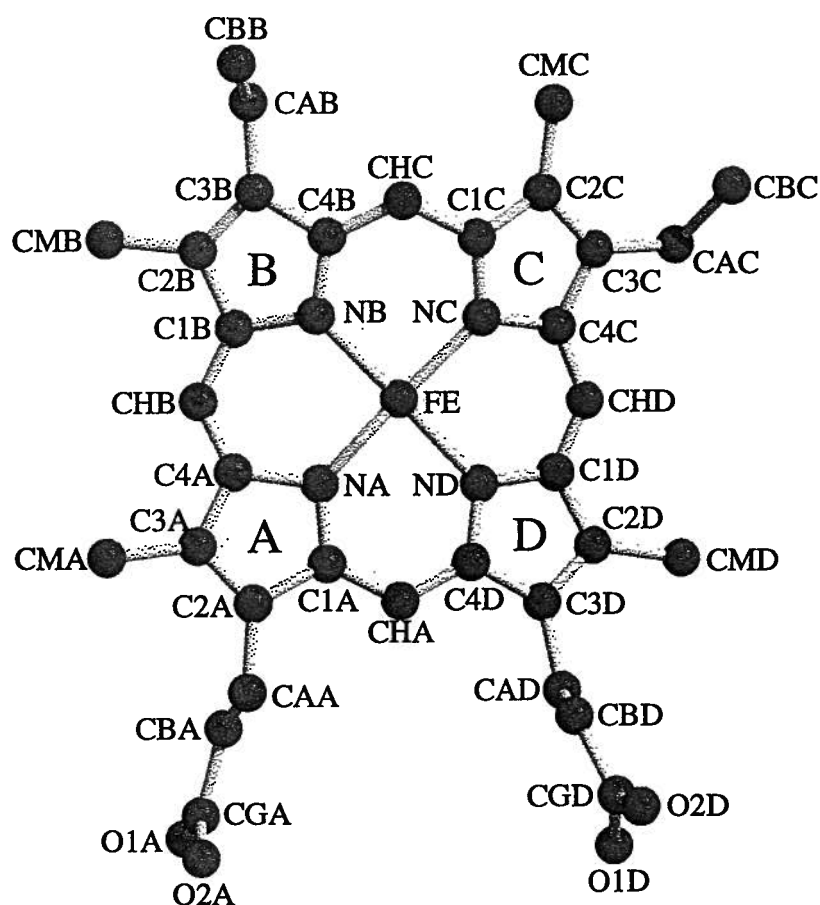
Figure 1.2: A schematic diagram of iron protoporphyrin IX with all non-hydrogen atoms shown as grey balls. These atoms and the four pyrrole rings of the heme macrocycle are labeled according to the conventions of the Protein Data Bank (Bernstein *et al.*, 1977). In eukaryotic cytochromes *c*, this porphyrin ring is covalently attached to the protein through two thioether linkages (Cys14 SG - heme CAB; Cys17 SG - heme CAC) and the iron atom is hexacoordinate, with the four pyrrole nitrogen atoms, His18 NE2 and Met80 SD providing the ligands. In the view presented, the solvent exposed heme edge observed in cytochromes *c* is located at the right, the histidine ligand is behind the porphyrin ring and the methionine ligand is positioned in front.

sulfite oxidase (McLeod *et al.*, 1961; Cohen & Fridovich, 1971) while in yeast systems, cytochrome *c* donates electrons to cytochrome *c* peroxidase (Altschul *et al.*, 1940; Abrams *et al.*, 1942) and accepts electrons from flavocytochrome b_2 (Bach *et al.*, 1942a,b). Thus an important aspect of the mechanism by which cytochrome *c* mediates electron transfer is how this protein is capable of interacting with such a wide variety of electron transfer partners.

1.2 The Structure of Cytochrome c

The amino acid sequences of cytochromes *c* from a variety of eukaryotic organisms have been determined and the overall length of the polypeptide chain is found to vary from 103 to 113 residues. A high degree of conservation is observed in the alignment of the 94 sequences available (those of *Euglena gracilis* and *Tetrahymena pyriformis* were excluded due to gaps in their sequences), with 27 residues being invariantly conserved and a further 16 amino acids being highly conserved (Hampsey *et al.*, 1986, 1988; Moore & Pettigrew, 1990). Table 1.1 contains the aligned sequences of 5 cytochromes *c* of particular relevance to the studies conducted in this thesis and indicates those residues that are found to be invariant or highly conserved in all such proteins. As one might expect, many of these invariant residues are absolutely required for the structural and functional integrity of cytochrome *c*. Nevertheless, a surprising result is that amino acid substitutions at some invariant sites have resulted in mutant cytochrome *c* proteins which are functionally viable (Pielak *et al.*, 1985; Hampsey *et al.*, 1988). This raises questions concerning the necessity of having these particular residues in cytochrome *c* and the cause of their observed invariant conservation.

The three dimensional structures of several eukaryotic cytochromes *c* have been determined to atomic resolution by X-ray crystallographic methods. These include the two isozymes of cytochrome *c* from yeast, iso-1 (Louie & Brayer, 1990; Berghuis & Brayer, 1992) and iso-2 (Murphy *et al.*, 1992), as well as the cytochromes *c* from tuna (Takano & Dickerson, 1981a,b), horse (Bushnell *et al.*, 1990), rice (Ochi *et al.*, 1983) and bonito (Tanaka *et al.*, 1975). More recently, the structures of yeast iso-1 and horse cytochrome *c* have also been studied by NMR

Table 1.1: Alignment of the sequences of yeast iso-1, yeast iso-2, tuna, horse and rice cytochromes *c*

```
        -9              1              10            20
         •              •        •            o   ••••  o         o      o •
Iso-1  - - - - T E F K A[G]S A K K[G]A T L[F]K T R[C]L[Q C H T]V E K[G]G P H[K]V[G]
Iso-2  A K E S T G F K P[G]S A K K[G]A T L[F]K T R[C]Q[Q C H T]I E E[G]G P N[K]V[G]
Tuna   - - - - - - - - -[G]D V A K[G]K K T[F]V Q K[C]A[Q C H T]V E N[G]G K H[K]V[G]
Horse  - - - - - - - - -[G]D V E K[G]K K I[F]V Q K[C]A[Q C H T]V E K[G]G K H[K]T[G]
Rice   - A S F S E A P P[G]N P K A[G]E K I[F]K T K[C]A[Q C H T]V D K[G]A G H[K]Q[G]

        30            40            50            60
        • o •    •    o •    •      o     •    o •          •
Iso-1  [P N L]H[G]I[F G R]H S[G]Q A E[G]Y S[Y]T D[A N]I K K N V L[W]D E N N M S E
Iso-2  [P N L]H[G]I[F G R]H S[G]Q V K[G]Y S[Y]T D A N I N K N V K[W]D E D S M S E
Tuna   [P N L]W[G]L[F G R]K T[G]Q A E[G]Y S[Y]T D A N K S K G I V[W]N N D T L M E
Horse  [P N L]H[G]L[F G R]K T[G]Q A P[G]F T[Y]T D A N K N K G I T[W]K E E T L M E
Rice   [P N L]N[G]L[F G R]Q S[G]T T P[G]Y S[Y]S T A N K D M A V I[W]E E N T L Y D

          70          80         •     •   90    •   o o      o o   100
        •• •  o • • • • o o o • • o • •
Iso-1  [Y L]T[N P J K Y I P G T K M]A[F]G[G]L[K K]E K D[R]N[D L]I T[Y]L K K[A]C E -
Iso-2  [Y L]T[N P J K Y I P G T K M]A[F]A[G]L[K K]E K D[R]N[D L]I T[Y]M T K[A]A K -
Tuna   [Y L]E[N P K K Y I P G T K M]I[F]A[G]I[K K]K G E[R]Q[D L]V A[Y]L K S[A]T S -
Horse  [Y L]E[N P K K Y I P G T K M]I[F]A[G]I[K K]K T E[R]E[D L]I A[Y]L K K[A]T N E
Rice   [Y L]L[N P J K Y I P G T K M]V[F]P[G]L[K J]P Q E[R]A[D L]I S[Y]L K E[A]T S -
```

The sequences of yeast iso-1 (Smith *et al.*, 1979), yeast iso-2 (Montgomery *et al.*, 1980), tuna (Kreil, 1965), horse (Margoliash *et al.*, 1961) and rice (Mori & Morita, 1980) cytochromes *c* have been aligned so as to maximize the structural homology present. The single letter code is used to identify amino acids and the residue numbering is based on the sequence of tuna cytochrome *c*. Residues 52 and 54 in rice cytochrome *c* are listed as asparagine and aspartate, respectively, as opposed to the aspartate at position 52 and the asparagine at position 54 reported by Mori and Morita (1980). The present assignments for these residues fit the current chemical data and are more consistent with other related sequences (Moore & Pettigrew, 1990). Note the single letter code J is used to denote ε-N-trimethyl lysines. Those amino acid residues identical in all five protein sequences are enclosed in boxes. Residues which are invariant in 94 eukaryotic sequences are marked with a filled dot (•) and those which are conserved in at least 90 sequences are marked with an open circle (o).

Table 1.2: Secondary structural elements present in yeast iso-1 cytochrome *c*

Secondary structural element	Residues involved
α-helix	2–14
β-turn (type II)	21–24
γ-turn	27–29
β-turn (type II)	32–35
β-turn (type II)	35–38
β-turn (type II)[†]	43–46
α-helix	49–55
α-helix	60–70
α-helix	70–75
β-turn (type II)	75–78
α-helix	87–102

[†]mediated through a water molecule.

techniques (Moench & Satterlee, 1989; Busse *et al.*, 1990; Gao *et al.*, 1990, 1991; Qi, 1994a,b). All these cytochromes *c* share a common polypeptide fold, with significant conformational differences occurring primarily in flexible surface loops (Bushnell *et al.*, 1990). In the following discussion, yeast iso-1 cytochrome *c* is used as an example to describe the general structural features of these proteins since it has not only been determined to the highest resolution (1.2 Å; Louie & Brayer, 1990), but it also forms the basis of the structural studies described herein.

The global polypeptide fold of yeast iso-1 cytochrome *c* is illustrated in Figure 1.1 and the details of the positioning of all main and side chain atoms are shown in Figure 1.3. This protein has a high α-helical content; a list of residues involved in these and other secondary structural features is given in Table 1.2. The heme prosthetic group of cytochrome *c* is found buried within the hydrophobic core of the protein, with only one edge of this group being exposed to
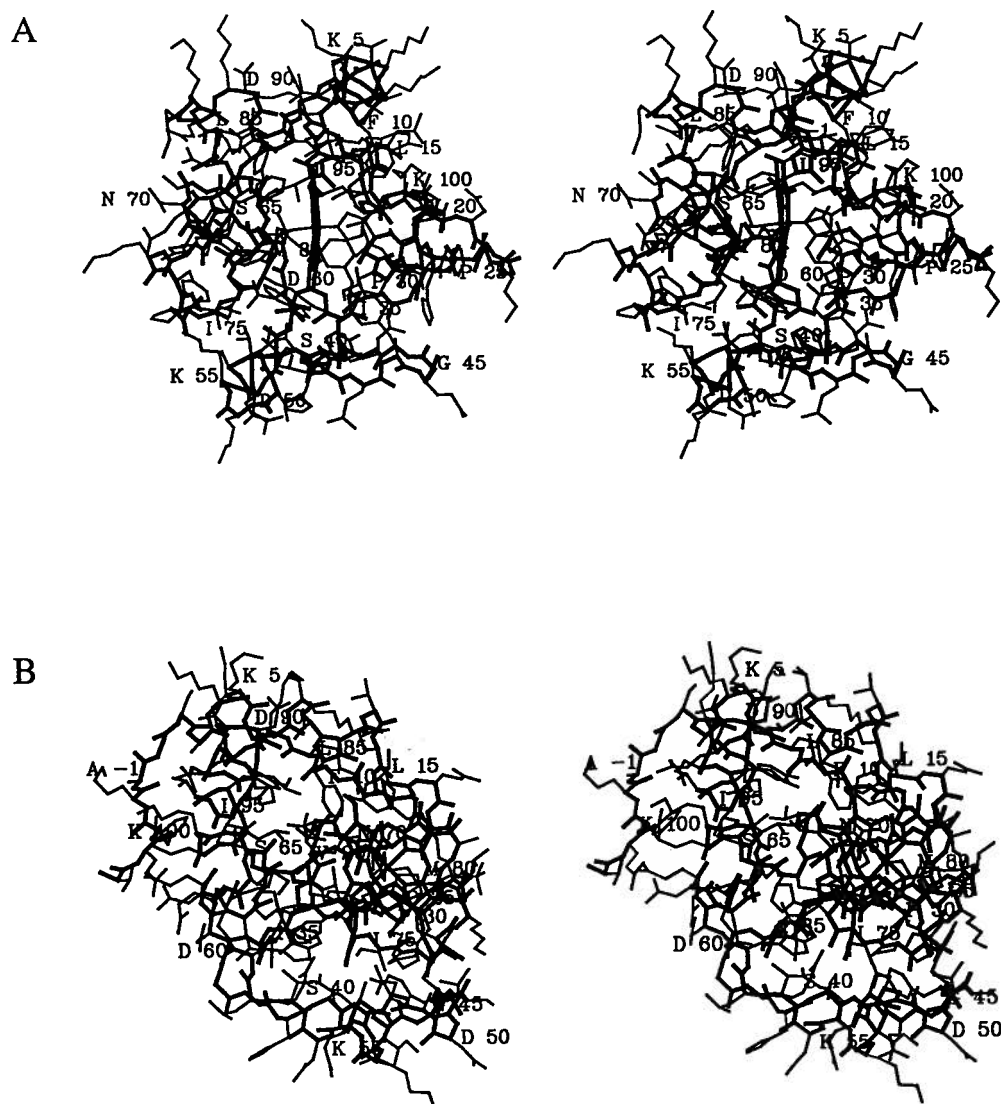
Figure 1.3: Stereo diagrams of yeast iso-1 cytochrome c showing the positions of all main chain (thick lines) and side chain (thin lines) atoms in (a) the standard heme edge-on view and (b) a view rotated by 90° that looks down on the face of the heme plane. The heme group has also been drawn with thick lines, along with the two heme ligand bonds to His18 and Met80 and the two covalent thioether linkages to Cys14 and Cys17. Every fifth α-carbon atom has been labeled with its one letter amino acid designation and sequence number.

the external solvent environment (Figure 1.4). Also sequestered within the interior of the protein are the two propionate groups of the heme moiety which participate in an extensive network of hydrogen bonds with polar side chains and buried water molecules. Two of these water molecules, Wat166 and Wat121 (Figure 1.5), are conserved among all eukaryotic cytochrome *c* structures determined to date (Bushnell *et al.*, 1990; Louie & Brayer, 1990; Murphy *et al.*, 1992; Qi *et al.*, 1994a). Changes in the internal hydrogen bonding network about the heme propionates are found to accompany the transition of cytochrome *c* between the reduced and oxidized states (Takano & Dickerson, 1981a; Berghuis & Brayer, 1992; Qi *et al.*, 1994b).

Two other notable structural features are present in the hydrophobic core of yeast iso-1 cytochrome *c*. The first of these is an internal cavity which is defined by one edge of the heme macrocycle and the side chains of Leu32, Ile35, Met64 and Leu98 (Louie & Brayer, 1990). Although this cavity is large enough to accommodate a water molecule, none is observed, likely due to a lack of hydrogen bonding partners available in this region of the protein. The second notable feature is a cluster of conserved leucine residues, consisting of Leu9, Leu68, Leu85, Leu94 and Leu98, whose side chains pack against each other. This leucine cluster is located adjacent to the heme moiety, the internal heme pocket hydrophobic cavity and the intersection of the N and C-terminal α-helices of yeast iso-1 cytochrome *c* (Figure 1.6). These latter α-helices pack against each other in a roughly perpendicular manner and are notable in that they are thought to be involved in the initiation of the folding of this protein (Roder *et al.*, 1988).

1.3 The Reduction Potential of Cytochrome c

The difference in the midpoint reduction potentials of two proteins represents the driving force for the transfer of an electron between them. Among eukaryotic cytochromes *c*, the value of the midpoint reduction potential is highly conserved ($\sim$270 ± 20 mV; Mathews, 1985; Pettigrew & Moore, 1987), likely as a functional requirement for optimal transfer of electrons both to and from physiological redox partners. A significant alteration of the reduction potential of cytochrome *c* would result in a change in the driving force of its electron transfer reactions and
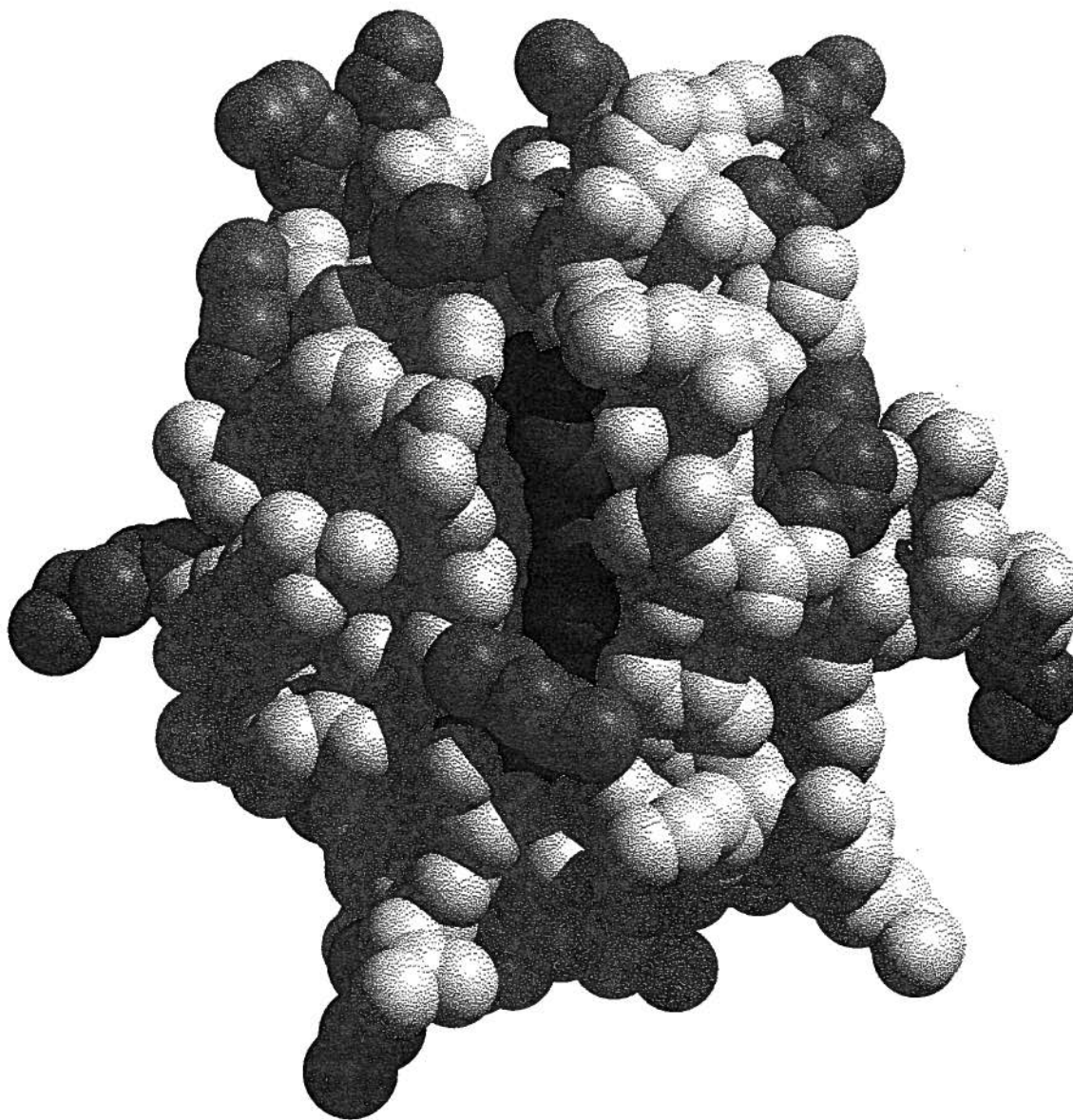
Figure 1.4: A space filling representation of yeast iso-1 cytochrome c showing the exposure of the edge of the heme prosthetic group (in black) to the external environment. Shown in grey are the side chains of lysine and arginine residues thought to be important in the formation of electron transfer complexes between cytochrome c and its redox partner proteins.
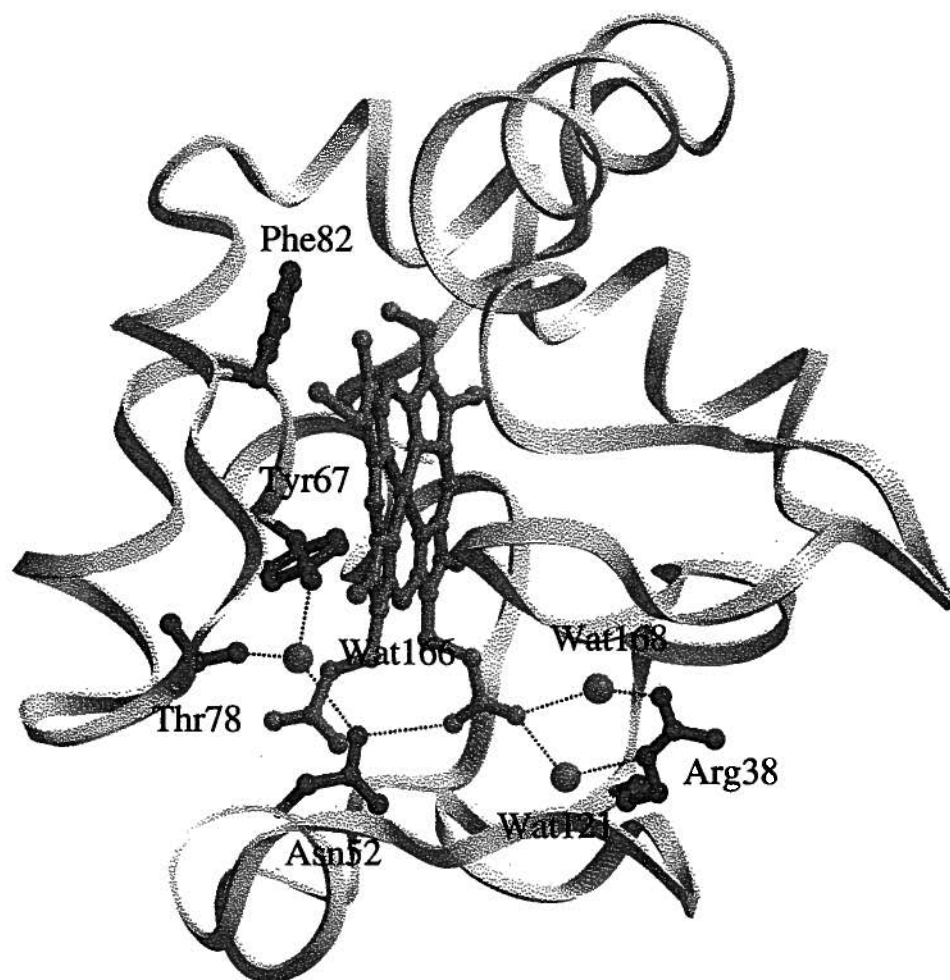
Figure 1.5: A diagram showing the hydrogen bonds formed (dotted lines) between three internal water molecules, heme propionate A and several conserved amino acids in yeast iso-1 cytochrome *c*. The overall polypeptide chain is represented as a ribbon, whereas a ball-and-stick representation is used to illustrate the heme group (light shading) and the side chains of Arg38, Asn52, Tyr67, Thr78 and Phe82 (dark shading). The three internal water molecules are shown as larger single spheres.
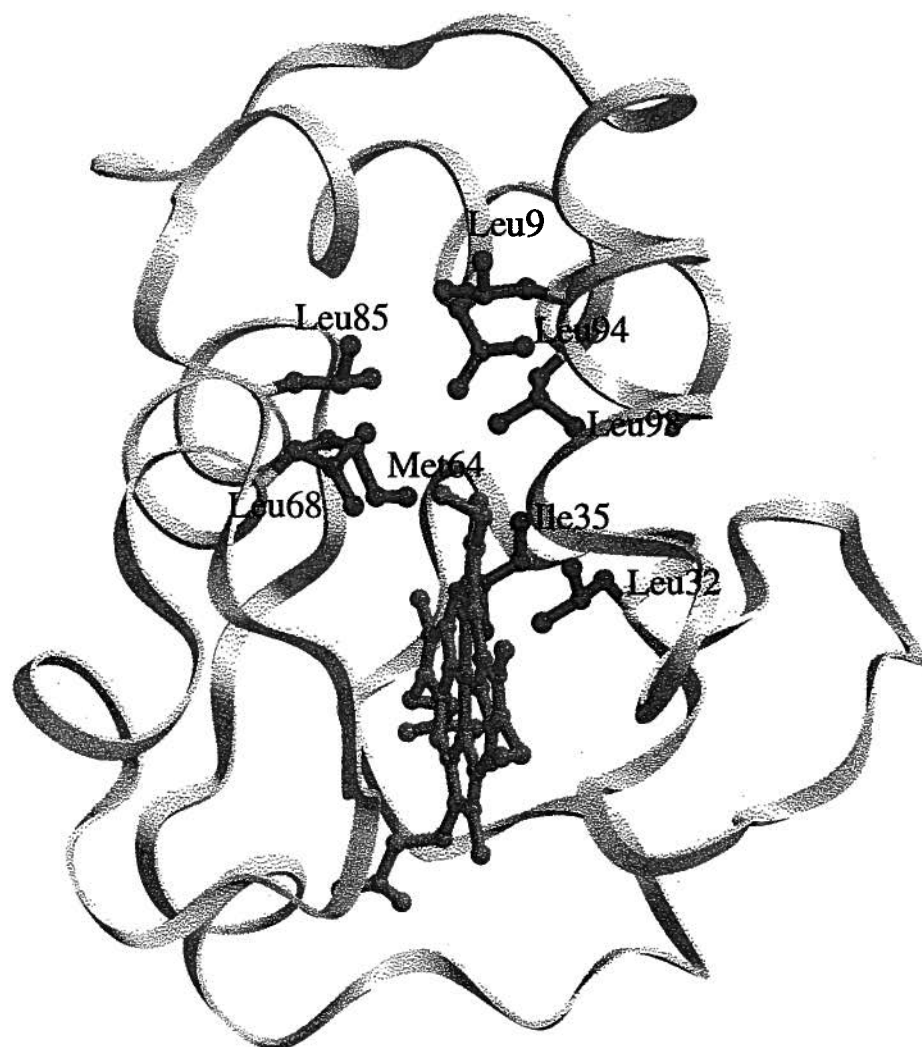
Figure 1.6: A diagram of a conserved leucine cluster found in the hydrophobic core of yeast iso-1 cytochrome *c* as well as residues forming the outer boundaries of a large internal cavity found at the back of the heme pocket. Also drawn is the conformation of the central heme group. The side chains of leucines 9, 68, 85, 94 and 98 make up the leucine cluster while the side chains of Leu32, Ile35, Met64 and Leu98 and one edge of the heme group define the outer limits of the internal hydrophobic cavity.

therefore, this would be expected to adversely impact the control and efficiency of such reactions. However, studies of mutant yeast cytochromes c having significantly decreased reduction potentials have found that this does not inhibit the growth of yeast cells (McLendon *et al.*, 1991; Komar-Panicucci *et al.*, 1992). Thus these studies have raised questions concerning the functional requirement for the maintenance of the reduction potential of cytochrome c.

1.3.1 Factors which regulate reduction potential

Due to the biological importance of electron transfer reactions, there has been much interest in understanding the factors which determine the midpoint reduction potentials of proteins involved in these reactions (Moore & Williams, 1977). Towards this end, many studies have focused on the members of the cytochrome family, which have midpoint reduction potentials spanning a range of nearly 800 mV (Churg & Warshel, 1986). From this range of reduction potentials, the identity of the axial ligands to the heme iron atom account for a variation of $\sim$150 mV (Harbury *et al.*, 1965), while an additional variation of the same magnitude can be attributed to substitutions to the porphyrin ring, such as the thioether linkages in c-type cytochromes (Marchon *et al.*, 1982). However, reduction potentials can vary by nearly $\sim$500 mV among cytochromes having identical heme iron ligands and porphyrin ring substituents (Cusanovich *et al.*, 1988). Thus this large variation must arise from the differences between the environments provided by the polypeptide matrices of these proteins.

1.3.2 Effect of heme pocket polarity on reduction potential

Measurements of the midpoint reduction potential of iron porphyrin ring groups have been shown to be dependent on the dielectric constant of the solution in which the experiment is performed (Kassner, 1972). Thus the polarity of the heme environment likely plays a large role in determining the reduction potential of a heme protein (Kassner, 1972, 1973; Churg & Warshel, 1986). Nonetheless, proteins having heme environments of similar polarity have been observed to have reduction potentials which vary by as much as 300 mV. This variation of

reduction potential has been correlated with the exposure of the heme moiety to the external solvent environment (Stellwagen, 1978). Although this would seem to indicate that reduction potential is dependent on solvent exposure rather than the polarity of the heme binding pocket, it must be noted that the heme groups of the proteins examined had varying axial ligands and porphyrin ring substituents. Furthermore, the notion that reduction potential is also dependent on heme solvent exposure is consistent with the idea that the polarity of the heme environment as a whole is the primary determinant of reduction potential since an increase in heme solvent exposure in a protein would result in a corresponding increase in the polarity of the heme environment.

1.3.3 Effect of electrostatic groups on reduction potential

Studies have shown that there is a relationship between the presence of charged protein groups and observed heme reduction potential. It has been proposed that this contribution is straightforward, based on the observation of a direct correlation between the global net charge of a protein and its reduction potential (Rees, 1985). However, this simple correlation has been shown to be overly simplistic and cannot consistently account for the influence of electrostatic effects on protein reduction potential (Moore *et al.*, 1986). Despite the apparent complexity of the relationship between electrostatics and reduction potential, it has been shown that particular charged groups can have a specific and appreciable effect on reduction potential. For example, it has been demonstrated that the reduction potential of cytochrome *c* can be altered in a predictable manner through the chemical modification of lysine residues (Schejter *et al.*, 1982). In another example, the substitution of Arg38 in cytochrome *c* by uncharged residues resulted in a decrease in the reduction potential (Cutler *et al.*, 1989). Also a factor in this latter case are differences in heme propionate charge which have been proposed to lead to midpoint reduction potential variations (Moore *et al.*, 1984). Not only does Arg38 have a charged side chain but it also interacts with the heme propionate A of cytochrome *c* (Figure 1.5). While it is evident that electrostatic contributions to heme reduction potential can be substantial, it is

also clear that much further work needs to be done to elucidate the precise factors involved in this process.

1.4 Cytochrome c in Electron Transfer Complexes

Cytochrome *c* function is also dependent on its ability to form complexes with its electron transfer partners. The contact surface between two electron transfer proteins must allow for the formation and dissolution of a viable complex while providing a suitable medium through which electrons can travel between the proteins. Extensive studies have been performed on cytochrome *c* aimed at determining the nature of the protein surface involved in the formation of such complexes (for reviews see Margoliash & Bosshard, 1983; Mathews, 1985; Pettigrew & Moore, 1987). Many of these studies have focused on the lysine and arginine residues which are located around the exposed heme edge of cytochrome *c* (Figure 1.4). It appears that these charged residues provide much of the impetus for complex formation and determine the specific configurations of these complexes through the formation of intermolecular electrostatic interactions (Ferguson-Miller *et al.*, 1979). However, important contributions to the stabilization of such electron transfer complexes also come from hydrophobic surface residues (Mauk *et al.*, 1986; Guillemette *et al.*, 1994) and other surface groups capable of forming hydrogen bonds (Mauk *et al.*, 1991).

Computer generated models of complexes formed between cytochrome *c* and various electron transfer partners have been used as one way to understand the relative functional importance of different regions of cytochrome *c*. The model complexes formed with cytochrome b_5 (Salemme, 1976; Mauk *et al.*, 1986) and cytochrome *c* peroxidase (Poulos & Kraut, 1980) have been the most extensively studied since the three-dimensional structures of both electron transfer proteins are known. These models are described separately in the following sections, along with the recent determination of the structure of the complex of cytochrome *c* with cytochrome *c* peroxidase (Pelletier & Kraut, 1992). In other studies, the regions of cytochrome *c* which interact with cytochrome *c* oxidase and cytochrome *c* reductase have been mapped (Pettigrew

& Moore, 1987), but models of these complexes have not been developed since the structures of these latter two proteins are not known. However, it has been shown that the region around the exposed heme edge of cytochrome c, including several charged residues, interacts with these two redox partners (Rieder & Bosshard, 1980). Other model complexes studied include those formed between cytochrome c and flavocytochrome b_2 (Tegoni *et al.*, 1993), flavodoxin (Matthew *et al.*, 1983) and plastocyanin (Roberts *et al.*, 1991).

1.4.1 The cytochrome c: cytochrome b₅ complex

The complex formed between cytochrome c and cytochrome b_5 has been the subject of numerous studies examining interprotein electron transfer (for example, see Eltis *et al.*, 1988; Qin *et al.*, 1991; Willie *et al.*, 1992, 1993; Meyer *et al.*, 1993). This was the first protein-protein electron transfer complex for which a model was proposed based on the structures of the individual proteins (Salemme, 1976). It was built by matching the complementary electrostatic surfaces of cytochrome c and cytochrome b_5 and then docking the structures of these proteins together. This model complex has been further subjected to theoretical analysis using electrostatic (Mauk *et al.*, 1986; Eltis *et al.*, 1991), molecular dynamics (Wendoloski *et al.*, 1987), Brownian dynamics (Eltis *et al.*, 1991; Northrup *et al.*, 1993) and energy minimization (Guillemette *et al.*, 1994) techniques. Figure 1.7 shows one such enhanced model of the cytochrome c-cytochrome b_5 complex. Although the models generated by these techniques likely do not completely duplicate the ensembles of closely related complexes which occur in solution (Hartshorn *et al.*, 1987; Burch *et al.*, 1990), they nevertheless provide a general outline of the residues involved in electron transfer between these proteins. Two such residues implicated by modeling and which are the focus of the studies in this thesis are those at positions 82 and 85 in cytochrome c (Wendoloski *et al.*, 1987; Burch *et al.*, 1990).
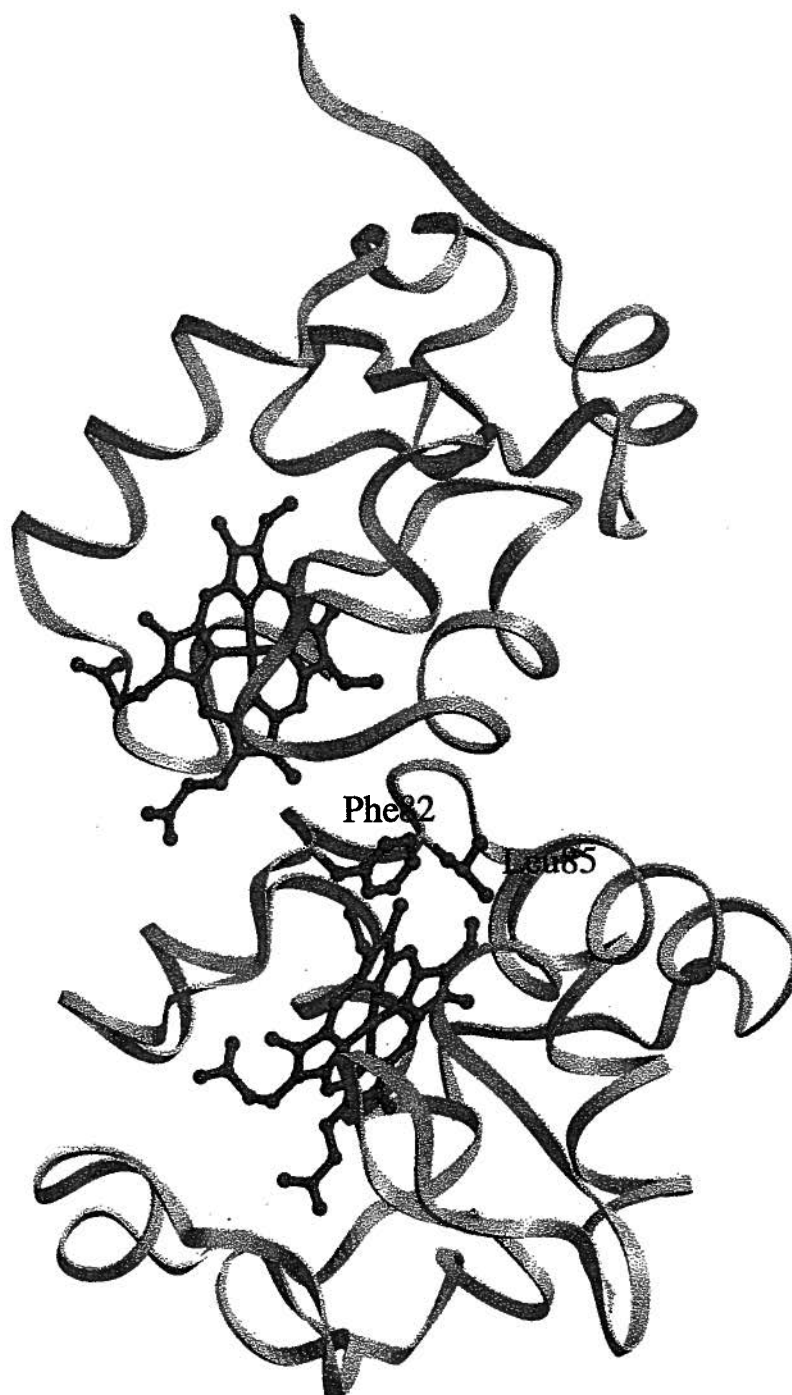
Figure 1.7: A model of the complex formed between yeast iso-1 cytochrome *c* (bottom) and bovine cytochrome *b*₅ (top). A ribbon representation is used to depict the two polypeptide backbones while the heme groups of the two proteins are shown in a ball and stick representation, as are the side chains of Phe82 and Leu85 in cytochrome *c*. This model represents the most common conformation observed in a Brownian Dynamics simulation of the complex (Northrup *et al.*, 1993); energy minimization was used to optimize intermolecular interactions (Guillemette *et al.*, 1994).

1.4.2   The cytochrome c: cytochrome c peroxidase complex

Another complex intensively studied to understand the nature of the electron transfer process has been that formed between cytochrome *c* and cytochrome *c* peroxidase (for example, see Erman *et al.*, 1991; Everest *et al.*, 1991; Nocek *et al.*, 1991; Beratan *et al.*, 1992; Corin *et al.*, 1993). This complex has also been the subject of a number of modeling studies (Poulos & Kraut, 1980; Poulos & Finzel, 1984; Lum *et al.*, 1987) and more recently, the structure of this complex has been determined by crystallographic methods to 2.3 Å resolution (Pelletier & Kraut, 1992). The structure determined for this complex, which is illustrated in Figure 1.8, has proven to be a valuable tool in understanding redox partner complexation. It has also revealed significant deficiencies in the earlier model complexes that had been constructed, especially with respect to the identity of the interactive surface region of cytochrome *c* peroxidase. However, both this complex structure and earlier modeling suggest that the surface of cytochrome *c* around the exposed heme edge is located at the site of intermolecular contact. It should be noted that while the structural determination outlines the general aspects of cytochrome *c*-cytochrome *c* peroxidase complex formation, this does not preclude the existence of alternate docking geometries for these two proteins such as those suggested by Brownian Dynamics studies (Northrup *et al.*, 1988). In fact, there is strong evidence that two distinct binding regions for cytochrome *c* exist on the surface of cytochrome *c* peroxidase (Stemp & Hoffman, 1993; Zhou & Hoffman, 1993; Mauk *et al.*, 1994; Zhou & Hoffman, 1994).

1.5   Mutants of Cytochrome c

In the past, classical mutagenesis methods have provided valuable insight into cytochrome *c* function (Hampsey *et al.*, 1988; Sherman, 1990). A more recently developed technique that allows considerable extension of these studies is site-directed mutagenesis, which allows the rational design of specific mutant proteins (Zoller & Smith, 1983; Smith, 1986). Using this method, both the roles of individual amino acids in cytochrome *c* and more global aspects of function can be probed. Of particular interest to the work in this thesis are the factors
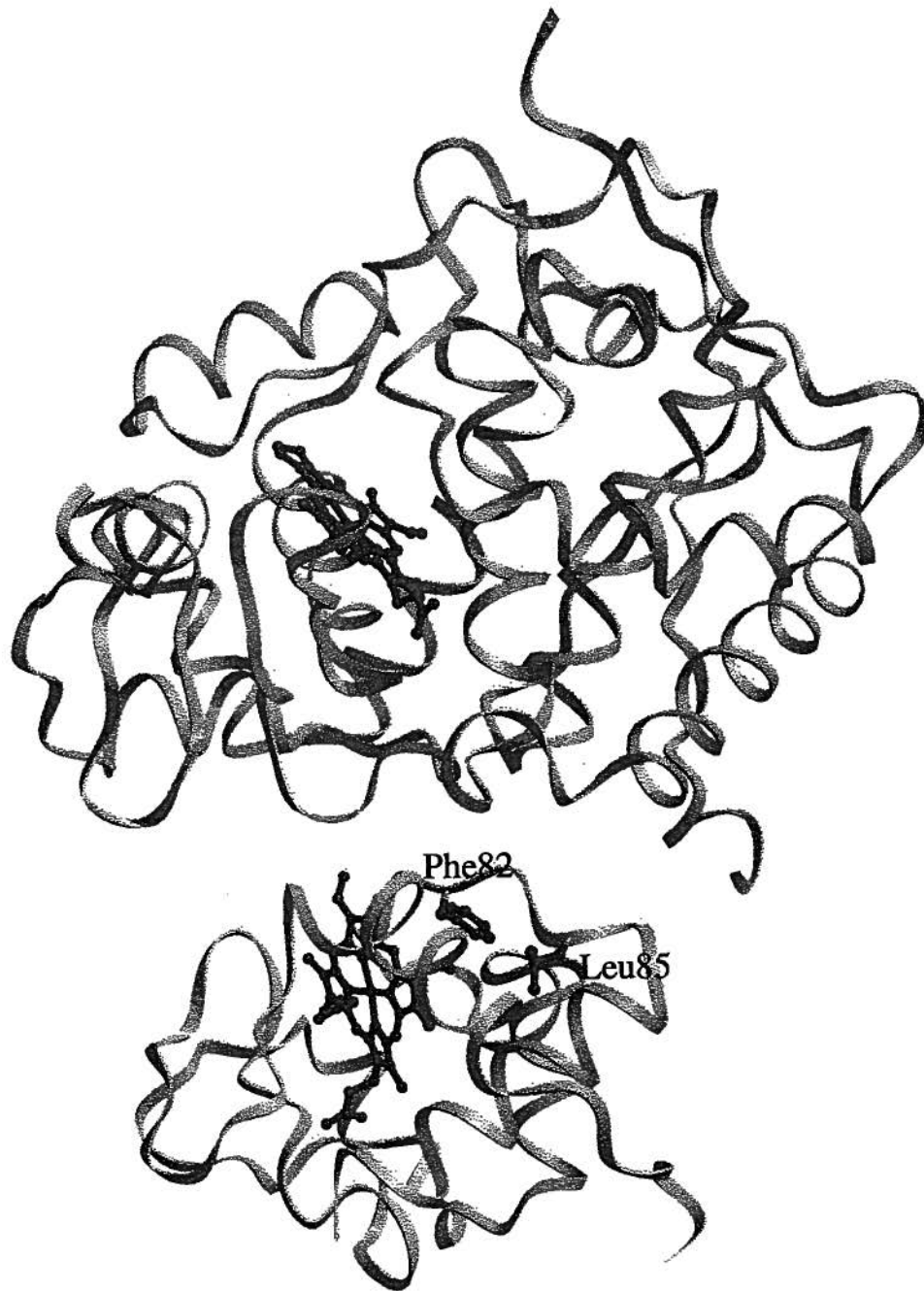
Figure 1.8: The structure of the complex formed between yeast iso-1 cytochrome *c* (bottom) and yeast cytochrome *c* peroxidase (top) as determined by Pelletier & Kraut (1992). A ribbon representation is used to depict the two polypeptide backbones. The heme groups of the two proteins are shown in a ball and stick representation, as are the side chains of Phe82 and Leu85 in cytochrome *c*.

involved in the maintenance of heme reduction potential, the nature of the interactive face of cytochrome *c* with electron transfer partners, and the roles of internal structural features such as hydrophobic cavities and clusters of leucine side chains.

Two amino acids that appear to have roles in these functional and structural aspects of cytochrome *c* are Phe82 and Leu85. These two residues form the focus of the studies discussed in this thesis, wherein specifically designed mutant proteins having single substitutions or combinations of substitutions at these and other related positions in the polypeptide chain are made, with the goal being to gain a better understanding of how Phe82 and Leu85 influence the function of cytochrome *c*. The overall placement of these residues in yeast iso-1 cytochrome *c* is shown in Figure 1.9. A brief description of the extent of knowledge concerning these residues which was available at the onset of this work is given in the following sections. A more complete analysis of structure-function relationships found for Phe82 and Leu85 on the basis of structural studies conducted as part of this thesis is presented in Chapters 3–6.

1.5.1 The role of phenylalanine 82

This residue is invariantly conserved in the sequences of cytochrome *c* and it is believed to have multiple functional roles. Substitution of Phe82 in yeast iso-1 cytochrome *c* with other amino acids has a significant effect on the ability of this protein to support growth of yeast on non-fermentable carbon sources, although no such mutation was found to completely abolish this function (Hilgen & Pielak, 1991; Inglis *et al.*, 1991). Mutants of this type also have an effect on measured heme reduction potential (Pielak *et al.*, 1985; Rafferty *et al.*, 1990). Structural studies have found that the side chain of this residue forms a part of the hydrophobic heme pocket of cytochrome *c*, with its aromatic ring packing against the face of the heme group in a coplanar fashion (Takano & Dickerson, 1981a,b; Louie *et al.*, 1988a; Bushnell *et al.*, 1990). Subsequent structural studies of the F82S (Louie *et al.*, 1988b) and F82G (Louie & Brayer, 1989) mutants of yeast iso-1 cytochrome *c* have revealed some aspects of the relationship between Phe82 and heme reduction potential, indicating the latter is correlated to the degree of heme
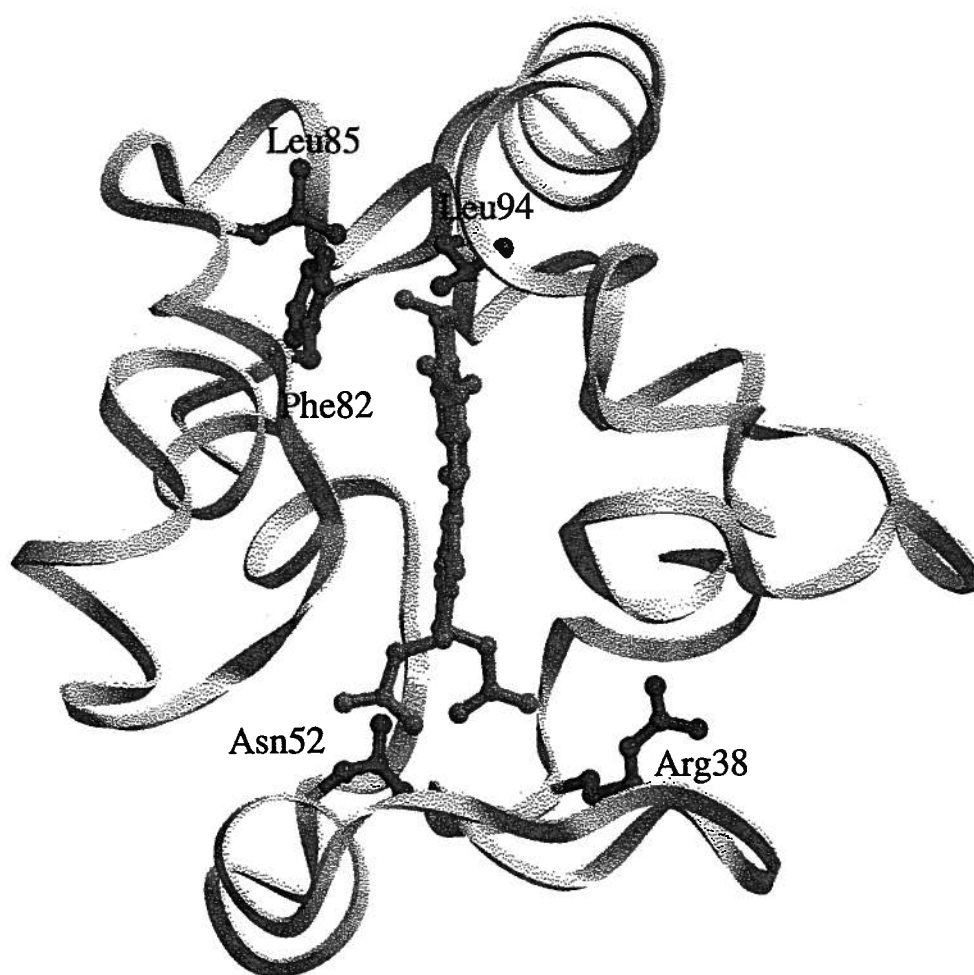
Figure 1.9: A ribbon diagram of the polypeptide fold of yeast iso-1 cytochrome *c* showing the location of the side chains of Phe82 and Leu85 which form the focus of structural studies discussed in this thesis. Related residues that were also examined include Arg38, Asn52 and Leu94. As part of these studies, all of these amino acids were replaced either singly or in groups by site-directed mutagenesis techniques.

solvent exposure and the proximity of polar groups.

The side chain of Phe82 is also partially exposed to solvent in the surface region of cytochrome *c* believed to form complexation interactions with electron transfer partners. The importance of this residue in the formation of electron transfer complexes has been suggested by modeling (Poulos & Kraut, 1980), NMR (Burch *et al.*, 1990) and molecular dynamics methods (Wendoloski *et al.*, 1987), and this has been confirmed by the structure determination of one such complex (Pelletier & Kraut, 1992). Figures 1.7 and 1.8 illustrate the putative positioning of Phe82 in complexes of this type. In regard to the functional role of Phe82, mutant proteins with replacements at this residue show alterations in steady-state electron transfer activity (Pielak *et al.*, 1985; Michel *et al.*, 1989) and intracomplex electron transfer kinetics (Everest *et al.*, 1991; Hazzard *et al.*, 1992).

1.5.2 The role of leucine 85

Relatively little study has been conducted on the role of the conserved Leu85 residue, although it has been implicated as an element at the interactive face of complexes formed by cytochrome *c* with cytochrome *c* peroxidase (Nocek *et al.*, 1991; Pelletier & Kraut, 1992). On the basis of modeling (Salemme, 1976; see Figure 1.7) and NMR studies (Burch *et al.*, 1990), Ile85 in horse cytochrome *c* appears to play a comparable role in complexes with cytochrome b_5. In terms of location, the side chain of Leu85 in yeast iso-1 cytochrome *c* is partially exposed to solvent, packs against the side chain of Phe82, and forms a portion of the hydrophobic heme binding pocket (see Figure 1.9; Louie & Brayer, 1990). Leu85 is one of a cluster of such residues (Leu9, Leu68, Leu94, Leu98) that is found along the most buried edge of the heme group. Furthermore, this leucine cluster is adjacent to an internal hydrophobic cavity in the heme pocket of yeast iso-1 cytochrome *c*. To this point, no study of the role of this leucine cluster or the nearby cavity has been conducted.

1.5.3   The roles of related residues

As part of studies conducted on Phe82 and Leu85 in this thesis, a number of other nearby or functionally related amino acids were examined. One of these is the highly conserved Leu94 which is part of the heme pocket leucine cluster that includes Leu85. The side chain of Leu94 packs directly against both the side chain of Leu85 and the heme group. Furthermore, this residue is located at the intersection point of the N and C-terminal helices of cytochrome *c* (Figure 1.9), a structural feature believed to be part of an early folding event in this protein (Roder *et al.*, 1988). It has been shown that replacement of Leu94 by alternative amino acids results in reduced activity *in vivo* (Hampsey *et al.*, 1988) and this has been attributed to possible alterations in the interaction between these N and C-terminal helices.

In order to study the role of Phe82 in the maintenance of heme reduction potential and its relationship to other residues that are also a factor in this property, proteins with multiple mutations involving Phe82, Asn52 and Arg38 were examined. Arg38 is an invariant residue positioned adjacent to the buried propionate A group of the heme to which it forms interactions mediated by two water molecules (Figure 1.5). It has been shown that replacement of this residue with other amino acids decreases the observed reduction potential of the resultant mutant protein (Cutler *et al.*, 1989) without causing large conformational shifts in the polypeptide chain (Barker *et al.*, 1991; Thurgood *et al.*, 1991).

Mutation of the invariant Asn52 to other residues can also have a significant effect on reduction potential (Burrows *et al.*, 1991; Langen *et al.*, 1992), as well as on the rate of electron transfer with cytochrome b_5 (Whitford *et al.*, 1991) and *in vivo* function (McLendon *et al.*, 1991). This residue is completely buried in the structure of cytochrome *c* near the plane of the heme group and the Met80 heme ligand. In yeast iso-1 cytochrome *c*, Asn52 also forms a part of a hydrogen bonding network to a conserved internal water molecule, Wat166 (Figure 1.5). A particularly novel feature of the mutation of Asn52 to isoleucine is that this acts to suppress the effects of other mutations that would otherwise disable the function of cytochrome *c* (Das *et al.*, 1989; Berroteran & Hampsey, 1991). It has been found that this replacement results in a

large increase in the thermal stability of cytochrome *c* (Das *et al.*, 1989; Hickey *et al.*, 1991) and subsequent structural analyses have investigated the source of this stabilization (Berghuis *et al.*, 1994a). Both Arg38 and Asn52 are structurally remote from Phe82 and the goal of combining mutations at these sites is to determine to what extent these residues act, independently or in unison, in maintenance of heme reduction potential and other properties related to the stability and function of cytochrome *c*.

1.6 Research Objectives

The goals of this thesis were fourfold and were centered on the use of a structure-function-mutagenesis approach in the study of Phe82, Leu85 and associated residues of cytochrome *c*. The first objective was to investigate the roles of Phe82 and Leu85 as elements at the complexation interface formed between cytochrome *c* and electron transfer partners. Clearly, this feature is central to cytochrome *c* function and there has been considerable interest in defining the role of these two residues in this process. Further studies were then designed to elucidate the contributions of Phe82 and Leu85 to other aspects of cytochrome *c* function. Thus a second objective was to characterize the nature of an internal hydrophobic leucine cluster to which Leu85 belongs, and which forms a substantial portion of the structure of the heme binding pocket. Associated with this work was an analysis of the highly conserved leucine cluster participant, Leu94, which is positioned at the juncture of the interaction of the N and C-terminal helical regions of cytochrome *c*. This helix-helix interaction is also an important structural element in forming the heme binding pocket. As part of the study of the leucine cluster, the possible role of an adjacent internal cavity, which is found next to the most buried edge of the heme group, was examined, along with the relationship between alterations in the volume of this cavity and functional aspects of cytochrome *c*.

The third objective of this work was to expand our understanding of the factors which govern heme reduction potential and particularly the role that Phe82 plays in this regard. Specifically targeted were aliphatic side chain replacements for Phe82. Also examined in conjunction with

these studies were the effects of mutations at Leu85 and Leu94. In a related fourth objective, an attempt was made to place these results in a larger context by looking simultaneously at Phe82 and two other distally located residues (Arg38 and Asn52), all of which have a significant role in the maintenance of heme reduction potential. The goal was to establish the degree of interplay between these sites with regards to this property. These studies also provided information concerning the contribution of each of these sites to the overall stability of cytochrome c and the effects on stability of introducing simultaneous mutations at these sites.

Overall, the chapters in this thesis are organized in the order of the objectives just discussed. Beyond Chapter 2, which deals with general aspects of experimental procedure, Chapter 3 focuses on the interactive complexation face of cytochrome c, Chapter 4 looks at the conserved leucine cluster in cytochrome c and the associated internal heme pocket cavity, Chapter 5 documents the influence of Phe82 on reduction potential, and Chapter 6 examines the individual and cumulative contributions of Arg38, Asn52 and Phe82 to heme reduction potential and overall protein stability.

It must be emphasized that although structural analyses are central to the work completed in this thesis, the interpretation of results of this type are greatly assisted and enhanced by associated functional analyses. For this reason structural studies were planned as part of a comprehensive program of mutagenesis and functional analyses in collaboration with two other groups. One of these was based at the University of British Columbia (J. G. Guillemette, A. G. Mauk and M. Smith) and focused on the structural and functional roles of residues at the interactive face of cytochrome c. The second group of collaborators was based at the University of Rochester (S. Komar-Panicucci, F. Sherman, G. McLendon), with the focus being interactions between distal residues in cytochrome c and the investigation of the cumulative and synergistic effects of introducing multiple substitutions of these residues. The efforts of these collaborators were directed toward the site-directed mutagenesis of cytochrome c, as well as the functional characterization of the resultant mutant proteins. My role in these collaborative efforts centered on the initial modeling and design of amino acid substitutions at the residues of interest, the

crystallization and determination of the three-dimensional structures of mutant proteins, and the detailed analysis of these protein structures with regard to correlating observed changes in the functional behavior of mutant proteins with their three-dimensional structures. The results of the work presented in this thesis have been published as a number of articles in scientific journals as summarized in the Addendum at the end of the thesis.

Chapter 2

Experimental Methods

An overview of the methodology used to study the structures of mutants of yeast iso-1 cytochrome c is described in this chapter. The details of each structural determination are given in following chapters.

2.1   General Experimental Approach

The general scheme used in this thesis to investigate structure-function relationships in yeast iso-1 cytochrome c is shown in Figure 2.10. This process was initiated by the design of mutations which would provide insight into the roles of Phe82 and Leu85 in particular, as well as associated residues that were involved in common structural features or related functionalities. The specific goals in studying each individual mutant protein designed are discussed in detail in the introductory sections of each of Chapters 3–6. Once mutant proteins had been expressed and purified, each was subjected to two streams of study. One of these was a series of functional tests; the other the elucidation of its three-dimensional structure using X-ray diffraction techniques. In the interpretive phase of this work the collected functional and structural data were assessed as to the impact of the introduced mutation(s) by comparison to the observed data for wild-type yeast iso-1 cytochrome c. In this assessment, a particular emphasis was placed on defining the role of the amino acid(s) which had been replaced. Yeast iso-1 cytochrome c is an ideal candidate for this type of study given the existing extensive knowledge base of the structural and functional attributes of the wild-type protein, as well as the ability to specifically alter this protein by site-directed mutagenesis.
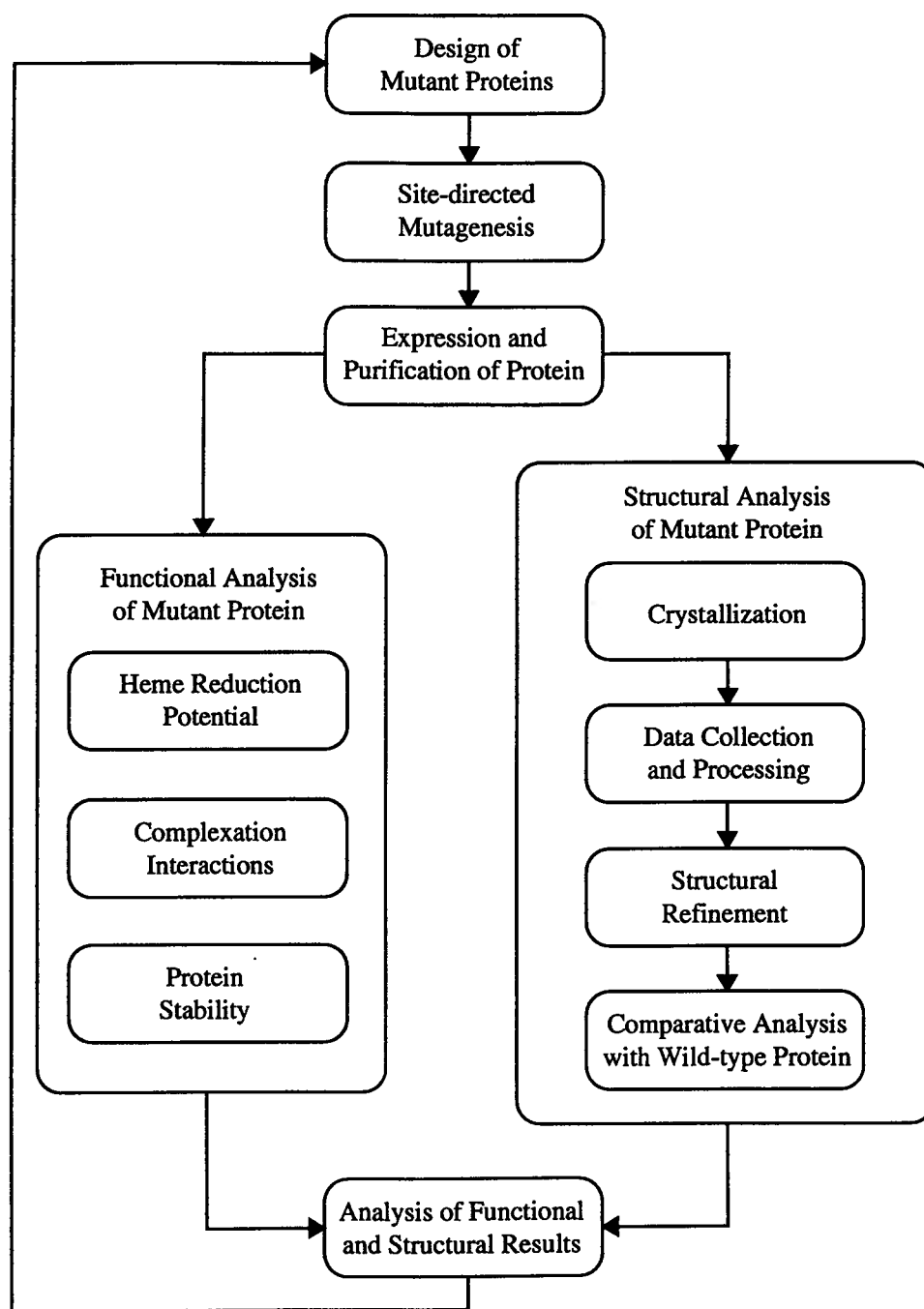
Figure 2.10: General scheme used to study structure-function relationships in yeast iso-1 cytochrome *c*.

2.2 Design of Mutant Cytochromes c

The design of each mutant yeast cytochrome c was based on a number of factors. These took into consideration not only the available structural and functional data available for yeast cytochrome c, but also those of related cytochromes c. Primary considerations were comparisons of the known amino acid sequences of eukaryotic cytochromes c, the high resolution structures of yeast iso-1 cytochrome c and the related tuna, horse and yeast iso-2 cytochromes c, and available data concerning the manner in which cytochrome c forms complexation interactions with electron transfer partners such as cytochrome c peroxidase and cytochrome b_5.

In a procedural sense a number of steps were followed in the development of each mutant protein. Initially, the amino acid of interest was studied in terms of its impact on functionality and its location within the protein. An analysis was then made of all the available alternative amino acids which might be substituted to determine which one(s) might most directly be useful to assess the functional characteristics of interest. Naturally many substitutions were inappropriate because they would likely lead to unwanted alterations and therefore be of limited use in interpreting or understanding the targeted functional property. An example of this is the substitution of small side chains with large ones leading to substantial steric conflicts that disrupt a whole range of functional properties over and above the one of interest. Also avoided were substitutions likely to result in substantial polypeptide chain refolding, which would again produce too many global shifts to make the interpretation of functional data meaningful for the targeted residue. The goal of choosing substitutions was to find suitable replacements that would only alter one particular facet of cytochrome c function and therefore allow a clear assessment of the role of the residue involved. The detailed rationale for designing each of the mutant proteins studied in this thesis is documented in the introductory sections of Chapters 3–6.

An important element in the determination of suitable substitutions was the use of molecular graphics to examine the structural environment of the residue of interest and to visualize possible replacement residues. Modeling of possible amino acid replacements was based on the

high resolution structure of yeast iso-1 cytochrome c (Louie & Brayer, 1990). The primary tool used to accomplish this was the program MMS (Dempsey, 1986) running on either a Silicon Graphics 3130 or 4D/340 workstation. In this way amino acid(s) that might be substituted at a given position could be inserted and adjusted manually to evaluate the structural consequences that might arise. This was particularly useful in assessing the potential for substituted residues to lead to structural conflicts. Amino acid substitutions were also screened as to their potential effects with regards to the electron transfer complexes formed by cytochrome c. This was accomplished by examining modeled mutations in the context of models of the complexes formed between cytochrome c and cytochrome c peroxidase (Poulos & Kraut, 1980) and cytochrome b_5 (Salemme, 1976).

Another consideration concerning the design of specific mutants of yeast iso-1 cytochrome c and the study of their properties should be noted. Specifically the wild-type form of this protein has the tendency to form homodimers through the free cysteine residue at position 102 (Bryant *et al.*, 1985; Moench & Satterlee, 1989). This interferes with both functional and structural analyses of this protein and a number of investigators have chemically modified the sulfhydryl group of Cys102 to prevent dimer formation (Zuniga & Nall, 1983; Ramdas *et al.*, 1986; Hickey *et al.*, 1991). However, this approach perturbs the structure of yeast iso-1 cytochrome c in its C-terminal region and thereby complicates the analysis of changes induced by mutations introduced at other locations. To avoid this problem we have chosen to modify Cys102 to either an alanine or threonine in our analyses of mutants of yeast iso-1 cytochrome c. These two substitutions occur naturally at position 102 in other eukaryotic cytochrome c sequences (Hampsey *et al.*, 1988; Moore & Pettigrew, 1990). Previous studies have shown that the C102A and C102T substitutions have a minimal impact on the structural and functional properties of yeast iso-1 cytochrome c (Cutler *et al.*, 1987; Hickey *et al.*, 1991; Berghuis & Brayer, 1992).

It should be emphasized that even though the best efforts go into the design of mutant proteins, often the structural alterations that occur at the site of mutation are more extensive than anticipated. Furthermore it is not uncommon for amino acid substitutions to induce

shifts far removed from the mutation site in ways that are difficult to predict given our current understanding of the factors involved in protein folding and stability. This appears to be particularly true for cytochrome *c* where previous studies of mutant proteins have uncovered unexpected polypeptide chain refolding (Louie & Brayer, 1989), positional shifts in side chains and internally bound water molecules (Louie *et al.*, 1988b; Berghuis *et al.*, 1994a), and changes in polypeptide chain mobility (Berghuis *et al.*, 1994a,b). In the absence of structural studies, these unforeseen changes would have led to incorrect interpretation of functional data since the assumption would have been made that, other than at the mutation site, the structure of these mutant proteins had remained the same. For these reasons special diligence was applied in the studies conducted in this thesis to characterize any unanticipated structural alterations induced by mutagenesis so as to achieve the best interpretation of the functional perturbations observed.

2.3 The Crystalline State

The utility of using X-ray diffraction techniques in the analysis of the structures of proteins requires that these proteins be in the crystalline state. A protein crystal consists of a well ordered three-dimensional lattice of a large number of individual protein molecules packed in a symmetrical manner. Such crystals are held together by intermolecular interactions, otherwise known as lattice contacts, formed between neighboring molecules. The fundamental repeating unit within a protein crystal is the unit cell which contains one or more identical asymmetric units related to each other through defined symmetry operations. The goal of the X-ray diffraction experiment is the determination of the atomic structure of the protein molecule(s) that are within the asymmetric unit.

Before structural analyses by X-ray diffraction can proceed, it is necessary to grow suitable crystals of the protein to be investigated. In this section a general overview of the methods used to grow diffraction quality crystals of mutants of yeast iso-1 cytochrome *c* is given. In this work two major methods of crystallization were used, the hanging drop vapour diffusion and free

interface diffusion approaches, both of which were supplemented by various seeding techniques. For a more detailed discussion of these and other crystallization methods the reader is referred to excellent reviews in McPherson (1982, 1990) and Carter, Jr. (1990).

2.3.1 The hanging drop vapour diffusion method

In this method, an inverted drop containing the protein solution is placed over a well containing the precipitant solution or "mother liquor", as illustrated in Figure 2.11. This protein drop contains a low concentration of precipitant whereas the mother liquor contains a high concentration of precipitant, resulting in the formation of a concentration gradient within the crystallization well. Due to this gradient, the protein drop and the mother liquor equilibrate over time through the diffusion of water vapour, causing a gradual increase in the precipitant concentration in the protein drop as the system reaches equilibrium. As the precipitant concentration in the drop increases, this solution becomes saturated and the protein comes out of solution, forming either a precipitate or the desired result, crystals. In order to encourage crystal formation, the protein drop can be seeded with either macro-crystals (Thaller *et al.*, 1985) or micro-crystals (Leung *et al.*, 1989) which can assist the formation of nucleation sites for crystal growth.

A typical hanging drop crystallization experiment was carried out using a twenty-four well Linbro plate (Flow Laboratories, McLean VA) to allow one to scan different variables to optimize the conditions for crystallization. In general these plates permitted two variables to be screened at one time. Variables studied included type of precipitant, pH, temperature, concentration of protein and precipitant in the protein drop and in the well solution, as well as the effect of reducing agents and other additives in the protein droplet. In crystallization trials, 1 ml of precipitant solution was placed in each well of the test plate and hanging protein drops containing 5–20 μl of protein solution (40–100 mg/ml) were dispensed onto coverslips. Coverslips were pre-treated with Sigmacote (Sigma Chemical Company, St. Louis), a siliconizing agent which prevented the protein drop from spreading out on the glass surface. Silicone grease was applied to the rim of each well to form an airtight seal between the well and the coverslip.
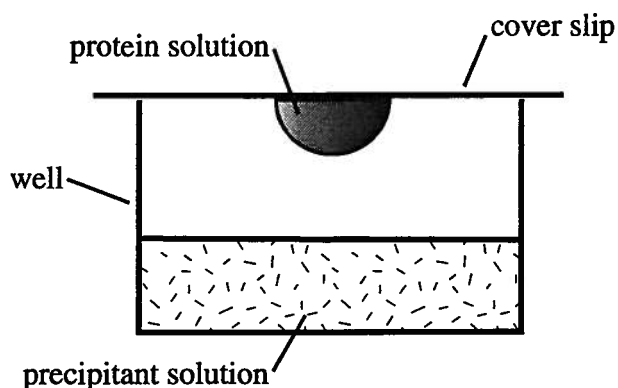
Figure 2.11: Schematic diagram of the hanging drop vapour diffusion method used in the crystallization of mutant yeast iso-1 cytochromes *c*.

In experiments utilizing crystal seeding, seeds were introduced into the protein drop just before placing the coverslip over its well on the Linbro plate. After assembly, each crystallization plate was further protected for storage by being wrapped in a thin plastic film.

2.3.2 The free interface diffusion method

A second method used to grow protein crystals was the free interface diffusion technique (Salemme, 1972). The setup for this method is illustrated in Figure 2.12 and involves placing a layer of protein solution on top of a layer of precipitant solution within a small diameter capillary tube and allowing these solutions to slowly mix by diffusion through the interface formed between these two layers. The main difference between this method and the hanging drop method is that the protein solution and mother liquor are in direct contact with one another and gradually mix across the contact interface. A consequence of this direct mixing is that protein initially encounters a supersaturating concentration of precipitant upon introduction into the capillary tube and this favors the formation of crystal nucleation sites at the interface between solutions. The largest crystals are often found to grow at this interface.

A typical free interface diffusion experiment was carried out using a capillary tube with
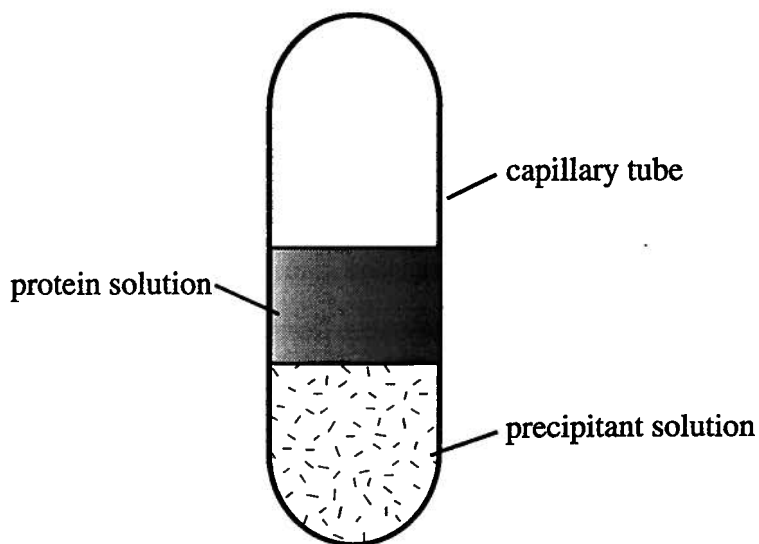
Figure 2.12: Schematic diagram of the free interface diffusion method used in the crystallization of mutant yeast iso-1 cytochromes *c*.

an inner diameter of 1.5 mm. Between 30-50 μL of precipitant solution was injected into the capillary with a syringe followed by the introduction of a layer of 5-10 μL of the protein solution directly on top of the precipitant solution. Manual centrifugation was employed to force the solutions to the bottom of the capillary tube and then the top of the tube was sealed using a bunsen burner. In experiments that utilized supplementary crystal seeding, these seeds were introduced into the protein solution layer before sealing the capillary tube. Capillary tubes were stored upright in styrofoam trays.

2.3.3 Conditions for the crystallization of mutant proteins

Yeast iso-1 cytochrome *c* mutant protein crystals grown using the hanging drop vapour diffusion method used high concentrations of ammonium sulphate ($(NH_4)_2SO_4$) as the precipitant agent inducing crystallization. In a process referred to as "salting out", water molecules preferentially solvate salt ions rather than the protein molecules as the concentration of the salt ions is

increased. Under these conditions, the protein molecules either precipitate out of solution or, if the conditions are favorable, form crystals where lost protein-solvent interactions are replaced with ordered protein-protein interactions. In a typical hanging drop experiment the starting concentration of ammonium sulphate was $\sim$70% saturation in the droplet and $\sim$90% saturation in the reservoir. Also essential for crystallization of cytochrome c was the addition of a reducing agent such as dithiothreitol (DTT) or sodium dithionite ($Na_2S_2O_4$) to keep this protein in the reduced state. A summary of conditions under which crystals were obtained for diffraction studies is shown in Table 2.3. In all cases, crystallizations were carried out at room temperature ($\sim$20°C), at which the best crystals were found to grow.

The use of the free interface diffusion method for crystallizing yeast iso-1 cytochrome c mutants employed conditions similar to those used in the hanging drop method, with ammonium sulphate being the crystallizing agent. However no precipitant was initially present in the layer containing the protein solution since the ammonium sulphate from the precipitant solution was able to diffuse directly into the protein solution. In the case of the F82L cytochrome c mutant protein, crystals could only be obtained for diffraction analysis by the free interface diffusion method. The conditions used are listed in Table 2.3 and involved a starting precipitant solution of 75% saturated ammonium sulphate.

Extensive scanning of crystallization conditions was required to achieve the growth of diffraction quality crystals of yeast iso-1 cytochrome c mutants. As shown in Table 2.3, the concentration of ammonium sulphate used to induce crystallization varied considerably (75%–94%) and the optimum pH varied from 5.3 to 6.5. In addition to the wide variance of potential conditions, crystallization trials were hampered by the narrow range of conditions under which each individual mutant protein would form satisfactory crystals. As a rule, variation of ammonium sulphate concentration by as little as 2% or the pH of the protein droplet by 0.1 units would be sufficient to result in precipitation of the protein rather than the formation of usable crystals. This is in contrast to other systems such as that of mutants of bacteriophage T4 lysozyme which has a higher tolerance for variations in crystallization conditions (Brennan *et al.*, 1988).

Table 2.3: Growth conditions and maximum size of crystals formed by mutant yeast iso-1 cytochromes c

Iso-1 cytochrome c mutant	Crystallization conditions	Crystal size (mm)
R38A/N52I (C102A)	88% $(NH_4)_2SO_4$; 70 mM $Na_2S_2O_4$; 0.1 M sodium phosphate, pH 6.5	0.4×0.3×0.05
R38A/N52I/F82S (C102A)	88% $(NH_4)_2SO_4$; 70 mM $Na_2S_2O_4$; 0.1 M sodium phosphate, pH 6.5	0.5×0.4×0.2
R38A/F82S (C102A)	88% $(NH_4)_2SO_4$; 70 mM $Na_2S_2O_4$; 0.1 M sodium phosphate, pH 6.5	0.15×0.05×0.02
N52I/F82S (C102A)	88% $(NH_4)_2SO_4$; 70 mM $Na_2S_2O_4$; 0.1 M sodium phosphate, pH 6.5	0.5×0.13×0.1
F82I (C102T)	85% $(NH_4)_2SO_4$; 150 mM NaCl; 70 mM $Na_2S_2O_4$; 0.1 M sodium phosphate, pH 6.4	0.17×0.17×0.05
F82L (C102T)	75% $(NH_4)_2SO_4$; 70 mM $Na_2S_2O_4$; 0.1 M sodium phosphate, pH 5.6	0.32×0.15×0.13
F82M (C102T)	90% $(NH_4)_2SO_4$; 140 mM $Na_2S_2O_4$; 0.1 M sodium phosphate, pH 6.2	0.15×0.08×0.05
F82Y (C102T)	90% $(NH_4)_2SO_4$; 20 mM DTT; 0.1 M sodium phosphate, pH 6.0	0.5×0.4×0.1
F82Y/L85A (C102T)	90% $(NH_4)_2SO_4$; 30 mM DTT; 0.1 M sodium phosphate, pH 5.3	0.4×0.4×0.1
L85A (C102T)	94% $(NH_4)_2SO_4$; 80 mM $Na_2S_2O_4$; 0.1 M sodium phosphate, pH 5.5	0.5×0.43×0.15
L85C (C102T)	90% $(NH_4)_2SO_4$; 70 mM $Na_2S_2O_4$; 0.1 M sodium phosphate, pH 6.4	0.3×0.28×0.1
L85F (C102T)	92% $(NH_4)_2SO_4$; 70 mM DTT; 0.1 M sodium phosphate, pH 6.3	0.28×0.28×0.1
L85M (C102T)	92% $(NH_4)_2SO_4$; 70 mM DTT; 0.1 M sodium phosphate, pH 6.2	0.58×0.35×0.13
L94S (C102T)	92% $(NH_4)_2SO_4$; 70 mM $Na_2S_2O_4$; 0.1 M sodium phosphate, pH 6.5	0.43×0.43×0.05

Further complicating the growth of suitable crystals for diffraction experiments was the requirement for seeding with micro-crystals. In almost all cases, suitable crystals could not be obtained without the introduction of seeds by a hair-seeding technique (Leung *et al.*, 1989). In this method, yeast iso-1 cytochrome *c* crystals were crushed in a solution of mother liquor to produce microscopic seed crystals. A human hair was passed through this seed solution and then through the protein solution used in the crystal growth trial. Even though the micro-crystalline seeds introduced into the protein drop by this process were too small to be observed under a microscope, this process proved critical in initiating nucleation sites for crystal growth. A further major advantage of this method is that the resultant crystals of mutant proteins were isomorphous to crystals of the wild-type protein, greatly simplifying the determination of the structures of these mutant proteins.

Even with a knowledge of the general conditions required for the crystallization of iso-1 cytochrome *c* mutant proteins and the application of the hair-seeding method to assist this process, the growth of diffraction quality crystals was neither straightforward nor guaranteed. This was reflected in the large variability in time required to grow diffraction quality crystals of these proteins. Although in optimal cases crystals appeared two weeks after initiation of the crystallization experiment and grew to full size after a further two weeks, the time required for the appearance of crystals could be as much as one year. In the extreme case of the F82L mutant protein, crystals of sufficient quality appeared only after nearly 2 years of growth.

It was also necessary to grow crystals large enough to produce acceptable experimental diffraction intensities, particularly for those mutant proteins studied using the laboratory Enraf Nonius CAD4 diffractometer which was equipped with only a sealed beam X-ray tube. However, many of the mutant proteins studied yielded only very tiny crystals which could not be used for X-ray diffraction analysis. Even after repeated attempts to increase crystal size by successive rounds of micro- or macro-seeding with these very tiny crystals, only small crystals could be obtained for structural analysis in some cases (Table 2.3). This size requirement was greatly

relieved by the installation of a Rigaku R-AXIS area detector equipped with a rotating anode X-ray generator, which made possible diffraction analyses of those crystals too small to be studied with the CAD4 diffractometer. In some cases, even small crystals could not be obtained after extensive crystallization trials. For example, over many years of crystallization trials employing the hanging drop vapour diffusion method, the free interface diffusion method and various other techniques, crystals were never obtained for the F82A, F82H, F82R or F82W mutants of yeast iso-1 cytochrome c.

With the exception of the F82L mutant protein, which is discussed in greater detail in Chapter 5, all of the iso-1 cytochrome c mutant proteins studied formed crystals which were isomorphous to those of wild-type iso-1 cytochrome c. These crystals belong to the tetragonal space group $P4_32_12$ and for the wild-type protein have unit cell parameters of $a = b = 36.46$ Å, $c = 136.86$ Å. Cell dimensions obtained for mutant protein crystals are discussed in each of the individual experimental sections in Chapters 3–6. Both wild-type and mutant protein crystals displayed a deep red color characteristic of cytochrome c and were shaped like pillows (Louie *et al.*, 1988a), with the crystallographic c axis being coincident with the thinnest dimension. These crystals have a solvent content of $\sim$30% and the asymmetric unit contains a single molecule of cytochrome c.

2.4 Theoretical Aspects of X-ray Diffraction

This section briefly describes the fundamentals of X-ray diffraction theory as it applies to the determination of the three-dimensional structures of proteins. Its purpose is to provide the reader who is unfamiliar with diffraction methods with sufficient background to follow the crystallographic aspects of the research described in this thesis. A more advanced discussion of these techniques is available in a number of excellent texts (for examples see Blundell & Johnson (1976), Ladd & Palmer (1985), Stout & Jensen (1989), McRee (1993) and Drenth (1994)).

2.4.1 Diffraction of X-rays by protein crystals

The determination of a protein structure by X-ray diffraction analysis requires an understanding of the way in which X-rays interact with matter. An object will scatter an incident X-ray in a defined manner and this scattering is dependent on the distribution of the object's electron density as follows:

$$F(\mathbf{S}) = \int_v \rho(\mathbf{r}) \, \exp\left(2\pi i \, \mathbf{r} \cdot \mathbf{S}\right) dv \qquad (2.1)$$

In this equation the total scattered wave F in the direction of the reciprocal space vector $\mathbf{S}$ is the sum of the individual waves scattered by the electron density ρ at real space positional vector $\mathbf{r}$ integrated over the whole volume v of the scattering object. Thus the total set of scattered waves represents the Fourier transform of the object's electron density distribution.

Two advantageous consequences arise when a protein crystal is the scattering object. The first of these is the multiplication of the intensity of the scattered waves to a measurable level brought about by the presence of large numbers of protein molecules in the crystal lattice. The second consequence is that the waves diffracted from a crystal are discrete due to the periodic nature of the crystal lattice. This periodicity allows for the simplification of Equation 2.1 by the replacement of the scattering vector $\mathbf{S}$ with a discrete direction specified by the Miller indices *hkl* of a reflection. Thus Equation 2.1 can be rewritten in the following way for diffraction from a crystal:

$$F_{hkl} = \int_v \rho(x, y, z) \, \exp 2\pi i (hx + ky + lz) \, dv \qquad (2.2)$$

This is the equation which relates a structure factor F_{hkl}, which is composed of both an amplitude and a phase, to the electron density $\rho(x, y, z)$ present in the unit cell.

2.4.2 Calculation of electron density from structure factors

In order to reconstruct an image of the protein of interest, a map of the distribution of the electron density in the unit cell of the crystal is required. The calculation of such a map is based on Equation 2.2, which can be inverted mathematically to give:

$$\rho(x,y,z) = \frac{1}{V} \sum_h \sum_k \sum_l F_{hkl} \exp -2\pi i(hx + ky + lz) \tag{2.3}$$

where V is the volume of the unit cell. Thus the electron density at any real space position (x, y, z) in the unit cell can be calculated from a summation of the structure factors, thereby allowing a three-dimensional map of the overall distribution of electron density within the unit cell to be constructed. In turn, examination of such a map allows the determination of the positions of atoms within the unit cell.

A major obstacle in this process arises from the fact that each structure factor F_{hkl} has both an amplitude $|F_{hkl}|$ and a phase α_{hkl}. To reflect this, Equation 2.3 can be rewritten as:

$$\rho(x,y,z) = \frac{1}{V} \sum_h \sum_k \sum_l |F_{hkl}| \exp i\alpha_{hkl} \exp -2\pi i(hx + ky + lz) \tag{2.4}$$

The structure factor amplitudes in this equation can be obtained directly from the intensities of the reflections measured in the X-ray diffraction experiment. Unfortunately, the phases of the structure factors cannot be obtained directly. Thus the calculation of an initial electron density map for a crystallized protein requires that estimates be made of the phases of the structure factors. This step represents a significant impediment to the determination of protein structures by X-ray diffraction.

2.4.3 Mutant protein structure determination

In the current work, two different methods have been employed to obtain initial starting models of mutant proteins. The method chosen for each mutant protein depended on whether it crystallized isomorphously to wild-type yeast iso-1 cytochrome c or in some other space group. The general outline of these approaches are presented in the two following sections.

2.4.3.1 Isomorphous crystal forms

A distinct advantage of the growth of mutant cytochrome c crystals having the same space group and unit cell as those of the known structure of wild-type yeast iso-1 cytochrome c is that this greatly facilitates the process of structure solution. This can be seen if we express the

structure factor equation (Equation 2.2) in terms directly related to the atomic centers within the unit cell as follows:

$$F_{hkl} = K \sum_j f_j(s_{hkl}) \, \exp\, -B_j s_{hkl}^2 \, \exp\, 2\pi i(hx_j + ky_j + lz_j) \tag{2.5}$$

In this equation, K is a scale factor and s_{hkl} is equal to $(\sin\theta)/\lambda$ for the reflection with Miller indices hkl. Each atom, j, is defined by its atomic position (x_j, y_j, z_j), its atomic scattering factor f_j, which is dependent only on the identity of the atom (ie: its atomic number), and its thermal parameter B_j, which is a measure of the mean square displacement of the atom from its average position. This form of the structure factor equation can be used to calculate structure factors directly from knowledge of the positional and thermal parameters of the atoms within a unit cell. Therefore if a starting model for a mutant protein in the unit cell can be constructed, this can be used to estimate the phases of the observed structure amplitudes that have been experimentally measured. For a mutant protein which crystallizes isomorphously to its wild-type counterpart, the structure of the wild-type protein provides an excellent starting model. This was the approach taken for many of the yeast iso-1 cytochrome c mutants studied.

Another advantage of crystallizing both mutant and wild-type proteins isomorphously is that an electron density map which shows the structural differences between these two proteins can be calculated. The modified version of Equation 2.4 needed to calculate such an electron density map is as follows:

$$\Delta\rho(x, y, z) =$$
$$\frac{1}{V} \sum_h \sum_k \sum_l (|F_{mut,hkl}| - |F_{wt,hkl}|) \, \exp\, i\alpha_{wt,hkl} \, \exp\, -2\pi i(hx + ky + lz) \tag{2.6}$$

In this equation, $\Delta\rho(x, y, z)$ represents the differences between the electron density distributions in the mutant and wild-type protein crystals, $|F_{mut,hkl}|$ are the structure factor amplitudes observed in the X-ray diffraction experiment for the mutant protein, $|F_{wt,hkl}|$ are the structure factor amplitudes observed for the wild-type protein, and $\alpha_{wt,hkl}$ are the phases of the relevant wild-type structure. This difference electron density map shows positive electron density peaks where there are atoms present in the mutant structure that are absent in the wild-type protein

and vice versa for the negative peaks. Three examples of initial difference electron density maps of this type for the F82Y, L85A and F82Y/L85A mutant proteins of yeast iso-1 cytochrome c are shown in Figure 2.13. Inspection of such maps was used to confirm the presence of amino acid substitutions within mutation sites and allow preliminary modeling of the positioning of these residues. In this way, a more representative starting model for a mutant protein could be constructed for use in structural refinement.

2.4.3.2   Non-isomorphous crystal forms

When a mutant protein crystallizes with a unit cell different than that of wild-type yeast iso-1 cytochrome c, a molecular replacement approach (Rossman, 1972) is necessary to assist in structure determination. In this thesis, the analysis of the F82L mutant protein falls into this category. The details of this specific analysis are given in Chapter 5 while a general discussion of this approach is presented here. A key ingredient in the molecular replacement method is the calculation of an experimental Patterson map according to the following equation:

$$P(u,v,w) = \frac{1}{V} \sum_h \sum_k \sum_l |F_{hkl}|^2 \exp{-2\pi i(hu + kv + lw)} \tag{2.7}$$

This calculation requires only the availability of the experimentally observed structure factor amplitudes for the mutant protein. In contrast to an electron density map where peaks occur at the positions of atoms in the unit cell, the Patterson map has peaks at positions corresponding to all interatomic vectors within the unit cell. Thus a peak at (u,v,w) in the Patterson map indicates that in the unit cell there are two atoms related positionally such that $u = x_1 - x_2$, $v = y_1 - y_2$ and $w = z_1 - z_2$. In practice, an experimental Patterson map is too complex to be directly interpreted unless there are only a few atoms in the unit cell.

Molecular replacement methods can make use of the experimentally observed Patterson map to correctly position a search model of the mutant protein in its unit cell. For the structure solution of the F82L mutant protein, the structure of wild-type yeast iso-1 cytochrome c makes a good starting model for this search. The search for this positioning is carried out in two stages. To begin, a rotation function is used to correctly orient the search model. This process
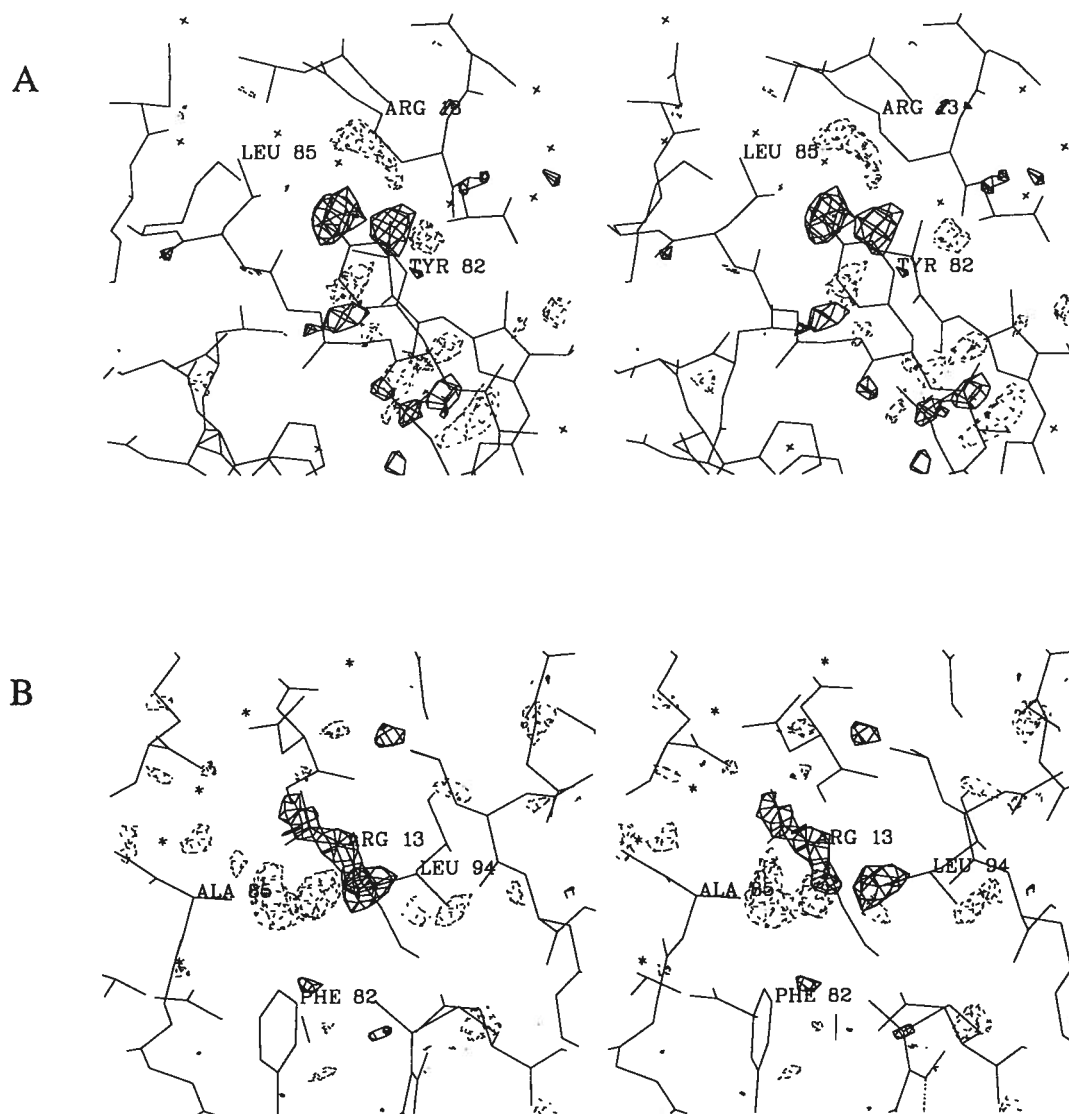
Figure 2.13: continued on next page.

C
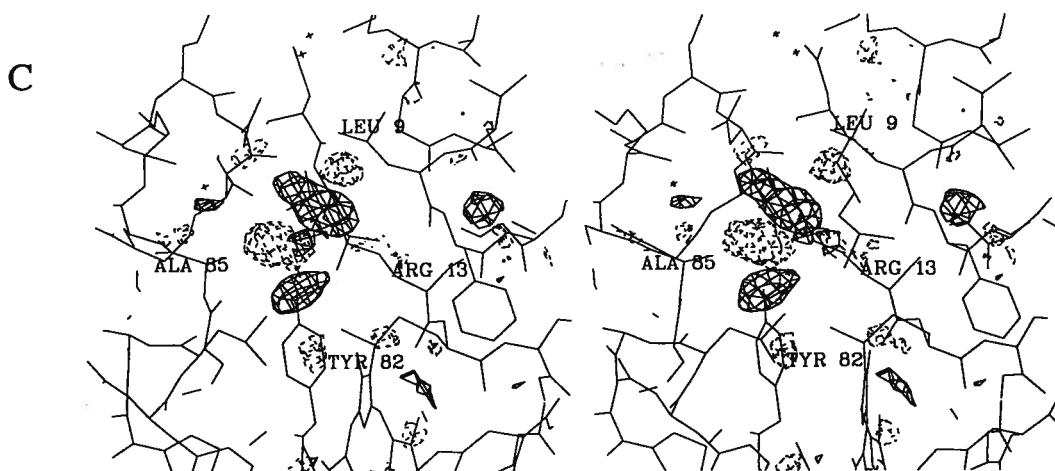
Figure 2.13: continued. $F_{mutant} - F_{wild-type}$ difference electron density maps drawn in the immediate vicinity of the mutated residues in (a) F82Y, (b) L85A and (c) F82Y/L85A yeast iso-1 cytochromes c. These maps were calculated using Equation 2.6 (Section 2.4.3.1) with positive electron density shown as solid contours and negative electron density shown as dashed contours. Overlaid are the final refined mutant protein structures obtained. Water molecule positions are shown as small crosses. Difference electron density for the addition of the Tyr82 hydroxyl group in the F82Y and F82Y/L85A mutant proteins is readily apparent. Also present are difference electron density peaks representing the loss of the Leu85 side chain and movement in the side chain of Arg13 in the L85A and F82Y/L85A mutant proteins.

involves the calculation of a set of intramolecular interatomic vectors for the search model which is then systematically rotated in steps about three axes and compared with the experimental Patterson map calculated with the observed diffraction data. This comparison is restricted to short vectors so that only intramolecular interatomic vectors in the observed vector set are included. Maximal superposition of the modeled and observed sets of interatomic vectors will be realized when the orientation of the search model coincides with that of the molecule in the new unit cell of the mutant protein crystal.

When the correct rotational orientation of the search model has been achieved, a translation function is utilized to position this model at the correct location within the unit cell. To start, a symmetry element is chosen and the correctly oriented search model is systematically translated within the unit cell. Depending on the chosen symmetry element, this systematic translation can be restricted to specific Harker sections. At each position during this process, the molecule related to the search model by the chosen symmetry element is generated along with the associated set of intermolecular vectors. These vectors are then compared against the experimentally derived Patterson map to determine the best correlation. In this way the positioning of the search model with respect to this and other symmetry related molecules can be determined to ultimately define the correct translational positioning of the search molecule. With the correct rotational and translational positioning of the search model, phase estimates can be made for the experimentally observed structure factor amplitudes and an initial electron density map computed. This then allows for subsequent structural refinement of the mutant protein structure.

Another potentially useful component of the molecular replacement approach is the self rotation search. This can be applied when multiple copies of a protein, which are related by non-crystallographic symmetry, are present within the asymmetric unit of the unit cell. This procedure is similar to the rotation function search described previously with the exception that the Patterson map derived from the experimental structure factor amplitudes is also used as the search Patterson map.

2.5 Practical Aspects of Diffraction Data Collection

In this section, a brief description of the various steps involved in mounting crystals for X-ray diffraction analysis, the collection of diffraction data and the processing of this data, is provided. Specific details pertaining to data acquisition for individual mutants of yeast iso-1 cytochrome *c* are given in Chapters 3–6. It should be pointed out that midway through the studies documented in this thesis, the laboratory changed from collecting data on an Enraf-Nonius CAD4-F11 diffractometer fitted with a sealed beam X-ray tube, to a newly acquired Rigaku R-AXIS II imaging plate area detector mounted on a RU300 rotating anode system. The additional intensity of the rotating anode X-ray beam and increased sensitivity of the imaging plate detector not only greatly improved the quality of diffraction data that could be collected, but also allowed for structure determinations where only very small crystals of mutant proteins could be grown. The approach taken by the diffractometer and area detector data collection methods are substantially different and general aspects of the methodology used for each are described below.

2.5.1 Mounting crystals for data collection

Protein crystals require special handling since they are soft and easily deformed. A further consideration is the need to keep these crystals moist due to their high solvent content. To protect crystals during data collection these were mounted in thin walled glass capillary tubes having diameters varying from 0.7–1.5 mm, depending on crystal size. Before crystal mounting, a solution identical to the original crystallization well solution, except for a 5–10% higher ammonium sulphate concentration, was prepared for use in the transfer of the crystal from its growth well to the capillary tube. After mounting, a limited amount of buffer was left near the crystal, with any excess being wicked away using either thin strips of filter paper or microcapillary tubes. Also included in the glass capillary before it was sealed with beeswax were columns of mounting solution placed above and below the crystal to ensure that it did not dry out during data collection. One end of the capillary was then glued into a mounting pin at

the appropriate height for data collection and placed on a goniometer head.

2.5.2 Diffractometer data collection and processing

X-ray diffraction data sets for crystals of the F82Y, F82Y/L85A, L85A, L85F, L85M and L94S mutants of yeast iso-1 cytochrome c were collected using an Enraf Nonius CAD4-F11 diffractometer. The sizes of each of the crystals used in data collection are summarized in Table 2.3. The diffractometer used was equipped with a helium filled beam tunnel and the distance between the crystal and detector was set to 36.8 cm. A nickel-filtered copper-target X-ray tube with focal spot 0.75 mm × 0.15 mm was used to generate the incident radiation and was operated at 26 mA and 40 kV. The ambient temperature during data collection was maintained at 15°C.

The strategy used in data collection was chosen to maximize the amount of data that could be collected from any one crystal, employing fairly narrow scan widths coupled with relatively slow scan speeds. Typically, continuous Ω scans of 0.6° at a speed of 0.55°/minute were used. Data collection was carried out in shells based on resolution, with higher resolution shells being collected earlier to offset the greater decay in the intensities of these reflections. Following the acquisition of a complete diffraction data set, when time permitted and the decay in the intensities of high resolution reflections had not progressed beyond ∼30%, repeat measurements of the high resolution data shells were made. The total time required to collect each complete data set varied between three weeks and one month.

The measurement of each reflection was divided into three parts. The middle 2/3 of each scan was assigned as representing the intensity of the reflection, whereas the first and final 1/6 of each scan was used to assess the background radiation and thereby provide a means of correcting the reflection intensity for this factor. An improvement on this background correction could be achieved by employing background averaging (Murphy *et al.*, 1992). In this method, an estimate of the background radiation for a reflection is not only based on the background measurements of that reflection but also on the backgrounds of reflections which are nearby

in reciprocal space. From experience, it was found that using the backgrounds from 8–12 neighboring reflections for this purpose gave the best results.

For each data collection, an absorption correction was applied using the empirical method of North *et al.* (1968). This was necessitated primarily by the non-spherical shape of the crystals used. In this method, a reflection aligned along the ϕ axis of data collection is used. The measured intensity of this ϕ independent reflection (monitored in 5° increments) varies with rotation of the ϕ axis due to absorption and this variation can be used to determine the amount of correction required for a general reflection.

Also performed was a correction for intensity decay occurring due to crystal degradation during X-ray exposure. This correction was based on the periodic measurement of standard reflections over the course of the full exposure time. Generally monitor reflections were grouped according to resolution so that the decay correction could be applied on this basis as well since higher resolution reflections are in general more sensitive to crystal decay than their lower resolution counterparts.

Following correction of measured intensities for background, absorption and decay effects, two additional corrections are required. The Lorentz correction is necessary because the reflection intensity is dependent on the geometry of the data collection method. The polarization correction adjusts for the variation of reflection intensity with the amount of refracted X-ray beam polarization. Once these two corrections are made, the data are converted into structure factors by taking the square roots of the reflection intensities.

2.5.3 Area detector data collection and processing

With the installation of a Rigaku R-AXIS II imaging plate area detector system and RU300 rotating anode, all subsequent data collections were collected using these instruments. This includes data from crystals of all mutant proteins not specifically listed at the beginning of Section 2.5.2. Unlike the CAD4 diffractometer where each reflection is measured individually, on the Rigaku area detector many reflections are simultaneously measured in a manner similar

to the photographic rotation method (Arndt & Wonacott, 1977). The physical basis of measurement used by this area detector consists of two radiation sensitive phosphor plates, each of which allows up to $\sim$10,000 diffraction intensities to be measured in a single exposure under optimal conditions. The end result is that on the area detector a complete data set can be collected much more rapidly and usually within 2–3 days, whereas diffractometer data collections required on the order of 3–4 weeks. A further advantage of the area detector system is its sensitivity which allows for the measurement of data to higher resolution and from crystals that would be too small for use with a diffractometer. An important factor here is also the greatly increased intensity of the X-ray beam generated by the rotating anode source.

One disadvantage of the area detector is that due to geometric reasons it is not always possible to collect 100% of the available data. Nonetheless, by using multiple scans at alternative settings, almost all the available data is usually accessible. To assure that data collection is as complete as possible, a software program is used to model data collection based on the proposed collection parameters. These parameters can then be adjusted as necessary to optimize data collection. For data collections of mutant yeast iso-1 cytochrome c crystals, it was found that by doing two separate series of scans, one of which was collected with an adapter that offset the spindle axis of the capillary holding the crystal by 45° from the ϕ axis of the area detector, that >95% of the theoretically available diffraction data could be collected.

For data collected on the area detector, the rotating anode generator was operated at 90–100 mA and 50–60 kV. The sizes of the crystals used in these data collections are summarized in Table 2.3 for each mutant protein. Data were collected using the oscillation method in which the crystal was moved through a ϕ angle of 1.0° and exposed to the X-ray beam for 20–30 minutes for each frame collected. Since the method of data collection is similar to the screenless oscillation or rotation method, processing of the collected data resembles the procedure described by Rossman *et al.* (1979), as implemented by Higashi and coworkers (Higashi, 1990; Sato *et al.*, 1992). In this method, corrections for background, Lorentz and polarization effects are initially applied to the individual diffraction intensities measured on each frame of data. The background correction

applied to a particular diffraction measurement is based on the level of background radiation detected in the vicinity of that reflection. Following these corrections, the frames collected are scaled to account for crystal decay and absorption effects in a resolution dependent manner. Only fully recorded diffraction intensities are included in the computation of scaling factors. After scaling, multiple measurements of intensities are merged and then reduced to structure factor amplitudes.

2.5.4 Determination of absolute scale

Structure factors obtained after data processing are on a relative scale and before the refinement of a model structure can proceed these must be multiplied by a scale factor so that they can be compared to calculated structure factors. The absolute scale factor is initially estimated and then later improved upon during subsequent structural refinement.

Estimation of the absolute scale factor can be accomplished by the method developed by Wilson (1942), requiring that only a knowledge of the chemical composition of the unit cell contents be available. This method assumes the atomic contents of the unit cell are randomly distributed and therefore the theoretical mean value of diffraction intensities as a function of resolution is given by:

$$\overline{I}_{abs} = \sum_{j} f_j^2 \; \exp \; -2B\left(\frac{\sin\theta}{\lambda}\right)^2 \tag{2.8}$$

where $\overline{I}_{abs}$ is the theoretical average intensity. The unit cell contents are represented by the atomic scattering factors f_j of all the atoms, j, in the unit cell and the thermal motion of these atoms is represented by the thermal factor B.

If the average observed intensity $\overline{I}_{rel}$ is related to $\overline{I}_{abs}$ by scale factor C, then Equation 2.8 can be rewritten as:

$$\ln\left(\frac{\overline{I}_{rel}}{\sum_j f_j^2}\right) = \ln C - 2B\left(\frac{\sin\theta}{\lambda}\right)^2 \tag{2.9}$$

This relationship can then be plotted to give a straight line with a slope of $-2B$ and an intercept of $\ln C$. As can be seen in the example given in Figure 2.14, at medium and high resolution
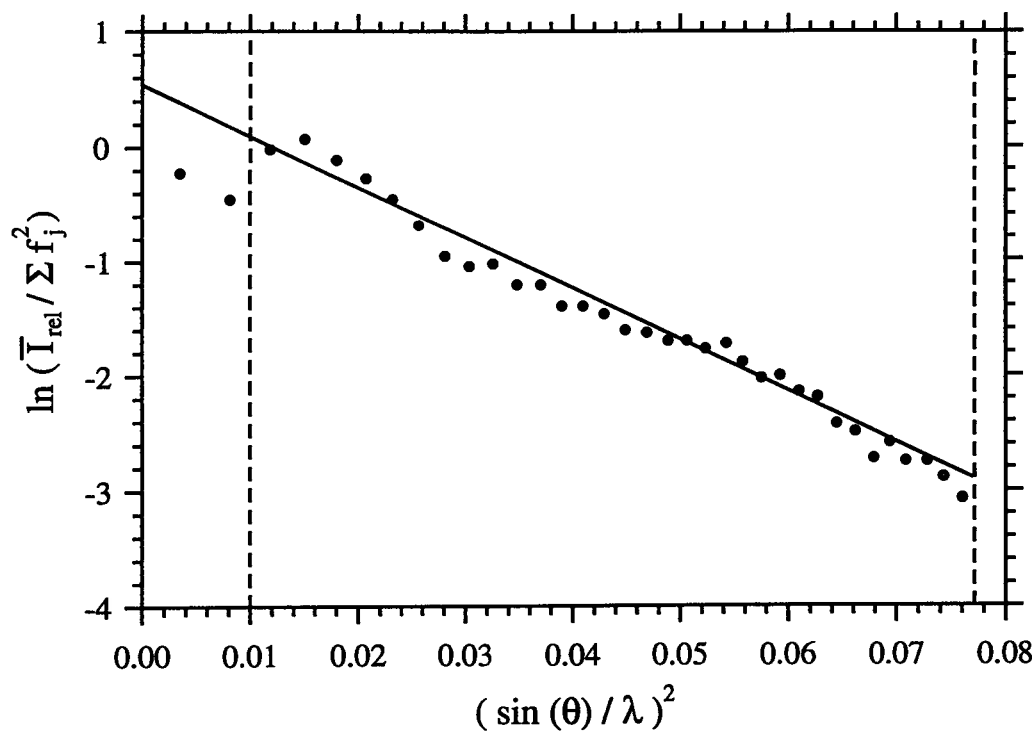
Figure 2.14: An example of a Wilson plot based on the R38A/N52I/F82S yeast iso-1 cytochrome c diffraction data set and used to determine the absolute scale factor. For this analysis reciprocal space was divided into shells according to resolution with each containing at least 250 reflections. To determine the absolute scale factor, a least-squares fit line (solid) to the data points was calculated using only those data points between 5.0–1.8 Å resolution (indicated by the vertical dashed lines). This analysis suggested that the absolute scale factor for this data set was 0.76.

a straight line is found as predicted, but at low resolution the data points fit less well. In practice, this poor fit at low resolution arises from the fact that the contents of the unit cell are not randomly distributed at this resolution. Thus in the determination of absolute scale factor it is common practice to apply resolution cutoffs, after which a line is least-squares fit to the data and used to obtain this value. The scale factor thus obtained can be used to scale the observed diffraction data set and the overall estimate of thermal factor serves as a useful indicator of the isotropic thermal *B* for the structure as a whole.

2.6 Refinement of Structural Models

Once an initial model of a mutant protein has been derived by the methods outlined in Section 2.4.3, further optimization is necessary to achieve the best fit between the observed structure factors and those that can be calculated from the structural model. This process involves successive cycles of computational refinement, reference to difference electron density maps and manual readjustments. One way in which the progress of structural refinement is typically monitored is by periodic calculation of the crystallographic R-factor as follows:

$$R = \frac{\sum_{hkl} \left| \, |F_{o,hkl}| - |F_{c,hkl}| \, \right|}{\sum_{hkl} |F_{o,hkl}|} \tag{2.10}$$

where $|F_{o,hkl}|$ are the observed structure factor amplitudes measured from the mutant protein crystal and $|F_{c,hkl}|$ are those calculated from the corresponding model structure by Equation 2.5. Thus the crystallographic R-factor is a direct measure of the agreement between the experimental data and the model structure, with a lower R-factor implying a better fit between these. For well refined protein structures, the value for the R-factor can vary between 0.10 and 0.25.

2.6.1 Stereochemically restrained refinement

The primary method employed in structural refinement in this thesis is the restrained parameter least-squares technique (Hendrickson, 1985). This refinement method operates by minimizing the differences between the structure factor amplitudes observed in the X-ray diffraction experiment and those calculated from the model structure (by Equation 2.5), while ensuring that

the stereochemistry of the protein structure remains within acceptable limits through the use of geometric restraints. This is accomplished by minimizing the following equation:

$$\Phi = \sum_{hkl} \frac{1}{\sigma_F^2(hkl)}(|F_{o,hkl}| - |F_{c,hkl}|)^2 + \sum \phi_{geometric} \tag{2.11}$$

where σ_F determines the relative weight of the structure factor terms in the equation and $\phi_{geometric}$ are the terms defining the geometric restraints.

The geometric terms in Equation 2.11 serve to restrain the relative atomic positions of the protein structure so that the stereochemical parameters associated with these positions do not deviate significantly from expected values. For example, the geometric term used to restrain the distances between individual atoms connected through covalent bonds is:

$$\phi_{distances} = \sum_{j}^{distances} \frac{1}{\sigma_D^2(j)}(d_{ideal,j} - d_{model,j})^2 \tag{2.12}$$

where σ_D is the expected standard deviation for the distribution of the distances, $d_{ideal,j}$ is the ideal distance between an atom pair j, and $d_{model,j}$ is the value for this distance calculated from the model structure. Other geometric terms serve to restrain planar groups, chiral centers, non-bonded contacts, torsion angles and thermal parameters.

2.6.2 Simulated annealing refinement

A primary constraint of stereochemically restrained refinement is its relatively small radius of convergence. As discussed in detail in Chapter 5 for the F82L and F82M mutant proteins, this can lead to unsatisfactory refinements when larger structural corrections are required. One technique that is useful under these circumstances is simulated annealing refinement (Brünger *et al.*, 1987) which is capable of sampling possible structural conformations beyond the local conformational energy minimum. This is carried out by linking the minimization of the differences between the observed and calculated structure factor amplitudes to a molecular dynamics simulation. Such a simulation involves the solution of Newton's equations of motion for each individual atom over a fixed span of time, with these atomic motions being dependent on the

interaction of this atom with every other atom in the simulation. These interactions are represented in the form of a potential energy function which consists of the sum of the energies which define the forces that act on each atom. In the simulated annealing method, the potential energy function is modified by the inclusion of a term representing the diffraction data:

$$E_{total} = w_{xray} \sum_{hkl} (|F_{o,hkl}| - |F_{c,hkl}|)^2 + \sum E_{geometric} \qquad (2.13)$$

where E_{total} is the total energy in the system, w_{xray} determines the relative weight of the structure factor terms in the equation and $E_{geometric}$ are the potential energy terms calculated from the geometry of the molecule. Although this equation is similar to Equation 2.11, its application is different. Whereas in conventional least-squares refinement Equation 2.11 is minimized, in simulated annealing refinement the total energy in Equation 2.13 is set to an arbitrarily high level and large time-dependent structural fluctuations of the molecule are simulated to search conformational space for the best fit between the observed and calculated structure factor amplitudes.

An example of a term in the potential energy function related to structural geometry during simulated annealing refinement is the following:

$$E_{bonds} = \sum_{j}^{bonds} k_j (d_{model,j} - d_{average,j})^2 \qquad (2.14)$$

where k_j is a constant describing the variability about the average length $d_{average,j}$ of bond j. As the bond distance calculated from the model structure deviates from the expected average bond distance, the potential energy of the bond increases to an unfavorable level. Other potential energy terms representing bond angles, dihedral angles, van der Waals' contacts and electrostatic interactions are also calculated.

2.6.3 General considerations in refinement of mutant proteins

2.6.3.1 X-ray diffraction data sets

A number of factors can affect a particular X-ray diffraction data set. For example the completeness of data collected from crystals of yeast iso-1 cytochrome c mutant proteins was dependent

on the size of these that could be grown (Table 2.3). Thus bigger crystals resulted in a greater number of observable reflections being collected than for small crystals where a larger portion of the reflections were too weak to be recorded. For example, only very small crystals could be grown for the F82M and F82I mutant proteins. Using the best of these, 2143 and 2460 reflections (6.0–2.3 Å resolution range), respectively, out of the ~4300 theoretically available could be measured using an Enraf-Nonius CAD4-F11 diffractometer equipped with a sealed beam X-ray tube.

Beyond crystal size, another significant factor in the numbers of reflections that can be measured from a given crystal is the detection instrumentation used. As noted earlier, midway through the studies conducted in this thesis, the laboratory acquired a Rigaku R-AXIS II area detector and RU300 rotating anode generator. The increase in X-ray beam intensity available, coupled with the increased sensitivity of the area detector, meant that more complete diffraction data sets could be collected even when crystal size was a severely limiting parameter. For example, for the F82M and F82I mutant protein crystals discussed above, collection of diffraction data using the area detector resulted in 2913 and 3727 observed reflections, respectively. These significantly improved data sets greatly facilitated the structural refinements of these mutant proteins (Chapter 5). However, it should be noted that despite this improvement, the limitations imposed by only being able to grow relatively small crystals could not be entirely overcome and a number of reflections from the F82I and F82M mutant protein crystals remained too weak to be observed. For those crystals of other mutant proteins for which only the CAD4 diffractometer was available during the collection of X-ray diffraction data, the completeness of the data sets measured is poorer, corresponding to the less intense X-ray source used and therefore the overall weaker intensity of the data available. A plot of data completeness versus resolution for each mutant protein diffraction data set is provided in the experimental sections of Chapters 3–6.

After collecting the best possible diffraction data set, another concern is how the weakest, and therefore most inaccurately measured, reflections should be handled. These reflections are

the most likely to contribute to noise in electron density maps, thereby obscuring the interpretation of such maps during the process of structural refinement. To remedy this situation, it is common to impose a threshold value or σ cutoff to filter reflections used in refinements. A survey of the literature reveals that there is a wide range of σ cutoffs in use, with the most common values ranging from $|F| \geq (0\text{--}3)\sigma(F)$ (McRee, 1993; Watkin, 1994). Close scrutiny of the effects of using different cutoffs of this magnitude to exclude weak data show that these do not adversely affect the structure resulting from refinement (Stenkamp & Jensen, 1975; Smalas & Hordvik, 1993).

In the current structural studies a consistent σ cutoff of $2\sigma(F)$ was employed, except for the L85A mutant protein data set where a $2.5\sigma(F)$ cutoff was applied (problems with crystal slippage were encountered during data collection for the L85A mutant protein — see Chapter 3). Experience showed that this cutoff level met the dual goals of including the greatest amount of data possible and being able to facilitate structure refinement with the clearest electron density maps. For data collected on the CAD4-F11 diffractometer, these cutoffs did affect a fair number of reflections depending on the size of the crystal used. In contrast, data sets collected on the Rigaku area detector had very few reflections falling below this threshold value, with the worst case involving the F82M mutant protein data set where only 51 reflections fell into this category.

To assess the utility of the $2\sigma(F)$ cutoff imposed, a test was made with the L85M mutant protein data set which had been collected with the CAD4-F11 diffractometer. Using the final refined structure of this protein, an additional eight cycles of restrained parameter least-squares refinement (Section 2.6.1) were carried out using all observed data between 6.0 and 1.9 Å resolution (6396 reflections, 83% completeness). This resulted in an average cumulative positional shift of 0.07 Å for all atoms over the 8 cycles of refinement, a value similar to the cumulative shift of 0.06 Å observed over the last 6 cycles for the original data set with a $2\sigma(F)$ cutoff. Therefore, at the end of structural refinement, shifts with the inclusion of all data were of the same order as those with the $2\sigma(F)$ cutoff and a comparison of the two refined structures showed there were no significant structural differences. One factor that was affected was the crystallographic

R-factor which was 0.208, compared to 0.178 for the 5210 reflections with $|F| \geq 2\sigma(F)$ in the same resolution range (Table 4.15; Chapter 4). Thus as expected, inclusion of all data has little impact on structural shifts while leading to a considerably higher R-factor and noisier electron density maps.

Two other factors affecting diffraction data were contributions resulting from the disordered solvent continuum and alternative crystal lattice packing arrangements. The first of these is a dominant contributor to low resolution reflections; to account for this, diffraction data below 6.0 Å resolution were excluded from refinement (Blundell & Johnson, 1976; Schoenborn, 1988). An example of the latter factor was found for the F82L mutant protein crystals which were found to be of a different space group than those grown for other mutant proteins. As discussed in Chapter 5, these crystals diffracted relatively poorly even when crystal size was taken into account. This resulted in a correspondingly higher rate of fall off in the number of observed reflections at high resolution as illustrated in Figure 5.30. For this protein, even with the use of the Rigaku area detector system, the resolution of the best structure that could be obtained was 2.5 Å.

2.6.3.2 Difference electron density maps

During structural refinements, it was necessary to carry out manual fittings on poorly behaved amino acids based on reference to different types of difference electron density maps. In addition, such maps covering the whole of the polypeptide chain were calculated periodically (from 4–7 times) during refinements to provide a means of checking the course of refinement and for any other adjustments to the structure that might be necessary. This approach also provided the primary means for locating solvent molecules bound to the protein surface or within the protein itself.

All of the difference electron density maps utilized were based on the calculation shown in Equation 2.6, but for which different structure factor and phase coefficients were used. In one case this was a simple difference map with coefficients of $|F_{o,hkl}| - |F_{c,hkl}|$ and $\exp i\alpha_{c,hkl}$.

Here, $|F_{o,hkl}|$ represents the experimentally measured structure factor amplitudes and $|F_{c,hkl}|$ and $\alpha_{c,hkl}$ are the structure factor amplitudes and phases computed from the refinement model. A related difference electron density map calculated with coefficients of $2|F_{o,hkl}| - |F_{c,hkl}|$ and $\exp i\alpha_{c,hkl}$ also proved very useful in assessing the fit of the refinement model to its electron density. A third type of map that particularly facilitated interpretations in those regions where it proved difficult to fit the polypeptide chain was the omit difference electron density map. Here the atoms of the structural feature being analyzed (this might be just a few atoms or those of several amino acids) are excluded and structure factor amplitudes $|F_{omit,hkl}|$ and phases $\alpha_{omit,hkl}$ are calculated based on the resultant structural model. In this way a difference electron density map can be calculated by using the coefficients $|F_{o,hkl}| - |F_{omit,hkl}|$ and $\exp i\alpha_{omit,hkl}$ in a formulation of Equation 2.6. In this map the excluded feature should be present as a large positive peak and thereby facilitate fitting of this part of the structure. The use of these three types of difference electron density maps was a powerful tool in achieving the best fit of mutant protein structural models to their electron density maps.

2.6.3.3   Course of a typical refinement

The course of the refinement of the N52I/F82S mutant of yeast iso-1 cytochrome c is illustrated in Figure 2.15 and provides a typical example of that followed for other mutant proteins. Note that the precise details for this and other mutant protein structural refinements are given in Chapters 3–6. After initial placement of the starting model for the N52I/F82S structure in the unit cell as discussed in Section 2.4.3.1, a series of refinement cycles was conducted using lower resolution data until the crystallographic R-factor was sufficiently lowered. Then further refinement was carried out with higher resolution data, interspersed with rounds of manual interventions based on difference electron density maps. The water molecules associated with the protein structure were also examined during each manual intervention and were added or deleted to the refinement model as necessary. Possible water molecules were also identified by a peak search of a $F_o - F_c$ difference electron density map or with the assistance of an
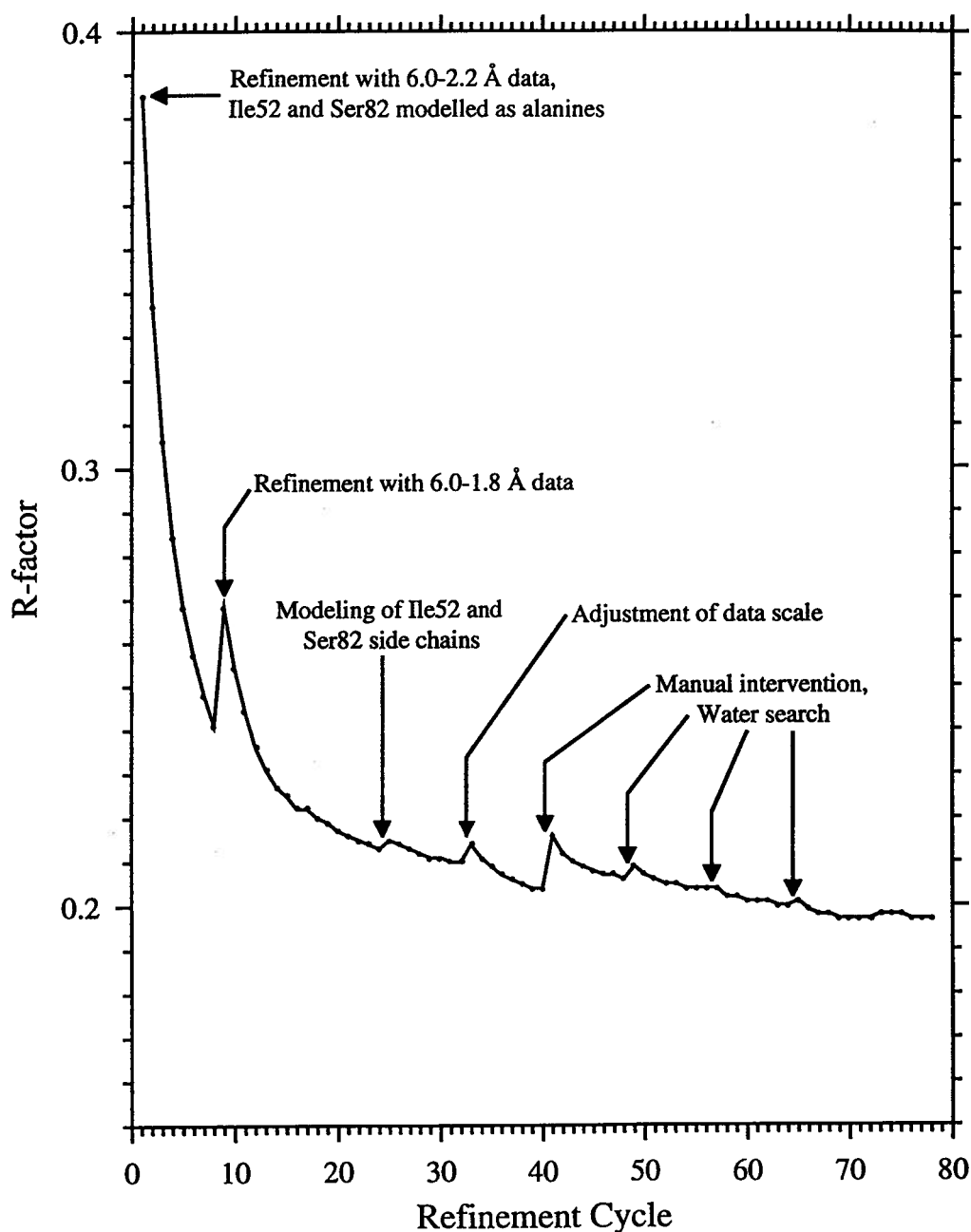
Figure 2.15: The course of the structural refinement of N52I/F82S yeast iso-1 cytochrome c by the restrained parameter least-squares method. This plot shows the crystallographic R-factor (Equation 2.10) as a function of refinement cycle number. Modeling of the side chains of Ile52 and Ser82 into $F_o - F_c$ difference electron density maps occurred after refinement cycle 24. Manual interventions during which the fit of the entire polypeptide chain was examined and a water search conducted using $2F_o - F_c$, $F_o - F_c$ and omit difference electron density maps are indicated.

automated procedure utilizing alternating cycles of peak searching and refinement cycles (Tong *et al.*, 1994). The criteria for the inclusion of a water molecule into the protein structure were that the potential water position had to be within 3.5 Å of a hydrogen bond donor or acceptor atom and that it refine to an isotropic thermal factor under 50 $Å^2$. The refinement process was continued until convergence was reached for both positional shifts and the crystallographic R-factor. A paramount consideration during refinements was that acceptable stereochemistry be maintained for the mutant protein structure. A compilation of stereochemical values and the restraint weighting used during refinements is given in Table 2.4. Values pertaining to individual mutant proteins can be found in Chapters 3–6.

2.6.3.4 Calculation of atomic coordinate errors

In this thesis, error estimates for the atomic coordinates of iso-1 cytochrome *c* mutant structures were determined by two methods. One method was that of Luzzati (1952) where overall coordinate errors are estimated by comparison of the dependence of the crystallographic R-factor on resolution with theoretical estimates of this dependence assuming that these errors are the only source of differences between observed and calculated structure factors. Luzzati plots for each of the mutant protein structures determined are presented as part of the experimental sections of Chapters 3–6. Coordinate errors estimated by this method ranged between 0.16 and 0.26 Å for the fourteen mutant iso-1 cytochromes *c* studied. In a second method (Cruickshank, 1949, 1954), the errors in the coordinates of a given atomic position are dependent on the fit between observed and calculated structure factors, the atom type and the thermal factor of the atom. Estimates for the overall r.m.s. coordinate error using this method ranged between 0.12 and 0.21 Å for all mutant protein structures studied. In general there was a close correspondence between the error estimates obtained by the Luzzati and Cruickshank methods. Nonetheless it must be remembered that these are both empirical methods relying on assumptions that are not completely valid and care must be taken when using such error estimates as an absolute measure of coordinate error.

Table 2.4: Compilation of stereochemistry observed in refined yeast iso-1 cytochrome c mutant structures

Stereochemical parameter	r.m.s. deviation from ideal values	Restraint weighting value
Distances (Å)		
Bond (1-2)	0.019	0.020
Angle (1-3)	0.037–0.051	0.030
Planar (1-4)	0.045–0.057	0.045
Planes (Å)	0.012–0.015	0.018
Chiral volumes (Å^3)	0.132–0.202	0.120
Non-bonded contacts (Å)[†]		
Single torsion	0.211–0.229	0.250
Multiple torsion	0.179–0.220	0.250
Possible hydrogen bonds	0.185–0.239	0.250
Torsion angles (°)		
Planar (0° or 180°)	1.9–2.5	2.5
Staggered (±60°,180°)	19.0–28.4	20.0
Orthonormal (±90°)	17.4–27.1	15.0

[†] The r.m.s. deviations from ideality for this class of restraint incorporates a reduction of 0.2 Å from the radius of each atom involved in a contact.

Chapter 3

The Roles of Residues 82 and 85 at the Interactive Face of Cytochrome c

3.1 Introduction

The objective of the studies conducted in this chapter is to examine the roles of Phe82 and Leu85 as participants in forming a part of the interactive surface between cytochrome c and complexed electron transfer partners. The side chain of Phe82 forms an integral part of the hydrophobic heme pocket in cytochrome c and packs directly against the heme prosthetic group in a coplanar fashion. The side chain of Leu85, in turn, packs against the distal edge of the aromatic ring of Phe82, as illustrated in Figure 1.9. The side chains of both of these residues are exposed to the external solvent environment in that surface region of cytochrome c which, along with the exposed edge of the heme moiety, is located at the putative site of complex formation and electron transfer between cytochrome c and its redox partner proteins. Evidence for the involvement of Phe82 and Leu85 in the formation of electron transfer complexes has come from molecular modeling (Salemme, 1976; Poulos & Kraut, 1980; Mauk *et al.*, 1986; Lum *et al.*, 1987), computational studies (Wendoloski *et al.*, 1987; Eltis *et al.*, 1991; Northrup *et al.*, 1993), NMR (Pielak *et al.*, 1988; Burch *et al.*, 1990), X-ray crystallography (Pelletier & Kraut, 1992) and comparative studies of electron transfer kinetics (Nocek *et al.*, 1991). Following chapters deal in greater depth with other aspects of the contributions of Phe82 (Chapters 5 and 6) and Leu85 (Chapter 4) to the structural and functional properties of cytochrome c.

Phe82 is a phylogenetically invariant residue (Hampsey *et al.*, 1988; Moore & Pettigrew, 1990) and it has been shown that substitution of this residue by glycine, serine or tyrosine results in decreased steady-state rates of electron transfer between cytochrome c and cytochrome c peroxidase (Pielak *et al.*, 1985) and cytochrome c oxidase (Michel *et al.*, 1989). Furthermore,

these substitutions and others at Phe82 also have a detrimental effect on yeast growth rates (Hilgen & Pielak, 1991; Inglis *et al.*, 1991) and modify the kinetics of electron transfer mediated by cytochrome *c* (Everest *et al.*, 1991; Hazzard *et al.*, 1992). These results serve to emphasize the important role Phe82 plays in the formation of complexes between cytochrome *c* and redox partner proteins.

With respect to the electrochemical reduction potential of cytochrome *c*, Phe82 also appears to play an important role that is related to the close packing of the side chain of this residue next to the heme group (Rafferty *et al.*, 1990). Previous structural studies of the F82S and F82G mutants of yeast iso-1 cytochrome *c* revealed that the lowered reduction potentials observed for these two mutant proteins arise from changes in the hydrophobic heme environment (Louie *et al.*, 1988b; Louie & Brayer, 1989). Specifically, the mutation of Phe82 to serine results in the introduction of a solvent channel into the heme pocket and the substitution of glycine at this location causes a conformational change in the local polypeptide backbone that places polar groups next to the heme moiety. Both substitutions substantially disrupt the hydrophobic nature of the heme pocket and thereby provide an explanation for the changes observed in the functional behavior of these mutant proteins.

For the case of the substitution of tyrosine for Phe82, it is surprising that there is little impact on heme reduction potential (Rafferty *et al.*, 1990) even though this replacement has a significant impact on electron transfer complex formation (Pielak *et al.*, 1985) and overall protein stability (Greene *et al.*, 1993). Molecular graphics modeling of the F82Y amino acid replacement, as described in Section 2.2, indicates that a structural conflict is likely to arise between the hydroxyl group of Tyr82 and the side chain of the adjacent Leu85. This conflict would be expected to necessitate a shift in either of the side chains of Tyr82 or Leu85, or perhaps in both. An earlier NMR study has tentatively assigned the residue shifted as being Leu85 (Pielak *et al.*, 1988; Greene *et al.*, 1993). Although this result provides an adequate explanation for the maintenance of heme reduction potential, it does not explain the significant impact this mutation has on the formation of electron transfer protein complexes.

In this chapter, to address the issue of precisely what structural changes occur as the result of replacement of Phe82 by tyrosine, the three-dimensional structure of this mutant protein has been elucidated using X-ray diffraction techniques. Furthermore the role of Leu85 in these structural shifts was assessed by examining the structure of the F82Y/L85A mutant protein in which the steric conflict that would normally occur between these residues should be relieved. To assure that the L85A mutation in itself does not lead to unexpected structural consequences, the structure of the mutant protein having this single amino acid substitution was also determined. By examining the structures of all three of these mutant proteins and that of wild-type yeast iso-1 cytochrome c, it was hoped that a comprehensive structural understanding of the relationship between Phe82 and Leu85 could be achieved in light of the available functional studies. Note that the studies in this chapter form an important part of the following chapters where additional mutations at both Phe82 and Leu85 are examined. The results of the structural analyses in the present chapter have been published in Lo *et al.* (1995a).

3.2 Experimental Procedures

Crystals of the F82Y, L85A and F82Y/L85A mutants of yeast iso-1 cytochrome c were grown under reducing conditions as discussed in Section 2.3. For these proteins the hanging drop vapour diffusion method was augmented with either seeding from macro-crystals or hair-seeding from micro-crystals. As summarized in Table 3.5, crystals of all three mutant proteins grew isomorphously to those of wild-type yeast iso-1 cytochrome c.

Following the methods outlined in Section 2.5.2, each mutant cytochrome c data set was collected from a single crystal on an Enraf Nonius CAD4-F11 diffractometer having a crystal to counter distance of 36.8 cm and equipped with a helium filled beam tunnel. A nickel-filtered copper-target X-ray tube with a focal spot of 0.75 mm × 0.15 mm and operated at 26 mA and 40 kV was used to generate the incident radiation. The ambient temperature was maintained at 15°C during data collection.

During data collection for the L85A mutant protein, an examination of the reflections used

Table 3.5: Data collection parameters for F82Y, L85A and F82Y/L85A yeast iso-1 cytochromes c

Parameter	Iso-1 cytochrome c mutant		
	F82Y	L85A	F82Y/L85A
Space group	$P4_32_12$	$P4_32_12$	$P4_32_12$
Cell dimensions (Å)			
$a = b$	36.43	36.60	36.52
c	136.67	138.30	136.74
Number of reflections collected	7073	12191	10278
Number of unique reflections	6173	6909	5408
Resolution (Å)	1.97	1.9	2.0

to monitor decay and slippage indicated that the crystal was gradually shifting within the X-ray capillary tube, probably due to the presence of excess mounting buffer around the crystal. To correct this, the X-ray capillary tube was unsealed and the excess buffer was removed with a microcapillary pipette, with special care being taken to avoid disturbing the protein crystal. The column of buffer above the crystal was then replaced with fresh mounting buffer and the X-ray capillary was resealed with wax. Following this process, the matrix defining the orientation of the L85A mutant protein crystal relative to the diffractometer was redetermined to confirm that no significant shift in the position of the crystal within the X-ray capillary had occurred. No further problem with slippage of this crystal was encountered.

The intensity data sets for all three mutant proteins were corrected for backgrounds, absorption (North *et al.*, 1968), crystal decay, and Lorentz and polarization effects as described in Section 2.5.2. In order to statistically improve high resolution intensity measurements for the three diffraction data sets, local background averaging was employed (Louie & Brayer, 1990;

Murphy *et al.*, 1992). Prior to structural refinement, the diffraction data sets for the F82Y, L85A and F82Y/L85A mutant proteins were placed on an absolute scale by the method of Wilson (1942) (Section 2.5.4).

Starting models for the three mutant protein structure refinements were constructed based on the wild-type reduced iso-1 cytochrome *c* structure determined to 1.2 Å resolution (Louie & Brayer, 1990). The initial $F_{mutant} - F_{wild-type}$ difference electron density maps for each mutant structure are shown in Chapter 2 (Figure 2.13) and have clear positive electron density peaks for the addition of the Tyr82 hydroxyl groups in the F82Y and F82Y/L85A mutant proteins, along with negative electron density peaks representing the truncation of the Leu85 side chain in the L85A and F82Y/L85A mutant proteins. In addition, these maps have electron density peaks representing conformational shifts in the side chains of Arg13 and Leu94 in the L85A mutant protein and in the side chain of Arg13 in the F82Y/L85A mutant protein. Examination of these maps allowed the modeling of the new positions of the side chains of Arg13, Tyr82 and Leu94 into the starting models for the structural refinement of these mutant proteins. All ordered waters with refined isotropic thermal factors under 50 Å^2 from the high resolution wild-type structure were used in the starting models except for those which were in close proximity (< 4 Å) to the mutation sites. The sulphate anion bound to the amino terminal end of the α-helix comprised of residues 3 through 12 in the wild-type structure was also included in the starting models of all three mutant proteins.

Structural refinements were carried out using a restrained parameter least-squares approach (Hendrickson, 1985) following the general protocols outlined in Section 2.6. This process utilized structure factors having a resolution greater than 6.0 Å and a $F/\sigma(F)$ ratio greater than 2.0 (2.5 in the case of the L85A data set) as discussed in Section 2.6.3.1, and employed the restraint weights listed in Table 2.4. The solvent water molecules included in structural refinement were modeled as neutral oxygen atoms with full occupancies. Overall, between 60–90 individual cycles of least-squares computational refinement were carried out for each structure determination. During structure refinements, an average of 5–8 sequential examinations of the

entire polypeptide chain using omit, $F_o - F_c$ and $2F_o - F_c$ difference electron density maps were conducted at regular intervals to check the progress of refinement and make manual corrections where necessary. These manual corrections included the identification of additional solvent waters by searching for strong difference electron density peaks within 3.5 Å of hydrogen bond donor or acceptor atoms, and the deletion of weakly resolved water molecules. Additional examinations of specific areas of each protein were required using $F_o - F_c$ and omit difference electron density maps due to poorly defined electron density resulting from the high thermal motion of these regions. The most significant of these problem areas were the first 5 amino-terminal residues of each protein and the placement of various surface side chains including that of Arg13 in the F82Y mutant protein. Whereas the side chain of Arg13 is substantially disordered in the F82Y and wild-type proteins, in the case of the L85A and F82Y/L85A mutant structures well ordered electron density is present for Arg13 as demonstrated in Figure 2.13. This feature of Arg13 is probably due to the replacement of Leu85 by alanine as discussed in the results section of this chapter. The final refined structures of all three mutant proteins exhibit good stereochemistry and this is summarized in Table 3.6 along with the final refinement parameters for these structures.

Atomic coordinate errors for mutant protein structures have been estimated using two methods (see Section 2.6.3.4). Inspection of the Luzzati (1952) plot drawn in Figure 3.16 indicates that these errors are in the range of 0.18–0.22 Å. Overall atomic coordinate errors can also be estimated by evaluating the individual atomic errors (Cruickshank, 1949, 1954). On the basis of this method, the estimated overall r.m.s. coordinate error is 0.16 Å for the F82Y structure, 0.18 Å for the L85A structure, and 0.20 Å for the F82Y/L85A structure.

3.3   Results

To allow for a comprehensive analysis of the effects of mutations in the F82Y, L85A and F82Y/L85A mutant proteins, all the available coordinate sets, along with that of wild-type yeast iso-1 cytochrome c, were superimposed using a least-squares procedure based on all α-carbon

Table 3.6: Refinement results and stereochemistry for the F82Y, L85A and F82Y/L85A yeast iso-1 cytochrome c mutant structures

	F82Y	L85A	F82Y/L85A
1. Refinement results			
Resolution range (Å)	6.0–1.97	6.0–1.9	6.0–2.0
Number of observed reflections	4546	4886	3761
Completeness in resolution range (%)	66.4	62.3	57.2
Number of protein atoms	895	891	892
Number of solvent atoms	70	79	72
Average thermal factors (Å^2)			
Protein atoms	14.8	15.4	16.6
Solvent atoms	23.4	27.2	27.4
R-factor	0.186	0.196	0.185

2. Stereochemistry of final models	r.m.s. deviation from ideal values		
Distances (Å)			
Bond (1-2)	0.019	0.019	0.019
Angle (1-3)	0.038	0.039	0.039
Planar (1-4)	0.045	0.046	0.045
Planes (Å)	0.013	0.012	0.013
Chiral volumes (Å^3)	0.163	0.138	0.159
Non-bonded contacts (Å)[†]			
Single torsion	0.212	0.216	0.226
Multiple torsion	0.192	0.220	0.207
Possible hydrogen bonds	0.215	0.239	0.234
Torsion angles (°)			
Planar (0° or 180°)	2.0	1.9	2.0
Staggered (±60°,180°)	24.7	23.1	23.6
Orthonormal (±90°)	21.7	19.5	17.4

[†]The r.m.s. deviations from ideality for this class of restraint incorporates a reduction of 0.2 Å from the radius of each atom involved in a contact.
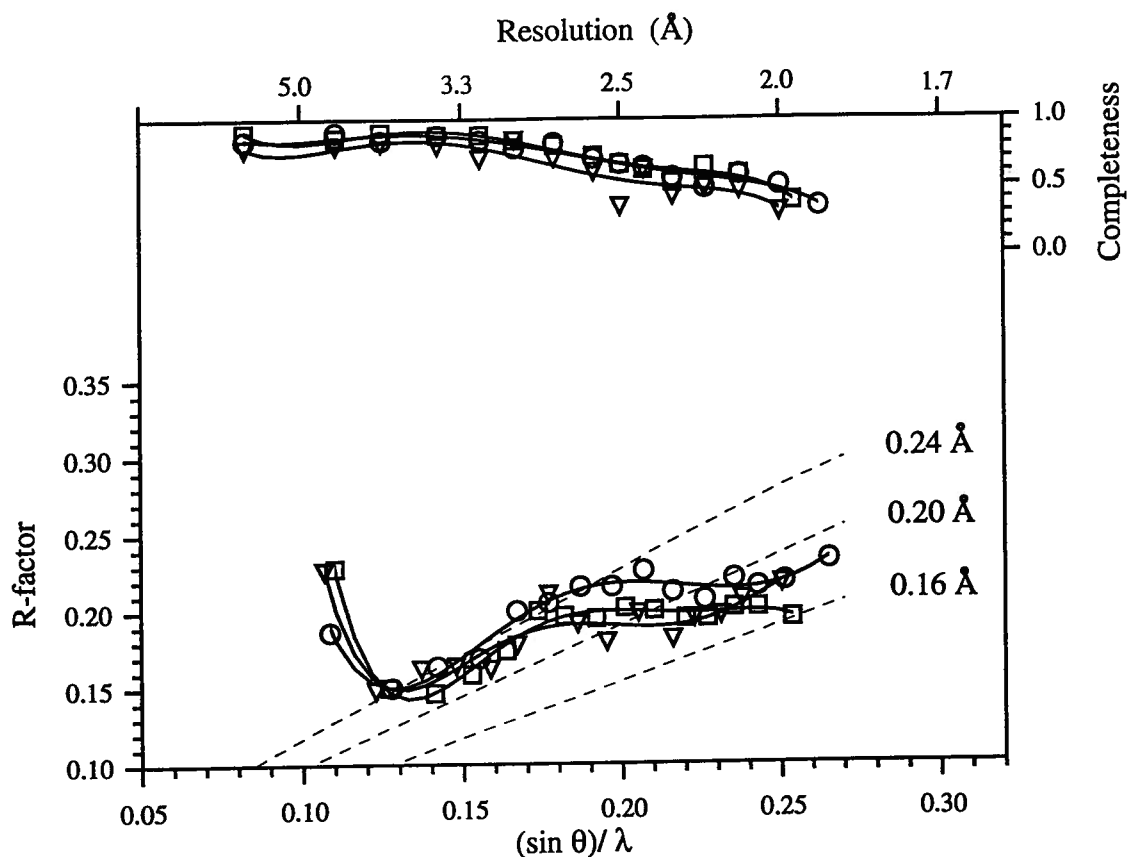
Figure 3.16: A plot of the crystallographic R-factor at the end of refinement as a function of resolution for the F82Y ($\square$), L85A ($\bigcirc$) and F82Y/L85A ($\triangledown$) mutants of yeast iso-1 cytochrome c. The theoretical dependence of R-factor on resolution assuming various levels of r.m.s. error in the atomic positions of the model (Luzzati, 1952) is shown as broken lines. This analysis suggested an overall r.m.s. coordinate error for the mutant structures of between 0.18 and 0.22 Å. The top portion of this figure (axes at top and right) shows the fraction of reflections observed and used in refinement as a function of resolution.

Table 3.7: Overall average positional deviations (Å) between wild-type yeast iso-1 cytochrome c and the F82Y, L85A and F82Y/L85A mutant proteins

Atom groups	Iso-1 cytochrome c mutant		
	F82Y	L85A	F82Y/L85A
All common protein atoms	0.31	0.37	0.35
All main chain atoms	0.18	0.21	0.22
All common side chain atoms	0.47	0.57	0.52
All heme atoms	0.13	0.15	0.15

atoms. This comparison is shown in Figure 3.17 and reveals that the overall polypeptide chain fold of yeast iso-1 cytochrome c is retained upon introduction of these mutations at residues 82 and 85. As indicated in Table 3.7, average deviations for main chain atoms between the wild-type and three mutant proteins are on the order of 0.18–0.22 Å.

Plots of the average positional deviations of residues along the polypeptide chain of the mutant proteins are shown in Figure 3.18. The N-terminal residues, Thr(-5) and Glu(-4), are substantially disordered and therefore the large positional deviations seen at these positions are likely the result of positional mobility rather than a reflection of the induced mutations. Tables 3.8 and 3.9 show that the overall geometry and solvent exposure of the heme group of each mutant protein is comparable to that of wild-type cytochrome c. For each individual mutant protein, specific structural alterations are observed at or near the sites of mutation and these are discussed in detail in the following sections.
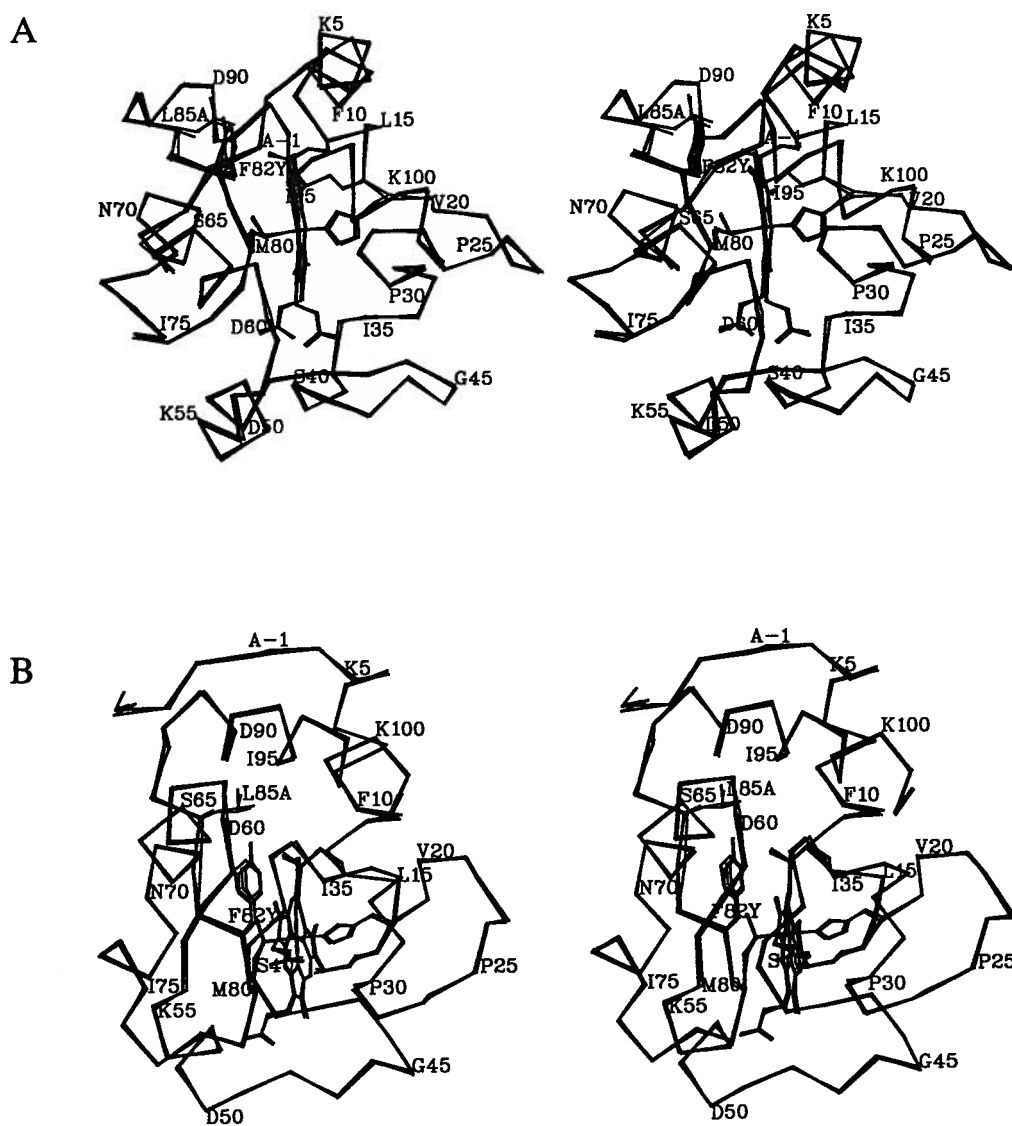
Figure 3.17: Stereo diagrams of the α-carbon backbones of the wild-type, F82Y, L85A and F82Y/L85A iso-1 cytochrome c structures in (a) the standard view looking at the heme edge-on and (b) an alternate view looking directly down into the mutation sites at residues 82 and 85. Also drawn are the side chains of the mutated residues, Phe82 and Leu85, and the heme moieties of all four proteins, along with the ligands to the heme iron atom (His18 and Met80) and cysteines 14 and 17, which form covalent thioether bonds to the heme porphyrin ring. Every fifth amino acid residue is indicated by its one-letter amino acid designation and sequence number.

A

B
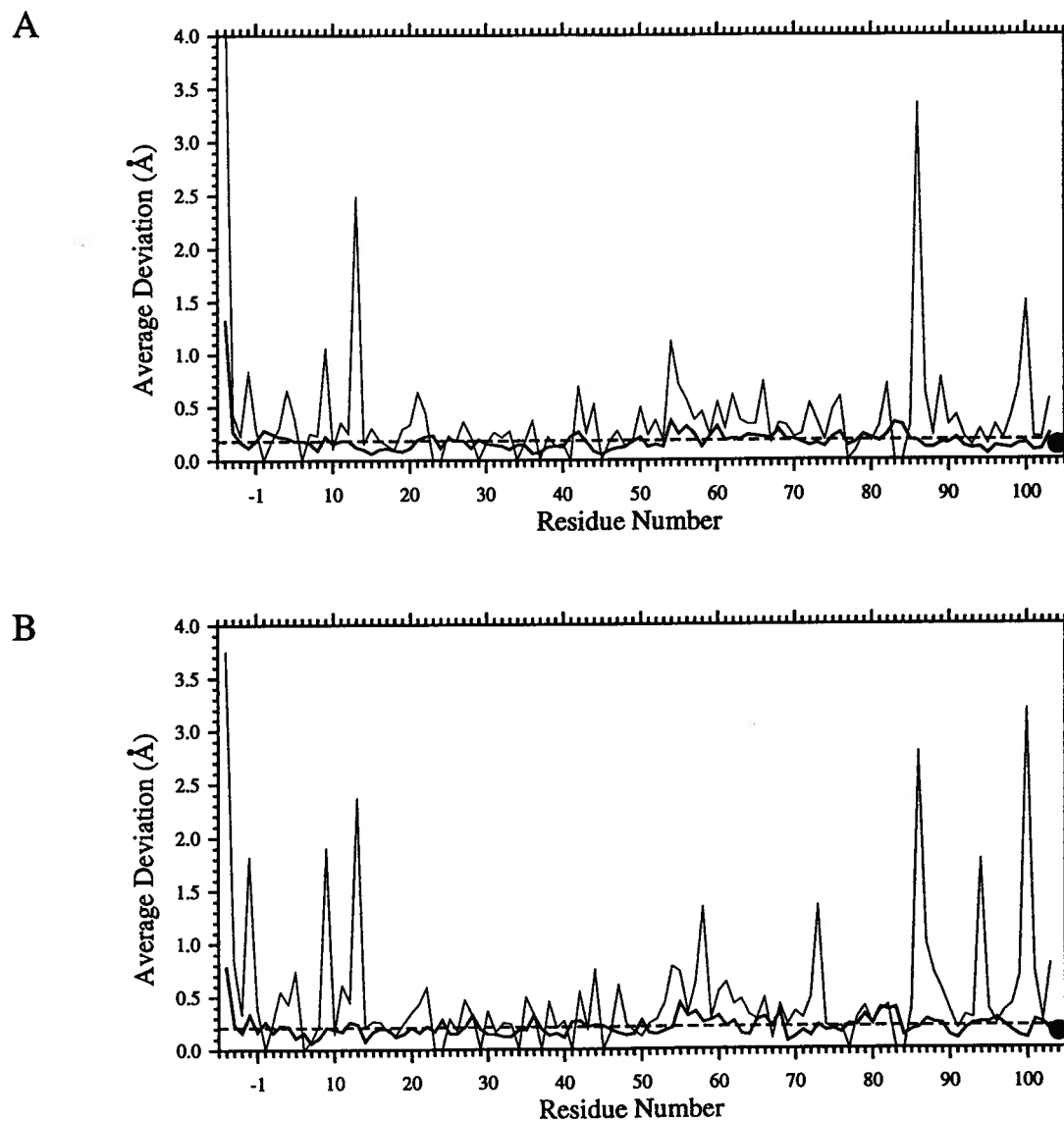
Figure 3.18: continued on next page.
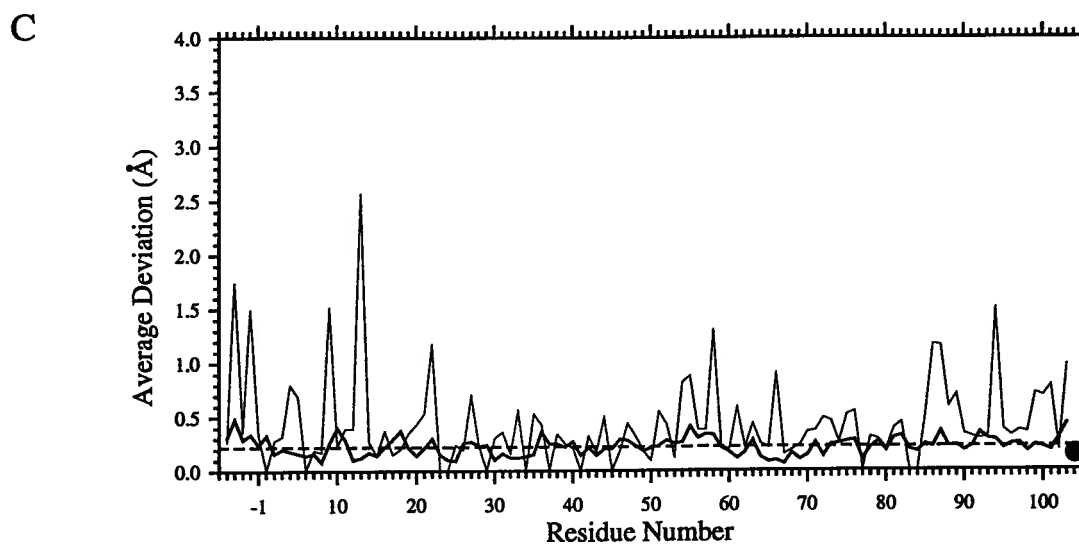
Figure 3.18: continued. Plots of average positional deviations from the wild-type iso-1 cytochrome c structure for the (a) F82Y, (b) L85A and (c) F82Y/L85A mutant proteins. Thick lines indicate average deviations of main chain atoms while thin lines indicate average deviations of the equivalent side chain atoms. In each diagram, the filled circle at residue position 104 represents the average positional deviation of the heme group and the horizontal dashed line represents the average positional deviation for all main chain atoms.

Table 3.8: Heme geometry of F82Y, L85A, F82Y/L85A and wild-type yeast iso-1 cytochromes *c*

	Wild-type	F82Y	L85A	F82Y/L85A

1. Angular deviations (°) between the pyrrole nitrogen plane normal and the four individual pyrrole ring plane normals and the heme coordinate bonds.

	Wild-type	F82Y	L85A	F82Y/L85A
A	9.4	9.0	9.2	13.5
B	11.1	11.2	8.8	11.6
C	8.8	8.5	9.2	10.1
D	8.1	9.5	10.2	10.2
Fe - His18 NE2	2.2	2.8	3.3	8.3
Fe - Met80 SD	4.9	2.1	4.3	5.6

2. Angular deviations (°) between the porphyrin ring plane normal and the four pyrrole ring plane normals, the pyrrole nitrogen plane normal and the heme coordinate bonds.

	Wild-type	F82Y	L85A	F82Y/L85A
A	6.7	5.9	5.7	7.9
B	11.9	10.7	10.1	12.4
C	9.8	10.8	9.8	10.5
D	6.0	7.0	6.7	4.7
NNNN	2.6	3.1	3.4	5.6
Fe - His18 NE2	3.2	4.7	0.3	2.9
Fe - Met80 SD	7.5	4.9	7.9	11.1

3. Bond distances (Å) between the heme iron atom and its six ligands.

	Wild-type	F82Y	L85A	F82Y/L85A
His18 NE2	1.98	1.95	1.92	2.14
Met80 SD	2.36	2.28	2.38	2.33
Heme NA	1.97	1.98	1.99	2.01
Heme NB	2.00	2.02	1.98	2.00
Heme NC	1.99	2.02	1.98	2.02
Heme ND	2.01	2.05	2.11	2.01

The pyrrole nitrogen plane is defined by the four pyrrole nitrogens of the heme group. The four pyrrole ring planes are each defined by the five atoms of the ring and the first carbon atom attached to each of the four carbons of the ring. The porphyrin ring is defined by the five atoms in each of the four pyrrole rings, the four bridging methine carbon atoms, the first carbon atom of each of the eight side chains of the heme and the central iron atom of the heme. The heme atom nomenclature used in this table follows the conventions of the Protein Data Bank (see Figure 1.2).

Table 3.9: Heme solvent accessibility in F82Y, L85A, F82Y/L85A and wild-type yeast iso-1 cytochromes c

| | Yeast iso-1 cytochrome c structure | | | |
	Wild-type	F82Y	L85A	F82Y/L85A
1. Solvent accessible heme atoms and surface area exposed (Å^2)				
CHD	2.9	2.9	2.8	3.1
CMC	9.2	11.2	12.3	9.2
CAC	3.4	4.1	3.3	4.4
CBC	20.1	20.6	18.4	18.3
CMD	10.8	11.2	10.3	10.1
2. Total heme exposure (Å^2)	46.4	50.0	47.1	45.1
3. Total heme surface (Å^2)	513.1	515.0	514.7	512.2
4. % heme surface area exposed	9.0	9.7	9.2	8.8

Solvent exposure was determined by the method of Connolly (1983) with a probe sphere having a 1.4 Å radius.

3.3.1 Structure of F82Y cytochrome c

In wild-type yeast iso-1 cytochrome c, the side chain of Leu85 lies directly adjacent to the distal edge of the aromatic ring of the side chain of Phe82. Thus, mutation of Phe82 to a tyrosine places the additional hydroxyl group into direct spatial conflict with the Leu85 side chain. As the current structural analysis shows, this potential conflict is resolved by the side chain of Tyr82 undergoing a significant positional displacement ($\Delta d = 0.7$ Å), involving a rotation toward the surface of the protein ($\Delta\chi_1 = 3°$; $\Delta\chi_2 = 10°$; Figure 3.19). At this location, the side chain of Tyr82 exhibits significantly increased thermal mobility ($\Delta B = \sim 8$ Å^2; Table 3.10) and the hydroxyl group of this residue hydrogen bonds to a new surface water molecule. Also having increased thermal mobilities are the main chain atoms of residues 81 and 82. In contrast, the Leu85 side chain is shown to retain a position comparable to that in the wild-type structure, with an average deviation of 0.3 Å for side chain atoms. Tyr82 displacement also decreases the angle between the normal of its planar group and that of the heme to 9° from the 23° observed in the wild-type protein. The difference in these values, 14°, is significantly larger than the 4° and 5° observed in the L85A and F82Y/L85A structures, respectively.

Leu9 and Arg13 are two residues in the region of the mutation site which adopt altered conformations. The average side chain deviations observed are 1.1 Å and 2.5 Å, respectively (Figure 3.19). The shift of the side chain of Tyr82 to a more solvent exposed position necessitates the displacement of the nearby side chain of Arg13. The new conformation of Arg13 as well as the positional shift of Tyr82 toward the protein surface (Figure 3.19) account for the marked increase in the solvent exposure of the aromatic ring of Tyr82 (Table 3.11). In contrast, the altered position of the side chain of Arg13 partially masks the side chain of Leu85 from solvent exposure (Table 3.11). A further spatial consequence of Arg13 movement is the displacement of the side chain of Leu9. The conformation observed for Leu9 ($\chi_1 = -104°$; $\chi_2 = 128°$) in the F82Y protein corresponds well to an alternative conformation observed for this side chain in the high resolution wild-type structure ($\chi_1 = -111°$; $\chi_2 = 123°$; Louie & Brayer, 1990). In wild-type yeast iso-1 cytochrome c, this alternative site appears to have an occupancy of $\sim 30\%$.
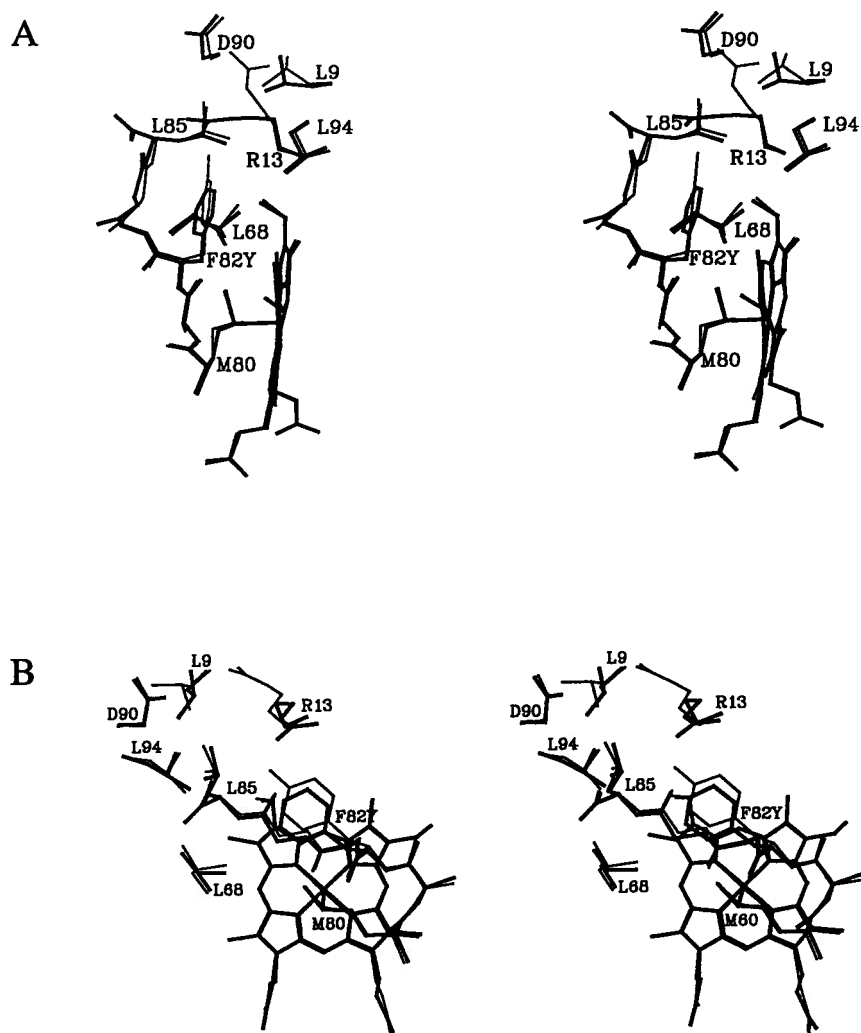
Figure 3.19: Stereo diagrams showing two views of the region about Tyr82 in F82Y iso-1 cytochrome *c*. In each diagram the wild-type protein structure has been superimposed and is shown with thick lines, while the mutant protein structure is depicted by thin lines. Altered side chain conformations for Leu9, Arg13 and Tyr82 are clearly evident.

Table 3.10: Average thermal factors ($Å^2$) of residues 80 through 85 in F82Y, L85A, F82Y/L85A and wild-type yeast iso-1 cytochromes c

Atom groups	Yeast iso-1 cytochrome c structure			
	Wild-type	F82Y	L85A	F82Y/L85A
Met80 main chain	9.9	9.5	10.7	7.4
Met80 side chain	5.2	5.5	8.0	6.2
Ala81	12.0	16.7	11.5	10.7
Phe/Tyr82 main chain	15.2	20.4	13.6	12.1
Phe/Tyr82 side chain	16.9	25.2	10.9	13.2
Gly83	19.0	21.2	16.4	12.4
Gly84	17.4	21.2	17.2	14.3
Leu/Ala85 main chain	13.8	16.3	12.8	13.6
Leu/Ala85 side chain	17.9	12.6	12.9	8.9
All heme atoms	5.3	6.0	7.9	7.6

The average thermal factor for all protein atoms of the wild-type iso-1 cytochrome c structure was 16.5 $Å^2$. The distributions of protein atomic thermal factors for the three mutants were normalized to this value for this comparison.

Table 3.11: Solvent accessibility of residues 82 and 85 in F82Y, L85A, F82Y/L85A and wild-type yeast iso-1 cytochromes *c*

	Yeast iso-1 cytochrome *c* structure			
	Wild-type	F82Y	L85A	F82Y/L85A[†]
Side chain surface area exposure (Å^2)				
Phe/Tyr82 CD2	10.9	11.8	8.6	10.3
Phe/Tyr82 CE2	6.8	14.2	11.4	12.9
Tyr82 OH	—	6.9	—	5.7
Leu85 CD2	13.3	8.7	—	—
Total Phe/Tyr82 aromatic ring exposure (Å^2) (atoms CD2 and CE2)	17.7	26.0	20.0	23.2

Solvent exposed areas were calculated by the method of Connolly (1983) with a probe sphere of 1.4 Å radius.

[†]The internal water molecules numbered 224 and 248 were considered to be an integral part of the protein for this calculation.

Other prominent features in Figure 3.18a involving side chain groups represent amino acids in the disordered amino terminal region of the polypeptide chain or polar side chains extending from the protein into solvent (Lys54, Lys86 and Lys100).

3.3.2 Structure of L85A cytochrome c

Mutation of leucine 85 to a much smaller alanine residue would be expected to create considerable free volume in this region. The current structural studies show that in response, the
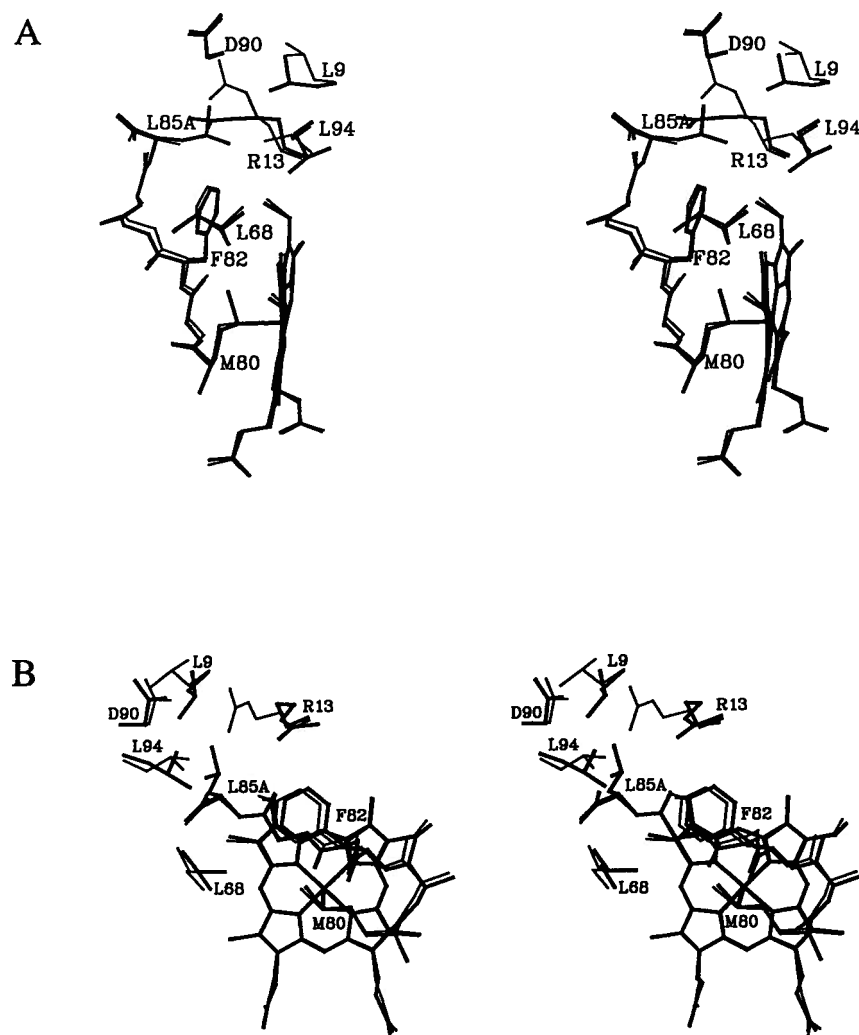
Figure 3.20: Stereo diagrams showing two views of the region about Ala85 in L85A iso-1 cytochrome *c*. In each diagram the wild-type protein structure has been superimposed and is shown with thick lines, while the mutant protein structure is depicted by thin lines. Altered side chain conformations for Leu9, Arg13 and Leu94 are clearly evident.

nearby side chains of Leu9, Arg13 and Leu94 have all adopted new conformations (Figures 3.18b and 3.20). The side chain of Leu94 is found to shift ($\Delta d = 1.8$ Å) into the additional space available near Ala85. The side chain of Arg13 also moves toward Ala85 ($\Delta d = 2.4$ Å) and at this alternate location forms a new interaction with the side chain of Asp90 (Arg13 NH1-Asp90 OD1; d = 3.6 Å). This new interaction has a marked effect on the thermal factors of the atoms of the Arg13 side chain, which have an average B of 32.4 Å^2 in the wild-type structure and 16.7 Å^2 in the L85A protein. The movements of both Leu94 and Arg13 appear to cause a shift in the side chain of Leu9 away from the mutation site ($\Delta d = 1.9$ Å) in order to avoid spatial conflicts with these residues. The new conformation of Leu9 differs from both of those seen in the wild-type protein (Louie & Brayer, 1990).

3.3.3 Structure of F82Y/L85A cytochrome c

As can be seen in Figure 3.21, in the F82Y/L85A mutant protein the removal of the side chain of Leu85 allows the additional hydroxyl group of Tyr82 to be accommodated with minimal perturbation of the overall position of the phenyl ring of this residue ($\Delta d = 0.4$ Å). This hydroxyl group is found to point directly into the region formerly occupied by the Leu85 side chain in the wild-type protein. In addition, two new water molecules are bound in this region, one of which (Wat 248) forms a hydrogen bond to the hydroxyl group of Tyr82. The second water molecule (Wat224) hydrogen bonds to the guanidinium group of Arg13 as well as to Wat248 (Figure 3.21).

As observed for the L85A protein, the side chain of Arg13 in the F82Y/L85A double mutant moves toward the region vacated by the Leu85 side chain ($\Delta d = 2.6$ Å) and forms a new interaction with the side chain of Asp90 (Arg13 NH1-Asp90 OD1; d = 3.3 Å). The average thermal factor for Arg13 side chain atoms is 19.3 Å^2 and, as in the L85A mutant protein, this is considerably lower than found in the wild-type protein. New conformations are also assumed by both Leu9 ($\Delta d = 1.5$ Å) and Leu94 ($\Delta d = 1.5$ Å). As seen in Figure 3.21, the Leu9 side chain has shifted away from the mutation site to avoid spatial conflicts with the
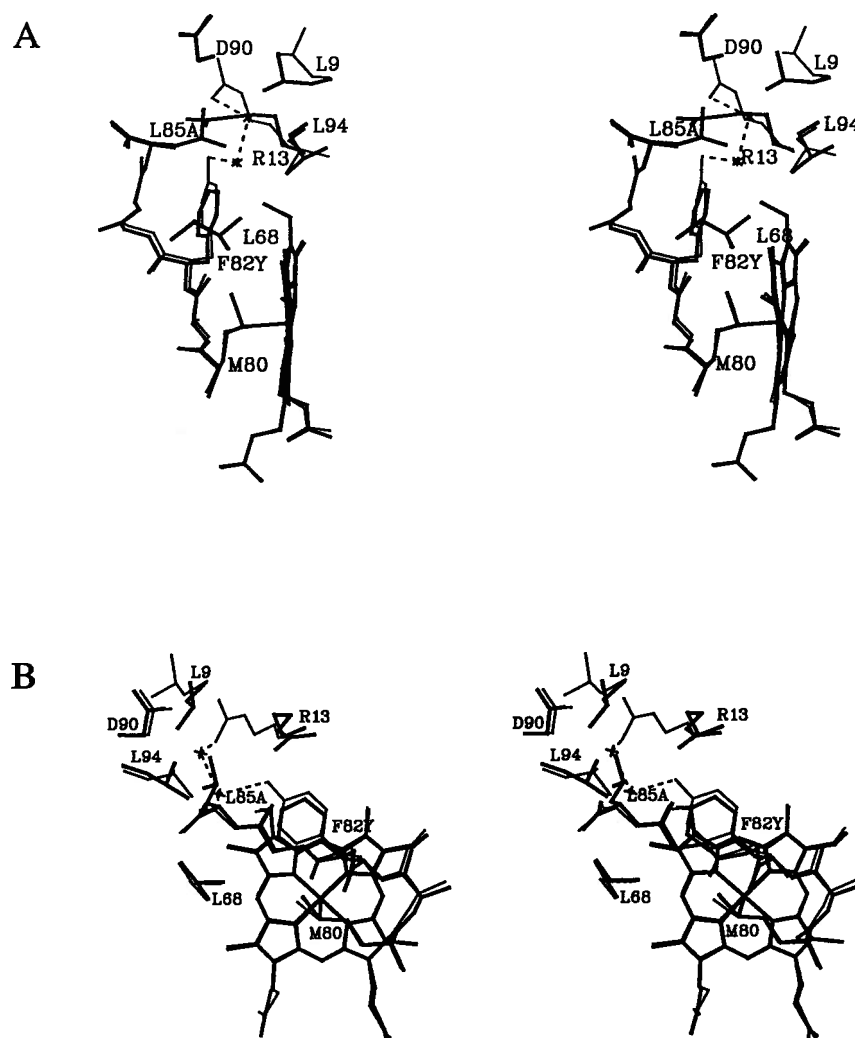
Figure 3.21: Stereo diagrams showing two views of the region about the mutated residues in F82Y/L85A iso-1 cytochrome c. In each diagram the wild-type protein structure has been superimposed and is shown with thick lines, while the mutant protein structure is depicted by thin lines. Altered side chain conformations for Leu9, Arg13 and Leu94 are clearly evident. Two internally bound water molecules (Wat224 and Wat248) observed in the mutant protein are depicted as asterisks.

repositioned side chain of Arg13. Unlike the Leu94 shift observed in the L85A mutant protein, in the F82Y/L85A double mutant, reorientation of this residue is more localized likely due to the two newly bound internal water molecules in this region.

3.4 Discussion

3.4.1 Structural consequences of residue 82 and 85 mutations

A summary of the structural changes seen in the F82Y, L85A and F82Y/L85A mutants of yeast iso-1 cytochrome c is given in Table 3.12. From this overview it can be seen that most of the structural changes present are localized to the region about the mutation sites. In the F82Y protein, increased spatial requirements for the larger tyrosyl side chain appear to be the dominant factor and lead to the rotation of the side chain of Tyr82 toward the protein surface where its hydroxyl group hydrogen bonds to a surface water molecule. The increased thermal mobility of the side chain of this residue is indicative of less than optimal packing of this side chain with neighboring amino acids which may explain the observed decrease in the stability of this mutant protein (Greene et al., 1993). Interestingly, earlier modeling and NMR studies of the F82Y mutant protein suggested that the Tyr82 side chain occupied a position equivalent to that of the Phe82 side chain in wild-type iso-1 cytochrome c and that the side chain of Leu85 had an altered conformation (Pielak et al., 1988; Greene et al., 1993). These results are in disagreement with the present structural analysis. However, the clarity of the current $F_{mutant} - F_{wild-type}$ (Figure 2.13a), fragment deleted and $2F_o - F_c$ difference electron density maps in the vicinity of residues 82 and 85 clearly indicate that Tyr82 as opposed to Leu85 is shifted in the F82Y mutant protein. It should be noted that crystalline lattice contacts are not likely to be a potential factor in the disagreement with earlier data since the region about Leu85 and Tyr82 is unconstrained by such interactions.

The induced structural incompatibility between Tyr82 and Leu85 in the F82Y mutant protein is relieved in the F82Y/L85A mutant protein. The mutation of Leu85 to alanine opens up additional space next to the Tyr82 side chain so that it can retain a conformation comparable

Table 3.12: Summary of positional differences observed between the F82Y, L85A and F82Y/L85A mutant yeast iso-1 cytochromes c and the wild-type protein

F82Y	L85A	F82Y/L85A
1. Tyr82 side chain shifts towards surface of protein and its hydroxyl group interacts with a surface water molecule	1. Leu94 side chain moves towards Ala85	1. Leu9 and Leu94 side chains adopt new conformations
2. Tyrosyl 82 ring rotates 14° relative to heme plane	2. Leu9 and Arg13 side chains adopt new conformations	2. Arg13 and Asp90 side chains form a new interaction
3. Leu9 and Arg13 side chains adopt new conformations	3. Arg13 and Asp90 side chains form a new interaction	3. Two water molecules are introduced into the mutation site
		4. Tyr82 retains original Phe82 position with its hydroxyl group interacting with a newly introduced internal water molecule

to that of the normally resident Phe82. This additional space also allows the hydrogen bonding potential of the hydroxyl group of Tyr82 to be satisfied by permitting the binding of two new internal water molecules. In the L85A mutant protein, the hydrophobic cavity that otherwise would be created is filled by the side chain of Leu94 and the nonpolar portion of the side chain of Arg13. No internal water molecules are found in this highly hydrophobic interior region and the positioning of the aromatic group of Phe82 is not affected.

A further point of interest arising from these studies is that the conformation of Arg13 is clearly dependent on the presence of both Phe82 and Leu85 in the structure of wild-type yeast iso-1 cytochrome *c*. One role of the side chains of Phe82 and Leu85 may be to restrict the potential interaction of Arg13 and Asp90 in order for the former residue to be fully available at the interactive face of cytochrome *c* with redox partners (Pelletier & Kraut, 1992; Northrup *et al.*, 1993; Guillemette *et al.*, 1994; Huang *et al.*, 1994). Shifts in the side chain of Arg13 have also been observed in other mutant proteins with replacements at Phe82 (Louie *et al.*, 1988b; Louie & Brayer, 1989). Overall, the structural changes observed for the three mutant proteins examined in this chapter are directly related to satisfying the spatial requirements of new side chains, the minimization of unoccupied internal space and the solvent exposure of hydrophobic groups, as well as attaining the maximal hydrogen bonding between available polar groups.

3.4.2 Impact of mutations on reduction potential

The dielectric constant of the heme pocket is a primary determinant in setting the reduction potential of cytochrome *c* (Kassner, 1973; Louie & Brayer, 1989; Moore & Pettigrew, 1990). Two essential factors affecting the heme pocket dielectric constant are the solvent exposure of the heme moiety and the polarity of amino acids in close proximity to this group. One important structural element in this regard is the side chain of Phe82. For example, the mutation of this residue to serine leads to the creation of a solvent channel into the heme pocket (Louie *et al.*, 1988b), thereby dramatically increasing heme solvent exposure and decreasing the observed reduction potential of this mutant protein (ΔE_m = -35 mV; Rafferty *et al.*, 1990). Similarly,

the introduction of polar groups into the heme pocket, occurring as the result of polypeptide rearrangements in the F82G mutant protein (Louie & Brayer, 1989), has a pronounced effect on reduction potential (ΔE_m = -43 mV). By examining a wide range of side chain replacements for Phe82, it is possible to determine that this residue's contribution to the observed +290 mV reduction potential of wild-type yeast iso-1 cytochrome *c* is ~+40 mV (Rafferty *et al.*, 1990).

Replacement of Phe82 by a tyrosine has a modest impact on heme reduction potential (ΔE_m = -10 mV; Table 3.13). The increased polarity of the tyrosyl side chain might be expected to have a larger effect, but this is apparently offset by a small positional shift in this group so that the tyrosyl hydroxyl group is oriented out toward the protein surface where it can interact with solvent molecules (Table 3.11). In this conformation, the Tyr82 hydroxyl group is quite distant (d = 6.5 Å) from the porphyrin ring of the heme and is shielded from direct heme plane contact by the CBB side chain atom of the heme group. In addition, the hydrophobicity of the heme pocket remains intact since the tyrosyl ring remains in position to shield the heme from any significant increase in solvent exposure (Table 3.9).

In both the L85A and F82Y/L85A mutant cytochromes *c*, even smaller effects are seen on heme reduction potential (Table 3.13). For the L85A mutant protein, this is to be expected since the side chain of Phe82 retains its wild-type conformation and the internal cavity left by replacement of Leu85 is filled by the hydrophobic portions of other side chains (Figure 3.20). Thus the hydrophobic integrity of the heme pocket is preserved in this mutant protein and the reduction potential is not significantly perturbed.

Although the hydroxyl group of Tyr82 takes on a more internal positioning and two new water molecules are bound in the F82Y/L85A mutant (Figure 3.21, Table 3.9), this has only a small effect on heme reduction potential (Table 3.13). This result is somewhat surprising given the larger impacts of the glycine and serine substitutions at Phe82 (Louie *et al.*, 1988b; Louie & Brayer, 1989). However this might be explained by the fact that the tyrosyl hydroxyl and the two newly bound internal water molecules which contribute to increased polarity in the mutation site are substantially further removed from the heme plane than are the polar

Table 3.13: Reduction potentials for F82Y, L85A, F82Y/L85A and wild-type yeast iso-1 cytochromes *c*

Cytochrome *c*	E_m (mV)
Wild-type	290±2
F82Y	280±2
L85A	285±3
F82Y/L85A	283±3

Experimental conditions were: 25°C, pH 6.0 and $\mu = 0.1$ M. Values are listed relative to a standard hydrogen electrode reference. The first two values listed were taken from Rafferty *et al.* (1990) while the last two values have resulted from collaborative work performed in conjunction with this thesis and presented in Guillemette *et al.* (1994).

groups introduced in the F82S and F82G mutant proteins. In these latter proteins, the newly introduced polar groups not only are located immediately adjacent to the central face of the heme plane, but are also near the central heme iron atom. In the F82Y/L85A protein, the tyrosyl hydroxyl group is projected away from the heme porphyrin ring (d = 6.5 Å) and the new internal water molecules are located along the heme edge where heme substituent side chains shield direct access to the porphyrin ring. The shortest heme porphyrin ring plane to water distance is 5.4 Å. Thus it appears that the increased local polarity introduced into the F82Y/L85A mutant protein is too distant from the central heme porphyrin core to substantially affect heme reduction potential.

3.4.3 Electron transfer in mutant proteins

The steady-state rate of the electron transfer reaction of yeast iso-1 cytochrome c with yeast cytochrome c peroxidase varies considerably upon mutation of Phe82, with the F82Y, F82S and F82G proteins having 30%, 70% and 20% of wild-type activity, respectively (Pielak *et al.*, 1985). Similar trends were observed for the activity of these mutants in the electron transfer reaction with bovine cytochrome c oxidase (Michel *et al.*, 1989). Such decreases in reaction rate may arise from perturbation of either the intrinsic rate of electron transfer within these protein-protein complexes or the interactions that are a part of the formation of such complexes. Recent studies have shown that the multiphasic kinetics observed in the electron transfer reaction between reduced iso-1 cytochrome c and a Zn-substituted cytochrome c peroxidase porphyrin π cation radical does not require the presence of an aromatic residue at position 82 of cytochrome c (Everest *et al.*, 1991). Studies of electron transfer between bovine cytochrome c oxidase and iso-1 cytochromes c with replacements of Phe82 produced similar conclusions (Hazzard *et al.*, 1992).

The fact that the kinetics of intracomplex electron transfer involving Phe82 mutants of iso-1 cytochrome c do not correspond to the steady-state activity decreases observed for these proteins suggests that complex formation with redox partners is the major factor influencing these changes in steady-state activity. This is supported by the proposed interactive surface of cytochrome c as elucidated by modeling of such complexes (Poulos & Kraut, 1980; Lum *et al.*, 1987; Northrup *et al.*, 1988) and the recent determination of the structure of the complex formed between yeast iso-1 cytochrome c and cytochrome c peroxidase (Pelletier & Kraut, 1992). In this latter complex, Phe82 is completely sequestered within the region of protein-protein interactions, although the side chain of Arg13 and several water molecules prevent Phe82 from making direct contact with the cytochrome c peroxidase molecule. In the case of the F82Y mutant protein, the side chain of Tyr82 would protrude off the surface of the protein into the site of complexation and, in conjunction with corresponding movements of the Arg13 side chain, would disrupt the formation of a productive electron transfer complex. This could

explain the considerably lower steady-state activity of this mutant protein. In contrast, the mutation of Phe82 to serine does not present such a physical intrusion into the interaction region of the complex and steady-state activity is affected to a lesser extent. The lower rate of the Ser82 protein could be attributed to the increase of solvent molecules in this region leading to somewhat less specific complex surface interactions. Another example of a large change in the contour of the complex contact surface can be found in the mutation of Phe82 to glycine in which the exposed face of cytochrome c is drastically altered (Louie & Brayer, 1989). As would be expected from the present work, this greatly reduces the steady-state electron transfer rate.

Thus there appears to be a close relationship between the integrity of the complexation surface of cytochrome c and the overall electron transfer activity observed. The importance of this factor is further emphasized by the observed species specificity in attaining optimal protein-protein electron transfer reactions involving cytochrome c (Ho *et al.*, 1985; Nocek *et al.*, 1991; Moench *et al.*, 1992, 1993). Such effects on electron transfer most likely arise from differences in the makeup of the interactive surface of cytochrome c between species, not unlike the structural changes that have been introduced by site-directed mutagenesis.

Chapter 4

Replacements in a Conserved Leucine Cluster in the Hydrophobic Heme Pocket of Cytochrome c

4.1 Introduction

In Chapter 3, the structural and functional effects arising from the introduction of the F82Y and L85A substitutions into cytochrome c were examined along with the complementary F82Y/L85A double mutant protein having both of these amino acid replacements. The objective of the experiments presented in this chapter is to expand on studies of the role of Leu85 in cytochrome c as well as the role of the adjacent Leu94 residue. These two leucine residues, along with leucines 9, 68 and 98, form a cluster of conserved leucines in the hydrophobic heme pocket of cytochrome c. This leucine cluster is also adjacent to, and in part forms the boundary of, an internal hydrophobic cavity that is positioned toward the back of the heme pocket near one edge of this moiety. In addition to these features, previous studies have implicated Leu85 as being a primary hydrophobic contact point in complexes formed between cytochrome c and its electron transfer partners. Evidence for this arises not only from the results of modeling studies (Salemme, 1976; Northrup et al., 1993) but also from the results of studies utilizing NMR that indicate a shift in the side chain of residue 85 in the complex of cytochrome c with cytochrome b_5 (Burch et al., 1990). It has also been pointed out that amino acid replacements or conformational shifts at Leu85 may influence the kinetics of cytochrome c function as these would require different packing restraints with complexed electron transfer partners (Pielak et al., 1988; Nocek et al., 1991). Such replacements and conformational shifts of Leu85 have previously been examined in conjunction with structure-function studies of the adjacent Phe82 residue (see Chapter 3; Pielak et al., 1988; Greene et al., 1993).

To evaluate Leu85 from both the structural and functional perspectives, a family of variant proteins has been constructed in which this residue is replaced with several alternative amino acids. In almost all species for which the amino acid sequence of cytochrome c is known, residue 85 is either a leucine or an isoleucine. In those few instances where this is not the case, this residue is phenylalanine or methionine (Hampsey *et al.*, 1988; Moore & Pettigrew, 1990). Past work has shown the conformation of an isoleucine at residue 85 as the result of the structure determination of horse cytochrome c (Bushnell *et al.*, 1990). In addition, the structure of the L85A variant of yeast iso-1 cytochrome c was described in Chapter 3 as part of an assessment of the role of the nearby invariant Phe82 residue.

In the current chapter, the L85F and L85M variants of yeast iso-1 cytochrome c, containing the two other residues that naturally occur at this position, are examined. Both of these replacement amino acids should alter the interactive face of cytochrome c in this region significantly and therefore act as probes of complexation interactions. These substitutions, one being aromatic and the other a longer unbranched hydrophobic residue, are also likely to have altered packing interactions within the leucine cluster in which the side chain of Leu85 normally resides. Also constructed was the L85C variant, with the cysteine side chain potentially providing two useful functions. First, as a considerably smaller side chain one would expect the formation of a cavity within the leucine cluster but with a more moderate effect than that observed for the L85A substitution (see Chapter 3). Second, the L85C mutation provides the opportunity to form a crosslink, via a disulfide bond, to a suitably altered and complexed electron transfer partner in future experiments.

Leu94 is also of interest, not only because it is part of the leucine cluster in yeast iso-1 cytochrome c, but in addition its side chain packs directly against that of Leu85 and the central heme group (Louie & Brayer, 1990). Also of importance is the location of this residue at the highly conserved interface formed by the nearly perpendicular packing of the N-terminal (residues 2 to 14) and C-terminal (residues 87 to 102) helices in the structure of cytochrome c.

This helix-helix packing arrangement has been linked to early events in the folding of cytochrome c (Roder *et al.*, 1988).

An analysis of 100 cytochrome c amino acid sequences from different organisms (Hampsey *et al.*, 1988; Fredericks & Pielak, 1993) shows that Leu94 is highly conserved, with a leucine occurring at this position in 95 sequences, an isoleucine in 3 sequences and a valine in 2 sequences. Interestingly, mutagenic studies have shown substitution of serine at residue 94 or similar substitutions at the related leucine cluster residues Leu68 and Leu98 has a significant and deleterious effect on yeast iso-1 cytochrome c function (Hampsey *et al.*, 1986, 1988). Thus despite nearly normal amounts of cytochrome c being observed for the L94S variant, only 30% of the normal yeast growth rate was observed at 22°C. At 30°C, substantially less folded protein was present, indicating that this substitution had an effect on protein stability and that the variant protein was thermally labile (Hampsey *et al.*, 1988). This led to the proposal that the L94S substitution prevents proper folding of cytochrome c. Similar results were obtained by Fredericks and Pielak (1993) who examined a wider range of substitutions at Leu94. These authors propose that the helix-helix interface at Leu94 is conformationally flexible and shifts in helical positions adjust to substitutions made in residues in this region. To assess the degree to which this helix interface can adjust and at the same time study the role of Leu94 in the function of cytochrome c and as part of the hydrophobic leucine cluster in the heme pocket, yeast iso-1 cytochrome c with the substitution of serine at this position has been constructed and examined in this chapter.

At this point, little attention has been focused on the contributions of hydrophobic interactions on the stability of cytochrome c complexes with electron transfer partners or the roles that a heme pocket leucine cluster, an adjacent internal cavity and a nearby helix-helix interface play in the function of this protein. Previous studies have shown that two residues important to these features are leucines 85 and 94. To gain further insight into their functional and structural roles in cytochrome c, the work in this chapter examines a total of four variant proteins with substitutions at these residues. This work has been published in Lo *et al.* (1995c).

Table 4.14: Data collection parameters for the L85C, L85F, L85M and L94S mutant yeast iso-1 cytochromes c

	Iso-1 cytochrome c mutant			
Parameter	L85C	L85F	L85M	L94S
Space group	$P4_32_12$	$P4_32_12$	$P4_32_12$	$P4_32_12$
Cell dimensions (Å)				
$a = b$	36.51	36.55	36.46	36.50
c	137.11	138.24	137.55	136.63
Data collection method	RAXIS	CAD4	CAD4	CAD4
Number of reflections collected	35500	12913	12574	10787
Number of unique reflections	7920	6435	6741	6197
Resolution (Å)	1.81	1.9	1.9	1.9

4.2 Experimental Procedures

The L85C, L85F, L85M and L94S yeast iso-1 cytochrome c mutant proteins were initially crystallized by the hanging drop vapour diffusion method under reducing conditions as discussed in Section 2.3. Diffraction quality crystals were obtained after further seeding with micro-crystals (Leung et al., 1989). All crystals obtained were of the space group $P4_32_12$ and were found to be isomorphous with those of wild-type yeast iso-1 cytochrome c. Unit cell dimensions obtained for mutant protein crystals are listed in Table 4.14.

Each of the X-ray diffraction data sets for the L85F, L85M and L94S mutant proteins was collected from a single crystal on an Enraf Nonius CAD4-F11 diffractometer as described in Section 2.5.2. The incident radiation was generated by a nickel-filtered copper-target X-ray tube operating at 26 mA and 40 kV, with the crystal to counter distance set to 36.8 cm and the ambient temperature maintained at 15°C during data collection. Corrections to intensity

data sets were applied to account for background radiation (Murphy *et al.*, 1992), absorption (North *et al.*, 1968), crystal decay (Louie *et al.*, 1988a), and Lorentz and polarization effects as described in Section 2.5.2. Diffraction data for the L85C mutant protein was collected from a single crystal on a Rigaku R-AXIS II imaging plate area detector as described in Section 2.5.3. The incident radiation was generated by a RU-300 rotating anode generator operating at 100 mA and 60 kV. Crystals were oscillated through a ϕ angle of 1.0° for each frame. Processing of this data set was carried out using the R-AXIS II data processing software (Higashi, 1990; Sato *et al.*, 1992) as described in Section 2.5.3. All four mutant protein data sets were put on an absolute scale by inspection of Wilson (1942) plots as discussed in Section 2.5.4.

The crystals used for the collection of the diffraction data sets for the L85F and L94S mutants of yeast iso-1 cytochrome *c* were particularly small, as indicated in Table 2.3. The small size of these crystals was reflected in the relatively weak intensity data measured for these mutant protein data sets and the correspondingly higher number of unobserved reflections. Although the size of the crystal used in the collection of the L85C mutant protein diffraction data set was comparable to that of the L85F mutant protein (Table 2.3), this data collection benefited greatly from the increased intensity of the incident X-ray beam produced by the rotating anode generator of the R-AXIS area detector and the improved sensitivity of the imaging plate area detector, as discussed in Sections 2.5.3 and 2.6.3.1. Thus a correspondingly more complete data set to higher resolution was obtained for the L85C mutant protein (Table 4.15; Figure 4.22).

Starting models for structural refinement of mutant proteins were constructed from the coordinates of the wild-type iso-1 cytochrome *c* protein (Louie & Brayer, 1990). This was assisted by examining $F_{mutant} - F_{wild-type}$ difference electron density maps (Equation 2.6; Section 2.4.3.1). The replacement of Leu85 by cysteine and methionine, and the replacement of Leu94 by serine could be readily built into the starting models based on these difference electron density maps. For the L85F structure, the $F_{mutant} - F_{wild-type}$ difference electron density map was less clear and this residue was initially modeled as an alanine residue. Also included in the starting models used for structural refinement of the mutant proteins were water molecules

from the wild-type iso-1 cytochrome c structure having isotropic thermal factors below 50 Å^2 and a sulphate anion bound to the amino terminal end of the N-terminal helix of this structure.

The four cytochrome c mutant structures were refined using a restrained parameter least-squares approach (Hendrickson, 1985) following the methods described in Sections 2.6.3.1 and 2.6 and using the restraint weights listed in Table 2.4. The solvent water molecules included in structural refinement were modeled as neutral oxygen atoms with full occupancies. During refinement, as many as 80 individual cycles of least-squares refinement were carried out for each mutant protein structure. The side chain of Phe85 in the L85F mutant protein structure, which as discussed above could not initially be satisfactorily modeled, was clearly visualized in a $2F_o - F_c$ difference electron density map obtained after 11 cycles of least-squares refinement and the appropriate missing side chain atoms were added at this point. During the refinement of each mutant protein structure, at least 3, and in some cases up to 6 (L85F structure), complete examinations of the entire polypeptide chain and all associated solvent molecules were made with the aid of omit, $F_o - F_c$ and $2F_o - F_c$ difference electron density maps to allow for manual corrections to the refinement models. In addition to these overall examinations of the polypeptide chain structure, less comprehensive manual interventions were carried out during the course of the refinements, consisting for the most part of the adjustment of the conformations of individual side chains and the addition and deletion of water molecules. A water molecule was included in the structural model if it was found to be within 3.5 Å of a hydrogen bond donor or acceptor atom and refined to a thermal factor of less than 50 Å^2. The final refinement parameters and structural stereochemistry for all four mutant protein structures are summarized in Table 4.15.

Atomic coordinate errors for the four structures studied were estimated by two methods as described in Section 2.6.3.4. Figure 4.22 shows the resultant Luzzati (1952) plot indicating coordinate errors ranging between 0.16 Å and 0.22 Å for these structures. The Cruickshank (1949) method produces overall atomic coordinate errors of 0.12 Å, 0.18 Å, 0.15 Å and 0.18 Å for the L85C, L85F, L85M and L94S structures, respectively.

Table 4.15: Refinement results and stereochemistry for the L85C, L85F, L85M and L94S yeast iso-1 cytochrome c mutant structures

	L85C	L85F	L85M	L94S
1. Refinement results				
Resolution range (Å)	6.0–1.81	6.0–1.9	6.0–1.9	6.0–1.9
Number of observed reflections	7614	4466	5210	4223
Completeness in resolution range (%)	85.8	57.2	67.3	55.3
Number of protein atoms	892	897	894	892
Number of solvent atoms	76	63	69	83
Average thermal factors (Å^2)				
Protein atoms	21.6	15.9	15.3	14.6
Solvent atoms	33.3	24.4	27.6	24.7
R-factor	0.200	0.190	0.178	0.189

2. Stereochemistry of final models	r.m.s. deviation from ideal values			
Distances (Å)				
Bond (1-2)	0.019	0.019	0.019	0.019
Angle (1-3)	0.037	0.040	0.039	0.039
Planar (1-4)	0.049	0.047	0.048	0.048
Planes (Å)	0.014	0.013	0.015	0.014
Chiral volumes (Å^3)	0.146	0.160	0.156	0.166
Non-bonded contacts (Å)[†]				
Single torsion	0.211	0.214	0.212	0.216
Multiple torsion	0.188	0.202	0.186	0.194
Possible hydrogen bonds	0.194	0.225	0.198	0.236
Torsion angles (°)				
Planar (0° or 180°)	2.3	1.9	2.5	2.2
Staggered (±60°,180°)	20.3	23.2	19.2	21.9
Orthonormal (±90°)	20.4	22.0	19.7	19.2

[†]The r.m.s. deviations from ideality for this class of restraint incorporates a reduction of 0.2 Å from the radius of each atom involved in a contact.
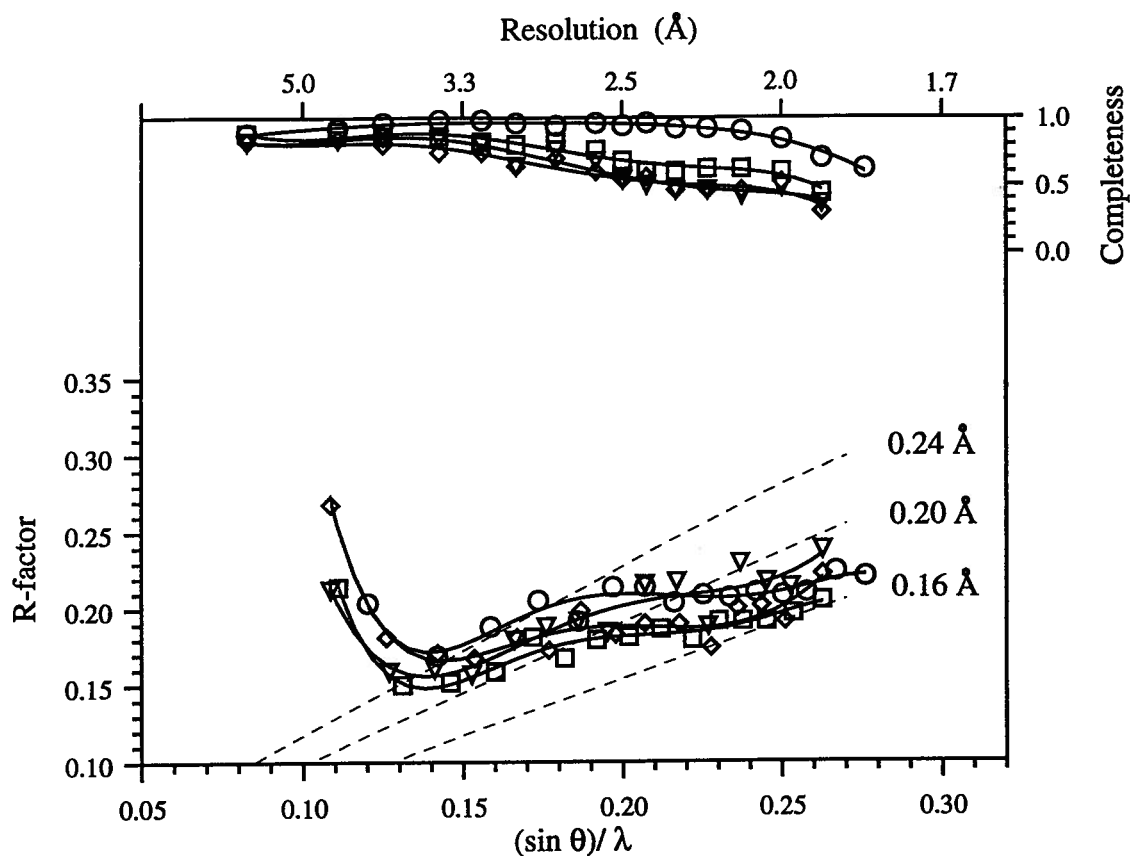
Figure 4.22: A plot of the crystallographic R-factor at the end of refinement as a function of resolution for the L85C (○), L85F (▽), L85M (□), and L94S (◇) mutants of yeast iso-1 cytochrome c. The theoretical dependence of R-factor on resolution assuming various levels of r.m.s. error in the atomic positions of the model (Luzzati, 1952) is shown as broken lines. This analysis suggested an overall r.m.s. coordinate error for the mutant structures of between 0.16 and 0.22 Å. The top portion of this figure (axes at top and right) shows the fraction of reflections observed and used in refinement as a function of resolution.

Table 4.16: Overall average positional deviations (Å) between wild-type yeast iso-1 cytochrome *c* and the L85C, L85F, L85M and L94S mutant proteins

Atom groups	Iso-1 cytochrome *c* mutant			
	L85C	L85F	L85M	L94S
All common protein atoms	0.19	0.39	0.27	0.30
All main chain atoms	0.13	0.25	0.15	0.19
All common side chain atoms	0.27	0.57	0.41	0.43
All heme atoms	0.10	0.17	0.14	0.13

4.3 Results

4.3.1 Structural comparison of mutant and wild-type cytochromes c

To facilitate structural comparisons, each of the four mutant protein structures was superimposed onto the backbone of the high resolution wild-type structure (Louie & Brayer, 1990) by a least-squares fit of α-carbon atoms. As shown in Table 4.16 and Figure 4.23, the global fold of the polypeptide chain of all four mutant proteins is similar to that found in wild-type yeast iso-1 cytochrome *c*. Plots of the average positional deviations of residues along the polypeptide chain of the mutant proteins are shown in Figure 4.24. The N-terminal residues, Thr(-5) through Phe(-3), are largely disordered in the wild-type protein (Louie & Brayer, 1990) and display large positional deviations in the mutant proteins. Other large positional deviations involve the side chains of Lys(-2), Lys4, Lys11, Lys54, Asn63, Glu66, Lys87, Lys89, Lys99, Lys100 and Glu103 which are all located on the protein surface and have large thermal factor values. The differences observed for these residues and those at the N-terminus are likely the result of positional disorder rather than a consequence of the mutations introduced in this study. Also
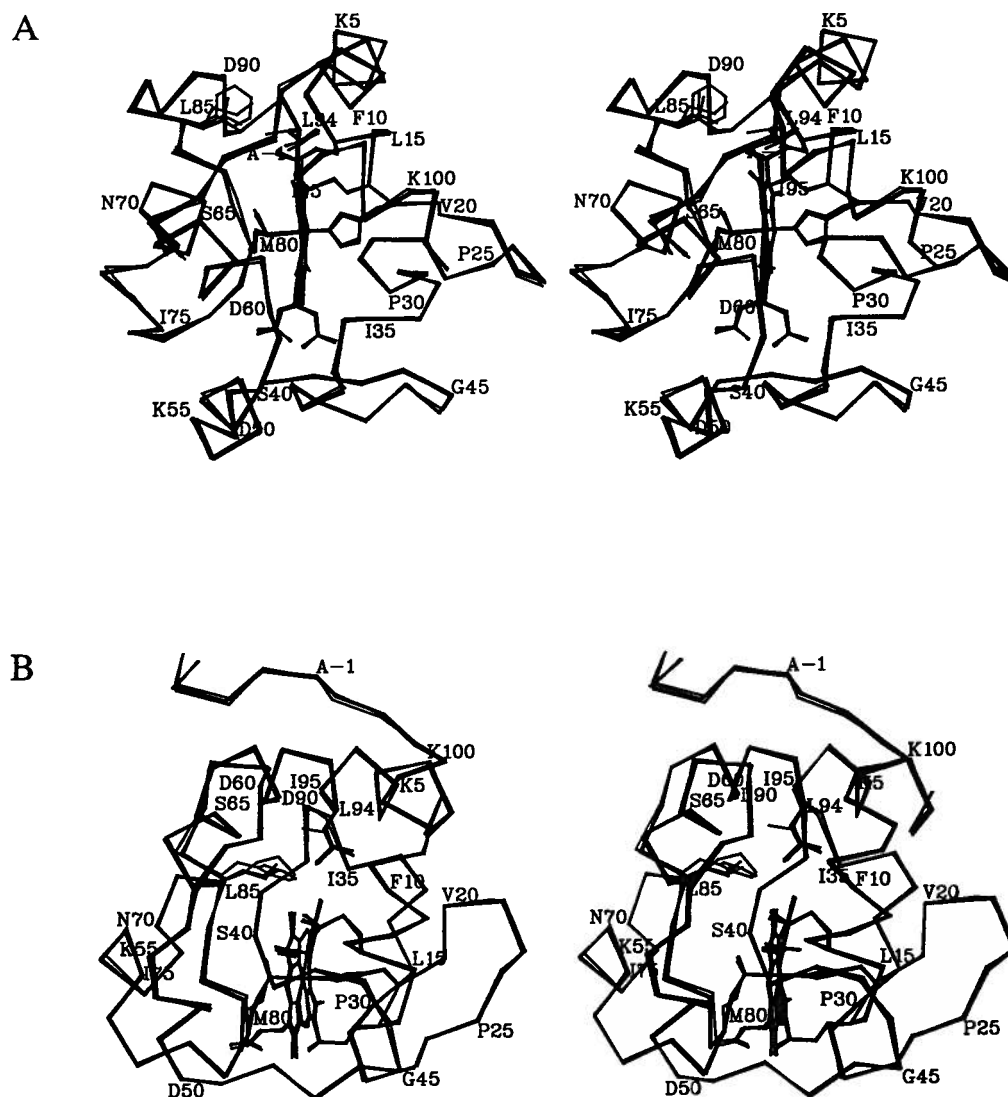
Figure 4.23: Stereo diagrams of the α-carbon backbones of the wild-type, L85C, L85F, L85M and L94S iso-1 cytochrome c structures in (a) the standard view looking at the heme edge-on and (b) an alternate view looking directly into the mutation sites at residues 85 and 94. Also drawn are the side chains of the mutated residues, Leu85 and Leu94, and the heme moieties of all five proteins, along with the ligands to the heme iron atom (His18 and Met80) and cysteines 14 and 17, which form covalent thioether bonds to the heme porphyrin ring. Every fifth amino acid residue is indicated by its one-letter amino acid designation and sequence number. Residue numbering is based on an alignment of the primary sequence of yeast iso-1 cytochrome c (Table 1.1) where the amino-terminal residue of this protein is designated as residue (-5).

A

B
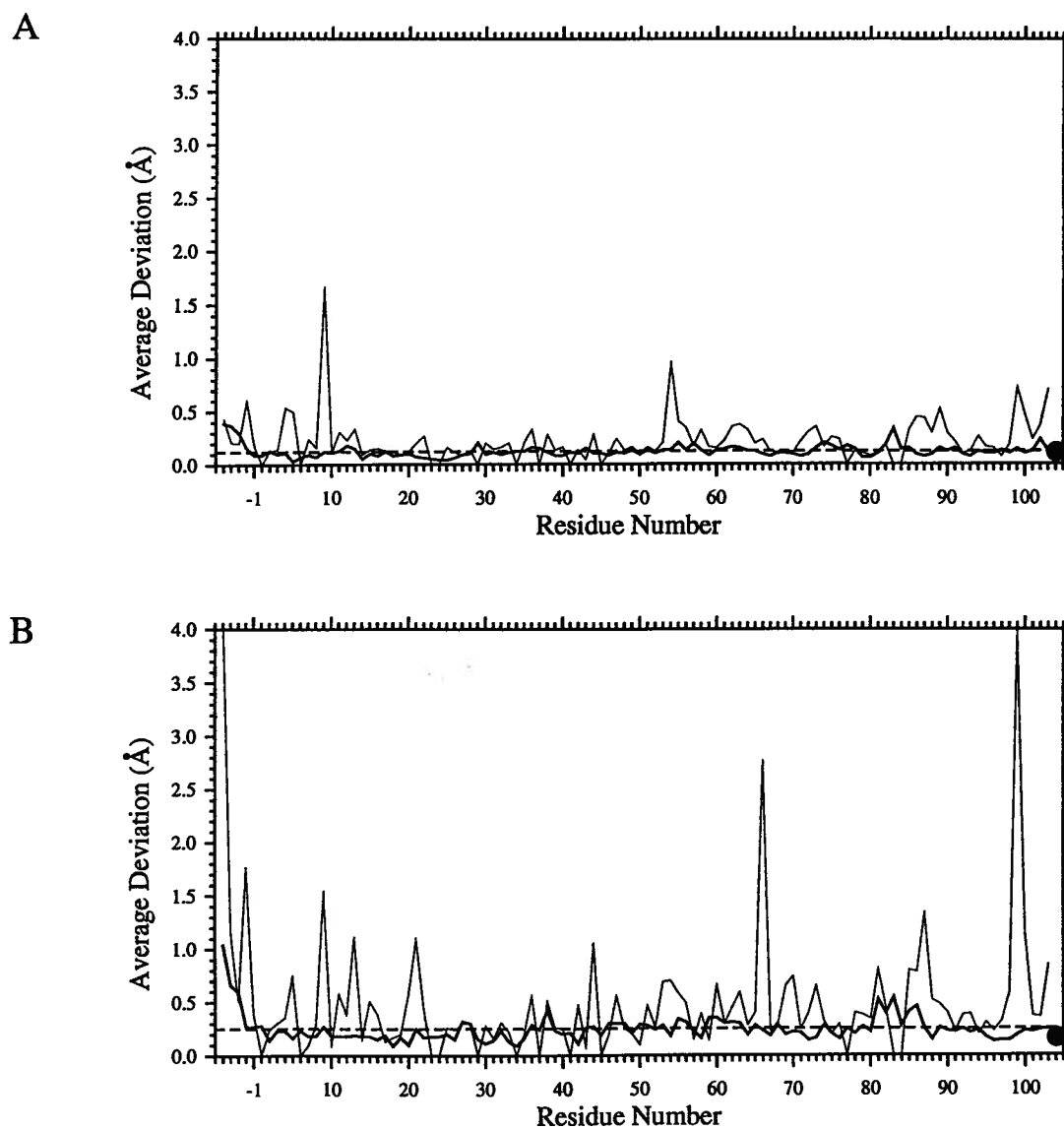
Figure 4.24: continued on next page.
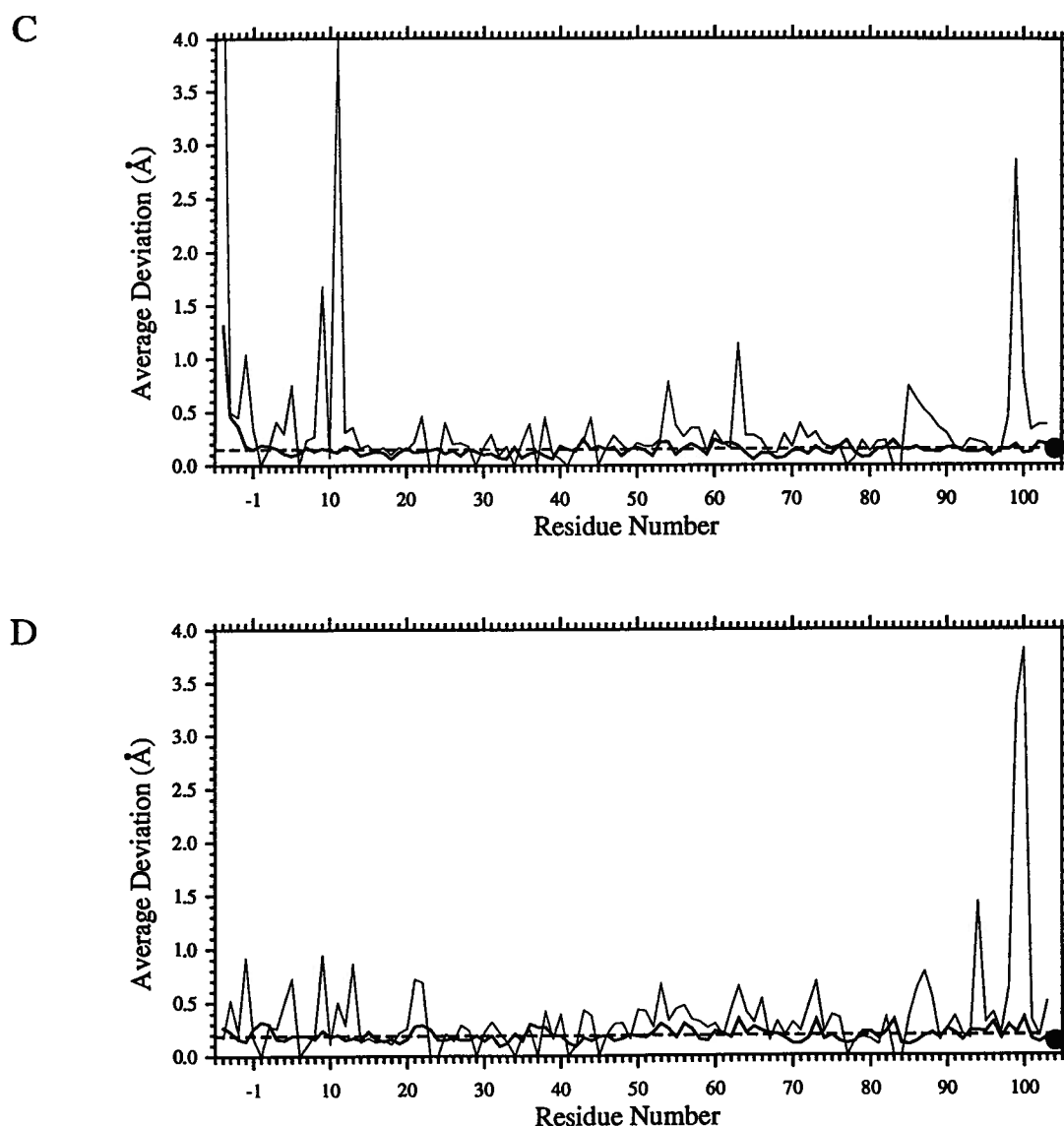
Figure 4.24: continued. Plots of average positional deviations from the wild-type yeast iso-1 cytochrome *c* structure for the (a) L85C, (b) L85F, (c) L85M and (d) L94S mutant proteins. Thick lines indicate average deviations of main chain atoms while the thin lines indicate average deviations of the equivalent side chain atoms. In each diagram the filled circle at residue position 104 represents the average positional deviation of the heme group. The plotted horizontal dashed line represents the average positional deviation for all main chain atoms.

examined between the four mutant proteins studied and wild-type yeast iso-1 cytochrome *c* were overall heme group geometry (Table 4.17) and solvent exposure (Table 4.18). Additional conformational differences are observed about substituted residues in each mutant cytochrome *c* and these are discussed below in subsequent sections.

4.3.2   Structure of L85C cytochrome c

Examination of the amino acid side chains directly in the mutation site reveals that the χ_1 torsion angle of Cys85 (-94°) is similar to that of the normally resident Leu85 in the wild-type structure (-95°). The SG atom of Cys85 is positioned close to the aromatic ring of Phe82, being only 5.0 Å from the ring centroid and 3.7 Å from the CZ atom. Thus, this sulfur atom forms a favorable nonpolar interaction with the edge of the Phe82 aromatic ring of the type described by Reid *et al.* (1985). The sulfur atom of Cys85 also forms a hydrogen bond (d = 2.8 Å) to a new water molecule, Wat227, which occupies a position similar to that of the CD2 atom of Leu85 in the wild-type protein. This latter group constitutes the branch of the leucine side chain projected toward the surface of the protein (Figure 4.25). Although the smaller size of a cysteine side chain at residue 85 might be expected to result in the formation of a direct interaction between the side chains of Arg13 and Asp90, as observed in the F82Y/L85A and L85A mutant proteins (Chapter 3), this is prevented in the current structure by the intervening Wat227 and the positioning of the sulfhydryl moiety of Cys85 (Figure 4.25), which together provide comparable steric bulk to that of the normally resident leucine side chain in the wild-type protein.

Although there is no corresponding replacement for the buried CD1 carbon atom of Leu85 in the L85C mutant protein and therefore no spatial constraint preventing reorientation of the side chain of Leu94, this latter residue does not exhibit the conformational rearrangement seen in the L85A mutant protein (Chapter 3). This may arise since the sulfur atom of Cys85 effectively excludes bulk solvent from the hydrophobic interior of the protein unlike the solvent channel formed when an alanine residue is substituted at this location. This would suggest that

Table 4.17: Heme geometry of L85C, L85F, L85M, L94S and wild-type yeast iso-1 cytochromes *c*

	Wild-type	L85C	L85F	L85M	L94S

1. Angular deviations (°) between the pyrrole nitrogen plane normal and the four individual pyrrole ring plane normals and the heme coordinate bonds.

	Wild-type	L85C	L85F	L85M	L94S
A	9.4	11.4	10.4	11.5	14.1
B	11.1	10.5	10.0	10.7	11.1
C	8.8	9.0	13.3	9.1	11.6
D	8.1	8.3	8.1	9.4	12.5
Fe - His18 NE2	2.2	3.9	3.5	4.2	4.6
Fe - Met80 SD	4.9	3.9	0.9	3.5	1.9

2. Angular deviations (°) between the porphyrin ring plane normal and the four pyrrole ring plane normals, the pyrrole nitrogen plane normal and the heme coordinate bonds.

	Wild-type	L85C	L85F	L85M	L94S
A	6.7	8.3	6.4	8.7	7.9
B	11.9	11.8	12.1	12.2	12.5
C	9.8	9.4	11.5	9.2	11.4
D	6.0	5.8	4.0	7.3	6.3
NNNN	2.6	3.3	4.5	3.3	6.2
Fe - His18 NE2	3.2	2.4	1.8	6.7	2.9
Fe - Met80 SD	7.5	7.1	5.1	6.7	5.7

3. Bond distances (Å) between the heme iron atom and its six ligands.

	Wild-type	L85C	L85F	L85M	L94S
His18 NE2	1.98	1.98	2.00	1.97	1.97
Met80 SD	2.36	2.28	2.43	2.28	2.34
Heme NA	1.97	2.01	2.01	1.98	1.99
Heme NB	2.00	2.00	2.01	2.03	2.03
Heme NC	1.99	2.01	1.98	2.01	2.01
Heme ND	2.01	2.06	2.05	2.04	2.04

The pyrrole nitrogen plane is defined by the four pyrrole nitrogens of the heme group. The four pyrrole ring planes are each defined by the five atoms of the ring and the first carbon atom attached to each of the four carbons of the ring. The porphyrin ring is defined by the five atoms in each of the four pyrrole rings, the four bridging methine carbon atoms, the first carbon atom of each of the eight side chains of the heme and the central iron atom of the heme. The heme atom nomenclature used in this table follows the conventions of the Protein Data Bank (see Figure 1.2).

Table 4.18: Heme solvent accessibility in L85C, L85F, L85M, L94S and wild-type yeast iso-1 cytochromes c

		Yeast iso-1 cytochrome c structure				
		Wild-type	L85C	L85F	L85M	L94S
1.	Solvent accessible heme atoms and surface area exposed (Å^2)					
	CHD	2.9	3.1	3.6	3.3	0.0
	CMC	9.2	9.8	9.7	10.4	9.7
	CAC	3.4	3.5	2.3	3.2	4.3
	CBC	20.1	19.5	20.2	19.4	20.9
	CMD	10.8	11.1	6.8	10.5	7.7
2.	Total heme exposure (Å^2) .	46.4	47.0	42.6	46.8	42.6
3.	Total heme surface (Å^2)	513.1	515.8	511.7	516.2	514.5
4.	% heme surface area exposed	9.0	9.1	8.3	9.1	8.3

Solvent exposure was determined by the method of Connolly (1983) with a probe sphere having a 1.4 Å radius.

Figure 4.25: Stereo diagrams showing two views of the region about Cys85 in the L85C mutant protein. In each diagram the structure of the wild-type protein (thick lines) has been superimposed on the mutant protein structure (thin lines). A water molecule (Wat227) which forms a hydrogen bond (d = 2.8 Å; dashed line) to the sulfur atom of Cys85 is depicted by an asterisk.

Leu94 side chain reorientation in the L85A protein is not a result of simple spatial compensation caused by the decrease in side chain size at residue 85, but arises from a need to minimize the exposure of its hydrophobic side chain to bulk solvent.

Other conformational changes in the vicinity of the mutation site involve Gly83 and Leu9 (Figure 4.24a). For Gly83, the average main chain deviation observed is 0.31 Å, which is more than two times the overall average deviation of 0.13 Å between the L85C and wild-type proteins (Table 4.16). It would seem that Gly83, being part of a flexible double glycine sequence which can readily adopt alternate conformations, is responding to the need to attain an optimal packing arrangement in the vicinity of the mutation site. Such compensatory behavior by Gly83 has been previously observed in the F82S (Louie *et al.*, 1988b) and F82G (Louie & Brayer, 1989) mutant proteins. In the wild-type iso-1 cytochrome *c* structure, the side chain of Leu9 is located at the protein surface and exhibits two distinct conformations (Louie & Brayer, 1990). The side chain of Leu9 in the L85C structure adopts neither of these, but has a conformation (χ_1 = -80°; χ_2 = 153°) which resembles that of Leu9 in L85A cytochrome *c* (χ_1 = -70°; χ_2 = 177°; Chapter 3). In this alternate conformation, the side chain of Leu9 is farther away from the newly bound Wat227 than would be the case if this residue were to adopt either of the conformations observed in the wild-type protein. This suggests that reorientation of the side chain of Leu9 arises in order to decrease the interaction of this aliphatic side chain with Wat227.

4.3.3 Structure of L85F cytochrome c

Introduction of a phenylalanine residue at position 85 allows the formation of a direct aromatic ring to aromatic ring interaction with Phe82. This occurs between the edge of the phenyl group of Phe82 and the face of the Phe85 aromatic ring (Figure 4.26), with the CZ atom of Phe82 being 4.0 Å from the centroid of the Phe85 ring. The centroids of these aromatic rings are 5.4 Å apart and the normals of their rings form an angle of 57°; values consistent with energetically favorable aromatic ring to aromatic ring interactions (Burley & Petsko, 1985; Singh & Thornton, 1985). Notably, the larger size of the phenylalanine replacement of Leu85
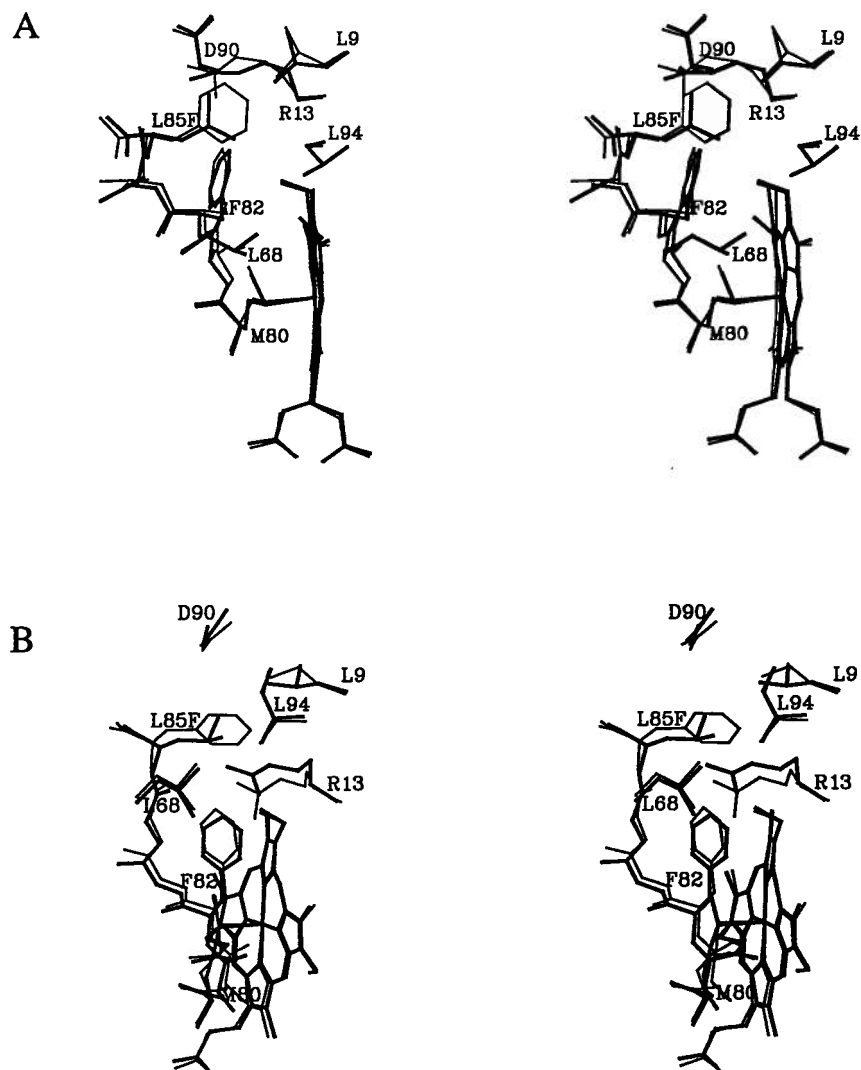
Figure 4.26: Stereo diagrams showing two views of the region about Phe85 in the L85F mutant protein. In each diagram the structure of the wild-type protein (thick lines) has been superimposed on the mutant protein structure (thin lines).

causes the α-carbon of Phe85 to be shifted toward the protein surface ($\Delta d = 0.4$ Å), requiring compensating adjustments in the conformations of nearby polypeptide chain, including the main chain atoms of residues 81 through 86 (Figures 4.24b and 4.26). Surprisingly, these shifts do not affect the orientation of the Phe82 side chain ($\Delta\chi_1 = 5°$; $\Delta\chi_2 = 4°$). Retention of side chain torsional angles in combination with the displacement of main chain segments is not an uncommon response to the mutation-induced repacking of protein interiors (Baldwin *et al.*, 1993).

Of the residue side chains which pack directly against the side chain of residue 85, Leu9 and Arg13 undergo the largest shifts upon mutation of Leu85 to phenylalanine (Figure 4.26). Leu9 assumes a novel side chain conformation not seen in either the wild-type protein or in other mutants with replacements of Leu85. Other nearby residues such as Leu68, Asp90 and Leu94 occupy positions similar to those seen in the wild-type protein (Figure 4.26).

4.3.4 Structure of L85M cytochrome c

The χ_1 torsion angle of Met85 exhibits a conformation (-154°) which differs from all other replacements at this position. If Met85 were to adopt a χ_1 conformation similar to that of Leu85 in the wild-type protein ($\chi_1 = -95°$), the SD atom of this residue would form an unfavorable interaction with the π-electron cloud of the aromatic ring of Phe82 (Reid *et al.*, 1985). Thus the Met85 orientation observed apparently arises from the need to position the delta sulfur atom of this residue away from the aromatic ring of Phe82. This is in contrast to the SG atom of Cys85 in the L85C mutant protein which makes an energetically favorable interaction with the edge of the side chain of Phe82. The added side chain length of Met85 also impinges upon the region occupied by Leu9 in the wild-type protein. This potential conflict causes Leu9 to adopt the conformation observed in Figure 4.27 ($\chi_1 = -80°$; $\chi_2 = 164°$) which is similar to that seen in the L85C and L85A mutant proteins.
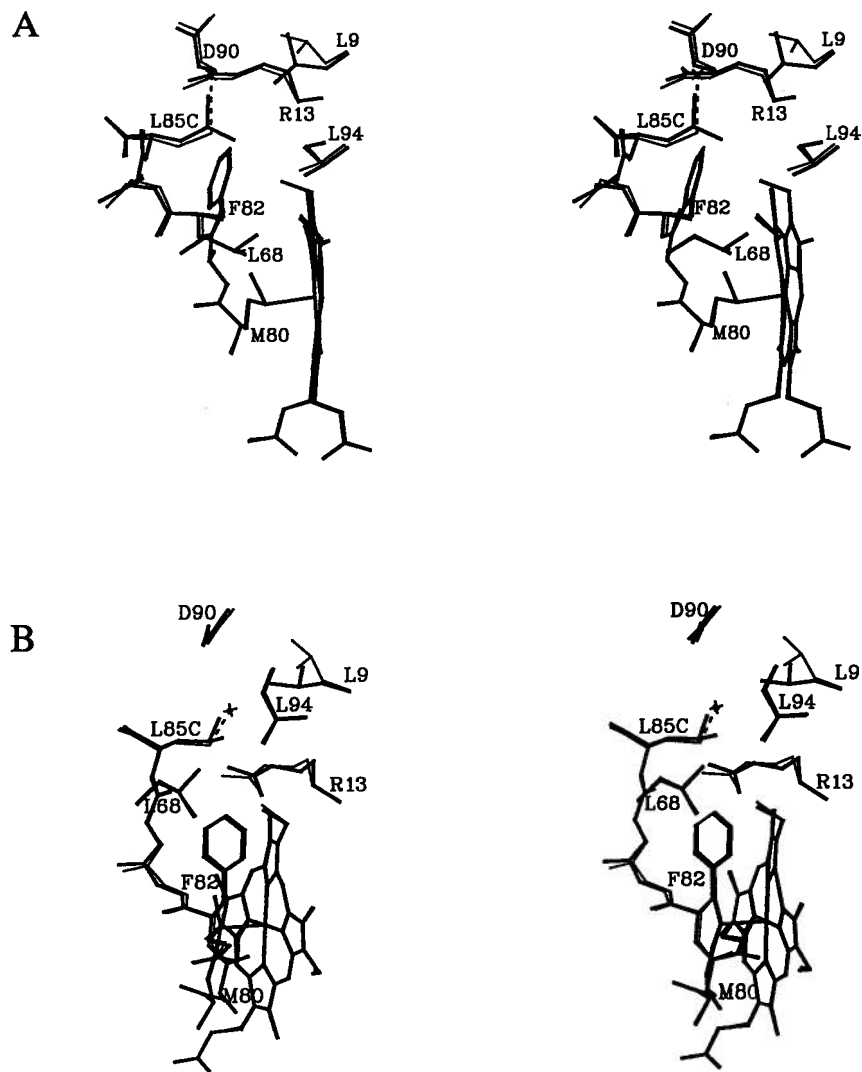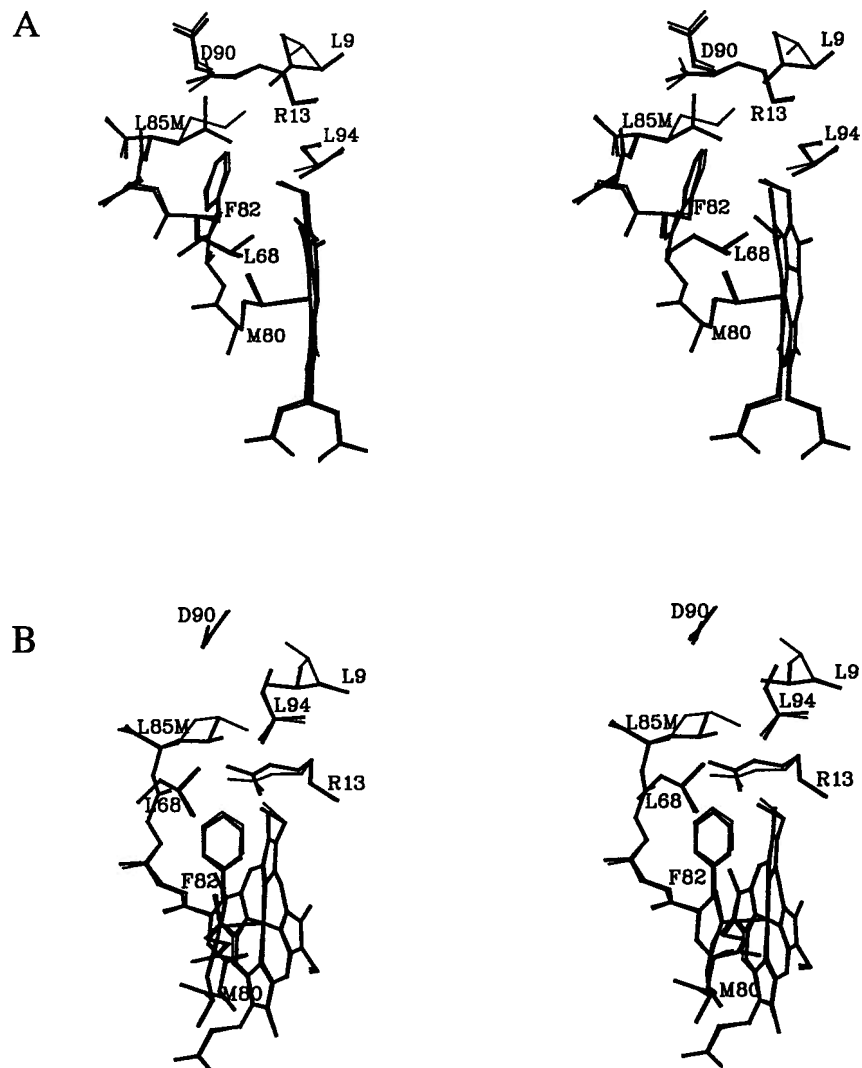
Figure 4.27: Stereo diagrams showing two views of the region about Met85 in the L85M mutant protein. In each diagram the structure of the wild-type protein (thick lines) has been superimposed on the mutant protein structure (thin lines).

4.3.5 Structure of L94S cytochrome c

In wild-type yeast iso-1 cytochrome *c* the side chain of Leu94 is buried in the hydrophobic heme pocket at the crossover point between the N (residues 2-14) and C (residues 87-102) terminal helices (Figure 4.28). To accommodate the hydrophilic nature of a serine side chain at this position, a novel conformation is adopted. The χ_1 torsion angle of Ser94 rotates by -135° with respect to that of Leu94, placing the OG atom in a position to form bifurcated hydrogen bonds to the main chain carbonyl atoms of Asp90 and Arg91 (Figure 4.28). Despite these new interactions, both of these carbonyl groups retain their hydrogen bonds to the main chain amide groups of Leu94 and Ile95, respectively. Conformations of serine residues in α-helices which allow hydrogen bonding between the side chain hydroxyl group and main chain carbonyl oxygen atoms of the previous helical turn are common when these residues are buried in the hydrophobic interiors of proteins (Gray & Matthews, 1984).

In response to the movement of Ser94 away from the interior of the protein, the side chain of Leu98 shifts toward the region vacated by residue 94 (Figure 4.28), with the CD1 atom of this residue moving by 1.3 Å. The Leu9 side chain orientation seen in this mutant protein (χ_1 = -129°; χ_2 = 137°) corresponds to an alternative conformation of this residue seen in the wild-type protein (χ_1 = -111°; χ_2 = 123°). It appears that this conformation of Leu9 is favored to avoid direct contact with the hydroxyl group of Ser94.

4.4 Discussion

4.4.1 Structural consequences of residue 85 and 94 mutations

As summarized in Table 4.19, significant structural changes observed in mutants of yeast iso-1 cytochrome *c* with replacements of the conserved leucines at positions 85 and 94 are localized to the vicinity of the mutation sites. These appear to arise primarily as a consequence of the spatial requirements of the new side chains and the need to optimize the new intramolecular interactions formed. For example both Cys85 and Phe85 are oriented to form energetically
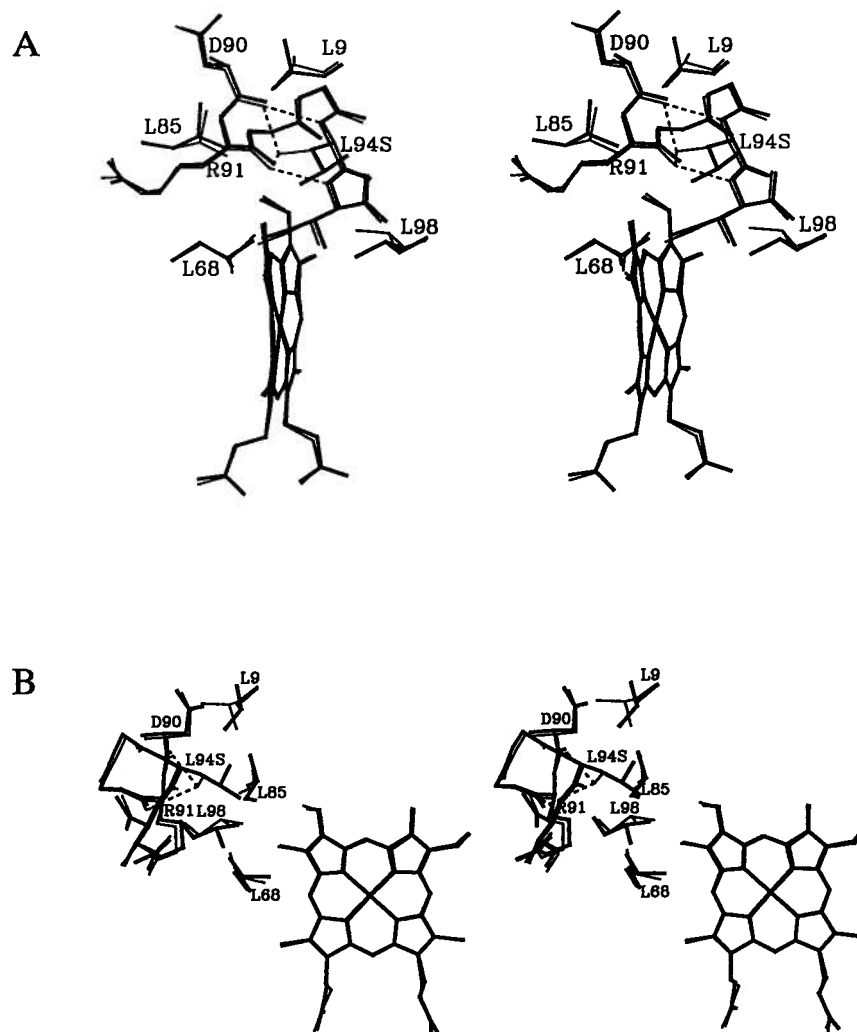
Figure 4.28: Stereo diagrams showing two views of the region about Ser94 in the L94S mutant protein. The structure of the wild-type protein has been superimposed and is shown with thick lines while the mutant protein structure is depicted by thin lines. Altered side chain conformations for Leu9 and Leu98 are clearly evident. Hydrogen bonds formed between the hydroxyl group of Ser94 and the main chain carbonyl oxygen atoms of Asp90 and Arg91 are represented by dashed lines. Intra-helical hydrogen bonds formed between these carbonyl groups and the amide nitrogen atoms of Leu94 and Ile95 are also represented by dashed lines.

Table 4.19: Summary of positional differences observed between the L85C, L85F, L85M and L94S mutant yeast iso-1 cytochromes c and the wild-type protein

L85C	L85F	L85M	L94S
1. Cys85 side chain interacts with edge of Phe82 aromatic ring	1. Phe82 and Phe85 side chains form an aromatic ring to aromatic ring interaction	1. Met85 adopts a conformation to prevent contact of SD atom with Phe82 π-electron cloud	1. Ser94 side chain hydrogen bonds to Asp90 and Arg91 main chain carbonyls
2. A new water molecule is bound in the mutation site	2. Main chain spanning residues 81 through 86 undergoes a positional shift	2. Leu9 side chain adopts a new conformation	2. Leu9 shifts away from Ser94 hydroxyl group
3. Leu9 side chain shifts away from newly bound water	3. Leu9 and Arg13 side chains adopt new conformations		3. Leu98 side chain adopts a new conformation
4. Gly83 adopts a new conformation			

favorable interactions with the edge of the aromatic ring of Phe82. The conformation of Cys85 is such that the SG atom of this residue interacts with the edge of the aromatic ring of Phe82 (Reid *et al.*, 1985) while for Phe85, an edge-face interaction with Phe82 is introduced (Burley & Petsko, 1985; Singh & Thornton, 1985). A similar perpendicular edge-face interaction between two phenylalanine rings was recently noted in a mutant of T4 lysozyme and resulted in the stabilization of that protein (Anderson *et al.*, 1993). Although the precise geometries of these two interactions are somewhat different, it is likely that this interaction in L85F cytochrome *c* would have a similar stabilizing effect. In contrast, in the L85M mutant protein, Met85 adopts a more distant conformation which prevents a potentially unfavorable interaction of its SD atom and the π-electron cloud of Phe82 (Reid *et al.*, 1985). Finally, the side chain of Ser94 in the L94S mutant protein adopts a conformation which allows interaction with two main chain carbonyl groups of the C-terminal α-helix (residues 90 and 91), thereby satisfying the hydrogen bonding potential of the Ser94 hydroxyl group.

4.4.2 Effects on reduction potential

An essential factor controlling cytochrome *c* reduction potential is the dielectric constant of the heme pocket (Kassner, 1973; Louie & Brayer, 1989; Moore & Pettigrew, 1990). This is dependent in large part on both the solvent exposure of the heme group and the polarity of those residues in the immediate heme environment. For example, the reduction potential of yeast iso-1 cytochrome *c* can be significantly decreased by an increase in either the solvent exposure of the heme moiety (Louie *et al.*, 1988b) or the polarity of protein substituents packing directly against the heme plane (Louie & Brayer, 1989). However, this effect rapidly drops off with distance so that the introduction of polar groups such as hydroxyl moieties or internal water molecules at distances greater than 5 Å from the heme porphyrin plane do not result in a significant decrease in reduction potential (Chapter 3).

The reduction potential of the L85C mutant protein is very similar to that of wild-type yeast iso-1 cytochrome *c* (Table 4.20), despite the introduction of a polar side chain and a

Table 4.20: Reduction potentials for L85C, L85F, L85M, L94S and wild-type yeast iso-1 cytochromes *c*

Cytochrome *c*	E_m (mV)
Wild-type	290±2
L85A	285±3
L85C	288±3
L85F	285±2
L85M	284±2
L94S	280±2

Experimental conditions were: 25°C, pH 6.0 and $\mu = 0.1$ M. Values are listed relative to a standard hydrogen electrode reference. The first value listed was taken from Rafferty *et al.* (1990) while the values for the mutant proteins have resulted from collaborative work performed in conjunction with this thesis and published in Lo *et al.* (1995c) and Guillemette *et al.* (1994).

newly bound water molecule (Figure 4.25). Examination of this structure shows that the sulfur atom of Cys85 is pointed toward the protein surface and is distant from the heme porphyrin ring (d = 7.1 Å), while Wat227 is located at an even greater distance (d = 9.1 Å). Thus these new features of the L85C mutant protein do not change the dielectric constant in the direct vicinity of the heme group. A further factor which preserves the hydrophobic pocket about the heme is the manner in which the orientation of the Cys85 side chain excludes entrance of bulk solvent into this region.

Replacement of Leu85 by either phenylalanine or methionine also does not result in reduction potentials which are significantly different from that of the wild-type protein (Table 4.20). This

is to be expected given that the substitutions are hydrophobic and the solvent exposure of the heme groups in these two proteins do not differ greatly from the wild-type protein (Table 4.18). These results indicate that conformational changes occurring to accommodate these amino acid replacements do not significantly impact the heme environment.

Replacement of Leu94 by a serine does result in a modest decrease in the reduction potential of cytochrome c ($\Delta E_m = -10$ mV; Table 4.20). This effect is unlikely to arise from changes in side chain polarity since the gamma oxygen atom of Ser94 is distant from the heme porphyrin plane (d = 7.4 Å). Temperature dependence measurements (data not shown) reveal that the decreased reduction potential of L94S cytochrome c is more the result of changes in the entropy of reduction, ΔS°_{cyt} (-12.6 e.u. in L94S; -9.1 e.u. in wild-type), rather than changes in the enthalpic contribution, ΔH° (-14.9 kcal/mol in L94S; -14.0 kcal/mol in wild-type). Two factors proposed to affect the entropy of reduction are the reordering of solvent around the polypeptide chain (Taniguchi *et al.*, 1980) and alteration of side chain packing in the hydrophobic core (Murphy *et al.*, 1992). It is possible that either or both of these factors may play a role in the decreased reduction potential of the L94S mutant protein given the structural changes observed.

4.4.3 Functional alterations

Earlier studies have implicated residue 85 in the formation of bimolecular electron transfer complexes involving cytochrome c (Pielak *et al.*, 1988; Burch *et al.*, 1990; Nocek *et al.*, 1991). However, a recent examination of model complexes formed between cytochrome c and cytochrome b_5 shows that Leu85 is not likely to reside at the interface between these two proteins (Northrup *et al.*, 1993; Guillemette *et al.*, 1994). Furthermore, measurements of the rate of electron transfer in this complex have revealed no significant changes when Leu85 of cytochrome c is replaced by either cysteine, phenylalanine or methionine (Guillemette *et al.*, 1994). Our results support the conclusion that Leu85 is not a major factor in bimolecular complexation with cytochrome b_5, given the absence of functional effects in light of the significant protein surface changes observed for the L85C, L85F and L85M mutant proteins.

In the case of Leu94 in cytochrome *c*, mutation to serine has been found to significantly decrease the growth of yeast (Hampsey *et al.*, 1986; Fredericks & Pielak, 1993). These effects have been ascribed to both defective formation of the hydrophobic heme pocket (Hampsey *et al.*, 1986) and alteration of the nature of the interaction between the N (residues 2-14) and C-terminal (residues 87-102) α-helices of cytochrome *c* (Fredericks & Pielak, 1993). Our results show that the L94S mutation does have a direct effect on the hydrophobic heme pocket, precipitating structural changes in the adjacent conserved leucine cluster and the hydrophobic internal cavity. However, the N and C-terminal helices which intersect in a nearly perpendicular manner (Figure 4.23) and appear to be an essential component in the folding of cytochrome *c* (Roder *et al.*, 1988) are unaffected (Figures 4.24 and 4.28) by the L94S mutation in terms of structural integrity and orientation. These results show that the yeast growth rate alterations caused by this mutation are most likely the result of disruption of the heme pocket region.

A study of a mutagenic library has also suggested that the large number of substitutions observed at Leu94 and at the adjacent Tyr97 are likely accommodated by shifts in the position of the interacting N and C-terminal helices (Fredericks & Pielak, 1993). Our results show that at least in the case of the L94S mutant protein, no such structural change is observed. It is likely that the presence of a cluster of leucine side chains in this region of the protein, including Leu9, Leu68, Leu85, Leu94 and Leu98, in conjunction with a nearby internal cavity, provide sufficient structural plasticity such that any of the mutant side chains introduced can be accommodated without shifts in the relative orientations of these two helices.

4.4.4 Hydrophobic internal cavity fluctuations

As illustrated in Figure 4.29, a large internal cavity is found in yeast iso-1 cytochrome *c*, bounded by the side chains of Leu32, Ile35, Met64 and Leu98, and one edge of the heme group (Louie & Brayer, 1990). There are no potential hydrogen bonding partners on the cavity surface and no water molecules are observed to be present. This cavity can be eliminated by the replacement of Leu98 by a methionine residue (Murphy *et al.*, 1992) or by a positional shift
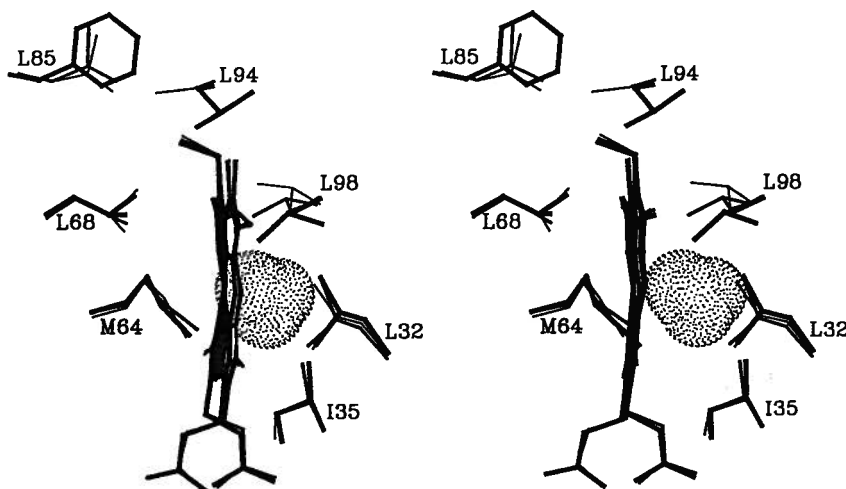
Figure 4.29: A stereo diagram showing the location of the hydrophobic internal cavity (dot surface) found in wild-type iso-1 cytochrome *c*. The heme group and nearby side chains that define the outer limits of this cavity in the L85F (thick lines) and L94S (thin lines) mutant proteins have been superimposed on the structure of the wild-type protein (medium lines). The different conformations observed for the Leu98 side chain are largely responsible for determining the size of this internal cavity. In the L85F mutant protein, the Leu98 side chain moves into the internal cavity, effectively eliminating this feature. In the L94S mutant protein, the Leu98 side chain moves toward the side chain of Ser94, causing an increase in cavity size. The volume and surface area of this cavity in a wide range of mutant proteins is tabulated in Table 4.21.

of the side chain of Leu98 (Murphy *et al.*, 1993). A tabulation of the volume and surface area of this hydrophobic cavity for a series of mutant proteins having replacements of Leu85 and Leu94, as well as Phe82, is presented in Table 4.21.

As evident in Table 4.21 there is a trend for the size of the internal cavity to be affected by volumetric changes brought about by mutagenesis, even if the site of mutation is not immediately adjacent to the cavity wall. For example, mutations in which one residue is replaced by a larger one (F82Y, L85F) tend to eliminate this cavity. Conversely, substitution of a smaller residue for the native amino acid (F82G, F82S, L85A, L94S) tends to cause an increase in cavity

Table 4.21: Surface area and volume of the hydrophobic internal cavity in mutant and wild-type yeast iso-1 cytochromes *c*

Protein	Surface area (Å^2)	Volume (Å^3)
Wild-type	40.4	35
F82G	54.1	42
F82S	50.0	40
F82Y[†]	—	—
F82Y/L85A	25.8	15
L85A	47.8	40
L85C[†]	—	—
L85F[†]	—	—
L85M	44.4	31
L94S	72.1	56

Surface areas and cavity volumes were calculated by the methods of Connolly (1983, 1985) with probe spheres of radius 1.4 Å and 1.2 Å, respectively. The values for surface areas and volumes are estimated to have errors of ± 5.0 Å^2 and ± 5 Å^3, respectively. The structure of the wild-type protein was from Louie & Brayer (1990); the F82G mutant from Louie & Brayer (1989); the F82S mutant from Louie *et al.* (1988b); and the F82Y, F82Y/L85A and L85A mutants from Chapter 3.

[†]no cavity could be detected with a 1.4 Å radius probe sphere.

size. Furthermore, mutation to a similar sized (L85M) residue seems to help maintain the size of the cavity. Although the behavior of the F82Y/L85A and L85C mutants would seem to contradict these trends, it must be realized that newly bound water molecules are introduced either into the protein interior (F82Y/L85A; Chapter 3) or onto the protein surface (L85C; Figure 4.25) in these mutants, causing a net increase in steric bulk.

The position of the side chain of Leu98 seems in large part to determine cavity size, with even small shifts of this residue having significant effects. In some cases, this dependence can be readily explained by changes in immediately adjacent residues such as in the L94S mutant protein (see Figure 4.29). However, in other mutant proteins, the cause for a positional shift in Leu98 and a subsequent change in cavity size is not as obvious. It is likely that small, cumulative changes in the positions of both main chain and side chain atoms result from the introduced mutations, and that there are subtle structural strains arising from these changes. It is possible that the combination of a hydrophobic internal cavity and the presence of the nearby flexible leucine cluster composed of not only Leu98, but also Leu9, Leu68, Leu85 and Leu94, can act as a structural buffer in these cases.

Previous studies of residue substitutions resulting in a decrease in side chain size can provide some insight into the current structural results. For example, such mutations in a hydrophobic protein core can result in either the creation of internal cavities (Eriksson *et al.*, 1992) or the contraction of the protein around the affected region (Katz & Kossiakoff, 1990; McRee *et al.*, 1990). From our results, we observe that for the internal L94S cytochrome c mutant, the nearby internal cavity has been enlarged by the largest amount (Table 4.21) without contraction of the protein, indicating that the immediate region has considerable structural rigidity. In contrast, the introduction of size decreasing mutations at protein surfaces can result in the reorganization of the local solvent structure around newly available hydrogen bonding protein moieties (Katz & Kossiakoff, 1990; Nair *et al.*, 1991; Nair & Christianson, 1993) or a combination of positional shifts in nearby side chains with the introduction of bound solvent molecules (Bone *et al.*, 1989; Varadarajan & Richards, 1992). While the former situation applies in the case of the L85C

cytochrome c mutant, a unique scenario was observed in the L85A mutant protein (Chapter 3). Without compensating structural changes, this latter mutation would result in the creation of a hydrophobic invagination exposed to bulk solvent. The presence of the flexible leucine cluster in this region of the protein allows compensatory adjustments which effectively exclude solvent from the hydrophobic protein interior. Although the effect of these adjustments increases the size of the internal cavity of iso-1 cytochrome c, the energetic cost involved appears to be adequately offset by the gain from preserving the hydrophobic environment of the protein interior. These examples show that the response to structurally disruptive mutations will vary depending on the rigidity of the protein backbone and the flexibility of nearby side chains.

Overall, our results suggest that the conserved leucine cluster found in cytochrome c along with an internal hydrophobic cavity allows this protein to retain a measure of conformational flexibility. Apart from an ability to adapt to mutations, it is also conceivable that these two features have a role in cytochrome c function from the standpoint of providing the flexibility to assist in the structural switch of this protein between oxidation states (Berghuis & Brayer, 1992). Many of those residues affected in an oxidation state dependent manner are located adjacent to the leucine cluster region, as well as the nearby internal hydrophobic cavity.

Chapter 5

Replacement of the Invariant Phenylalanine 82 in Cytochrome c by Aliphatic Residues

5.1 Introduction

The previous two chapters have dealt with the potential role of Phe82 and Leu85 in forming contact face interactions, as well as looking at the contribution of Leu85 to an internal hydrophobic leucine cluster and a related internal hydrophobic cavity. As part of this latter study Leu94 was also investigated since it contributes to both the leucine cluster and cavity structures in addition to being located at the juncture between the N and C-terminal helices of the cytochrome c fold. In the present chapter a closer study is made of the role of Phe82, in particular as this relates to its replacement by large aliphatic amino acids.

As discussed in Chapter 3, Phe82 is a phylogenetically invariant residue in cytochrome c (Hampsey *et al.*, 1988; Moore & Pettigrew, 1990) that plays a role in electron transfer complex formation (Pielak *et al.*, 1985; Michel *et al.*, 1989), electron transfer kinetics (Everest *et al.*, 1991; Hazzard *et al.*, 1992) and heme reduction potential (Rafferty *et al.*, 1990). Previous structural studies have looked at mutant proteins wherein Phe82 was replaced by glycine (Louie & Brayer, 1989), serine (Louie *et al.*, 1988b) or tyrosine (Chapter 3), but as yet these studies have not been extended to replacements by large aliphatic side chains.

Replacement of Phe82 by leucine, methionine or isoleucine leads to mutant proteins that exhibit unique functional properties and it is therefore of considerable interest to be able to correlate structural studies with these data. For example, these mutant proteins all behave differently in their kinetics of electron transfer with cytochrome b_5 (Willie *et al.*, 1993; Guillemette *et al.*, 1994) and cytochrome c peroxidase (Everest *et al.*, 1991; Nocek *et al.*, 1991). Especially

notable is the F82I mutant protein, in which 50× tighter binding with cytochrome *c* oxidase is observed (Michel *et al.*, 1989) along with strikingly different kinetics of electron transfer (Hazzard *et al.*, 1992).

Another aspect of cytochrome *c* function addressed in the present studies involves the reduction potential of cytochrome *c*. All three replacement aliphatic side chains are smaller and of different shape than that of the normally resident phenylalanine, and the substitution of each could be expected to result in the formation of a cavity or even potentially a solvent channel into the heme pocket. This would be expected to produce a concomitant decrease in heme reduction potential. While this result is observed in the F82I mutant protein, albeit to a smaller than expected degree, this is not the case for the F82L and F82M mutant proteins (Rafferty *et al.*, 1990). Thus the question arises as to how the side chains of leucine and methionine, when substituted for Phe82, act to preserve the hydrophobic nature of the heme pocket. The goal of the present chapter is to address this question and others related to the unique features demonstrated by the F82I, F82L and F82M mutants of cytochrome *c*. This work has been submitted for publication as part of Lo & Brayer (1995).

5.2 Experimental Procedures

5.2.1 Crystallization and data collection

Using the conditions detailed in Table 2.3, the F82I and F82M mutant proteins were crystallized by the hanging drop vapour diffusion method, while the F82L mutant protein was crystallized by the free interface diffusion technique. Both of these crystallization methods are described in Section 2.3. All crystallizations of these proteins were aided by seeding with micro-crystals (Leung *et al.*, 1989). Crystals of the F82I and F82M mutant proteins grew isomorphously to those of the wild-type protein and belong to the space group $P4_32_12$, with the cell dimensions listed in Table 5.22.

In contrast, the morphology of the crystals formed by the F82L mutant protein was unique and these crystals were not isomorphous to those found for wild-type yeast iso-1 cytochrome *c*.

Table 5.22: Data collection parameters for F82I, F82L and F82M yeast iso-1 cytochromes *c*

	Iso-1 cytochrome *c* mutant		
Parameter	F82I	F82L	F82M
Space group	$P4_32_12$	$I2_12_12_1$	$P4_32_12$
Cell dimensions (Å)			
a	36.49	62.92	36.52
b	36.49	69.15	36.52
c	136.87	104.26	138.33
Number of reflections collected	13825	13183	8514
Number of unique reflections	6250	5101	3820
Merging R-factor[†]	0.069	0.094	0.134
Resolution (Å)	1.9	2.5	2.1

[†] Merging R-factor $= \dfrac{\sum_{hkl}\sum_{i=1}^{n}|I_{i_{hkl}}-\bar{I}_{hkl}|}{\sum_{hkl}\sum_{i=1}^{n}I_{i_{hkl}}}$

Instead of the normally observed rounded pillow shape found for crystals of the wild-type and related mutant proteins, crystals of the F82L mutant protein were rectangular prisms with sharp well defined edges and faces. It is also notable that F82L mutant protein crystals required considerably more time to grow (nearly 2 years) than those of other mutant proteins. Precession photography and subsequent diffraction data collection indicated that these crystals were of either space group $I222$ or $I2_12_12_1$, with the cell dimensions listed in Table 5.22. Unfortunately, these two orthorhombic body-centered space groups are indistinguishable from one another on the basis of systematic absences, since the absences expected for the 2_1 screw axes of space group $I2_12_12_1$ form a subset of the general absences caused by body-centering in both space groups. It is of interest to note that if one assumes there is one protein molecule per asymmetric unit, a solvent content of ∼72% can be calculated for these crystals (Matthews,

1968). A solvent content of ~44% is expected if the assumption is made that there are two molecules per asymmetric unit. As both of these situations are theoretically possible, each was considered during the structure solution of this protein, as described below.

Diffraction data for the F82I, F82L and F82M mutant proteins were collected on a Rigaku R-AXIS II imaging plate area detector system with incident radiation provided by a RU-300 rotating anode generator operating at 90–100 mA and 50–60 kV, as discussed in Section 2.5.3. Crystals were oscillated through a ϕ angle of 1.0° for each frame, with the X-ray exposure time ranging between 20 and 30 minutes. X-ray intensity data were processed to structure factors following the procedures described in Section 2.5.3 using the R-AXIS II data processing software (Higashi, 1990; Sato *et al.*, 1992). The method of Wilson (1942) was used to put each mutant protein data set on an absolute scale as described in Section 2.5.4.

As illustrated in Figure 5.30, an examination of the diffraction data sets obtained for the F82I, F82L and F82M mutant proteins revealed that the crystals of all three proteins diffracted poorly, having a rapid fall off in intensities with increased resolution. For the F82I and F82M mutant proteins this was likely a consequence of the extremely small size of the crystals that could be grown (Table 2.3) despite numerous crystallization trials to improve on these. A primary factor in successful data collection in these cases was undoubtedly the sensitivity of the R-AXIS II area detector and the availability of a rotating anode X-ray source. As discussed in Section 2.6.3.1, earlier attempts to collect diffraction data sets from crystals of these two mutant proteins using a CAD4 diffractometer with a sealed beam X-ray tube were unsuccessful since the poor quality of the data sets obtained precluded their use in structural refinement.

For the F82L mutant protein, although the best crystal that could be grown was also relatively small, it was of a size comparable to a number of other crystals of mutant iso-1 cytochromes *c* used in structural analyses (Table 2.3). However, this F82L mutant protein crystal diffracted considerably poorer than might be expected at higher resolution. This result may be related to the very open packing of the alternative crystalline lattice of these crystals as discussed in later sections. As shown in Figure 5.30, the completeness of the diffraction data
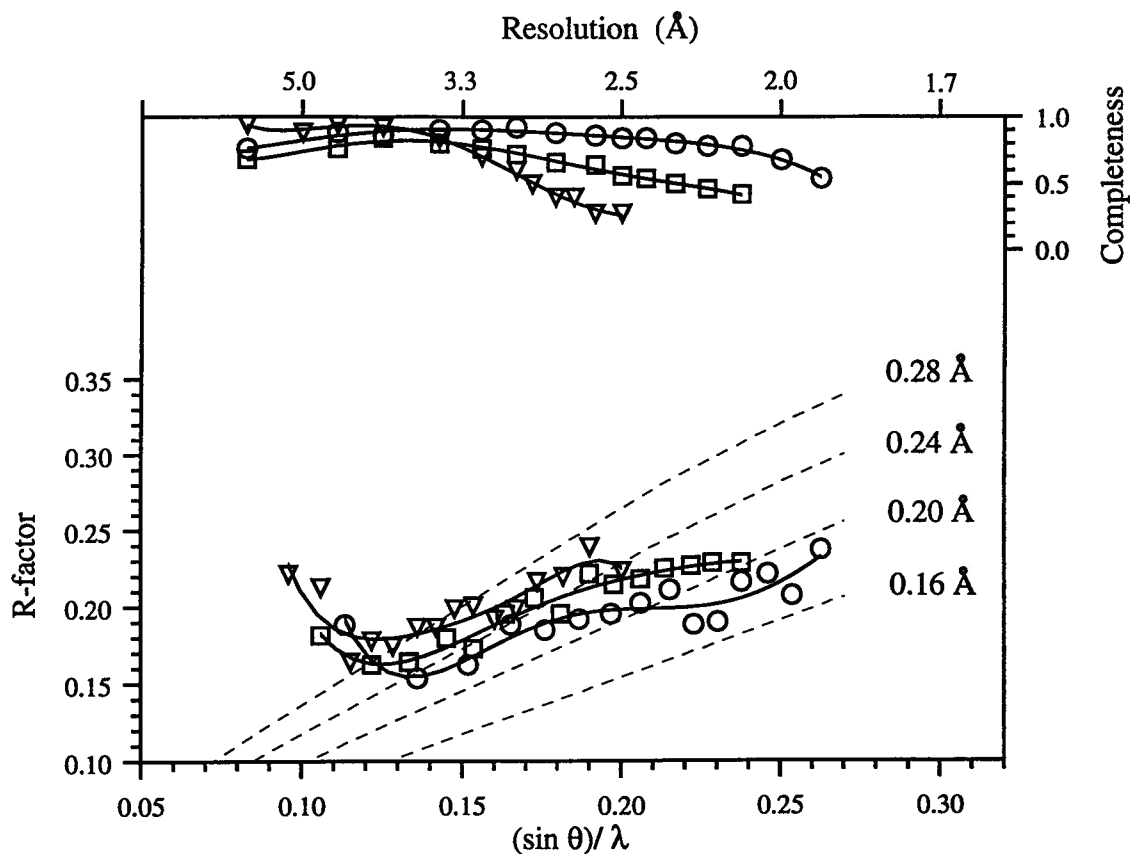
Figure 5.30: A plot of the crystallographic R-factor at the end of refinement as a function of resolution for the F82I (○), F82L (▽) and F82M (□) mutants of yeast iso-1 cytochrome c. The theoretical dependence of R-factor on resolution assuming various levels of r.m.s. error in the atomic positions of the model (Luzzati, 1952) is shown as broken lines. This analysis suggested an overall r.m.s. coordinate error for the mutant structures of between 0.20 and 0.26 Å. The top portion of this figure (axes at top and right) shows the fraction of reflections observed and used in refinement as a function of resolution.

that could be collected for the F82L mutant protein crystal was low beyond 3.0 Å resolution and was only 27.6% for the 2.6–2.5 Å resolution shell. Even though it was limited, the collection of diffraction data for the F82L mutant protein was extended to 2.5 Å resolution in the hope of getting a reasonable definition of the protein structure despite the weakness of the data at high resolution.

5.2.2 Structure solution for the F82L mutant protein using molecular replacement methods

Crystallization of F82L yeast iso-1 cytochrome c in a unique space group necessitated the use of the molecular replacement approach in the solution of the structure of this protein. A brief summary of the theoretical basis for this method is presented in Section 2.4.3.2. The set of molecular replacement programs used in these studies was the MERLOT package (Fitzgerald, 1988) running on a Silicon Graphics 4D/340 workstation.

A key factor in the success of a molecular replacement search is the quality of the initial search model. For mutant proteins with a small number of amino acid substitutions, molecular replacement analyses are facilitated since the search model that can be constructed closely resembles the target structure. The search model used in this case was based on the high resolution structure of wild-type yeast iso-1 cytochrome c (Louie & Brayer, 1990) and consisted of residues -1 through 103, the heme group and four internal water molecules. The four residues at the N-terminus were not included since these are largely disordered in the wild-type structure. The four internal water molecules included in the search model, Wat110, Wat121, Wat166 and Wat168, are highly conserved and can be considered to be an integral part of the protein structure. The side chain at residue 82 was modeled as an alanine since the conformation of a leucine at this position was not known.

The search model was initially centered at the origin of a $P1$ unit cell with $a=b=c=90$ Å and $\alpha=\beta=\gamma=90°$, and structure factors were calculated to 3.0 Å resolution. The thermal factors of all atoms were assumed to be 15.5 Å^2, the same as the average of the thermal factors of

the wild-type iso-1 cytochrome c atoms included in the search model. A fast rotation function search (Crowther, 1972) was carried out with data between 10.0 and 3.5 Å resolution. This search was performed for $0.0° \leq \alpha < 180.0°$ in $2.5°$ steps, $0.0° \leq \beta < 90.0°$ in $1.0°$ steps and $0.0° \leq \gamma < 360.0°$ using $5.0°$ steps. The radius of the search about the Patterson origin was limited to 19.0 Å and origin removal was applied. The highest peak observed was 6.2σ above background, with the next highest peak being of height 4.5σ as illustrated in Figure 5.31. Fine scans to optimize the best rotation function solution obtained (Lattman & Love, 1972) employed $1.0°$ steps spanning $\pm 5.0°$ in each of α, β and γ.

The translation function of Crowther and Blow (1967) was used to determine the translational positioning of the rotationally oriented model of the F82L mutant protein within the crystallographic unit cell. Due to crystallographic symmetry, there are four symmetry related rotation function solutions in each of the two orthorhombic body-centered space groups. The translation function search was applied to each different pair of rotationally related molecules utilizing diffraction data between 10.0 and 3.5 Å resolution. The height of the largest peak from each translation search ranged from 6.5σ to 8.3σ (Figure 5.32). This set of peaks was consistent with the $I2_12_12_1$ space group but not with the $I222$ space group. The correctly oriented and translated search model obtained from this molecular replacement search resulted in a starting crystallographic R-factor of 0.398 for data between 6.0 and 3.0 Å resolution.

Given the large size of the unit cell of the F82L mutant protein crystals ($\sim 72\%$ solvent content if only one molecule is present in the asymmetric unit), the possibility of a second protein molecule being present within the asymmetric unit was carefully assessed during and after the studies discussed above. In particular, application of translation function searches to the next highest peaks resulting from the rotation function search did not produce any additional solutions. Furthermore, a self rotation search was performed to determine if non-crystallographic symmetry elements were present. The results of this analysis were also negative. After the completion of refinement of the F82L mutant protein structure (discussed in Section 5.2.3), a further inspection of $2F_o - F_c$ and $F_o - F_c$ difference electron density maps also failed to show
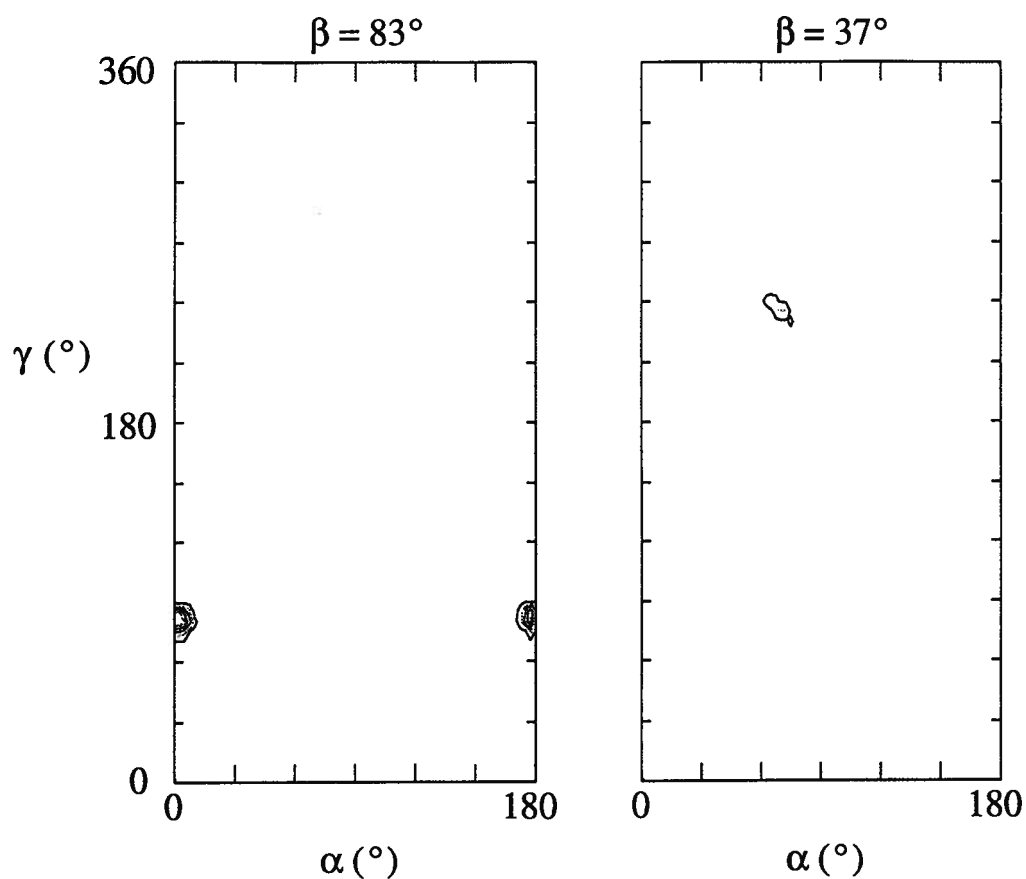
Figure 5.31: Two sections of the rotation function map calculated for F82L iso-1 cytochrome c. The correct solution ($\alpha = 1°$, $\beta = 83°$, $\gamma = 82°$), having a peak height 6.2σ above background, is shown on the left in the map section at $\beta = 83°$. For comparison, on the right is shown the map section having the second highest peak found ($\alpha = 70°$, $\beta = 37°$, $\gamma = 235°$) contoured at the same levels.
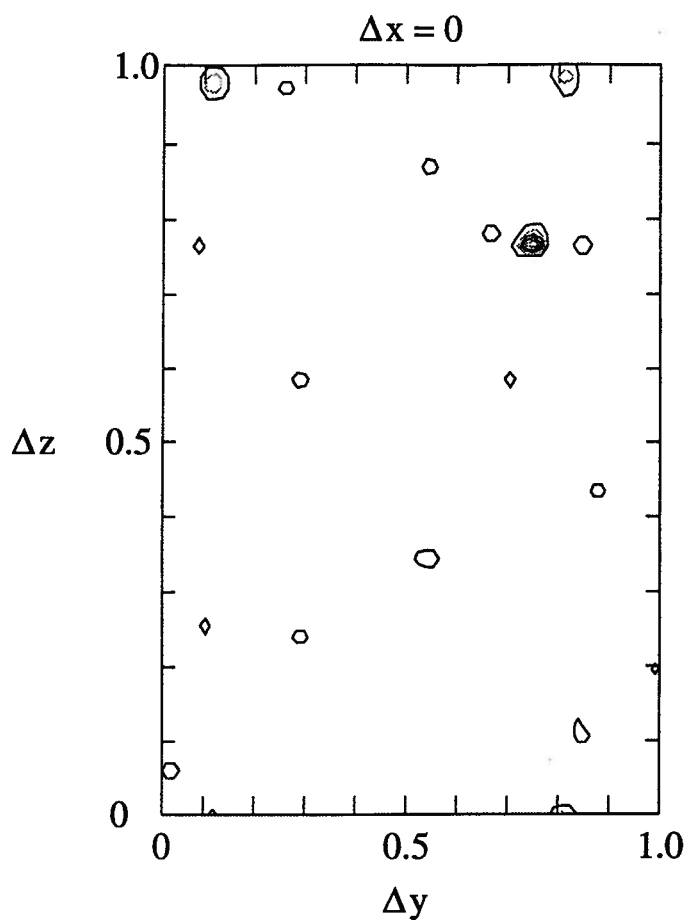
Figure 5.32: A section of a translation function map for F82L iso-1 cytochrome c. The correct translation function solution is represented by the highest peak in the map ($\Delta y = 0.75$, $\Delta z = 0.77$). This section was calculated at $\Delta x = 0$ for two molecules related to each other by a 180° rotation about the a axis. An equivalent solution exists in the section at $\Delta x = 0.50$ representing a molecule translated by half a unit cell length along each of the three orthogonal axes.

any evidence for an additional protein molecule in the asymmetric unit. Additional support for this result was the ability to refine the crystallographic R-factor for this structure to a value comparable to that of the other mutant proteins studied.

5.2.3 Refinement of mutant protein structures

The starting models for the refinement of the F82I and F82M mutant proteins consisted of the high resolution structure of wild-type yeast iso-1 cytochrome c (Louie & Brayer, 1990) in which residue 82 was represented as an alanine. With the exception of those near residue 82, all solvent molecules having isotropic thermal factors less than 50 Å^2 in the wild-type protein structure were included in these two starting models, as was a bound sulphate anion. For the F82L mutant protein, the starting model employed was that oriented in the molecular replacement analysis described in Section 5.2.2 where residue 82 was also represented as an alanine. Initial refinements of the three mutant proteins were carried out by the restrained parameter least-squares method (Hendrickson, 1985) as described in Section 2.6 using the restraint weights listed in Table 2.4.

In the case of the F82I mutant protein, the side chain of Ile82 was built into a $2F_o - F_c$ difference electron density map calculated after 14 cycles of refinement. Interspersed at 5 points during a subsequent 66 cycles of refinement were complete examinations of the entire polypeptide chain and all solvent molecules using omit, $F_o - F_c$ and $2F_o - F_c$ difference electron density maps as a guide, with manual adjustments being made as necessary. An iterative peak searching and refinement procedure was used to identify the likely location of additional water molecules (Tong *et al.*, 1994). Water molecules which refined to isotropic thermal factors greater than 50 Å^2 were eliminated from the refinement model, as were those more than 3.5 Å from hydrogen bond donor or acceptor atoms.

The structural refinements of the F82L and F82M mutant proteins proved to be considerably more difficult. For the F82L mutant protein, clearly defined electron density for the side chain of Leu82 was observed in a $F_o - F_c$ difference electron density map after 24 cycles of refinement

and on this basis this side chain was fit. The four amino-terminal residues which had been left out of the molecular replacement model were added after a further 8 cycles of refinement based on $2F_o - F_c$ and $F_o - F_c$ difference electron density maps. Despite the clarity of the Leu82 side chain in difference electron density maps, problems arose during refinement in maintaining the conformation of this residue within normally accepted geometric restraints. It proved fruitless to correct the conformation of this residue through manual fittings since further refinement simply resulted in a return to the original unacceptable conformation. In addition, the progress of the structural refinement of the F82L mutant protein as a whole proved unsatisfactory as indicated by convergence to a standard crystallographic R-factor of 0.250 after 72 cycles. For the F82M mutant protein, the side chain of Met82 was placed on the basis of a $F_o - F_c$ difference electron density map calculated after 32 cycles of least-squares refinement. Although refinement of the conformation of Met82 was within accepted norms, the overall progress of the refinement of the F82M mutant protein also proved unsatisfactory as indicated by convergence of the crystallographic R-factor to an unacceptably high value of 0.237.

To overcome the problems encountered in the refinement of the F82L and F82M mutant proteins, simulated annealing refinement using the program X-PLOR (Brünger, 1992) was performed. The objective of simulated annealing refinement is to conduct an enhanced search of conformational space while optimizing the fit of the observed and calculated structure factor amplitudes. The major advantage of this technique is that it permits the structural model access to a large number of alternative conformations which are beyond the local potential energy minimum and are not accessible in conventional least-squares refinement. A brief description of this method is presented in Section 2.6.2.

For the F82L and F82M iso-1 cytochrome c structures, the slow-cooling protocol (Brünger, 1990) was employed for simulated annealing refinement. The first step in this process involves the minimization of both structure factor and energy terms to optimize the conformation of the refinement model. In the second step, velocities are assigned to individual atoms based on the kinetic energy that would be present at an arbitrarily high temperature, in this case 2500 K. This

kinetic energy drives the conformational search of the model, allowing large barriers of potential energy to be overcome in the search for a best fit. In the third step, the molecular dynamics search is allowed to continue, with the kinetic energy of the system being periodically decreased in steps of 25 K until an energy representing 300 K is reached. Finally, the structural model is extensively refined to minimize both the crystallographic R-factor and the potential energy function, in effect giving the optimal structure in the local energy minimum. The simulated annealing refinement of the F82L and F82M mutant proteins resulted in significant overall shifts in the positions of atoms in these two structures ($\Delta d = 0.56$ Å for F82L; $\Delta d = 0.60$ Å for F82M). The phases of the calculated structure factors for these structures also underwent significant changes, averaging 32° and 41° for the F82L and F82M structures, respectively. Surprisingly, the overall crystallographic R-factors resulting from the simulated annealing process were found to be only slightly lowered (0.236 for F82L; 0.225 for F82M) from starting values.

Examination of electron density maps showed that despite the small lowering of R-factor observed, a much improved fit of polypeptide chain for both the F82L and F82M mutant proteins was observed after the application of simulated annealing refinement. Of special note was the conformation around Leu82, where a shift in nearby polypeptide chain allowed for an improved fit of this side chain that satisfied all normal stereochemical requirements. As had been hoped, these optimized structural fits allowed conventional restrained parameter least-squares refinement to proceed. Thus each of these two mutant protein structures were subjected to a further 60–70 cycles of refinement, in addition to 4 overall examinations of the complete polypeptide chain to allow for manual adjustment using difference electron density maps, as previously outlined for the F82I mutant protein. These manual interventions were concerned with optimizing the conformations of surface side chains, locating water molecules and adjusting the N-terminal region of these proteins (residues (-2)–(-5)). The final parameters and stereochemistry for the refinement of all three cytochrome c mutant protein structures studied in this chapter are given in Table 5.23.

The two methods described in Section 2.6.3.4 were used to estimate atomic coordinate

Table 5.23: Refinement results and stereochemistry for the F82I, F82L and F82M yeast iso-1 cytochrome c mutant structures

	F82I	F82L	F82M
1. Refinement results			
Resolution range (Å)	6.0–1.9	6.0–2.5	6.0–2.1
Number of observed reflections	5991	4482	3520
Completeness in resolution range (%)	78.3	59.5	61.3
Number of protein atoms	891	891	891
Number of solvent atoms	75	52	76
Average thermal factors (Å^2)			
Protein atoms	19.6	20.9	19.7
Solvent atoms	31.3	32.6	17.6
R-factor	0.188	0.197	0.192

	r.m.s. deviation from ideal values		
2. Stereochemistry of final models			
Distances (Å)			
Bond (1-2)	0.019	0.019	0.019
Angle (1-3)	0.042	0.051	0.042
Planar (1-4)	0.052	0.057	0.051
Planes (Å)	0.013	0.015	0.014
Chiral volumes (Å^3)	0.143	0.202	0.164
Non-bonded contacts (Å)[†]			
Single torsion	0.215	0.229	0.224
Multiple torsion	0.179	0.214	0.211
Possible hydrogen bonds	0.187	0.231	0.227
Torsion angles (°)			
Planar (0° or 180°)	2.3	2.5	2.1
Staggered (±60°,180°)	22.5	28.4	27.6
Orthonormal (±90°)	21.2	22.9	27.1

[†]The r.m.s. deviations from ideality for this class of restraint incorporates a reduction of 0.2 Å from the radius of each atom involved in a contact.

errors for the refined structures obtained. The Luzzati (1952) plot shown in Figure 5.30 gives estimates for overall coordinate errors for the F82I, F82L and F82M mutant proteins of 0.20 Å, 0.26 Å and 0.22 Å, respectively. Evaluation of overall atomic coordinate errors by the method of Cruickshank (1949) results in r.m.s. coordinate errors of 0.13 Å for the F82I structure, 0.18 Å for the F82L structure, and 0.21 Å for the F82M structure.

5.2.4 Direct electrochemistry

As part of the work described in this thesis, the midpoint reduction potential of the F82M mutant of yeast iso-1 cytochrome c was obtained by cyclic voltammetry using the methods of Rafferty *et al.* (1990). However, a detailed discussion of the theory and methodology used in the measurement of this value is beyond the scope of this work and the reader is referred to excellent descriptions of this technique in Rafferty *et al.* (1990) and Burrows *et al.* (1991).

The experimental apparatus used in this experiment was described by Rafferty *et al.* (1990) and the conditions employed are briefly described here. Prior to the measurement of the electrochemical potential of the F82M mutant protein, a gold disk electrode was carefully polished. This electrode was then cleaned by immersion in a solution of 100 mM $NaClO_4$ having 20 mM phosphate buffer and adjusted to pH 6, while cycling a current over a potential range of -1 to 1.2 V through the electrode. The gold surface of the electrode was then modified by immersion in a saturated solution of 4,4'-dithiodipyridine. This treatment promotes the transfer of electrons between the electrode and cytochrome c. A sample of F82M iso-1 cytochrome c (at ~0.4 mM concentration) in a buffer with ionic strength $\mu = 0.1$ M and at pH 6.0 (containing 50 mM KCl and enough sodium phosphate to provide the remaining ionic strength) was used for the determination of electrochemical potential. A voltammogram was obtained at 25°C by scanning a potential range of 44 to 544 mV at a rate of 20 mV s^{-1}. The midpoint reduction potential of the protein was calculated by averaging the peaks from the oxidizing and reducing currents.

Table 5.24: Overall average positional deviations (Å) between wild-type yeast iso-1 cyto-chrome *c* and the F82I, F82L and F82M mutant proteins.

	Iso-1 cytochrome *c* mutant		
Atom groups	F82I	F82L	F82M
All common protein atoms	0.23	0.77	0.63
All main chain atoms	0.15	0.54	0.43
All common side chain atoms	0.33	1.06	0.87
All heme atoms	0.10	0.32	0.43

The three N-terminal residues (Thr(-5) - Phe(-3)) were excluded from these calculations.

5.3 Results

5.3.1 Structural comparison of mutant and wild-type cytochromes c

Prior to a detailed analysis of the F82I, F82L and F82M mutant protein structures, all three were superimposed onto the wild-type yeast iso-1 cytochrome *c* structure using a least-squares fitting procedure that included all α-carbon atoms in the polypeptide chain with the exception of the three at the amino-terminal end. As discussed later, these three residues were found to have large positional deviations between these structures. Although the global fold of cytochrome *c* is retained in the mutant proteins (Figure 5.33), it is apparent from Table 5.24 that the main chain atoms of the F82L and F82M mutant proteins have undergone significant conformational changes. Plots of the average positional deviations of residues along the polypeptide chain of the mutant proteins are shown in Figure 5.34. For the F82L and F82M mutant proteins, particularly large positional deviations are observed for the N-terminal residues, Thr(-5) through Lys(-2),

and a number of flexible surface side chains.

5.3.2 Structure of F82I cytochrome c

The longer branch of the substituted Ile82 side chain is directed toward the interior of the protein ($\chi_1 = 66°$; $\chi_2 = 136°$) and resides near the bottom of the pocket normally occupied by the aromatic ring of Phe82. The α-carbon atom of Ile82 is found in a more surface exposed location relative to that of Phe82 and this appears to result in shifts in the flexible Gly83-Gly84 portion of the polypeptide chain ($\Delta d = 0.32$ Å; Figures 5.34a and 5.35). The shorter branch of the Ile82 side chain is projected toward the heme group and makes van der Waals' contact with the CMC methyl group of the heme (d = 3.2 Å). The conformation and geometry of the heme group in the F82I mutant protein is tabulated in Tables 5.24 and 5.25. As indicated in Table 5.26, there is a small increase in the heme solvent exposure in this mutant protein.

5.3.3 Structure of F82L cytochrome c

As shown in Figures 5.34b and 5.36, substitution of leucine for Phe82 results in significant shifts in nearby polypeptide chain backbone ($\Delta d = 0.70$ Å for residues 81–84). Other large main chain shifts occur around Gly23 ($\Delta d = 1.3$ Å for residues 22–23) and Lys54 ($\Delta d = 1.3$ Å for residues 53–54), as well as at the amino ($\Delta d = 5.7$ Å for residues (-5)–(-4)) and carboxy ($\Delta d = 1.0$ Å for residues 102–103) termini. At least some of the shifts in these latter four regions are likely due to alternative crystalline lattice packing interactions formed by the F82L mutant protein as compared to those found in crystals of wild-type yeast iso-1 cytochrome c. This is supported by a crystal packing analysis (Figure 5.37) which shows that three of these polypeptide chain segments do form different lattice interactions while the fourth, the C-terminus of the polypeptide chain, forms lattice interactions in wild-type protein crystals but not in those of the F82L mutant. This packing analysis also shows that large solvent channels are present between the protein molecules in crystals of the F82L mutant protein.

It is not clear what has led to the new space group observed for crystals of the F82L mutant
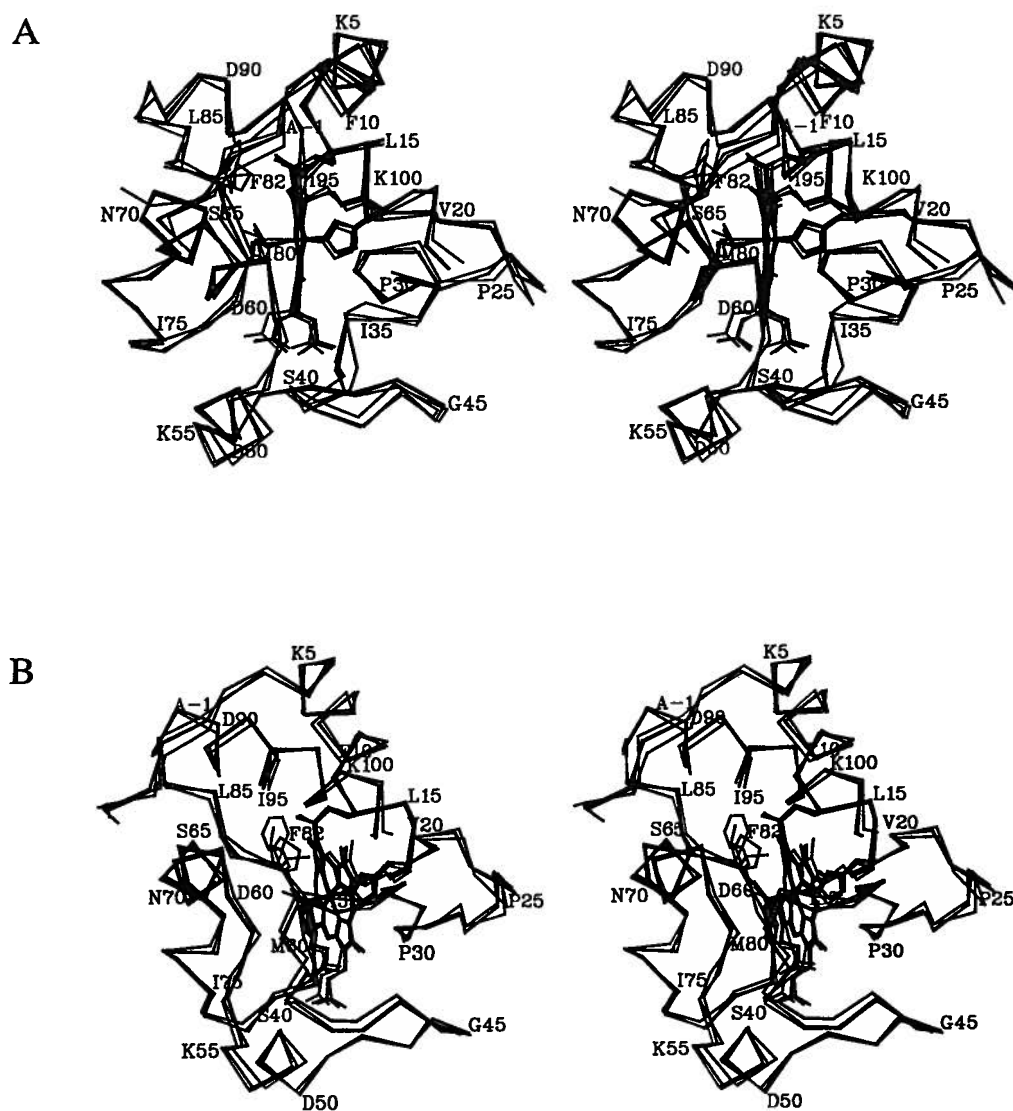
Figure 5.33: Stereo diagrams of the overlapped α-carbon backbones of the wild-type, F82I, F82L and F82M iso-1 cytochrome c structures in (a) the standard view looking at the heme edge-on and (b) an alternate view looking directly down into the mutation site at residue 82. Also drawn for all four proteins are the side chain of residue 82, the heme group, the ligands to the heme iron atom (His18 and Met80) and cysteines 14 and 17, which form covalent thioether bonds to the heme porphyrin ring. Every fifth amino acid residue is indicated by its one-letter amino acid designation and sequence number. A complete listing of the primary sequence of yeast iso-1 cytochrome c can be found in Table 1.1.

A

B
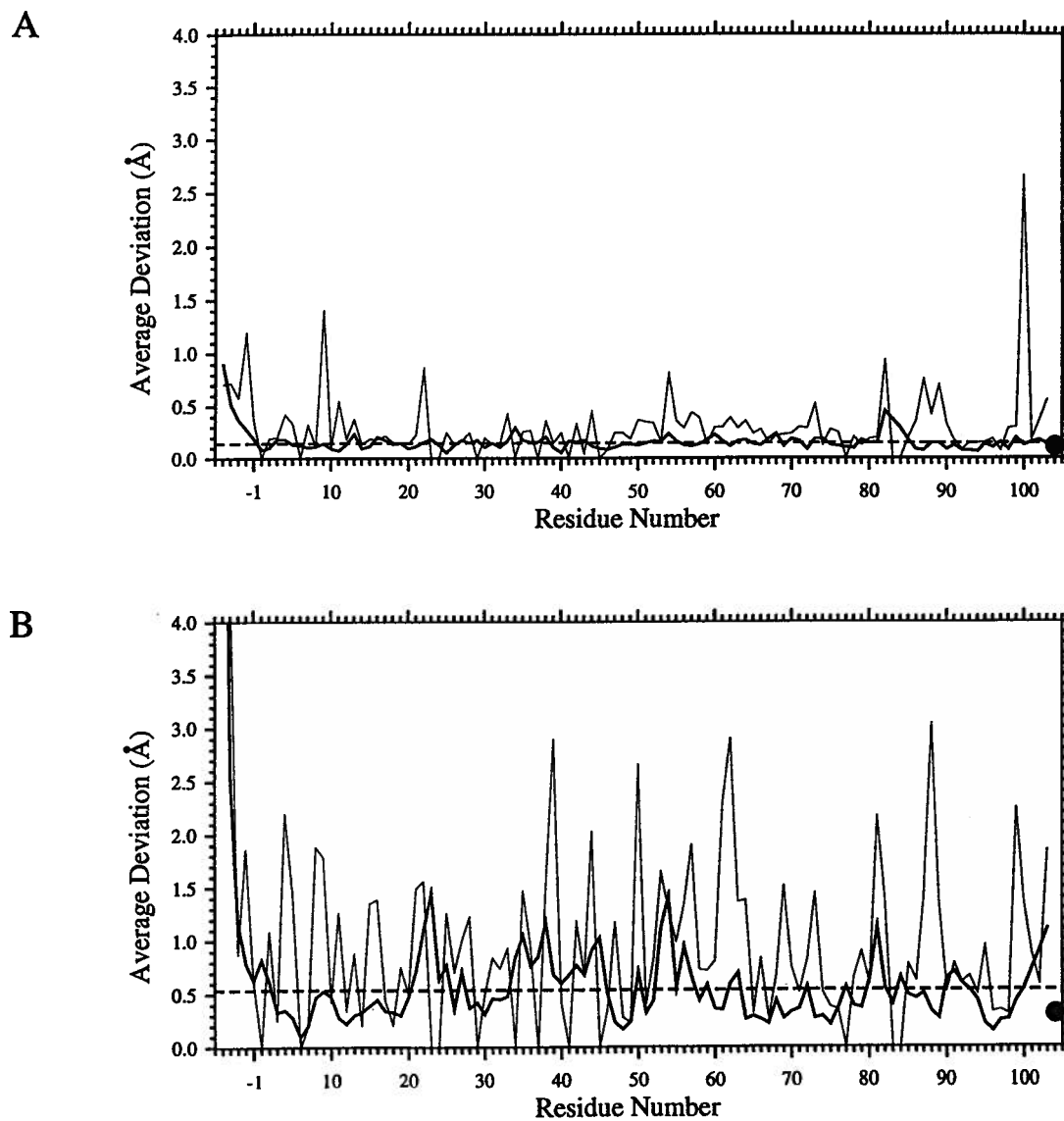
Figure 5.34: continued on next page.

C
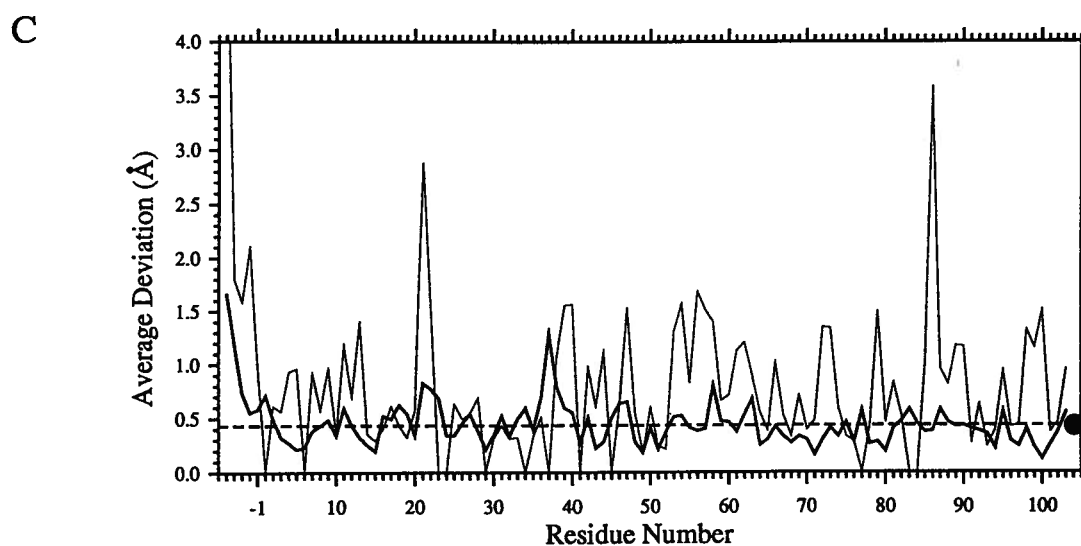
Figure 5.34: continued. Plots of average positional deviations from the wild-type iso-1 cytochrome c structure for the (a) F82I, (b) F82L and (c) F82M mutant proteins. Thick lines indicate average deviations of main chain atoms while thin lines indicate average deviations of the equivalent side chain atoms. In each diagram the filled circle at position 104 represents the average positional deviation of the heme group. For each structure, the average positional deviation for all main chain atoms (except those of the three N-terminal residues) is displayed as a horizontal dashed line.
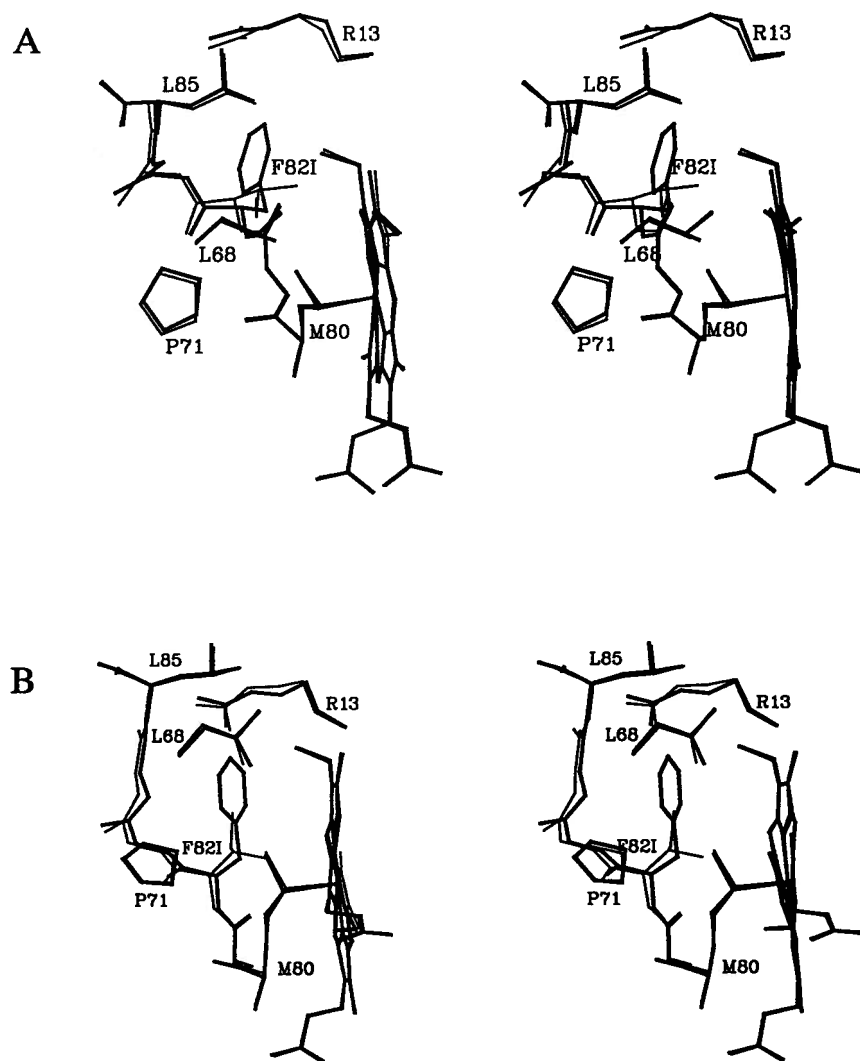
Figure 5.35: Stereo diagrams showing two views of the region about Ile82 in the F82I mutant protein. The structure of the wild-type protein (thick lines) has been superimposed on the mutant protein structure (thin lines).

Table 5.25: Heme geometry of F82I, F82L, F82M and wild-type yeast iso-1 cytochromes *c*

	Wild-type	F82I	F82L	F82M

1. Angular deviations (°) between the pyrrole nitrogen plane normal and the four individual pyrrole ring plane normals and the heme coordinate bonds.

	Wild-type	F82I	F82L	F82M
A	9.4	11.3	12.9	9.4
B	11.1	10.4	13.6	6.2
C	8.8	10.3	11.7	12.3
D	8.1	9.6	17.9	7.8
Fe - His18 NE2	2.2	5.5	4.9	6.8
Fe - Met80 SD	4.9	1.7	12.2	10.0

2. Angular deviations (°) between the porphyrin ring plane normal and the four pyrrole ring plane normals, the pyrrole nitrogen plane normal and the heme coordinate bonds.

	Wild-type	F82I	F82L	F82M
A	6.7	7.2	8.2	7.1
B	11.9	11.8	13.1	10.4
C	9.8	10.1	15.9	8.7
D	6.0	5.8	13.7	4.1
NNNN	2.6	4.3	4.8	4.2
Fe - His18 NE2	3.2	1.7	4.7	8.4
Fe - Met80 SD	7.5	5.5	16.9	8.2

3. Bond distances (Å) between the heme iron atom and its six ligands.

	Wild-type	F82I	F82L	F82M
His18 NE2	1.98	2.07	2.10	1.92
Met80 SD	2.36	2.21	2.03	2.20
Heme NA	1.97	1.98	2.00	2.05
Heme NB	2.00	2.02	2.02	1.99
Heme NC	1.99	2.00	2.03	1.98
Heme ND	2.01	2.04	2.01	2.02

The pyrrole nitrogen plane is defined by the four pyrrole nitrogens of the heme group. The four pyrrole ring planes are each defined by the five atoms of the ring and the first carbon atom attached to each of the four carbons of the ring. The porphyrin ring is defined by the five atoms in each of the four pyrrole rings, the four bridging methine carbon atoms, the first carbon atom of each of the eight side chains of the heme and the central iron atom of the heme. The heme atom nomenclature used in this table follows the conventions of the Protein Data Bank (see Figure 1.2).

Table 5.26: Heme solvent accessibility in F82I, F82L, F82M and wild-type yeast iso-1 cytochromes c

		Yeast iso-1 cytochrome c structure			
		Wild-type	F82I	F82L	F82M
1.	Solvent accessible heme atoms and surface area exposed (Å^2)				
	CBB	0.0	7.4	0.0	0.0
	CHD	2.9	2.6	0.0	4.4
	CMC	9.2	7.8	10.3	11.5
	CAC	3.4	2.8	4.7	1.4
	CBC	20.1	20.0	18.1	25.4
	CMD	10.8	10.8	12.6	12.5
2.	Total heme exposure (Å^2)	46.4	51.4	45.7	55.2
3.	Total heme surface (Å^2)	513.1	515.8	514.3	513.5
4.	% heme surface area exposed	9.0	10.0	8.9	10.7

Solvent exposure was determined by the method of Connolly (1983) with a probe sphere having a 1.4 Å radius.
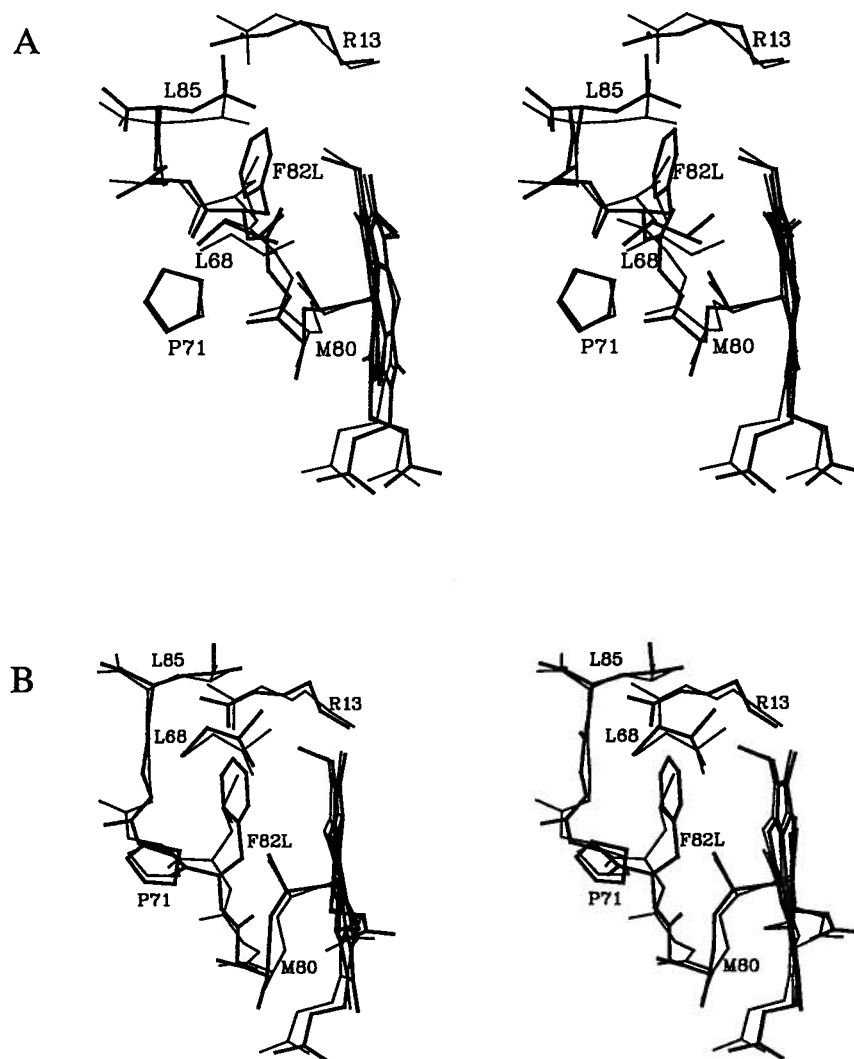
Figure 5.36: Stereo diagrams showing two views of the region about Leu82 in the F82L mutant protein. The structure of the wild-type protein (thick lines) has been superimposed on the mutant protein structure (thin lines).

A

B
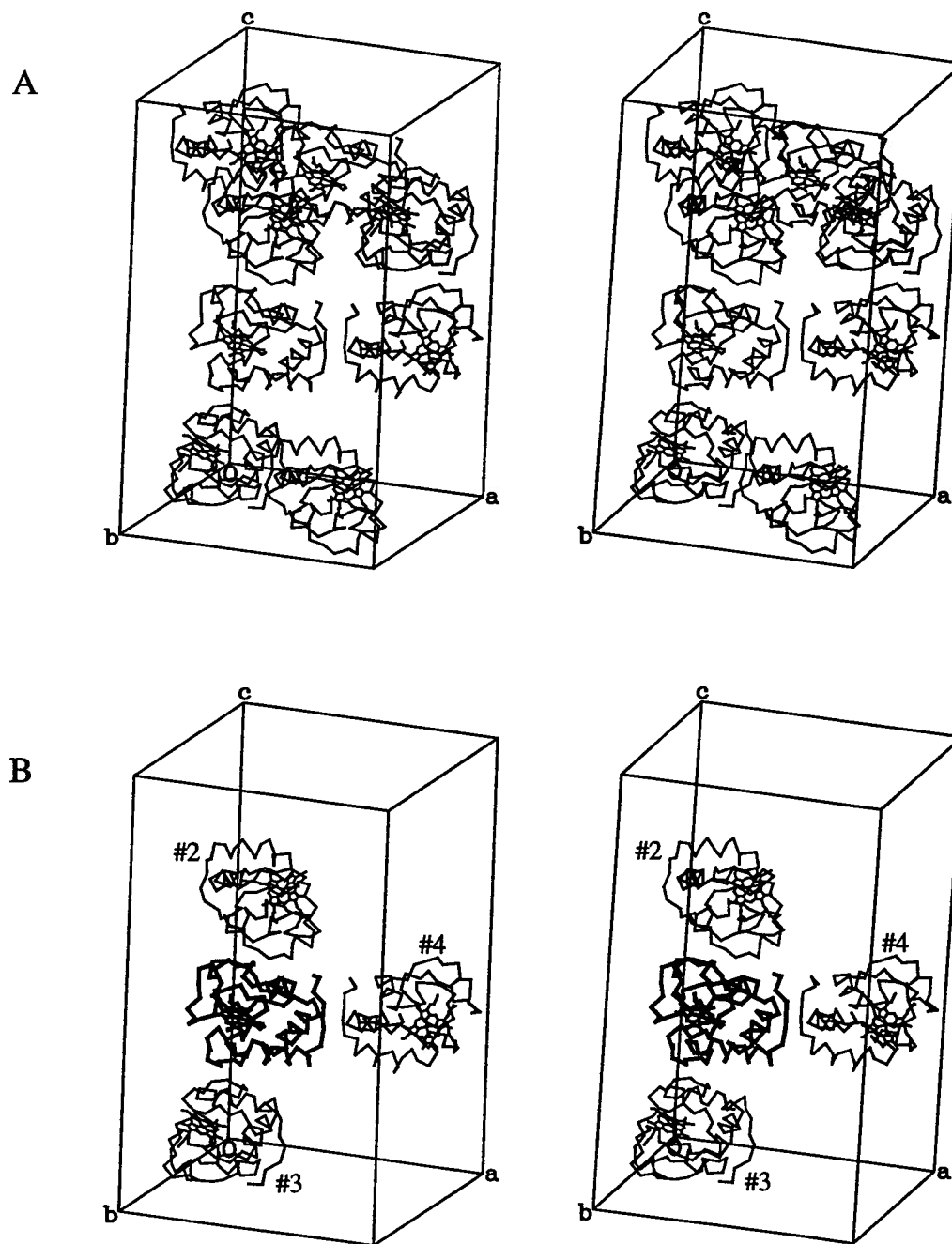
Figure 5.37: A packing diagram of the crystalline lattice containing the F82L iso-1 cytochrome c structure showing (a) the eight symmetry related molecules which pack within a single unit cell and (b) one such molecule (thick lines) and the three neighboring cytochrome c molecules (#2, #3, #4) with which it forms direct protein-protein contacts. These latter three molecules are related to the origin molecule by the following symmetry operations: #2:$(1/2 - x, y, -z)$; #3:$(x, -y, 1/2 - z)$; #4$(-x, 1/2 - y, z)$.

protein (Table 5.22). While there are significant conformational shifts in the vicinity of the mutation site, in light of other studies of related mutant proteins (for example see those having F82Y: Figure 3.19, Chapter 3; F82M: Figure 5.40; F82G: Louie & Brayer, 1989), these seem insufficient to promote alternative lattice packing. Other major polypeptide changes are in flexible exterior loop regions and as such, it is not surprising that these changes accompany a new lattice packing arrangement. It is notable that earlier crystallization screens of wild-type yeast iso-1 cytochrome *c* did result in crystals of the same morphology as those of the F82L mutant protein, although these were much too small for use in diffraction analyses. Apparently some feature of the F82L mutant protein enhances the ability of such crystals to attain a greater size.

A novel feature of the F82L structure is the unique orientation found for the N-terminal portion of its polypeptide chain (Figure 5.34b). This new conformation is accompanied by a significant decrease in average main chain thermal factors for the three N-terminal residues, Thr(-5) to Phe(-3) (47.4 Å^2 in wild-type; 31.4 Å^2 in F82L; Figure 5.38), allowing for much better definition of this region in electron density maps. This is likely due to the alternative lattice contacts formed by this region of the polypeptide chain in the F82L mutant protein crystals, as noted above. As shown in Figure 5.38, other regions of polypeptide have significant changes in main chain thermal factors, including increases about Leu9, Pro25, Ala43 and Lys79 and a decrease around Asp60. These changes in polypeptide chain mobility may be related to conformational changes observed in nearby segments of polypeptide chain (Figure 5.34b), or changes in the lattice packing contacts of these regions.

To demonstrate the good fit achieved, the final refined conformation of Leu82 overlaid on its corresponding omit difference electron density map is shown in Figure 5.39. It was anticipated that substitution of a smaller leucine side chain at residue 82 would lead to increased heme solvent exposure. Unexpectedly, this does not occur due to a shift in the main chain atoms of Ala81 and Leu82 toward the interior of the heme pocket (Table 5.26; Figure 5.36). As can be seen in Figure 5.36, the side chain of Leu82 is also found positioned much deeper in the
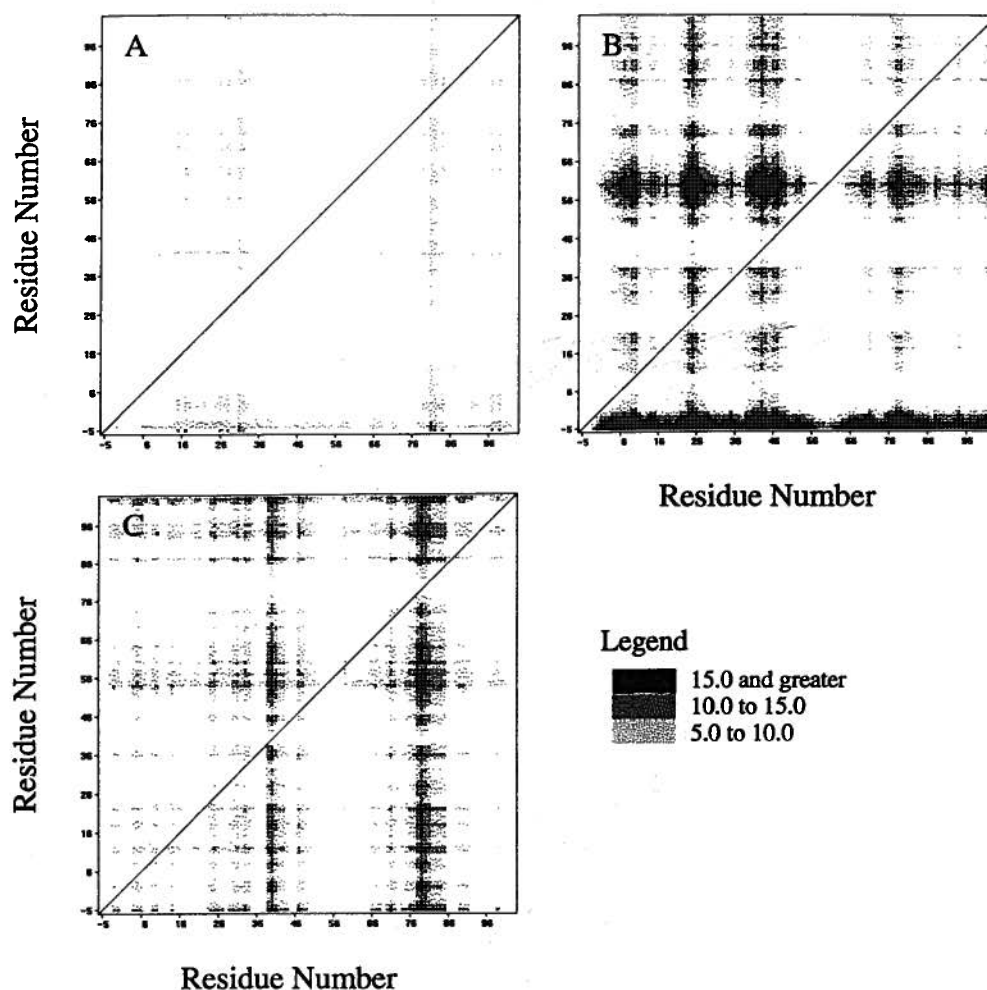
Figure 5.38: Thermal factor difference matrices from the comparison of wild-type iso-1 cytochrome c with the (a) F82I, (b) F82L and (c) F82M mutant proteins. Each matrix point $P_{x,y}$ represents a pairing of amino acids x and y. The value of the pairing is calculated from the equation: $P_{x,y} = (B_x - B_y)_{\text{mutant}} - (B_x - B_y)_{\text{wild-type}}$ where B_i is the average thermal factor (Å^2) of the main chain atoms of a given amino acid i. Positive matrix values are displayed according to the scale shown. Due to the inverse symmetry of the matrix across the diagonal, negative values are redundant and have been omitted. Amino acids producing vertical streaks within the matrix have significantly higher main chain thermal factors in the mutant structure relative to the wild-type structure while horizontal streaks indicate significantly lower main chain thermal factors in the mutant protein.

Figure 5.39: Omit difference electron density map of the F82L iso-1 cytochrome c structure in the vicinity of Leu82 computed with the omission of the whole of this residue. Contours are shown at the 3σ level. Superimposed on this map is the final refined structure of the F82L mutant protein.

hydrophobic pocket than expected. The main chain shift of residues 81 and 82 coupled with the formation of a close contact between the Leu82 CD2 side chain methyl group and the CE methyl group of Met80 (d = 3.1 Å; Figure 5.36), appear to play a role in perturbing the conformation of the side chain of Met80. Primarily affected are the length and orientation of the heme iron ligand bond formed by Met80 (Table 5.25).

5.3.4   Structure of F82M cytochrome c

Placement of a methionine at residue 82 is accompanied by positional shifts in nearby polypeptide chain, including residues 81–84 (Figure 5.40). A further adjustment in the side chain of Leu85 is observed, wherein it shifts toward the Met82 side chain (Δd = 1.1 Å; Figure 5.40) and fills much of the free volume created by the substitution of a smaller methionine for the normally resident phenylalanine. As discussed in Chapter 4 (Section 4.4.4), Leu85 also appears to have a certain amount of flexibility to respond to nearby mutations by virtue of belonging to a cluster of conserved leucines, including those at positions 9, 68, 94 and 98, which is able to accommodate structural changes in adjacent protein groups by undergoing positional displacements in concert with changes in the size of an adjacent internal hydrophobic cavity.

A methionine at position 82 also results in a conformational shift in the side chain of the Met80 heme ligand. As can be seen in Figure 5.40, the CE methyl group of Met82 points into the hydrophobic heme pocket where it forms a close contact with the CE methyl group of Met80 (d = 3.3 Å) and displaces this latter group by 0.9 Å from its normal position. This displacement occurs primarily via a rotation of -41° in the χ_3 torsion angle of Met80. While movement of Met80 CE avoids a potential steric conflict, it does result in an increase in the thermal parameters of the polypeptide backbone atoms of Met80 and the adjacent Lys79 (Figure 5.38). A contributing factor to these higher thermal factors may be the loss of a hydrogen bond between the side chain of Lys79 and the main chain carbonyl oxygen of Ser47 (d = 2.6 Å in wild-type; 4.0 Å in F82M mutant). This hydrogen bond is formed across the solvent exposed edge of the heme crevice and is believed to play a role in stabilizing the structure of cytochrome *c*
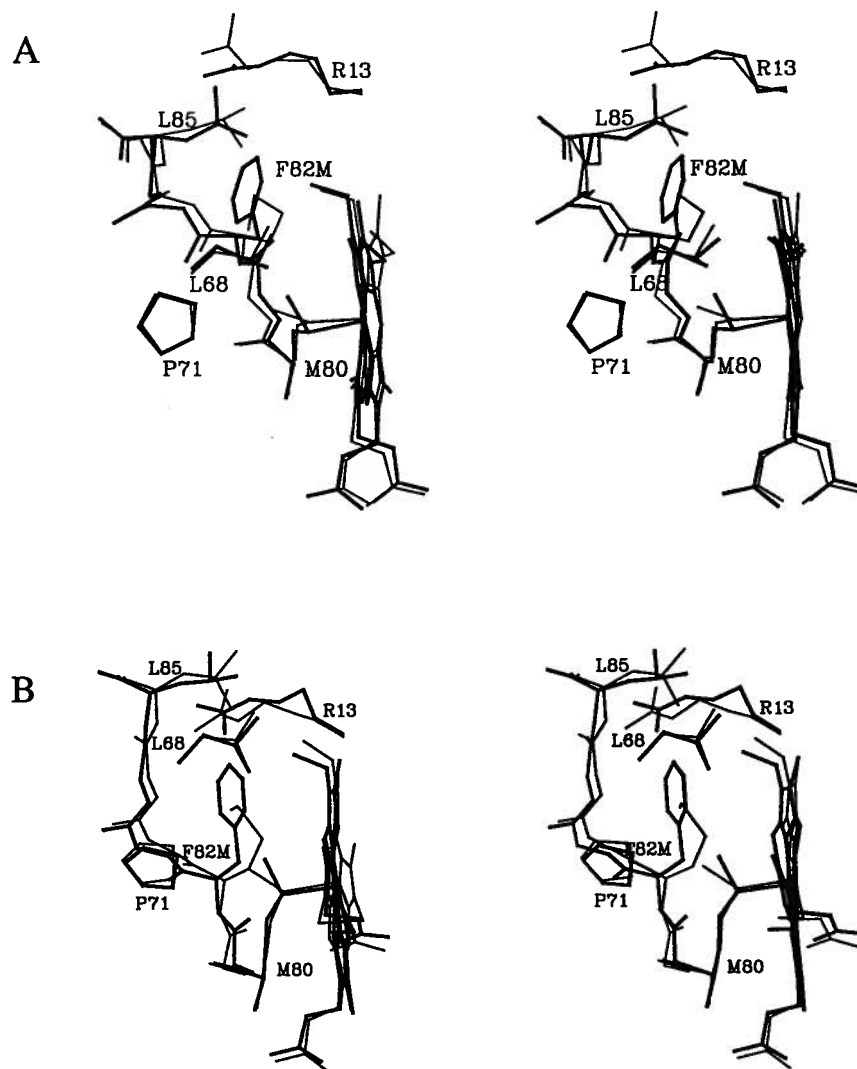
Figure 5.40: Stereo diagrams showing two views of the region about Met82 in the F82M mutant protein. The structure of the wild-type protein (thick lines) has been superimposed on the mutant protein structure (thin lines).

(Hampsey *et al.*, 1986).

One apparent consequence of the shift observed in the side chain of Met80 is a ~5° rotation of the heme moiety as a whole about an axis normal to the heme plane and running approximately through the heme NA atom. Heme rotation leads to a correspondingly large displacement of heme atoms in the F82M mutant protein compared to their positions in wild-type yeast iso-1 cytochrome c ($\Delta d = 0.43$ Å; Table 5.24), but does not greatly perturb the internal geometry of the heme (Table 5.25). Two heme substituents particularly perturbed include the CBC methyl group ($\Delta d = 0.5$ Å) which becomes more exposed to solvent (Table 5.26) and the CBB methyl group ($\Delta d = 1.1$ Å) which comes into contact with the CD2 methyl group of the side chain of Leu94 (d = 3.2 Å). This latter interaction may account for the positional shift observed for the side chain of Leu98 ($\Delta d = 1.4$ Å) and the subsequent abolition of the normally present internal hydrophobic cavity in the back of the heme pocket. The potential roles of Leu94 and this internal cavity are discussed in more detail in Chapter 4.

Another prominent structural change observed in the F82M mutant protein, but which is far removed from the mutation site at residue 82, involves the conformationally flexible region around residues 37 and 38, which forms part of a type II β-turn on the surface of yeast iso-1 cytochrome c (Table 1.2; Louie & Brayer, 1990). Here Gly37 has adopted a new conformation ($\phi = 168°$; $\psi = -77°$) which differs markedly from that found in the wild-type protein ($\phi = 87°$; $\psi = -11°$). Although conformational variability about Gly37 has previously been noted in different cytochromes c, this has been attributed to local amino acid substitutions (Murphy *et al.*, 1992). The current study suggests that while this may be a contributing factor, regional flexibility of the polypeptide chain is sufficient to result in different structural isoforms. In the F82M mutant protein it seems likely that heme group rotation is responsible for inducing this rearrangement.

In addition to conformational shifts in the main chain atoms of Arg38, the position of the side chain of this residue also undergoes a significant alteration in the F82M mutant protein ($\Delta d = 1.1$ Å). Normally, the guanidinium group of this side chain participates in hydrogen

bonding interactions with two conserved water molecules, Wat121 and Wat168, which are in turn hydrogen bonded to the propionate A group of the heme (Figure 1.5; Louie & Brayer, 1990). Heme rotation in the F82M mutant protein shifts the position of both the propionate A group ($\Delta d = 0.55$ Å) and Wat121 ($\Delta d = 0.73$ Å). The conformational shifts observed for Arg38 compensate for heme movement and preserve the hydrogen bonding interactions observed in the wild-type protein. However, as evident from Figure 5.38, these shifts do result in increased thermal mobility for residues 39–41.

5.4 Discussion

5.4.1 Structural implications

Replacement of Phe82 by the aliphatic residues isoleucine, leucine and methionine substantially alters the character of the side chain present at this position both in terms of bulk and overall shape. Surprisingly, substitution by isoleucine, which has the fewest degrees of side chain conformational freedom among these three residues, results in the smallest structural changes. The positional shifts observed (Figures 5.34a and 5.35) appear to be a consequence of the beta branching of the Ile82 side chain and the difficulty in packing this group into the shape of the available space. Particularly affected by this are Gly83 and Gly84 which provide some conformational flexibility in this region to compensate for this new group. The orientation of the side chain of Ile82 appears to be for the most part set by the close contact of the CG2 methyl group of this residue with the plane of the heme group. Some increased heme solvent exposure (Table 5.26) is observed but the conformation of Ile82 is such as to avoid the formation of a solvent channel into the hydrophobic heme pocket.

As illustrated in Figure 5.34b, substantive conformational shifts are found in the F82L mutant protein. These are evident both in the direct vicinity of the mutation site (Figure 5.36) as well as more globally about the outer surface of the protein. These latter changes are related to the new lattice packing arrangement adopted by this protein in the crystalline state, with the regions about Gly23, Lys54 and the N and C-termini being the most affected. All of these

regions form prominent lattice contacts in one or both of the F82L mutant and wild-type yeast iso-1 cytochromes c. Directly in the mutation site, significant shifts in the adjacent backbone of residues 81 to 84 are observed and these serve to partially fill open space present as the result of the smaller leucine side chain. These adjustments coupled with the positioning of this side chain further than expected into the hydrophobic heme pocket (Figure 5.36) mean that for this mutant protein no increase in heme solvent exposure is observed (Table 5.26). One result of the tight packing of Leu82 in the heme pocket is a close contact with the heme ligand residue Met80, which perturbs the nature of the heme ligand bond formed by this residue (Table 5.25).

A completely unexpected consequence of methionine substitution at Phe82 is the novel orientation observed for the heme group (Figure 5.40), which is found rotated by ~5° within the hydrophobic pocket in which it is bound. Heme rotation appears to be promoted by a close contact between the side chains of Met82 and the heme ligand Met80, and as a consequence the CD methyl group of the side chain of this latter residue is considerably displaced. The effects of heme rotation are widespread and include conformational changes in a cluster of conserved leucines, rearrangement of a surface β-turn formed by residues 35–38, positional shifts in the internal Wat121 and the side chain of Arg38, and an increase in the thermal mobility of the polypeptide segments involving residues 39–41 and 78–81 (Figure 5.38).

In the F82M mutant protein at the mutation site itself, the nearby backbone of residues 81 to 84, along with the side chain of Leu85, shift in toward the heme pocket and thereby fill in the free volume that would otherwise be created by the smaller Met82 side chain. Nevertheless a small increase in heme solvent exposure is observed for this protein (Table 5.26), which appears to be related to the observed rotation of the heme group. The heme atoms most affected (CMC, CBC and CMD) occur on the solvent exposed edge of this group (Figures 1.2 and 5.40), a region rotated up and further out into solvent. It is notable that in no other mutant form of yeast iso-1 cytochrome c has such a substantive and concerted movement of the heme group been observed. Much of the ability of the heme group to undergo this rotation is likely the result of the presence of an internal cavity and a nearby cluster of flexible leucine side chains at the

back of the heme pocket (see Chapter 4 for further discussion in this regard).

5.4.2   Functional effects

As discussed in Chapter 3, Phe82 occupies a central position in what is believed to be the contact face formed between cytochrome c and associated electron transfer partners. Changes in this interactive surface by mutation of Phe82 to other amino acids lead to alterations in the kinetics of electron transfer within such complexes (Willie *et al.*, 1993; Guillemette *et al.*, 1994). Especially notable is the behavior of the F82I mutant protein, which binds 50× tighter to cytochrome c oxidase than does the wild-type protein (Michel *et al.*, 1989). This might be related to the unique shape of the aliphatic side chain of Ile82 which permits a tighter and more extensive fit between cytochrome c and cytochrome c oxidase when these proteins are complexed. Figure 5.35 suggests this might result from the smaller size of the side chain of isoleucine and perhaps the positioning of this residue as dictated by its β-branched structure. Unfortunately, the structure of the complex formed between cytochrome c and cytochrome c oxidase has not been determined and therefore a more definitive understanding of the interactions occurring is not yet possible. It should be remembered that while Ile82 may lead to tighter binding in this complex, the invariant conservation of a phenylalanine at this position suggests that other factors are of greater importance in the overall scheme of the electron transfer pathway of which cytochrome c is only part.

Of all the mutant proteins studied, the F82I mutant protein alone has such a marked effect on cytochrome c complexation with cytochrome c oxidase, with other substitutions at Phe82 leading to less drastic changes in the interaction of these two electron transfer proteins. For example, the positional shifts in the polypeptide backbone observed in the F82L (Figure 5.36) and F82G (Louie & Brayer, 1989) mutant proteins lead to only slightly increased affinities for cytochrome c oxidase (Michel *et al.*, 1989). Furthermore, while the replacement of Phe82 by serine in the F82S mutant protein might be expected to allow for a closer approach of cytochrome c and cytochrome c oxidase, the polar nature of the serine side chain and the

introduction of a newly bound water molecule into a solvent channel in the heme pocket (Louie *et al.*, 1988b) appear to have a disruptive effect on complex formation. In the case of the F82M mutant protein, it is conceivable that a critical factor perturbing electron transfer protein complexation is the unexpected discovery that the heme group of this protein is rotated. A natural consequence of this will be the formation of altered interactions with the exposed heme edge in any complexes formed with this protein. Collectively these results show that the character and surface contour of cytochrome *c* in the region of residue 82 is a determinant in the ability of this protein to form productive electron transfer complexes, but that elucidation of the structures of a number of these will be required to understand all the factors involved.

The alterations in the association of cytochrome *c* with redox partners observed to result from amino acid substitutions at residue 82 account for the perturbation of the kinetics of electron transfer within the protein complexes formed (Everest *et al.*, 1991; Hazzard *et al.*, 1992). However, it should be pointed out that the relationship between complex formation and electron transfer kinetics is not straightforward since multiple docking geometries having different reactivities are possible for these complexes (Northrup *et al.*, 1993; Stemp & Hoffman, 1993; Zhou & Hoffman, 1993; Mauk *et al.*, 1994; Zhou & Hoffman, 1994). Further complicating matters is the dependence of electron transfer kinetics on environmental factors such as temperature and solvent (Nocek *et al.*, 1991). Thus it is difficult to obtain a quantitative correlation between the structural changes and electron transfer kinetics observed for the mutant proteins examined.

5.4.3 Effects on reduction potential

The reduction potential of cytochrome *c* is dependent on the dielectric constant of the hydrophobic heme pocket (Kassner, 1973; Louie & Brayer, 1989). However, as discussed in Chapters 3 and 4, when substitutions are made in or near the heme pocket, the effect on reduction potential can vary considerably and is dependent on the positioning of newly introduced groups relative to the heme moiety. For example, when water molecules are introduced into the heme pocket along the edge of the heme where intervening groups such as heme methyl substituents shield

the heme plane, the effect on heme reduction potential is small, even if these polar groups are close (5.4 Å) to the heme porphyrin ring (F82Y/L85A mutant protein; Chapter 3). In contrast, replacements which increase the polarity of the heme environment through the introduction of polar groups against the planar face of the heme have large effects on reduction potential. Two examples of this are found in the F82S mutant protein, in which a decrease in reduction potential results from the introduction of a polar hydroxyl group and a solvent channel into the heme pocket (Louie *et al.*, 1988b; see also Chapter 6), and the F82G mutant protein, in which the packing of polar main chain groups against the face of the heme porphyrin ring also results in a decrease in reduction potential (Louie & Brayer, 1989). Thus the parameters which influence heme reduction potential are complex and numerous, making predictions of final values based on modeling difficult.

The small decrease observed for the reduction potential of the F82I mutant cytochrome c (ΔE_m = -17 mV; Table 5.27) can be rationalized by its slightly increased heme solvent exposure (Table 5.26). This increase in solvent exposure is for the most part localized at the CBB methyl group which is normally completely buried in the hydrophobic heme pocket (Table 5.26). The observed decrease in reduction potential is not as large as that for the F82S mutant protein (ΔE_m = -45 mV; Rafferty, 1990) in which more of the CBB methyl group is exposed to solvent. In this latter case, the polar nature of the serine side chain and the binding of a new water molecule into the mutation site also contribute to the lower reduction potential observed.

In the case of the F82L mutant protein, very little change is observed in the midpoint reduction potential relative to that of the wild-type protein (Table 5.27). This result corresponds to the fact that residues 81–84 shift deeper into the heme pocket, preventing the formation of a solvent channel that would be expected from the simple replacement of Phe82 by leucine. Thus both the nonpolar heme environment (Table 5.26) and the midpoint reduction potential are preserved in the F82L mutant protein. Note that perturbations in the conformation of the Met80 ligand in this mutant protein do not appear to have any impact on reduction potential.

More difficult to explain are the results for the F82M mutant protein. Here an increase in

Table 5.27: Reduction potentials for F82I, F82L, F82M and wild-type yeast iso-1 cytochromes c

Cytochrome c	E_m (mV)
Wild-type[†]	290±2
F82I[†]	273±2
F82L[†]	286±2
F82M[‡]	288±2

Experimental conditions were: 25°C, pH 6.0 and $\mu = 0.1$ M. Values are listed relative to a standard hydrogen electrode reference.

[†]from Rafferty *et al.* (1990).

[‡]The protocol used to determine the reduction potential for the F82M mutant protein is described in Section 5.2.4.

heme solvent exposure is observed (Table 5.26) without a corresponding decrease in reduction potential (Table 5.27). A possible explanation for this discrepancy may be the fact that the increased heme solvent exposure originates with the rotation of the heme moiety within its binding pocket. Since the resultant increased heme solvent exposure occurs to one edge of the heme, it is possible its effect on heme reduction potential is muted due to shielding by heme substituent side chains as was previously observed in the F82Y/L85A (Chapter 3) and L94S (Chapter 4) mutant proteins.

Understanding the elements involved in regulation of reduction potential in the F82M mutant protein is further complicated by other structural features. Some of these involve shifts that occur in the immediate vicinity of the heme, including altered interactions between this group and its binding pocket, and a new conformation for the side chain of the heme ligand

Met80. Others involve more distant groups, which cannot be discounted as unimportant given that similar shifts in the packing of polypeptide groups distant from the heme have been shown to have a significant effect on heme reduction potential in other instances (Murphy *et al.*, 1993). In conclusion, the results for the F82M mutant protein show that heme solvent exposure by itself cannot be used as a simple predictor of the reduction potential of cytochrome *c* since many other factors contribute in different ways to the regulation of this functional property.

Chapter 6

The Structural and Functional Effects of Multiple Mutations at Distal Sites in Cytochrome c

6.1 Introduction

While an extensive analysis of the individual roles of Phe82 and Leu85 in the structure and function of cytochrome c has been made in Chapters 3–5, it must be remembered that these residues do not act in isolation and that other amino acids, both nearby and distally remote, influence many of the same properties. For example, two other regions of cytochrome c that make significant contributions to heme reduction potential, electron transfer rates and protein stability are those in the vicinity of Arg38 and Asn52. Both of these highly conserved amino acids have been studied individually with respect to the structural and functional consequences of making amino acid substitutions. Figure 1.9 illustrates the placement of Arg38, Asn52 and Phe82 within the structure of yeast iso-1 cytochrome c and shows that each is spatially distant (> 9 Å) from the others. The goal of the present chapter is to study simultaneous mutations at all three of these residues to gain insight into the interplay between these distal sites with respect to functional properties that they all influence in common.

Arginine 38 is an invariant residue (Hampsey *et al.*, 1988; Moore & Pettigrew, 1990) which is partially buried in the interior of cytochrome c. The side chain of this residue is involved in a hydrogen bonding network with propionate A of the heme group and two conserved internal water molecules, as illustrated in Figure 1.5. This residue is involved in the regulation of the heme reduction potential of cytochrome c through both the electrostatic stabilization provided by the charge on its guanidinium group and the electron withdrawing effect of this side chain on heme propionate A (Cutler *et al.*, 1989; Davies *et al.*, 1993). Previous studies have shown

157

that various amino acid substitutions at Arg38 result in a decrease in the midpoint reduction potential of cytochrome *c* (Cutler *et al.*, 1989). In structural terms, the substitution of Arg38 by alanine results in the removal of a positively charged side chain and creates an access point for bulk solvent (H. Tong, personal communication).

Asparagine 52 is a completely internal residue which is invariant among eukaryotic cytochrome *c* sequences (Moore & Pettigrew, 1990). This residue participates in a hydrogen bonding network that involves the conserved internal water molecule, Wat166 (Figure 1.5). This water appears to be an important component in the structural transition between oxidation states in cytochrome *c* (Berghuis & Brayer, 1992). Much interest has focused on the substitution of Asn52 by isoleucine since this has been found to increase protein stability dramatically (Hickey *et al.*, 1991) and act as a suppressor of mutations which would normally abolish functional activity in cytochrome *c* (Das *et al.*, 1989; Berroteran & Hampsey, 1991). The N52I substitution also results in a significant decrease in heme reduction potential (Burrows *et al.*, 1991; Guillemette *et al.*, 1994), likely as the result of the displacement of Wat166 and the resultant adjustment of internal hydrogen bonding (Berghuis *et al.*, 1994a).

The focus of the present studies is the analysis of mutant proteins having all possible combinations of the substitutions R38A, N52I and F82S. In the case of Phe82, the serine substitution was chosen because it has the largest impact on functional properties without leading to changes in polypeptide chain folding, a feature that might complicate interpretation of the results. The R38A and N52I mutations were chosen since individually each of these results in well characterized perturbations of the functional behavior of cytochrome *c*. In addition, the structures of the mutant proteins having each of the targeted substitutions at Arg38, Asn52 and Phe82 have been determined and therefore a baseline exists for documenting any additional effects that might occur in multiply mutated proteins. The basic question posed by these studies is whether Arg38, Asn52 and Phe82 act individually or in unison with respect to various properties of cytochrome *c*, and if the latter is the case, to what degree does this occur. This work has been published as part of Lo *et al.* (1995b).

Table 6.28: Data collection parameters for yeast iso-1 cytochromes c with multiple mutations

Parameter	Iso-1 cytochrome c mutant			
	R38A/N52I	R38A/F82S	N52I/F82S	R38A/N52I/ F82S
Space group	$P4_32_12$	$P4_32_12$	$P4_32_12$	$P4_32_12$
Cell dimensions (Å)				
$a = b$	36.42	36.75	36.10	36.48
c	137.03	137.39	137.47	137.28
Number of reflections collected	19351	20721	36008	71744
Number of unique reflections	6667	6291	8048	8999
Merging R-factor[†]	0.067	0.088	0.088	0.064
Resolution (Å)	1.8	1.9	1.8	1.8

[†]Merging R-factor $= \dfrac{\sum_{hkl}\sum_{i=1}^{n} |I_{i_{hkl}} - \bar{I}_{hkl}|}{\sum_{hkl}\sum_{i=1}^{n} I_{i_{hkl}}}$

6.2 Experimental Procedures

Crystals of reduced yeast iso-1 cytochrome c proteins containing combinations of the R38A, N52I and F82S mutations were grown from solutions of 88% ammonium sulphate and 70 mM sodium dithionite buffered at pH 6.5 by 0.1 M sodium phosphate (Table 2.3). The hanging drop vapour diffusion method (Section 2.3) was employed with seeding from micro-crystals (Leung *et al.*, 1989). The crystals grown for each of the four mutant proteins are of the space group $P4_32_12$ with unit cell dimensions as indicated in Table 6.28 and are isomorphous with crystals of wild-type yeast iso-1 cytochrome c.

For each of the four mutant cytochromes c, X-ray diffraction data were collected on a Rigaku R-AXIS II imaging plate area detector from a single crystal as described in Section 2.5.3. The

incident radiation was provided by a RU-300 rotating anode generator operating at 90–100 mA and 50–60 kV. For each frame, each crystal was oscillated through a ϕ angle of 1.0° and exposed to the X-ray beam for 20–30 minutes. The relatively low number of total measurements made for the R38A/N52I and R38A/F82S crystals (Table 6.28) was a result of these diffracting poorly to high resolution and having a much higher rate of intensity decay. As documented in Table 2.3, the best crystals that could be grown of these mutant proteins were less than ideal for analysis, with the R38A/N52I crystal having one very thin dimension and the R38A/F82S crystal being extremely small overall. X-ray intensity data were processed to structure factors (summarized in Table 6.28) using the R-AXIS II data processing software (Higashi, 1990; Sato *et al.*, 1992) and the procedures described in Section 2.5.3. Each mutant protein data set was put on an absolute scale using the Wilson (1942) plot method (Section 2.5.4).

Starting models for the structural refinement of the four mutant proteins were based on the high resolution structure of wild-type iso-1 cytochrome *c* (Louie & Brayer, 1990). New side chains at the three mutation sites were initially modeled as alanine residues. Also included in the starting models were all water molecules from the wild-type structure having isotropic thermal factors below 50 Å^2, with the exception of those in the vicinity of residues 38, 52 and 82. Additionally, the sulphate anion bound to the amino terminal end of the N-terminal helix of cytochrome *c* was included in each starting model.

The restrained parameter least-squares approach (Hendrickson, 1985) was employed for the refinement of each cytochrome *c* mutant structure as described in Section 2.6. The restraint weights listed in Table 2.4 were used for refinement and all water molecules were treated as fully occupied neutral oxygen atoms. Each of the four mutant proteins was initially subjected to 24 cycles of least-squares refinement, after which the first round of manual adjustments were made based on $F_o - F_c$ and $2F_o - F_c$ difference electron density maps at the three mutation sites. In this way mutation of Arg38 to alanine was confirmed by the lack of electron density for a longer side chain. Also observed in this case were electron density peaks representing new water molecules bound in the cavity created by this mutation. At this point the side chain of

Ile52 could be clearly visualized and fit. These difference maps also confirmed the concomitant elimination of the internal water molecule, Wat166, when Ile52 is present as opposed to the normally resident Asn52. In those mutant proteins where Phe82 was replaced by serine, the conformation of the Ser82 hydroxyl group was readily modeled, as was an adjacent newly bound water molecule.

For each of the four mutant proteins, a further 50–60 cycles of least-squares refinement were carried out. In addition, omit, $F_o - F_c$ and $2F_o - F_c$ difference electron density maps covering the entire course of the polypeptide chain were examined periodically during the course of this least-squares refinement, with each mutant protein being subjected to a thorough examination of this type a total of four times. These checks of the progress of refinement resulted in a number of manual corrections of the five amino-terminal residues of the polypeptide chain and in surface side chain positions. Water molecules considered for inclusion into refinement models were primarily found by the use of an iterative procedure involving alternating rounds of peak searching and reciprocal space refinement (Tong *et al.*, 1994). All water molecule positions determined by this method were also confirmed manually by reference to $F_o - F_c$ and $2F_o - F_c$ difference electron density maps. Final refinement parameters and stereochemistry for all four mutant protein structures are tabulated in Table 6.29.

Atomic coordinate errors for each of the four mutant protein structures have been estimated using the two methods described in Section 2.6.3.4. Inspection of a Luzzati (1952) plot (Figure 6.41) provides estimates of r.m.s. coordinate errors ranging from 0.18 Å for the R38A/N52I structure to 0.22 Å for the R38A/F82S structure. The N52I/F82S and R38A/N52I/F82S structures both have r.m.s. coordinate errors of 0.20 Å by this method. Overall atomic coordinate errors can also be estimated by evaluating individual atomic errors (Cruickshank, 1949, 1954). Based on this method, the estimated overall r.m.s. coordinate error is 0.13 Å for the R38A/N52I structure, 0.14 Å for the R38A/F82S structure, and 0.12 Å for the N52I/F82S and R38A/N52I/F82S structures.

Table 6.29: Refinement results and stereochemistry for the structures of yeast iso-1 cytochromes c with multiple distal mutations

	R38A/ N52I	R38A/ F82S	N52I/ F82S	R38A/N52I/ F82S
1. Refinement results				
Resolution range (Å)	6.0–1.8	6.0–1.9	6.0–1.8	6.0–1.8
Number of observed reflections	6358	6018	7740	8665
Completeness in resolution range (%)	70.8	77.1	87.4	95.3
Number of protein atoms	886	881	887	881
Number of solvent atoms	75	80	69	73
Average thermal factors ($\mathring{A}^2$)				
Protein atoms	22.5	21.0	21.2	23.9
Solvent atoms	34.5	29.0	34.4	36.8
R-factor	0.188	0.198	0.197	0.199

2. Stereochemistry of final models	r.m.s. deviation from ideal values			
Distances (Å)				
Bond (1-2)	0.019	0.019	0.019	0.019
Angle (1-3)	0.039	0.039	0.038	0.039
Planar (1-4)	0.050	0.046	0.047	0.049
Planes (Å)	0.014	0.014	0.014	0.015
Chiral volumes ($\mathring{A}^3$)	0.143	0.148	0.132	0.155
Non-bonded contacts (Å)[†]				
Single torsion	0.212	0.211	0.218	0.211
Multiple torsion	0.198	0.194	0.186	0.193
Possible hydrogen bonds	0.201	0.227	0.205	0.185
Torsion angles (°)				
Planar (0° or 180°)	2.3	2.2	2.2	2.5
Staggered (±60°,180°)	22.1	21.9	20.9	19.0
Orthonormal (±90°)	21.0	20.6	21.3	25.1

[†]The r.m.s. deviations from ideality for this class of restraint incorporates a reduction of 0.2 Å from the radius of each atom involved in a contact.
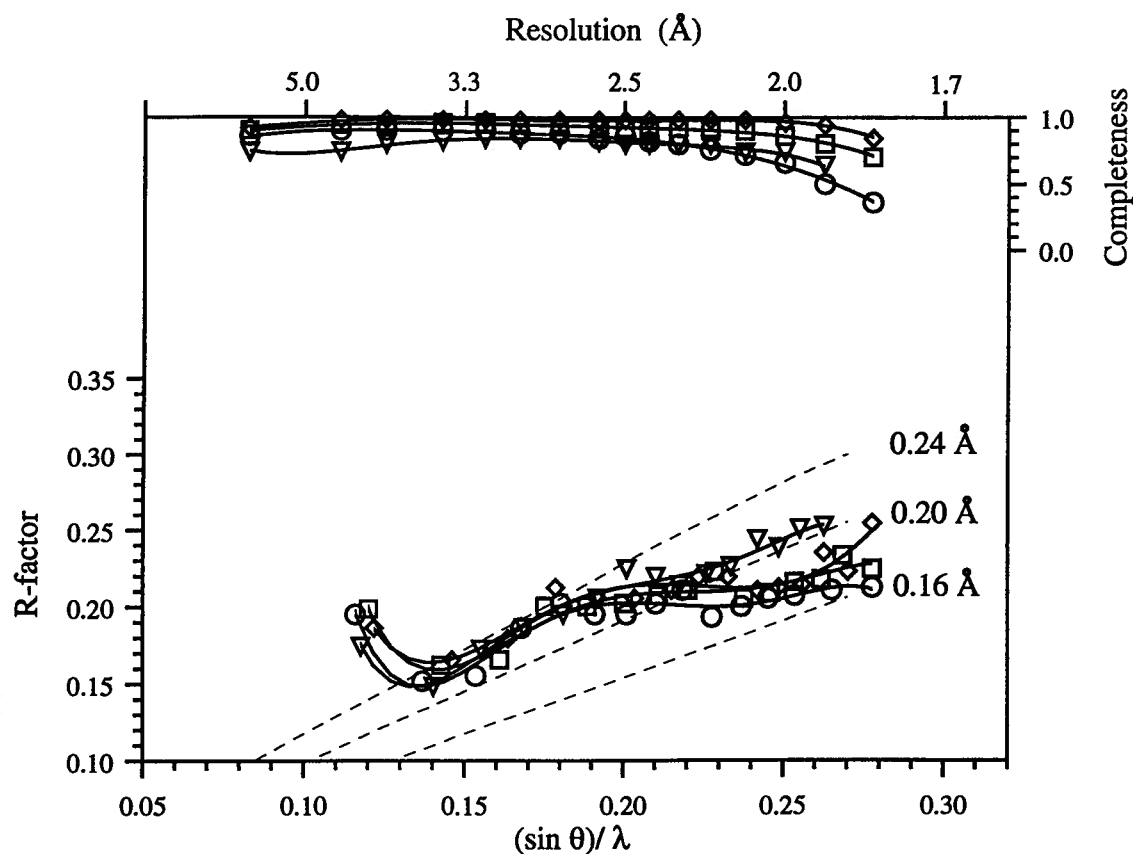
Figure 6.41: A plot of the crystallographic R-factor at the end of refinement as a function of resolution for the R38A/N52I (○), R38A/F82S (▽), N52I/F82S (□) and R38A/N52I/F82S (◇) mutants of yeast iso-1 cytochrome c. The theoretical dependence of R-factor on resolution assuming various levels of r.m.s. error in the atomic positions of the model (Luzzati, 1952) is shown as broken lines. This analysis suggested an overall r.m.s. coordinate error for the mutant structures of between 0.18 and 0.22 Å. The top portion of this figure (axes at top and right) shows the fraction of reflections observed and used in refinement as a function of resolution.

Table 6.30: Overall average positional deviations (Å) between yeast iso-1 cytochromes c with multiple distal mutations and the wild-type protein

	Iso-1 cytochrome c mutant			
Atom groups	R38A/N52I	R38A/F82S	N52I/F82S	R38A/N52I/ F82S
All common protein atoms	0.28	0.26	0.32	0.30
All main chain atoms	0.19	0.17	0.22	0.20
All common side chain atoms	0.38	0.36	0.44	0.42
All heme atoms	0.18	0.19	0.21	0.21

6.3 Results

6.3.1 Structural comparison of mutant and wild-type cytochromes c

To obtain an accurate assessment of the individual and cumulative structural effects of the R38A, N52I and F82S amino acid substitutions, the three-dimensional structures of the four mutant proteins were not only compared with each other, but also with the high resolution structure of wild-type yeast iso-1 cytochrome c (Louie & Brayer, 1990). Prior to these detailed comparisons, the structure of each mutant protein was superimposed onto the polypeptide chain of the wild-type protein by a least-squares fit of all α-carbon atoms. These structural analyses showed that significant changes were observed at each of the R38A, N52I and F82S mutation sites, and these are discussed individually in subsequent sections of this chapter. The conformational shifts involved are for the most part localized to these mutation sites, and no major disruptions to the overall fold of the polypeptide chain were observed (Table 6.30; Figure 6.42).

The distribution of average positional deviations over the course of the polypeptide chain
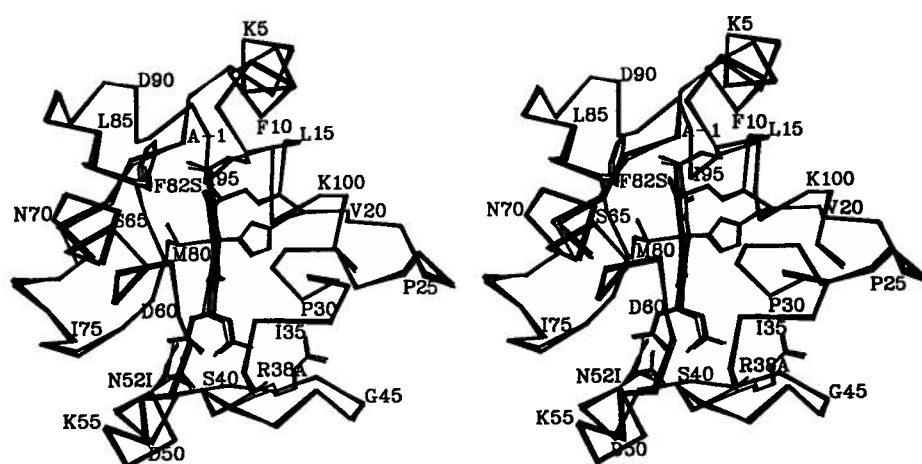
Figure 6.42: A stereo diagram of the α-carbon backbone of the wild-type iso-1 cytochrome c structure and those of the four mutant proteins with multiple distal mutations. The heme moieties of all five proteins are shown, along with the side chains of the mutated residues, Arg38, Asn52 and Phe82, the ligands to the heme iron atom, His18 and Met80, and cysteines 14 and 17, which form covalent thioether bonds to the heme porphyrin ring. Every fifth amino acid residue is indicated by its one-letter amino acid designation and sequence number.

is shown for each of the four mutant cytochromes c in Figure 6.43. Larger variations in the positions of the N-terminal residues Thr(-5) through Phe(-3) arise as a consequence of thermal disorder in this region of the protein (Louie & Brayer, 1990) rather than as a consequence of the introduced mutations. In addition, the hydrophilic side chains of Lys(-2), Lys4, Glu21, Glu44, Lys54, Lys55, Asn63, Glu66, Lys86, Lys87, Lys89 and Lys100 are all on the surface of the protein and are projected out into the surrounding solvent medium. As such, these side chains are substantially disordered and display large positional deviations between the various structures studied. Three hydrophobic residues on the protein surface also undergo apparent positional shifts, but these changes arise from either the presence of multiple residue conformations (Leu9), the high mobility of the local polypeptide backbone (Val57), or a combination of these factors (Leu58). These three residues display similar characteristics in wild-type yeast iso-1 cytochrome c (Louie & Brayer, 1990).

Examination of the heme geometry of the mutant proteins (Table 6.31) reveals that all four proteins are comparable to the wild-type protein in this regard. Of note is the shorter than expected ligand distance between the NE2 atom of His18 and the heme iron atom in the N52I/F82S protein. This apparently arises from movement of the side chain of His18 toward the heme group ($\Delta d = 0.2$ Å), and leads to a perturbation of the angle between this bond and the pyrrole nitrogen plane (becomes $\sim 7.2°$ instead of the average of $\sim 2.5°$; Table 6.31).

6.3.2 R38A mutation site

The replacement of Arg38 by an alanine represents a substantial decrease in side chain size as well as the elimination of a positive charge located partially in the interior of the protein in close proximity to the heme propionate A group. The space vacated by the Arg38 side chain is filled by two water molecules (Wat A and B) which serve to maintain the structure of the hydrogen bonding network centered around heme propionate A (Table 6.32; Figure 6.44). In the R38A/N52I/F82S mutant protein only Wat A is present. Spatially, these new water molecules are located at positions comparable to the NE and NH1 atoms of Arg38 and participate in
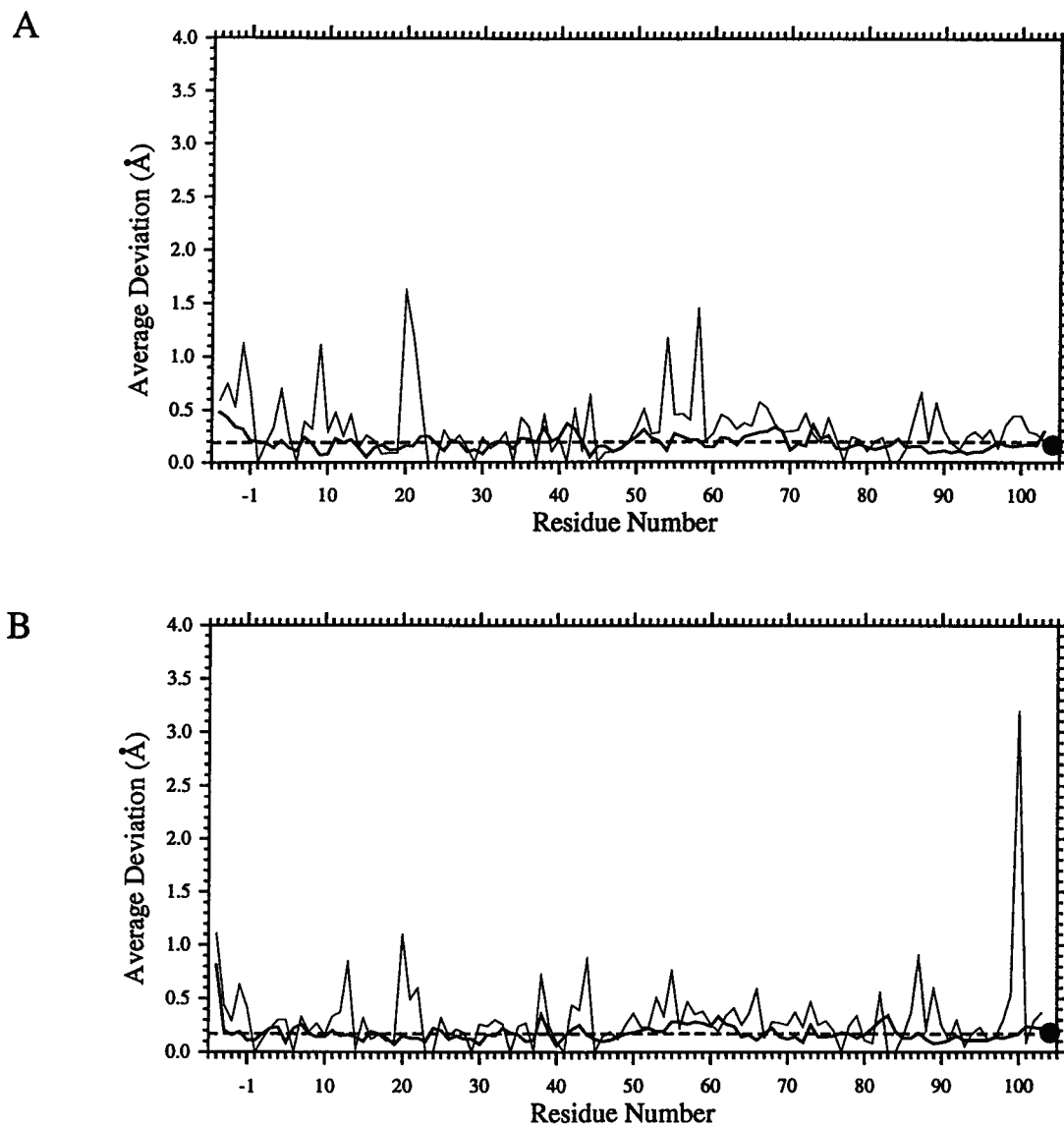
Figure 6.43: continued on next page.
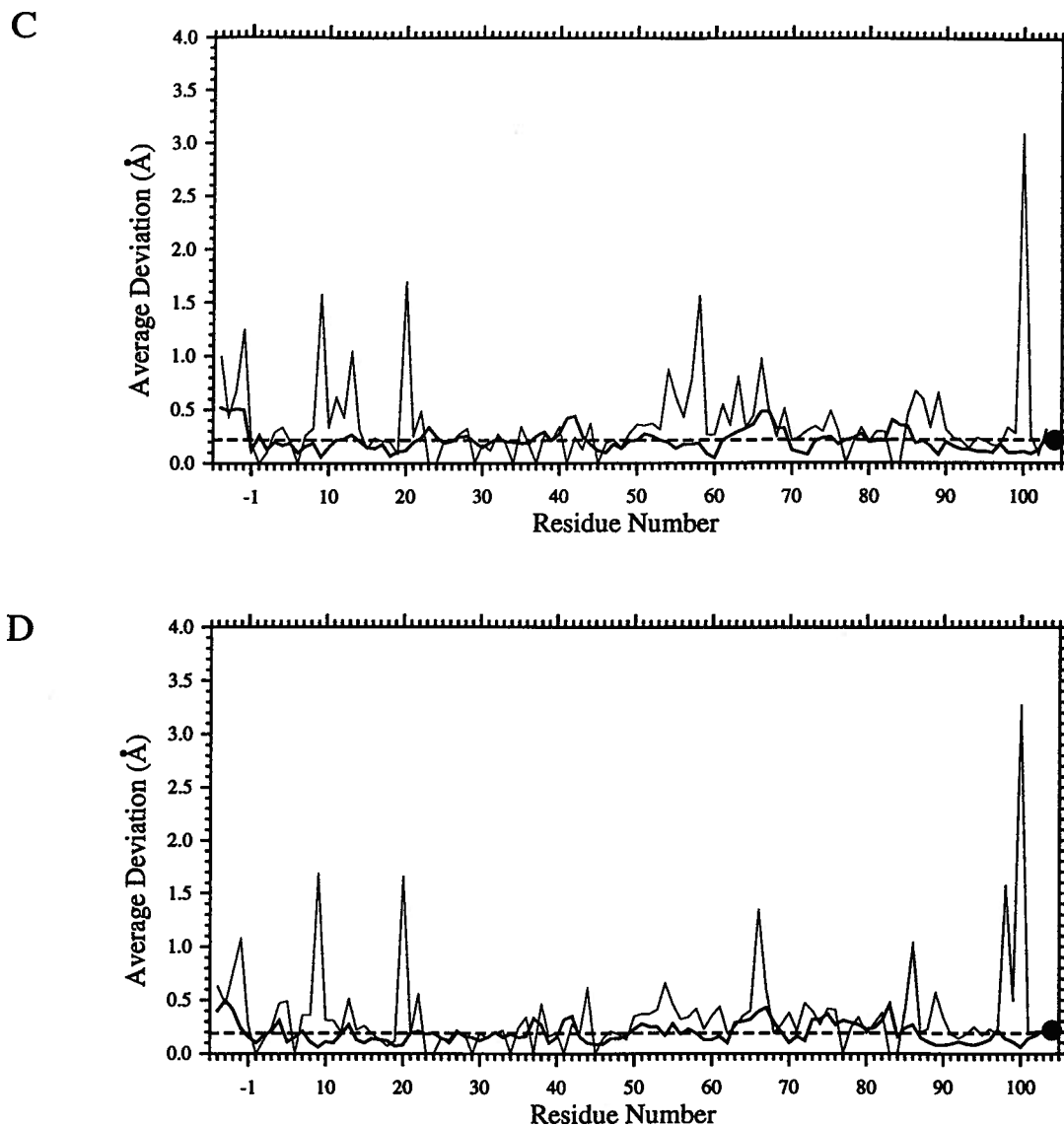
Figure 6.43: continued. Plots of average positional deviations from wild-type iso-1 cyto-chrome c along the course of the polypeptide chain for the (a) R38A/N52I, (b) R38A/F82S, (c) N52I/F82S and (d) R38A/N52I/F82S mutant proteins. Thick lines indicate average deviations of main chain atoms while thin lines indicate average deviations of the equivalent side chain atoms. In each diagram the filled circle at residue position 104 represents the average positional deviation of the heme group and the horizontal dashed line represents the average positional deviation for all main chain atoms (Table 6.30).

Table 6.31: Heme geometry of yeast iso-1 cytochromes c with multiple distal mutations

	Wild-type	R38A/N52I	R38A/F82S	N52I/F82S	R38A/N52I F82S

1. Angular deviations (°) between the pyrrole nitrogen plane normal and the four individual pyrrole ring plane normals and the heme coordinate bonds.

	Wild-type	R38A/N52I	R38A/F82S	N52I/F82S	R38A/N52I F82S
A	9.4	12.7	16.0	11.3	9.5
B	11.1	10.4	11.4	8.7	8.3
C	8.8	10.6	12.3	11.0	8.2
D	8.1	10.9	13.2	9.0	10.0
Fe - His18 NE2	2.2	2.1	4.2	7.2	1.5
Fe - Met80 SD	4.9	4.4	1.4	3.6	3.2

2. Angular deviations (°) between the porphyrin ring plane normal and the four pyrrole ring plane normals, the pyrrole nitrogen plane normal and the heme coordinate bonds.

	Wild-type	R38A/N52I	R38A/F82S	N52I/F82S	R38A/N52I F82S
A	6.7	9.1	11.9	6.6	5.4
B	11.9	12.3	14.8	10.6	9.1
C	9.8	10.9	11.4	10.3	9.2
D	6.0	7.5	9.1	4.2	5.9
NNNN	2.6	4.0	4.8	4.7	4.1
Fe - His18 NE2	3.2	3.0	4.5	2.8	2.5
Fe - Met80 SD	7.5	7.4	5.6	7.3	7.2

3. Bond distances (Å) between the heme iron atom and its six ligands.

	Wild-type	R38A/N52I	R38A/F82S	N52I/F82S	R38A/N52I F82S
His18 NE2	1.98	1.91	1.96	1.79	1.94
Met80 SD	2.36	2.34	2.39	2.34	2.38
Heme NA	1.97	1.98	1.97	1.99	2.00
Heme NB	2.00	2.00	2.01	2.01	2.04
Heme NC	1.99	2.00	2.03	1.98	2.03
Heme ND	2.01	2.06	2.02	2.08	2.04

The pyrrole nitrogen plane is defined by the four pyrrole nitrogens of the heme group. The four pyrrole ring planes are each defined by the five atoms of the ring and the first carbon atom attached to each of the four carbons of the ring. The porphyrin ring is defined by the five atoms in each of the four pyrrole rings, the four bridging methine carbon atoms, the first carbon atom of each of the eight side chains of the heme and the central iron atom of the heme. The heme atom nomenclature used in this table follows the conventions of the Protein Data Bank (see Figure 1.2).

Table 6.32: Heme propionate hydrogen bond interactions in yeast iso-1 cytochromes c with R38A, N52I and F82S replacements

Interaction		Distances (Å)							
		Wild-type	R38A[†]	N52I[‡]	F82S[¶]	R38A/ N52I	R38A/ F82S	N52I/ F82S	R38A/ N52I/ F82S
Heme O1A	Tyr48 OH	2.81	2.89	2.63	2.92	2.84	3.10	2.76	2.57
	Wat121	2.81	2.58	3.48	2.88	2.89	3.47	2.69	2.69
	Wat168	2.84	3.18	3.50	3.10	3.37	3.42	3.14	3.20
Heme O2A	Gly41 N	3.21	3.02	3.07	2.90	3.26	3.06	3.01	3.06
	Asn52 ND2	3.33	3.30	—	2.70	—	3.37	—	—
	Trp59 NE1	3.10	2.88	2.84	(3.71)	2.89	3.08	2.95	3.10
	Wat121	(4.01)	(3.50)	(3.91)	(3.70)	(3.91)	(4.22)	(3.74)	(3.56)
Heme O1D	Thr49 N	2.94	2.72	2.79	3.07	2.92	2.72	2.82	2.89
Heme O2D	Thr49 OG1	2.64	2.56	2.49	3.16	2.73	2.76	2.53	2.61
	Thr78 OG1	2.90	3.11	2.76	(3.67)	2.86	3.01	2.72	2.80
	Lys79 N	3.18	2.95	3.03	3.01	3.09	3.13	3.03	3.12
Wat121	Arg38 NE	2.81	—	2.97	(3.72)	—	—	3.09	—
	Wat168	(3.55)	(4.31)	(4.17)	(4.67)	(4.28)	(4.92)	(3.70)	(4.12)
	WatA[§]	—	(3.92)	—	—	2.54	2.47	—	3.31
Wat168	Arg38 NH1	2.56	—	2.93	3.33	—	—	2.63	—
	WatB[§]	—	3.22	—	—	2.89	2.74	—	—
WatA[§]	WatB[§]	—	2.91	—	—	2.60	2.79	—	—

Values listed are the distances between hydrogen donor and acceptor atoms. Values given in parentheses are not considered to be hydrogen bonds but are listed for comparison.

[†]from H. Tong, unpublished results.

[‡]from Berghuis *et al.* (1994a).

[¶]from Louie *et al.* (1988b).

[§]WatA and WatB are the water molecules which replace the Arg38 side chain and are closest to Wat121 and Wat168, respectively.
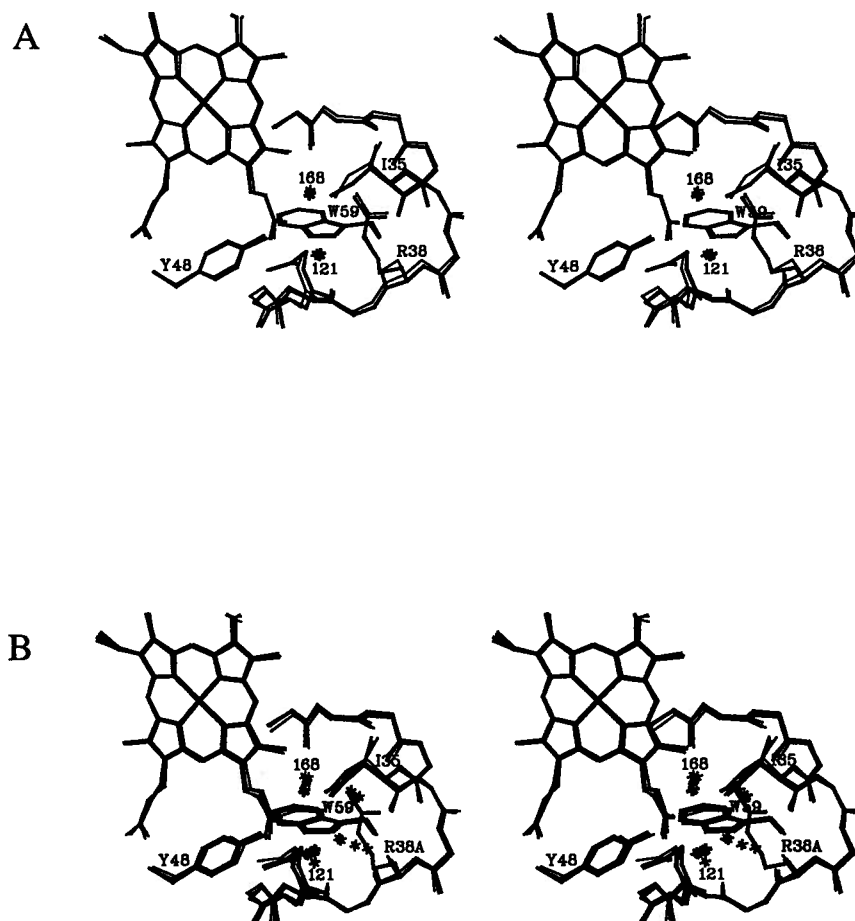
Figure 6.44: Stereo diagrams of the region around the R38A mutation site in yeast iso-1 cytochrome c. The structure of wild-type yeast iso-1 cytochrome c is drawn with thick lines and superimposed on the structures of (a) the N52I/F82S mutant protein (thin lines) and (b) the R38A, R38A/N52I, R38A/F82S and R38A/N52I/F82S mutant proteins (all drawn with thin lines). Water molecules are shown as asterisks, with the two conserved water molecules, Wat121 and Wat168, labeled.

similar hydrogen bonding interactions with two conserved water molecules, Wat121 and Wat168 (Table 6.32). In turn, the conserved Wat121 and Wat168 retain positions comparable to those found in the wild-type protein and form hydrogen bonds to the O1A atom of heme propionate A.

6.3.3 N52I mutation site

Substitution of Asn52 by isoleucine involves the exchange of a polar side chain for a nonpolar side chain of approximately equivalent size but of different shape. In the N52I single-site mutant protein, the highly conserved internal water molecule, Wat166, is excluded from the protein. In addition, the side chain of Tyr67 moves away from the side chain of Met80 ($\Delta d = 0.6$ Å) and toward that of Thr78, forming a new hydrogen bond interaction (Table 6.33; Figure 6.45; Berghuis *et al.*, 1994a). These changes are observed in all of the combinatorial mutant proteins having the N52I mutation (Table 6.33; Figure 6.45), with the Tyr67 side chain undergoing a positional shift of 0.5–0.6 Å.

6.3.4 F82S mutation site

The mutation of Phe82 to serine brings about the creation of a solvent channel directly into the heme pocket, thereby disrupting the nonpolar environment of the heme and leading to a significant drop in the reduction potential of cytochrome *c* (Louie *et al.*, 1988b). In the combination mutants containing the F82S mutation, a comparable phenomenon is observed, with a single water molecule being observed in the newly created solvent channel (Figure 6.46) and a significant increase in the solvent exposure of the heme porphyrin ring (Table 6.34; Louie *et al.*, 1988b). As apparent from Table 6.34, increased heme solvent exposure is caused primarily by the F82S mutation and is not affected by either the R38A or N52I mutations.

The side chain of Arg13 is in the vicinity of the F82S mutation site and shows considerable variability in the conformations adopted in the different combinatorial mutants (Figure 6.46). Nonetheless, the Arg13 side chain occupies the same general surface region in each case, and

Table 6.33: Wat166 hydrogen bond interactions in yeast iso-1 cytochromes c with R38A, N52I and F82S replacements

Interaction		Distances (Å)							
		Wild-type	R38A[†]	N52I[‡]	F82S[¶]	R38A/N52I	R38A/F82S	N52I/F82S	R38A/N52I/F82S
Wat166	Asn52 ND2	3.14	(3.72)	—	(4.13)	—	3.21	—	—
	Tyr67 OH	2.62	2.60	—	2.36	—	2.46	—	—
	Thr78 OG1	2.72	2.53	—	2.89	—	2.90	—	—
Tyr67 OH	Thr78 OG1	(4.18)	(4.21)	3.41	(3.73)	3.45	(4.10)	3.38	3.32
	Met80 SD	3.25	3.19	(3.63)	3.02	(3.61)	3.26	(3.43)	(3.60)

Values listed are the distances between hydrogen donor and acceptor atoms. Values given in parentheses are not considered to be hydrogen bonds but are listed for comparison.

[†]from H. Tong, unpublished results.

[‡]from Berghuis *et al.* (1994a).

[¶]from Louie *et al.* (1988b).
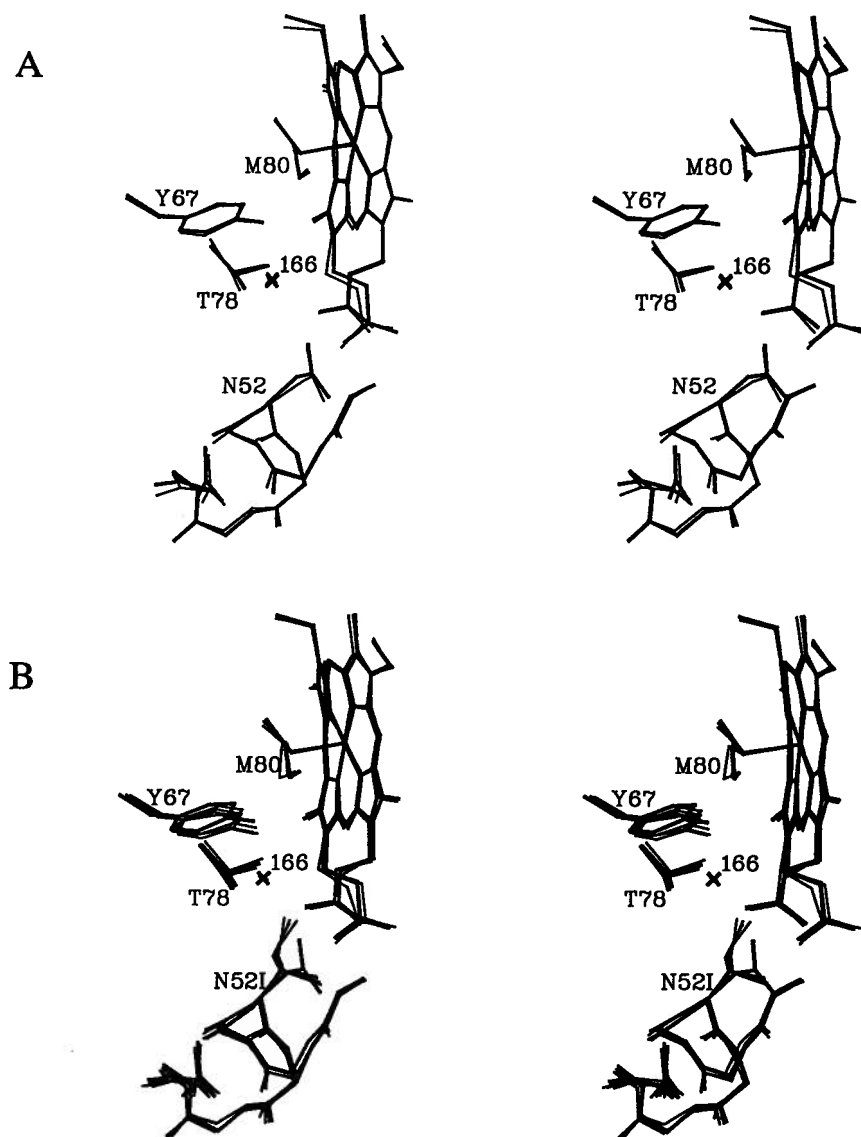
Figure 6.45: Stereo diagrams of the region around the N52I mutation site in yeast iso-1 cytochrome c. The structure of wild-type yeast iso-1 cytochrome c is drawn with thick lines and superimposed on the structures of (a) the R38A/F82S mutant protein (thin lines) and (b) the N52I, R38A/N52I, N52I/F82S and R38A/N52I/F82S mutant proteins (all drawn with thin lines). The internally bound Wat166 molecule, found in wild-type iso-1 cytochrome c and the R38A/F82S mutant protein and located adjacent to Asn52, Tyr67 and Thr78, is represented by an asterisk.

A

B
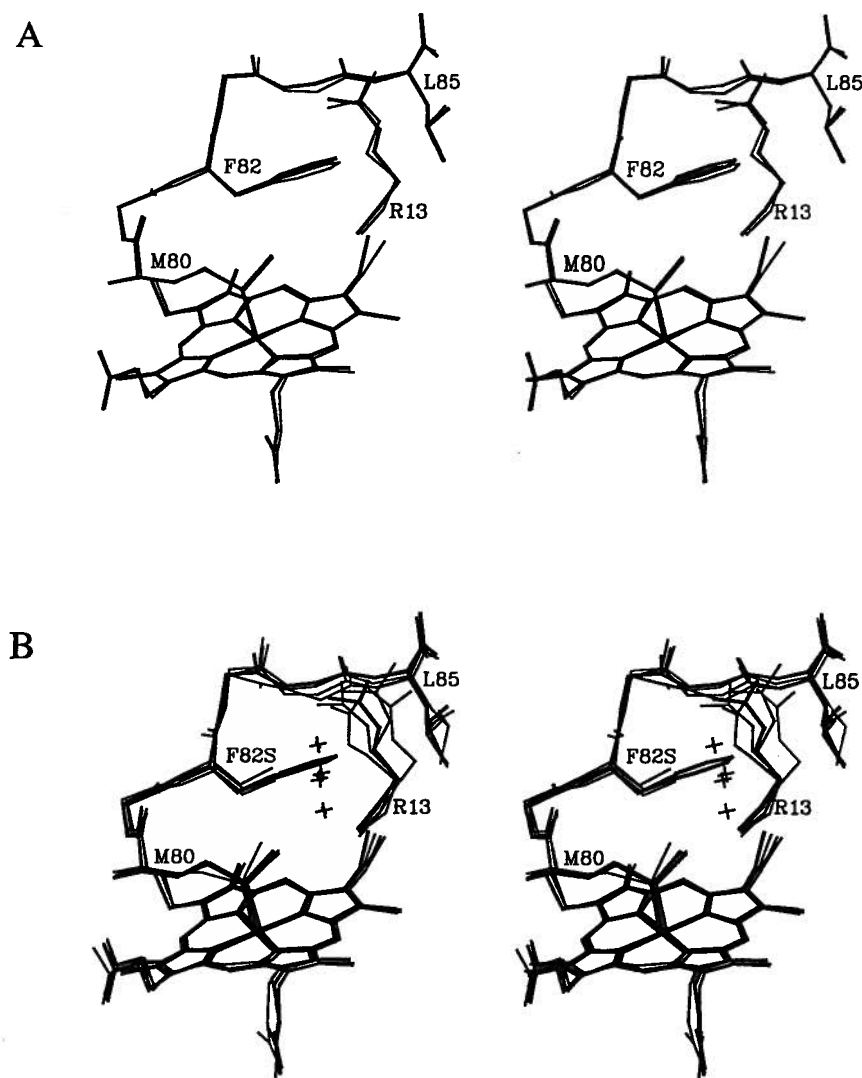
Figure 6.46: Stereo diagrams of the region around the F82S mutation site in yeast iso-1 cytochrome *c*. The structure of wild-type yeast iso-1 cytochrome *c* is drawn with thick lines and superimposed on the structures of (a) the R38A/N52I mutant protein (thin lines) and (b) the F82S, R38A/F82S, N52I/F82S and R38A/N52I/F82S mutant proteins (all drawn with thin lines). Water molecules bound in the solvent channel formed by the replacement of phenylalanine by serine at position 82 are shown as asterisks.

Table 6.34: Heme solvent accessibility in yeast iso-1 cytochromes c with R38A, N52I and F82S replacements

		Yeast iso-1 cytochrome c structure						
	Wild-type	R38A[†]	N52I[‡]	F82S[¶]	R38A/N52I[†]	R38A/F82S[†]	N52I/F82S	R38A/N52I/F82S[†]
1. Solvent accessible heme atoms and surface area exposed (Å^2)								
CBB	0.0	0.0	0.0	15.4	0.0	12.7	7.8	12.2
CHD	2.9	2.6	2.3	3.6	3.6	3.8	0.0	2.3
CMC	9.2	10.2	13.2	13.1	9.1	10.4	11.6	12.9
CAC	3.4	2.6	2.6	3.4	3.2	3.6	5.1	3.7
CBC	20.1	19.9	20.1	21.2	19.2	18.8	18.4	19.4
CMD	10.8	11.3	9.8	11.4	10.7	10.5	10.7	9.9
2. Total heme exposure (Å^2)	46.4	46.6	48.0	68.1	45.8	59.8	53.6	60.4
3. Total heme surface (Å^2)	513.1	516.2	521.2	511.8	512.4	512.2	514.5	511.0
4. % heme surface area exposed	9.0	9.0	9.2	13.3	8.9	11.7	10.4	11.8

Solvent exposure was determined by the method of Connolly (1983) with a probe sphere having a 1.4 Å radius.

[†]for all mutant proteins having the R38A mutation, Wat121 and Wat168 were considered an integral part of the protein structure. Results for the R38A single mutant protein were provided by H. Tong (personal communication).

[‡]from Berghuis *et al.* (1994a).

[¶]from Louie *et al.* (1988b).

the variability observed for this residue likely arises from the high thermal factors observed for this side chain (32.4 Å^2 in the wild-type protein; Louie & Brayer, 1990; average B is 38.5 Å^2 in F82S mutants).

A further structural change is an increase in thermal parameters for residue 82 and the two glycines at positions 83 and 84 (Figure 6.47; average B of these three residues is 17.1 Å^2 in wild-type and 32.3 Å^2 averaged over F82S mutants). This increase in thermal parameters is particularly marked for the N52I/F82S ($\Delta B = +15.0$ Å^2) and R38A/N52I/F82S ($\Delta B = +18.3$ Å^2) mutants (Figure 6.47). Increased mobility likely arises from the loss of the tight packing interactions formed by the aromatic ring of Phe82 which is sandwiched between this segment of polypeptide chain and the heme group. Another factor is that the water molecule introduced into the newly formed solvent channel at residue 82 can form a hydrogen bond to the carbonyl oxygen of Leu68 (d $= 3.2$ Å) and thereby interfere with the hydrogen bond normally found between this latter group and the main chain nitrogen atom of Leu85. This would allow more freedom of motion for the flexible Gly83-Gly84 segment of the polypeptide chain. Comparison of the thermal parameters for the F82S single mutant and the wild-type protein is not conclusive, probably due to the relatively low resolution (2.8 Å) of the structural determination for this mutant protein (Louie *et al.*, 1988b).

6.3.5   The conserved internal water, Wat166

In all eukaryotic cytochromes *c* examined thus far, a conserved water molecule is centrally located and hydrogen bonded to Asn52, Tyr67 and Thr78 (Bushnell *et al.*, 1990). A shift in the position of Wat166 toward the heme iron atom is observed in the structure of the oxidized form of yeast iso-1 (Δd $= 1.7$ Å) and other cytochromes *c* (Berghuis & Brayer, 1992). This oxidation state dependent shift results in the loss of the hydrogen bond between Wat166 and the side chain of Asn52. Similar structural changes are observed in both the reduced R38A (H. Tong, personal communication) and reduced F82S mutant proteins (Louie *et al.*, 1988b), suggesting that these structures shift toward the structure of the oxidized state. In the present study, all of
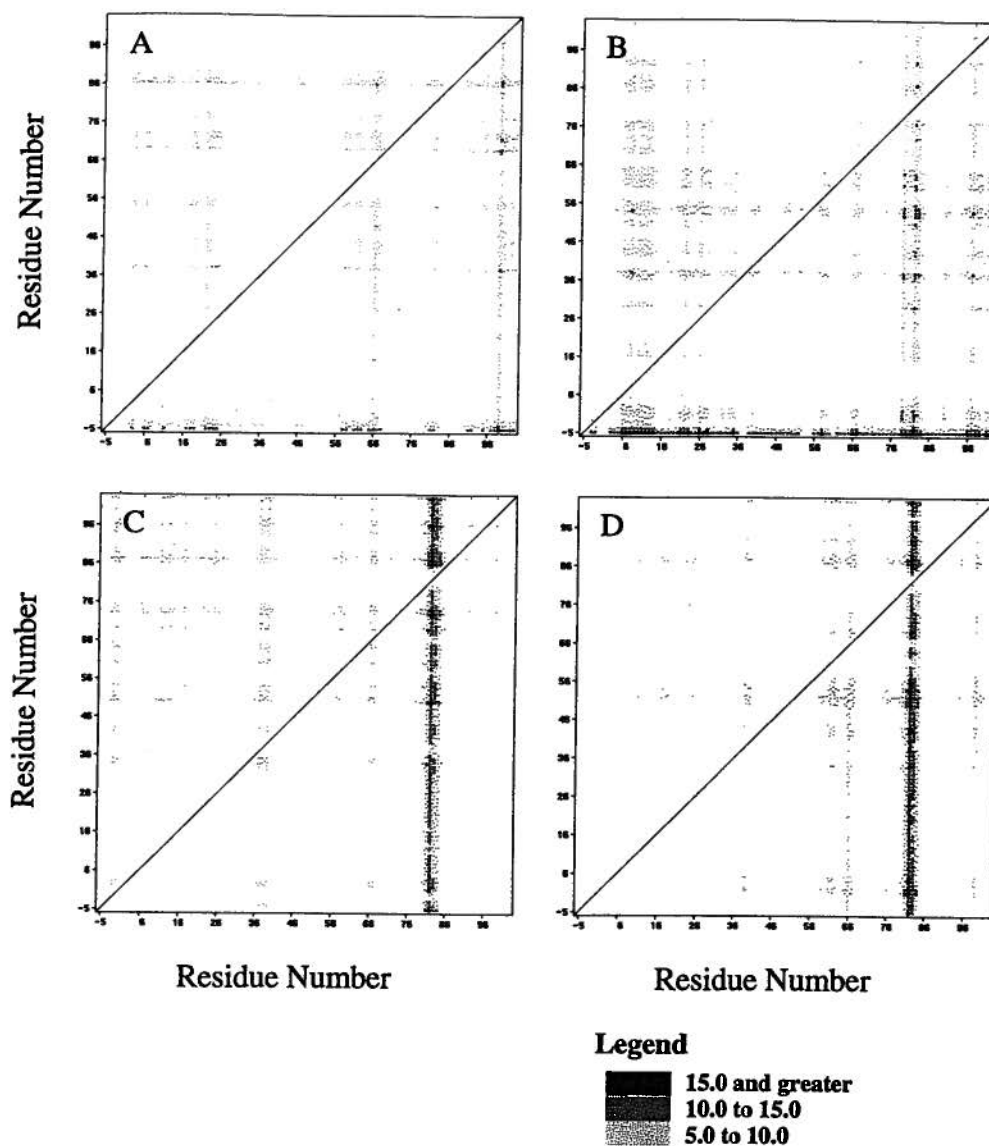
Figure 6.47: Thermal factor difference matrices from the comparison of wild-type iso-1 cytochrome c with the (a) R38A/N52I, (b) R38A/F82S, (c) N52I/F82S and (d) R38A/N52I/F82S mutants. Each matrix point $P_{x,y}$ represents a pairing of amino acids x and y. The value of the pairing is calculated from the equation: $P_{x,y} = (B_x - B_y)_{\text{mutant}} - (B_x - B_y)_{\text{wild-type}}$ where B_i is the average thermal factor (Å^2) of the main chain atoms of a given amino acid i. Positive matrix values are displayed according to the scale shown. Due to the inverse symmetry of the matrix across the diagonal, negative values are redundant and have been omitted. Amino acids producing vertical streaks within the matrix have significantly higher main chain thermal factors in the mutant structure relative to the wild-type structure while horizontal streaks indicate significantly lower main chain thermal factors in the mutant protein.

the protein structures determined were in the reduced state. Since the N52I mutation eliminates Wat166 from the protein interior, the only protein in the present study which retains this water molecule is the R38A/F82S double mutant. Surprisingly, Wat166 in the R38A/F82S protein does not move from the position it occupies in the reduced wild-type structure (Figure 6.45a) and it retains a hydrogen bond with Asn52 (Table 6.33).

6.4 Discussion

The site-directed mutagenesis technique provides the opportunity to specifically make multiple site mutations within a single protein. This can be useful in determining the extent of synergistic functional and structural changes which arise from the interaction of individual mutations. In the present work, a study has been made of the effects of introducing mutations at three distally separated sites of yeast iso-1 cytochrome *c* involving the invariant residues Arg38, Asn52 and Phe82. At these three residues, all four possible combinatorial mutant proteins were made with the three single replacements R38A, N52I and F82S. It appears that the degree of synergism between mutation sites can be quite different depending on the particular functional or structural aspect being assessed.

6.4.1 Structural effects

The replacement amino acids all represent substantial changes in side chain character and therefore it is not surprising that the introduction of each of these individual mutations into yeast iso-1 cytochrome *c* leads to significant structural and functional changes (Louie *et al.*, 1988b; Hickey *et al.*, 1991; Berghuis *et al.*, 1994a). The structural consequences of each mutation in the combinatorial mutant proteins are similar to those previously observed in the single mutant proteins (Louie *et al.*, 1988b; Berghuis *et al.*, 1994a). In general, the structural effects of each mutation are independent of the effects arising from mutations made at the other two sites. Thus for this set of mutant proteins with multiple distal substitutions, the structural effects observed do not have a synergistic component.

6.4.2 Protein stability

In terms of stability to guanidine hydrochloride denaturation (Komar-Panicucci *et al.*, 1992, 1994), the effect of individual mutation sites can be understood from the structural changes observed for each. For example, one structural role of the Arg38 side chain is to provide two hydrogen bonding groups to interact with two conserved water molecules, Wat121 and Wat168 (Table 6.32). These hydrogen bonds are replaced in the R38A mutant protein by the substitution of water molecules (Wat A and B) in place of the side chain of Arg38 (Table 6.32; Figure 6.44). Apparently, the maintenance of these hydrogen bonding interactions is sufficient to preserve the structural integrity of cytochrome *c*, thereby accounting for the negligible change in protein stability observed upon the introduction of this mutation (Table 6.35).

The N52I mutant protein is significantly more stable than wild-type yeast iso-1 cytochrome *c* (Table 6.35). This effect appears to be due to several factors, including replacement of a polar side chain by one of a hydrophobic nature within the hydrophobic core of the protein (Hickey *et al.*, 1991), displacement of an internal water molecule, Wat166 (Berghuis *et al.*, 1994a), and realignment of the hydrogen bonding network in this region (Table 6.33; Figure 6.45). Finally, the N52I mutation abolishes the structural transition between the reduced and oxidized states of the protein (Berghuis *et al.*, 1994a) and this is likely an important feature in maintaining the overall stability of the protein, especially in the oxidized state (Berghuis & Brayer, 1992).

The F82S replacement destabilizes yeast iso-1 cytochrome *c* (Table 6.35) by the introduction of a solvent channel and bound water molecule into the hydrophobic core of the protein (Figure 6.46; Louie *et al.*, 1988b). This is evident in the increased thermal parameters in the immediate vicinity of the mutation site (Figure 6.47). Such changes can also account for the lowering of the thermal stability of the heme pocket in the F82S protein relative to the wild-type protein (Hildebrandt *et al.*, 1991).

An analysis of the stability data for the four multiple mutant proteins for which structures were determined reveals the extent to which the R38A, N52I and F82S mutations interact in this regard (Table 6.35). The combination of the N52I and F82S mutations results in a net

Table 6.35: Unfolding of mutant and wild-type yeast iso-1 cytochromes c by guanidine hydrochloride

Cytochrome c	C_m [Gdn-HCl][†] (± 0.1 M)	m[‡]	ΔG°[§] (kcal/mol)
Wild-type	1.3	3.8	4.9
R38A	1.4	3.4	4.8
N52I	2.1	4.2	9.0
F82S	0.9	3.8	3.4
R38A/N52I	2.1	3.8	8.2
R38A/F82S	0.8	3.4	2.7
N52I/F82S	1.7	3.4	5.6
R38A/N52I/F82S	1.7	3.6	6.2

[†]Midpoints of unfolding by guanidine-hydrochloride were taken from Komar-Panicucci *et al.* (1992).

[‡]m is a measure of the cooperativity of the transition of the protein from the folded to the unfolded state and is derived from the slope of the linear region of a plot of ln ([folded protein] / [unfolded protein]) vs. [denaturant].

[§]$\Delta G^{\circ} \equiv$ free energy extrapolated to 0 M [Gdn-HCl]; $\Delta G^{\circ} = mC_m$

stabilization of cytochrome c due to the larger stabilizing contribution of the N52I replacement. This is not as large as in the N52I single mutant protein due to the destabilizing influence of the F82S mutation. Since the R38A mutation has a neutral effect on stability, the R38A/N52I double mutant protein has a stability similar to that of the N52I single mutant, whereas the R38A/F82S mutant protein is destabilized to the same extent as the F82S single mutant. Consistent with the stability of these double mutant proteins, the R38A/N52I/F82S triple mutant has a stability which is essentially the same as that of the N52I/F82S double mutant protein. Thus with respect to stability, the effects of each of the three mutations are independent and cumulative in the multiple mutant proteins. This is a reflection of the independent nature of the structural changes induced at each individual mutation site, which are distally located.

6.4.3 Reduction potential effects

Each of the mutant cytochromes c containing multiple substitution sites has a midpoint reduction potential significantly lower than that of either the wild-type protein or the related proteins with single site substitutions (Table 6.36). For the R38A/F82S and N52I/F82S mutant proteins, the observed reduction potentials are similar to what would be expected if the effect of each of the single mutations were independent and additive. In contrast, the R38A/N52I mutant has a reduction potential which is significantly higher than the expected value (Table 6.36). The triple mutant R38A/N52I/F82S protein has the lowest reduction potential observed, with a measured value which falls approximately midway within the range of values expected by combining the various reduction potentials observed for single and double site mutant proteins.

The higher than expected reduction potential observed for the R38A/N52I double mutant cytochrome c can be explained by a consideration of the individual contributions at each site of mutation. Arg38 likely contributes to the reduction potential of cytochrome c through two mechanisms. The first mechanism is the direct electrostatic stabilization of the reduced state of the heme group by the positively charged guanidinium side chain of this residue. The second mechanism is an electron withdrawing effect on the heme transmitted through

Table 6.36: Reduction potentials for yeast iso-1 cytochromes c with R38A, N52I and F82S replacements

Cytochrome c	E_m[†] (mV)	ΔE_m (mV)	Expected ΔE_m[‡] (mV)
Wild-type	285±2	—	—
R38A	239±2	-46	—
N52I	231±2	-54	—
F82S	247±2	-38	—
R38A/N52I	212±2	-73	-100
R38A/F82S	203±2	-82	-84
N52I/F82S	189±2	-96	-92
R38A/N52I/F82S	162±2	-123	-111 to -142[¶]

Experimental conditions were: 25°C, pH 6.0 and μ = 0.1 M. Values are listed relative to a standard hydrogen electrode reference.

[†]Electrochemical reduction potentials were taken from Komar-Panicucci *et al.* (1992).

[‡]based on a simple numerical addition of the effects of individual mutations.

[¶]range of values obtained by combining the various midpoint potentials observed for single and double site mutant proteins.

the hydrogen bonding network involving Wat121, Wat168 and the propionate A group of the heme (Figure 6.44; Cutler *et al.*, 1989; Davies *et al.*, 1993). The net result of these effects is a contribution of $\sim+45$ mV to the reduction potential of the protein. The contribution of Asn52 to the reduction potential of cytochrome *c* likely has three elements. The first consists of the maintenance of hydrogen bonding about Wat166, an internal water molecule (Figure 6.45; Berghuis & Brayer, 1992; Berghuis *et al.*, 1994a,b). Second is the dipole moment of the amide end of the side chain of Asn52 which is oriented to stabilize the reduced form of the heme iron (Langen *et al.*, 1992). A third element is the hydrogen bond formed between the side chain of Asn52 and the propionate A group of the heme which would be expected to have an electron withdrawing effect on the heme. These three factors result in a contribution to the midpoint reduction potential of $\sim+55$ mV.

Given that both Arg38 and Asn52 contribute to maintaining a high cytochrome *c* reduction potential through interaction with a common element, namely the heme propionate A group, a strict additive calculation of the effect of the R38A and N52I mutations could overestimate the drop in reduction potential expected. As shown experimentally (Table 6.36) this appears to be the case and suggests that in total, interactions with heme propionate A can only count toward raising the reduction potential of cytochrome *c* by some maximum value.

The mechanism by which substitution of Phe82 by serine affects reduction potential is different than that of either Arg38 or Asn52 substitution, and is independent of residue replacements at these latter two positions. The predominant role of Phe82 appears to be in forming a part of the hydrophobic heme pocket and in excluding solvent from this pocket, and it contributes $\sim+40$ mV to cytochrome *c* reduction potential through these mechanisms (Louie *et al.*, 1988b; Chapter 3). Phe82 does not appear to influence any structural features affected by either Arg38 or Asn52. This is supported by the observation that the reduction potentials of the R38A/F82S and N52I/F82S double mutant proteins can be simply calculated based on the addition of the individual effects of each single site substitution.

More difficult to analyze is the effect on reduction potential when all three substitutions are

combined in a single mutant protein. If it is assumed that all three mutations have independent and additive effects, the theoretical reduction potential (+147 mV) would be lower than the experimentally observed value (+162 mV; Table 6.36). As discussed previously, this discrepancy may be explained by the interdependence of the R38A and N52I mutations. However, addition of the effects of the R38A/N52I double mutant and the F82S mutant gives a theoretical reduction potential (+174 mV) which is greater than the observed experimental value (+162 mV). Therefore, the addition of the F82S mutation to the R38A/N52I double mutant has in some manner increased the net effect on the reduction potential of the protein. One possibility is that the cumulative alterations in side chain packing resulting from the multiple mutations have functional consequences in addition to their structural effects. For example, it has previously been observed that the disruption of hydrophobic packing at a site which is distant from the heme group can affect the reduction potential of this latter group (Murphy *et al.*, 1993). A second possibility arises from the fact that only one water molecule replaces the Arg38 side chain in the R38A/N52I/F82S mutant protein whereas two water molecules are found in the other mutant proteins with the R38A substitution (Table 6.32). The presence of only one hydrogen bonding group in this region of the protein may account for the discrepancy between the theoretical and observed reduction potentials. Evidence for this arises from consideration of the R38K mutant of yeast iso-1 cytochrome *c*, in which a drop in reduction potential of 23 mV is observed (Cutler *et al.*, 1989). In this case, the substitution of Arg38 by lysine results in a decrease of available hydrogen bonding groups while still maintaining the positive charge of the side chain.

To conclude, the introduction of multiple mutations within a single protein clearly affects functional and structural properties in different ways. In some cases the effects of multiple mutations are strictly additive, such as global protein stability in the present work, while the effects on other properties will be synergistic or partly so. This of course arises because within a single protein it is not uncommon that individual residues perform multiple functions and that these functions overlap among multiple residues. This poses a dilemma in understanding

the roles of residues in protein function, especially in sorting out the individual contributions of each residue to each property. It also suggests that attempts at protein engineering, whether in modification of existing proteins or in attempts to develop new activities *de novo*, will be fraught with difficulties in assessing and compensating for the multiple roles of individual amino acids.

Summary

The work described in this dissertation focused on understanding the contributions of Phe82, Leu85 and associated residues (Arg38, Asn52, Leu94) in mediating reduction potential, electron transfer, protein complex formation and protein stability in cytochrome c. Overall four specific objectives were pursued. The first of these concerned the roles of the invariant Phe82 and the highly conserved Leu85 in forming interactions at the complexation interface between cytochrome c and electron transfer partners. The importance of Phe82 to this process was clearly shown in an analysis of the F82Y mutant protein (Chapter 3) where the additional hydroxyl group of Tyr82 is in direct spatial conflict with the side chain of Leu85, leading to rotation of the side chain of Tyr82 out toward the protein surface. This alteration of the surface contour in this region of cytochrome c disrupts complex formation with redox partner proteins and leads to perturbation of electron transfer kinetics. It was further shown that this structural perturbation is mitigated when a smaller side chain, such as that of alanine, is substituted at Leu85. In contrast, despite earlier predictions that Leu85 is an important determinant in cytochrome c electron transfer complexation, the current studies show this is unlikely to be the case since the considerable surface contour perturbations made by various substitutions at this residue do not correspondingly translate into significant changes in this property. However, it was shown from these results that the placement of the side chain of Arg13 is dependent on the presence of both Phe82 and Leu85 and one role of these residues may be to restrict interactions of this side chain to the interactive face of cytochrome c.

A second objective of this thesis was to characterize the nature of an internal hydrophobic leucine cluster containing Leu85 and the nearby Leu94, as well as an adjacent internal hydrophobic cavity. Both of these features are found next to the most buried edge of the heme group. As shown in Chapter 4, much of the ability of cytochrome c to absorb the introduction

of mutations at Leu85 and Leu94 appears to be a consequence of the conformational flexibility afforded by this leucine cluster and the nearby internal cavity. Notably, these two structural features also facilitate large structural changes associated with heme rotation as observed in the F82M mutant protein. The leucine cluster and internal cavity may also play a functional role by providing structural flexibility between oxidation states in the course of cytochrome c electron transfer. Such conformational flexibility is not observed in an adjacent structural feature, the highly conserved interface formed by the nearly perpendicular packing of the N and C-terminal helices. The interaction between these helices is maintained despite structural changes in this region arising from substitutions at either Leu85 or Leu94.

A third objective was to investigate the factors regulating the reduction potential of cytochrome c, especially with respect to the role of Phe82 and the effect of aliphatic replacements at this site. Local structural changes in the F82L mutant protein were found to result in preservation of the hydrophobic heme environment and thus maintenance of heme reduction potential (Chapter 5). In contrast, the F82I mutant protein displays increased heme solvent exposure and a corresponding decrease in heme reduction potential. Although the F82M mutant protein also has an increased heme solvent exposure, no decrease in reduction potential is observed, possibly due to shielding of the heme from the solvent environment by heme substituent side chains. This shielding effect also mitigates the impact on reduction potential when polar groups are introduced into the heme environment as the result of substitutions at Phe82, Leu85 and Leu94.

The final objective of this thesis was to place our understanding of the role of Phe82 in a broader perspective by undertaking analyses of yeast iso-1 cytochromes c having multiple mutations at Phe82 and two other distally located sites. The multiple mutant proteins studied contained all possible combinations of the substitutions R38A, N52I and F82S, where each of these individual mutations by themselves would result in a significant decrease in heme reduction potential (Chapter 6). These studies showed that the structural consequences of each of these amino acid substitutions were independent, in agreement with observations related to

protein stability. However, in terms of heme reduction potential, two results were observed. For substitution of Phe82 by serine, the mechanism by which reduction potential is lowered is different than that occurring at either of the Arg38 and Asn52 sites, and is independent of residue replacements at these latter two positions. For Arg38 and Asn52, overlapping interactions lead to higher reduction potentials in proteins with multiple mutations than would be expected from a strict additive effect of substitutions at these residues. This appears to arise from interaction of these two amino acids with a common heme element, namely the heme propionate A group. Overall, the analysis of multiple mutations in cytochrome c shows that the consequences of individual mutations can be completely independent or alternatively show varying degrees of interdependence, depending on a given protein property and the manner in which mutations are combined. These studies and those discussed earlier point out the complex interrelationships that occur between amino acids in a protein and the significant challenge this presents when designing experiments to understand the individual roles of these residues in protein function.

Bibliography

Abrams, R., Altschul, A.M. & Hogness, T.R. (1942). Cytochrome c peroxidase. II. The peroxidase-hydrogen peroxidase complex. *J. Biol. Chem.* **142**, 303–316.

Altschul, A.M., Abrams, R. & Hogness, T.R. (1940). Cytochrome c peroxidase. *J. Biol. Chem.* **136**, 777–794.

Anderson, D.E., Hurley, J.H., Nicholson, H., Baase, W.A. & Matthews, B.W. (1993). Hydrophobic core repacking and aromatic-aromatic interaction in the thermostable mutant of T4 lysozyme Ser117→Phe. *Protein Sci.* **2**, 1285–1290.

Arndt, U.W. & Wonacott, A.J., eds. (1977). *The Rotation Method in Crystallography*. North-Holland Publishing Company, Amsterdam.

Bach, S.J., Dixon, M. & Keilin, D. (1942a). A new soluble cytochrome component from yeast. *Nature (London)*. **149**, 21.

Bach, S.J., Dixon, M. & Zerfas, L.G. (1942b). Lactic dehydrogenase of yeast. *Nature (London)*. **149**, 48–49.

Baldwin, E.P., Hajiseyedjavadi, O., Baase, W.A. & Matthews, B.W. (1993). The role of backbone flexibility in the accommodation of variants that repack the core of T4 lysozyme. *Science*. **262**, 1715–1718.

Barker, P.D., Mauk, M.R. & Mauk, A.G. (1991). Proton titration curve of yeast iso-1-ferricytochrome c. Electrostatic and conformational effects of point mutations. *Biochemistry*. **30**, 2377–2383.

Beratan, D.N., Onuchic, J.N., Winkler, J.R. & Gray, H.B. (1992). Electron-tunneling pathways in proteins. *Science*. **258**, 1740–1741.

Berghuis, A.M. & Brayer, G.D. (1992). Oxidation state-dependent conformational changes in cytochrome c. *J. Mol. Biol.* **223**, 959–976.

Berghuis, A.M., Guillemette, J.G., McLendon, G., Sherman, F., Smith, M. & Brayer, G.D. (1994a). The role of a conserved internal water molecule and its associated hydrogen bond network in cytochrome c. *J. Mol. Biol.* **236**, 786–799.

Berghuis, A.M., Guillemette, J.G., Smith, M. & Brayer, G.D. (1994b). Mutation of tyrosine-67 to phenylalanine in cytochrome c significantly alters the local heme environment. *J. Mol. Biol.* **235**, 1326–1341.

Bernstein, F.C., Koetzle, T.F., Williams, G.J.B., Meyer, E.F., Bruce, M.D., Rodger, J.R., Kennard, O., Shimanouchi, T. & Tasmui, M. (1977). The protein databank: a computer-based archival file for macromolecular structures. *J. Mol. Biol.* **112**, 535–542.

190

Berroteran, R.W. & Hampsey, M. (1991). Genetic analysis of yeast iso-1-cytochrome *c* structural requirements: suppression of Gly6 replacements by an Asn52 → Ile replacement. *Arch. Biochem. Biophys.* **288**, 261–269.

Blundell, T.L. & Johnson, L.N. (1976). *Protein Crystallography.* Academic Press, New York.

Bone, R., Silen, J.L. & Agard, D.A. (1989). Structural plasticity broadens the specificity of an engineered protease. *Nature (London).* **339**, 191–195.

Brayer, G.D. & Murphy, M.E.P. (1995). Structural studies of eukaryotic cytochromes *c*. In *The Cytochrome c Handbook.* (Mauk, A.G. & Scott, R.A., eds.). Plenum Press, New York. in press.

Brennan, R.G., Wozniak, J., Faber, R. & Matthews, B.W. (1988). Crystallization of mutant lysozymes from bacteriophage T4. *J. Crystal Growth.* **90**, 160–167.

Brünger, A.T. (1990). Slow-cooling protocols for crystallographic refinement by simulated annealing. *Acta Crystallogr. sect. A.* **46**, 585–593.

Brünger, A.T. (1992). *X-PLOR. Version 3.1. A System for X-ray Crystallography and NMR.* Yale University Press, New Haven.

Brünger, A.T., Kuriyan, J. & Karplus, M. (1987). Crystallographic R factor refinement by molecular dynamics. *Science.* **235**, 458–460.

Bryant, C., Strottmann, J.M. & Stellwagen, E. (1985). Refolding a disulfide dimer of cytochrome *c*. *Biochemistry.* **24**, 3459–3464.

Burch, A.M., Rigby, S.E.J., Funk, W.D., MacGillivray, R.T.A., Mauk, M.R., Mauk, A.G. & Moore, G.R. (1990). NMR characterization of surface interactions in the cytochrome b_5-cytochrome *c* complex. *Science.* **247**, 831–833.

Burley, S.K. & Petsko, G.A. (1985). Aromatic-aromatic interaction: a mechanism of protein structure stabilization. *Science.* **229**, 23–28.

Burrows, A.L., Guo, L.-H., Hill, H.A.O., McLendon, G. & Sherman, F. (1991). Direct electrochemistry of proteins. Investigations of yeast cytochrome *c* mutants and their complexes with cytochrome b_5. *Eur. J. Biochem.* **202**, 543–549.

Bushnell, G.W., Louie, G.V. & Brayer, G.D. (1990). High-resolution three-dimensional structure of horse heart cytochrome *c*. *J. Mol. Biol.* **214**, 585–595.

Busse, S.C., Moench, S.J. & Satterlee, J.D. (1990). One- and two-dimensional proton NMR studies of cys-102 S-methylated yeast isozyme-1 ferricytochrome *c*. *Biophys. J.* **58**, 45–51.

Carter, Jr., C.W., ed. (1990). *Protein and Nucleic Acid Crystallization.*, vol. 1 of *Methods.* Academic Press, San Diego.

Churg, A.K. & Warshel, A. (1986). Control of the redox potential of cytochrome *c* and microscopic dielectric effects in proteins. *Biochemistry.* **25**, 1675–1681.

Cohen, H.J. & Fridovich, I. (1971). Hepatic sulfite oxidase: purification and properties. *J. Biol. Chem.* **246**, 359–366.

Connolly, M.L. (1983). Solvent-accessible surfaces of proteins and nucleic acids. *Science.* **221**, 709–713.

Connolly, M.L. (1985). Computation of molecular volume. *J. Am. Chem. Soc.* **107**, 1118–1124.

Corin, A.F., Hake, R.A., McLendon, G., Hazzard, J.T. & Tollin, G. (1993). Effects of surface amino acid replacements in cytochrome *c* peroxidase on intracomplex electron transfer from cytochrome *c*. *Biochemistry.* **32**, 2756–2762.

Crowther, R.A. (1972). The fast rotation function. In *The Molecular Replacement Method.* (Rossman, M.G., ed.), pp. 173–178. Gordon & Breach, New York.

Crowther, R.A. & Blow, D.M. (1967). A method of positioning a known molecule in an unknown crystal structure. *Acta Crystallogr.* **23**, 544–548.

Cruickshank, D.W.J. (1949). The accuracy of electron-density maps in x-ray analysis with special reference to dibenzyl. *Acta Crystallogr.* **2**, 65–82.

Cruickshank, D.W.J. (1954). The accuracy of electron-density maps in x-ray analysis: correction. *Acta Crystallogr.* **7**, 519.

Cusanovich, M.A., Meyer, T.E. & Tollin, G. (1988). *c*-type cytochromes: oxidation-reduction properties. In *Heme Proteins.* (Eichorn, G.L. & Marzilli, J.G., eds.), vol. 7 of *Advances in Inorganic Biochemistry*, pp. 37–92. Elsevier, New York.

Cutler, R.L., Davies, A.M., Creighton, S., Warshel, A., Moore, G.R., Smith, M. & Mauk, A.G. (1989). Role of arginine-38 in regulation of the cytochrome *c* oxidation-reduction equilibrium. *Biochemistry.* **28**, 3188–3197.

Cutler, R.L., Pielak, G.J., Mauk, A.G. & Smith, M. (1987). Replacement of cysteine-107 of *Saccharomyces cerevisiae* iso-1-cytochrome *c* with threonine: improved stability of the mutant protein. *Protein Eng.* **1**, 95–99.

Das, G., Hickey, D.R., McLendon, D., McLendon, G. & Sherman, F. (1989). Dramatic thermostabilization of yeast iso-1-cytochrome *c* by an asparagine → isoleucine replacement at position 57. *Proc. Natl. Acad. Sci. USA.* **86**, 496–499.

Davies, A.M., Guillemette, J.G., Smith, M., Greenwood, C., Thurgood, A.G.P., Mauk, A.G. & Moore, G.R. (1993). Redesign of the interior hydrophilic region of mitochondrial cytochrome *c* by site-directed mutagenesis. *Biochemistry.* **32**, 5431–5435.

Dempsey, S. (1986). The UCSD Molecular Modeling System.

Drenth, J. (1994). *Principles of Protein X-ray Crystallography.* Springer-Verlag, New York.

Eltis, L.D., Herbert, R.G., Barker, P.D., Mauk, A.G. & Northrup, S.H. (1991). Reduction of horse heart ferricytochrome c by bovine liver ferrocytochrome b_5. Experimental and theoretical analysis. *Biochemistry.* **30**, 3663–3674.

Eltis, L., Mauk, A.G., Hazzard, J.T., Cusanovich, M.A. & Tollin, G. (1988). Kinetics of flavin semiquinone reduction of the components of the cytochrome c-cytochrome b_5 complex. *Biochemistry.* **27**, 5455–5460.

Eriksson, A.E., Baase, W.A., Zhang, X.-J., Heinz, D.W., Blaber, M., Baldwin, E.P. & Matthews, B.W. (1992). Response of a protein structure to cavity-creating mutations and its relation to the hydrophobic effect. *Science.* **255**, 178–183.

Erman, J.E., Kang, D.S., Kim, K.L., Summers, F.E., Matthis, A.L. & Vitello, L.B. (1991). Electron transfer within the cytochrome c-cytochrome c peroxidase complex: dependence of the transient-state and steady-state kinetics on ionic strength. *Mol. Cryst. Liq. Cryst.* **194**, 253–258.

Everest, A.M., Wallin, S.A., Stemp, E.D.A., Nocek, J.M., Mauk, A.G. & Hoffman, B.M. (1991). Aromatic hole superexchange through position 82 of cytochrome c is not required for intracomplex electron transfer to zinc cytochrome c peroxidase. *J. Am. Chem. Soc.* **113**, 4337–4338.

Ferguson-Miller, S., Brautigan, D.L. & Margoliash, E. (1979). The electron transfer function of cytochrome c. In *The Porphyrins. Volume VII.* (Dolphin, D., ed.), pp. 149–240. Academic Press, New York.

Fitzgerald, P.M.D. (1988). MERLOT: an integrated package of computer programs for the determination of crystal structures by molecular replacement. *J. Appl. Crystallogr.* **21**, 273–278.

Fredericks, Z.L. & Pielak, G.J. (1993). Exploring the interface between the N- and C-terminal helices of cytochrome c by random mutagenesis within the C-terminal helix. *Biochemistry.* **32**, 929–936.

Gao, Y., Boyd, J., Pielak, G.J. & Williams, R.J.P. (1991). Comparison of reduced and oxidized yeast iso-1-cytochrome c using proton paramagnetic shifts. *Biochemistry.* **30**, 1928–1934.

Gao, Y., Boyd, J., Williams, R.J.P. & Pielak, G.J. (1990). Assignment of proton resonances, identification of secondary structural elements, and analysis of backbone chemical shifts for the C102T variant of yeast iso-1-cytochrome c and horse cytochrome c. *Biochemistry.* **29**, 6994–7003.

Gray, T.M. & Matthews, B.W. (1984). Intrahelical hydrogen bonding of serine, threonine and cysteine residues within α-helices and its relevance to membrane-bound proteins. *J. Mol. Biol.* **175**, 75–81.

Greene, R.M., Betz, S.F., Hilgen-Willis, S., Auld, D.S., Fencl, J.B. & Pielak, G.J. (1993). Changes in global stability and local structure of cytochrome c upon substituting Phenylalanine-82 with tyrosine. *J. Inorg. Biochem.* **51**, 663–676.

Guillemette, J.G., Barker, P.D., Eltis, L.D., Lo, T.P., Smith, M., Brayer, G.D. & Mauk, A.G. (1994). Analysis of the bimolecular reduction of ferricytochrome c by ferrocytochrome b_5 through mutagenesis and molecular modelling. *Biochimie.* **76**, 592–604.

Hampsey, D.M., Das, G. & Sherman, F. (1986). Amino acid replacements in yeast iso-1-cytochrome c. Comparison with the phylogenetic series and the tertiary structure of related cytochromes c. *J. Biol. Chem.* **261**, 3259–3271.

Hampsey, D.M., Das, G. & Sherman, F. (1988). Yeast iso-1-cytochrome c: genetic analysis of structural requirements. *FEBS Lett.* **231**, 275–283.

Harbury, H.A., Cronin, J.R., Fanger, M.W., Hettinger, T.P., Murphy, A.J., Myer, Y.P. & Vinogradov, S.N. (1965). Complex formation between methionine and a heme peptide from cytochrome c. *Proc. Natl. Acad. Sci. USA.* **54**, 1658–1664.

Hartshorn, R.T., Mauk, A.G., Mauk, M.R. & Moore, G.R. (1987). NMR study of the interaction between cytochrome b_5 and cytochrome c. Observation of a ternary complex formed by the two proteins and $[Cr(en)_3]^{3+}$. *FEBS Lett.* **213**, 391–395.

Hazzard, J.T., Mauk, A.G. & Tollin, G. (1992). Laser flash photolysis studies of electron transfer mechanisms in cytochromes: an aromatic residue at position 82 is not required for cytochrome c reduction by flavin semiquinones or electron transfer from cytochrome c to cytochrome oxidase. *Arch. Biochem. Biophys.* **298**, 91–95.

Hendrickson, W.A. (1985). Stereochemically restrained refinement of macromolecular structures. *Methods Enzymol.* **115**, 252–270.

Hickey, D.R., Berghuis, A.M., Lafond, G., Jaeger, J.A., Cardillo, T.S., McLendon, D., Das, G., Sherman, F., Brayer, G.D. & McLendon, G. (1991). Enhanced thermodynamic stabilities of yeast iso-1-cytochromes c with amino acid replacements at positions 52 and 102. *J. Biol. Chem.* **266**, 11686–11694.

Higashi, T. (1990). Auto-indexing of oscillation images. *J. Appl. Crystallogr.* **23**, 253–257.

Hildebrandt, P., Pielak, G.J. & Williams, R.J.P. (1991). Structural studies of yeast iso-1 cytochrome c mutants by resonance Raman spectroscopy. *Eur. J. Biochem.* **201**, 211–216.

Hilgen, S.E. & Pielak, G.J. (1991). The function of the *Saccharomyces cerevisiae* iso-1-cytochrome c gene is independent of the codon at invariant residue Phe82 when the gene is present on a low-copy-number vector. *Protein Eng.* **4**, 575–578.

Ho, P.S., Sutoris, C., Liang, N., Margoliash, E. & Hoffman, B.M. (1985). Species specificity of long-range electron transfer within the complex between zinc-substituted cytochrome c peroxidase and cytochrome c. *J. Am. Chem. Soc.* **107**, 1070–1071.

Bibliography not available

Huang, Y., Beeser, S., Guillemette, J.G., Storms, R.K. & Kornblatt, J.A. (1994). Mutations of iso-1-cytochrome c at positions 13 and 90. Separate effects on physical and functional properties. *Eur. J. Biochem.* **223**, 155–160.

Inglis, S.C., Guillemette, J.G., Johnson, J.A. & Smith, M. (1991). Analysis of the invariant Phe82 residue of yeast iso-1-cytochrome c by site-directed mutagenesis using a phagemid yeast shuttle vector. *Protein Eng.* **4**, 569–574.

Ito, A. (1980a). Cytochrome b_5-like hemoprotein of outer mitochondrial membrane; OM cytochrome b. I: Purification of OM cytochrome b from rat liver mitochondria and comparison of its molecular properties with those of cytochrome b_5. *J. Biochem.* **87**, 63–71.

Ito, A. (1980b). Cytochrome b_5-like hemoprotein of outer mitochondrial membrane; OM cytochrome b. II: Contribution of OM cytochrome b to rotenone insensitive NADH-cyt c reductase activity. *J. Biochem.* **87**, 73–80.

Kassner, R.J. (1972). Effects of nonpolar environments on the redox potentials of heme complexes. *Proc. Natl. Acad. Sci. USA.* **69**, 2263–2267.

Kassner, R.J. (1973). A theoretical model for the effects of local nonpolar environments on the redox potentials of cytochromes. *J. Am. Chem. Soc.* **95**, 2674–2677.

Katz, B. & Kossiakoff, A. (1990). Crystal structures of subtilisin BPN′ variants containing disulfide bonds and cavities: concerted structural rearrangements induced by mutagenesis. *Proteins: Struct. Funct. Genet.* **7**, 343–357.

Komar-Panicucci, S., Bixler, J., Bakker, G., Sherman, F. & McLendon, G. (1992). Tuning the redox potential of cytochrome c through synergistic site replacements. *J. Am. Chem. Soc.* **114**, 5443–5445.

Komar-Panicucci, S., Weis, D., Bakker, G., Qiao, T., Sherman, F. & McLendon, G. (1994). Thermodynamics of the equilibrium unfolding of oxidized and reduced *Saccharomyces cerevisiae* iso-1-cytochromes c. *Biochemistry.* **33**, 10556–10560.

Kreil, G. (1965). Die C-terminale aminosauresequenz des tunfischcytochroms c. *Z. Physiol. Chemie.* **340**, 86–87.

Ladd, M.F.C. & Palmer, R.A. (1985). *Structure Determination by X-Ray Crystallography.* Plenum Press, New York.

Langen, R., Brayer, G.D., Berghuis, A.M., McLendon, G., Sherman, F. & Warshel, A. (1992). Effect of the Asn52→Ile mutation on the redox potential of yeast cytochrome c. Theory and experiment. *J. Mol. Biol.* **224**, 589–600.

Lattman, E.E. & Love, W.E. (1972). A rotational search procedure for detecting a known molecule in a crystal. *Acta Crystallogr. sect. B.* **26**, 1854–1857.

Lederer, F., Ghrir, R., Guiard, B., Cortail, S. & Ito, A. (1983). Two homologous cytochromes b_5 in a single cell. *Eur. J. Biochem.* **132**, 95–102.

Leung, C.J., Nall, B.T. & Brayer, G.D. (1989). Crystallization of yeast iso-2-cytochrome *c* using a novel hair seeding technique. *J. Mol. Biol.* **206**, 783–785.

Lo, T.P. & Brayer, G.D. (1995). Structural analyses of aliphatic residue replacements of the invariant phenylalanine 82 in cytochrome *c*. *Biochemistry, submitted.*

Lo, T.P., Guillemette, J.G., Louie, G.V., Smith, M. & Brayer, G.D. (1995a). Structural studies of the roles of residues 82 and 85 at the interactive face of cytochrome *c*. *Biochemistry.* **34**, 163–171.

Lo, T.P., Komar-Panicucci, S., Sherman, F., McLendon, G. & Brayer, G.D. (1995b). The structural and functional effects of multiple mutations at distal sites in cytochrome *c*. *Biochemistry, in press.*

Lo, T.P., Murphy, M.E.P., Guillemette, J.G., Smith, M. & Brayer, G.D. (1995c). Replacements in a conserved leucine cluster in the hydrophobic heme pocket of cytochrome *c*. *Protein Sci.* **4**, 198–208.

Louie, G.V. & Brayer, G.D. (1989). A polypeptide chain-refolding event occurs in the Gly82 variant of yeast iso-1-cytochrome *c*. *J. Mol. Biol.* **210**, 313–322.

Louie, G.V. & Brayer, G.D. (1990). The high resolution refinement of yeast iso-1-cytochrome *c* and comparison with other eukaryotic cytochromes *c*. *J. Mol. Biol.* **214**, 527–555.

Louie, G.V., Hutcheon, W.L.B. & Brayer, G.D. (1988a). Yeast iso-1-cytochrome *c*: a 2.8 Å resolution three-dimensional structure determination. *J. Mol. Biol.* **199**, 295–314.

Louie, G.V., Pielak, G.J., Smith, M. & Brayer, G.D. (1988b). The role of Phe-82 in yeast iso-1-cytochrome *c* and remote conformational changes induced by a serine residue at this position. *Biochemistry.* **27**, 7870–7876.

Lum, V.R., Brayer, G.D., Louie, G.V., Smith, M. & Mauk, A.G. (1987). Computer modelling of yeast iso-1-cytochrome *c*-yeast cytochrome *c* peroxidase complexes. *Protein Structure, Folding and Design.* **2**, 143–150.

Luzzati, V. (1952). Traitement statistique des erreurs dans la détermination des structures cristallines. *Acta Crystallogr.* **5**, 802–810.

Marchon, J.C., Mashiko, T. & Reed, C.A. (1982). How does nature control cytochrome redox potentials? In *Electron Transport and Oxygen Utilization.* (Ho, C., ed.), pp. 67–72. Elsevier, North, Amsterdam.

Margoliash, E. & Bosshard, H.R. (1983). Guided by electrostatics, a textbook protein comes of age. *Trends Biochem. Sci.* **8**, 316–320.

Margoliash, E., Smith, E.L., Kreil, G. & Tuppy, H. (1961). Amino acid sequence of horse heart cytochrome *c*. *Nature (London).* **192**, 1125–1127.

Mathews, F.S. (1985). The structure, function and evolution of cytochromes. *Progr. Biophys. Mol. Biol.* **45**, 1–56.

Matthew, J.B., Weber, P.C., Salemme, F.R. & Richards, F.M. (1983). Electrostatic orientation during electron transfer between flavodoxin and cytochrome c. *Nature (London)*. **301**, 169–171.

Matthews, B.W. (1968). Solvent content of protein crystals. *J. Mol. Biol.* **33**, 491–497.

Mauk, M.R., Barker, P.D. & Mauk, A.G. (1991). Proton linkage of complex formation between cytochrome c and cytochrome b_5: electrostatic consequences of protein-protein interactions. *Biochemistry.* **30**, 9873–9881.

Mauk, M.R., Ferrer, J.C. & Mauk, A.G. (1994). Proton linkage in formation of the cytochrome c-cytochrome c peroxidase complex: electrostatic properties of the high- and low-affinity cytochrome binding sites on the peroxidase. *Biochemistry.* **33**, 12609–12614.

Mauk, M.R., Mauk, A.G., Weber, P.C. & Matthew, J.B. (1986). Electrostatic analysis of the interaction of cytochrome c with native and dimethyl ester heme substituted cytochrome b_5. *Biochemistry.* **25**, 7085–7091.

McLendon, G., Hickey, D., Berghuis, A., Sherman, F. & Brayer, G. (1991). Effects of reaction free energy in biological electron transfer in vitro and in vivo. In *Electron Transfer in Inorganic, Organic, and Biological Systems.* (Bolton, J.R., Mataga, N. & McLendon, G., eds.), vol. 228 of *Advances in Chemistry Series*, pp. 179–189. American Chemical Society, Washington.

McLeod, R.M., Farkas, W., Fridovich, I. & Handler, P. (1961). Purification and properties of hepatic sulfite oxidase. *J. Biol. Chem.* **236**, 1841–1846.

McPherson, A. (1982). *Preparation and Analysis of Protein Crystals.* John Wiley & Sons, New York.

McPherson, A. (1990). Current approaches to macromolecular crystallization. *Eur. J. Biochem.* **189**, 1–23.

McRee, D.E. (1993). *Practical Protein Crystallography.* Academic Press, San Diego.

McRee, D.E., Redford, S.M., Getzoff, E.D., Lepock, J.R., Hallewell, R.A. & Tainer, J.A. (1990). Changes in crystallographic structure and thermostability of a Cu,Zn superoxide dismutase mutant resulting from the removal of a buried cysteine. *J. Biol. Chem.* **265**, 14234–14241.

Meyer, T.E., Rivera, M., Walker, F.A., Mauk, M.R., Mauk, A.G., Cusanovich, M.A. & Tollin, G. (1993). Laser flash photolysis studies of electron transfer to the cytochrome b_5-cytochrome c complex. *Biochemistry.* **32**, 622–627.

Michel, B., Mauk, A.G. & Bosshard, H.R. (1989). Binding and oxidation of mutant cytochromes c by cytochrome-c oxidase. *FEBS Lett.* **243**, 149–152.

Moench, S.J., Chroni, S., Lou, B.-S., Erman, J.E. & Satterlee, J.D. (1992). Proton NMR comparison of noncovalent and covalently cross-linked complexes of cytochrome c peroxidase with horse, tuna, and yeast ferricytochromes c. *Biochemistry*. **31**, 3661–3670.

Moench, S.J., Erman, J.E. & Satterlee, J.D. (1993). Species-specific differences in covalently crosslinked complexes of yeast cytochrome c peroxidase with horse and yeast iso-1 ferricytochromes c. *Int. J. Biochem.* **25**, 1335–1342.

Moench, S.J. & Satterlee, J.D. (1989). Proton NMR comparison of the *Saccharomyces cerevisiae* ferricytochrome c isozyme-1 monomer and covalent disulfide dimer. *J. Biol. Chem.* **264**, 9923–9931.

Montgomery, D., Leung, D., Smith, M., Shalit, P., Faye, G. & Hall, B. (1980). Isolation and sequence of a gene for iso-2-cytochrome c in *Saccharomyces cerevisiae*. *Proc. Natl. Acad. Sci. USA.* **77**, 541–545.

Moore, G.R., Harris, D.E., Leitch, F.A. & Pettigrew, G.W. (1984). Characterisation of ionisations that influence the redox potential of mitochondrial cytochrome c and photosynthetic bacterial cytochromes c_2. *Biochim. Biophys. Acta.* **764**, 331–342.

Moore, G.R. & Pettigrew, G.W. (1990). *Cytochromes c: Evolutionary, Structural and Physicochemical Aspects*. Springer-Verlag, Berlin.

Moore, G.R., Pettigrew, G.W. & Rogers, N.K. (1986). Factors influencing redox potentials of electron transfer proteins. *Proc. Natl. Acad. Sci. USA.* **83**, 4998–4999.

Moore, G.R. & Williams, R.J.P. (1977). Structural basis for the variation in redox potential of cytochromes. *FEBS Lett.* **79**, 229–232.

Mori, E. & Morita, Y. (1980). Amino acid sequence of cytochrome c from rice. *J. Biochem.* **87**, 249–266.

Murphy, M.E.P., Fetrow, J.S., Burton, R.S. & Brayer, G.D. (1993). The structure and function of omega loop A replacements in cytochrome c. *Protein Sci.* **2**, 1429–1440.

Murphy, M.E.P., Nall, B.T. & Brayer, G.D. (1992). Structure determination and analysis of yeast iso-2-cytochrome c and a composite mutant protein. *J. Mol. Biol.* **227**, 160–176.

Nair, S.K., Calderone, T.L., Christianson, D.W. & Fierke, C.A. (1991). Altering the mouth of a hydrophobic pocket. Structure and kinetics of human carbonic anhydrase II mutants at residue Val-121. *J. Biol. Chem.* **266**, 17320–17325.

Nair, S.K. & Christianson, D.W. (1993). Structural consequences of hydrophilic amino acid substitutions in the hydrophobic pocket of human carbonic anhydrase II. *Biochemistry*. **32**, 4506–4514.

Nocek, J.M., Stemp, E.D.A., Finnegan, M.G., Koshy, T.I., Johnson, M.K., Margoliash, E., Mauk, A.G., Smith, M. & Hoffman, B.M. (1991). Low-temperature, cooperative conformational transition within [Zn-cytochrome c peroxidase, cytochrome c] complexes: variation with cytochrome. *J. Am. Chem. Soc.* **113**, 6822–6831.

North, A.C.T., Phillips, D.C. & Mathews, F.S. (1968). A semi-empirical method of absorption correction. *Acta Crystallogr. sect. A.* **24**, 351–359.

Northrup, S.H., Boles, J.O. & Reynolds, J.C.L. (1988). Brownian dynamics of association of cytochrome c and cytochrome c peroxidase electron transfer proteins. *Science.* **241**, 67–70.

Northrup, S.H., Thomasson, K.A., Miller, C.M., Barker, P.D., Eltis, L.D., Guillemette, J.G., Inglis, S.C. & Mauk, A.G. (1993). Effects of charged amino acid mutations on the bimolecular kinetics of reduction of yeast iso-1-ferricytochrome c by bovine ferrocytochrome b_5. *Biochemistry.* **32**, 6613–6623.

Ochi, H., Hata, Y., Tanaka, N., Kakudo, M., Sakurai, T., Aihara, S. & Morita, Y. (1983). Structure of rice ferricytochrome c at 2.0 Å resolution. *J. Mol. Biol.* **166**, 407–418.

Pelletier, H. & Kraut, J. (1992). Crystal structure of a complex between electron transfer partners, cytochrome c peroxidase and cytochrome c. *Science.* **258**, 1748–1755.

Pettigrew, G.W. & Moore, G.R. (1987). *Cytochromes c: Biological Aspects.* Springer-Verlag, Berlin.

Pielak, G.J., Atkinson, R.A., Boyd, J. & Williams, R.J.P. (1988). Two-dimensional NMR as a probe of structural similarity applied to mutants of cytochrome c. *Eur. J. Biochem.* **177**, 179–185.

Pielak, G.J., Mauk, A.G. & Smith, M. (1985). Site-directed mutagenesis of cytochrome c shows that an invariant Phe is not essential for function. *Nature (London).* **313**, 152–154.

Poulos, T.L. & Finzel, B.C. (1984). Heme enzyme structure and function. In *Peptide and Protein Reviews.* (Hearn, M.T.W., ed.), vol. 4, pp. 115–171. Dekker, New York.

Poulos, T.L. & Kraut, J. (1980). A hypothetical model of the cytochrome c peroxidase-cytochrome c electron transfer complex. *J. Biol. Chem.* **255**, 10322–10330.

Qi, P.X., De Stefano, D.L. & Wand, A.J. (1994a). Solution structure of horse heart ferrocytochrome c determined by high-resolution NMR and restrained simulated annealing. *Biochemistry.* **33**, 6408–6417.

Qi, P.X., Urbauer, J.L., Fuentes, E.J., Leopold, M.F. & Wand, A.J. (1994b). Structural water in oxidized and reduced horse heart cytochrome c. *Nat. Struct. Biol.* **1**, 378–382.

Qin, L., Rodgers, K.K. & Sligar, S.G. (1991). Electron transfer between cytochrome b_5 surface mutants and cytochrome c. *Mol. Cryst. Liq. Cryst.* **194**, 311–316.

Rafferty, S.P., Pearce, L.L., Barker, P.D., Guillemette, J.G., Kay, C.M., Smith, M. & Mauk, A.G. (1990). Electrochemical, kinetic, and CD consequences of mutations at position-82 of yeast iso-1-cytochrome c. *Biochemistry*. **29**, 9365–9369.

Ramdas, L., Sherman, F. & Nall, B.T. (1986). Guanidine hydrochloride induced equilibrium unfolding of mutant forms of iso-1-cytochrome c with replacement of proline-71. *Biochemistry*. **25**, 6952–6958.

Rees, D.C. (1985). Experimental evaluation of the effective dielectric constant of proteins. *J. Mol. Biol.* **141**, 323–326.

Reid, K.S.C., Lindley, P.F. & Thornton, J.M. (1985). Sulphur-aromatic interactions in proteins. *FEBS Lett.* **190**, 209–213.

Rieder, R. & Bosshard, H.R. (1980). Comparison of the binding sites on cytochrome c for cytochrome c oxidase, cytochrome bc_1 and cytochrome c_1. Differential acetylation of lysyl residues in free and complexed cytochrome c. *J. Biol. Chem.* **255**, 4732–4739.

Roberts, V.A., Freeman, H.C., Olson, A.J., Tainer, J.A. & Getzoff, E.D. (1991). Electrostatic orientation of the electron-transfer complex between plastocyanin and cytochrome c. *J. Biol. Chem.* **266**, 13431–13441.

Roder, H., Elove, G.A. & Englander, S.W. (1988). Structural characterization of folding intermediates in cytochrome c by H-exchange labelling and proton NMR. *Nature (London)*. **335**, 700–704.

Rossman, M.G., ed. (1972). *The Molecular Replacement Method*. Gordon & Breach, New York.

Rossman, M.G., Leslie, A.G.W., Abdel-Meguid, S.S. & Tsukihara, T. (1979). Processing and post-refinement of oscillation camera data. *J. Appl. Crystallogr.* **12**, 570–581.

Salemme, F.R. (1972). A free interface diffusion technique for the crystallization of proteins for X-ray crystallography. *Arch. Biochem. Biophys.* **151**, 533–539.

Salemme, F.R. (1976). An hypothetical structure for an intermolecular electron transfer complex of cytochromes c and b_5. *J. Mol. Biol.* **102**, 563–568.

Sato, M., Yamamoto, M., Imada, K., Katsube, Y., Tanaka, N. & Higashi, T. (1992). A high-speed data-collection system for large-unit-cell crystals using an imaging plate as a detector. *J. Appl. Crystallogr.* **25**, 348–357.

Schejter, A., Aviram, I. & Goldkorn, T. (1982). The contribution of electrostatic factors to the oxidation-reduction potentials of c-type cytochromes. In *Electron Transport and Oxygen Utilization*. (Ho, C., ed.), pp. 95–99. Elsevier, North, Amsterdam.

Schoenborn, B.P. (1988). Solvent effect in protein crystals. A neutron diffraction analysis of solvent and ion density. *J. Mol. Biol.* **201**, 741–749.

Sherman, F. (1990). Studies of yeast cytochrome c: how and why they started and why they continued. *Genetics.* **125**, 9–12.

Singh, J. & Thornton, J.M. (1985). The interaction between phenylalanine rings in proteins. *FEBS Lett.* **191**, 1–6.

Smalas, A.O. & Hordvik, A. (1993). Structure determination and refinement of benzamidine-inhibited trypsin from the North Atlantic salmon (*Salmo salar*) at 1.82 Å resolution. *Acta Crystallogr. sect. D.* **49**, 318–330.

Smith, M. (1986). Site-directed mutagenesis. *Phil. Trans. Royal Soc. London ser. A.* **317**, 295–304.

Smith, M., Leung, D.W., Gillam, S., Astell, C.R., Montgomery, D.L. & Hall, B.D. (1979). Sequence of the gene for iso-1 cytochrome c in *Saccharomyces cerevisiae. Cell.* **16**, 753–761.

Stellwagen, E. (1978). Haem exposure as the determinate of oxidation-reduction potential of haem proteins. *Nature (London).* **330**, 86–88.

Stemp, E.D.A. & Hoffman, B.M. (1993). Cytochrome c peroxidase binds two molecules of cytochrome c: evidence for a low-affinity, electron-transfer-active site on cytochrome c peroxidase. *Biochemistry.* **32**, 10848–10865.

Stenkamp, R.E. & Jensen, L.H. (1975). Effects of data set thresholds. *Acta Crystallogr. sect. B.* **31**, 1507–1509.

Stout, G.H. & Jensen, L.H. (1989). *X-ray Structure Determination. A Practical Guide. Second Edition.* John Wiley & Sons, New York.

Takano, T. & Dickerson, R.E. (1981a). Conformation change of cytochrome c: ferricytochrome c refinement at 1.8 Å resolution and comparison with the ferrocytochrome structure. *J. Mol. Biol.* **153**, 95–115.

Takano, T. & Dickerson, R.E. (1981b). Conformation change of cytochrome c: ferrocytochrome c structure refined at 1.5 Å resolution. *J. Mol. Biol.* **153**, 79–94.

Tanaka, N., Yamane, T., Tsukihara, T., Ashida, T. & Kakudo, M. (1975). The crystal structure of bonito ferrocytochrome c at 2.3 Å resolution. *J. Biochem.* **77**, 147–162.

Taniguchi, V.T., Sailasuta-Scott, N., Anson, F.C. & Gray, H.B. (1980). Thermodynamics of metalloprotein electron transfer reactions. *Pure Appl. Chem.* **52**, 2275–2281.

Tegoni, M., White, S.A., Roussel, A., Mathews, F.S. & Cambillau, C. (1993). A hypothetical complex between crystalline flavocytochrome b_2 and cytochrome c. *Proteins: Struct. Funct. Genet.* **16**, 408–422.

Thaller, C., Eichele, G., Weaver, L.H., Wilson, E., Karlsson, R. & Jansonius, J.N. (1985). Seed enlargement and repeated seeding. *Methods Enzymol.* **114**, 132–135.

Thurgood, A.G.P., Pielak, G.J., Cutler, R.L., Davies, A.M., Greenwood, C., Mauk, A.G., Smith, M., Williamson, D.J. & Moore, G.R. (1991). Change in charge of an unvaried heme contact residue does not cause a major change of conformation in cytochrome c. *FEBS Lett.* **284**, 173–177.

Timkovich, R. (1979). Cytochrome c: the architecture of a protein-porphyrin complex. In *The Porphyrins. Volume VII.* (Dolphin, D., ed.), pp. 241–294. Academic Press, New York.

Tong, H., Berghuis, A.M., Chen, J., Luo, Y., Guss, J.M., Freeman, H.C. & Brayer, G.D. (1994). ASIR: an automatic procedure for determining solvent structure in protein crystallography. *J. Appl. Crystallogr.* **27**, 421–426.

Varadarajan, R. & Richards, F.M. (1992). Crystallographic structures of ribonuclease S variants with nonpolar substitutions at position 13: packing and cavities. *Biochemistry.* **31**, 12315–12327.

Watkin, D. (1994). The control of difficult refinements. *Acta Crystallogr. sect. A.* **50**, 411–437.

Wendoloski, J.J., Matthew, J.B., Weber, P.C. & Salemme, F.R. (1987). Molecular dynamics of a cytochrome c-cytochrome b_5 electron transfer complex. *Science.* **238**, 794–796.

Whitford, D., Gao, Y., Pielak, G.J., Williams, R.J.P., McLendon, G.L. & Sherman, F. (1991). The role of the internal hydrogen bond network in first-order protein electron transfer between *Saccharomyces cerevisiae* iso-1-cytochrome c and bovine microsomal cytochrome b_5. *Eur. J. Biochem.* **200**, 359–367.

Willie, A., McLean, M., Liu, R., Hilgen-Willis, S., Saunders, A.J., Pielak, G.J., Sligar, S.G., Durham, B. & Millett, F. (1993). Intracomplex electron transfer between ruthenium-65–cytochrome b_5 and position-82 variants of yeast iso-1-cytochrome c. *Biochemistry.* **32**, 7519–7525.

Willie, A., Stayton, P.S., Sligar, S.G., Durham, B. & Millett, F. (1992). Genetic engineering of redox donor sites: measurement of intracomplex electron transfer between ruthenium-65–cytochrome b_5 and cytochrome c. *Biochemistry.* **31**, 7237–7242.

Wilson, A.J.C. (1942). Determination of absolute scale from relative X-ray intensity data. *Nature (London).* **150**, 151–152.

Zhou, J.S. & Hoffman, B.M. (1993). Cytochrome c peroxidase simultaneously binds cytochrome c at two different sites with strikingly different reactivities: titrating a "substrate" with an enzyme. *J. Am. Chem. Soc.* **115**, 11008–11009.

Zhou, J.S. & Hoffman, B.M. (1994). Stern-Volmer in reverse: 2:1 stoichiometry of the cytochrome c-cytochrome c peroxidase complex. *Science.* **265**, 1693–1696.

Zoller, M.J. & Smith, M. (1983). Oligonucleotide-directed mutagenesis of DNA fragments cloned into M13 vectors. *Methods Enzymol.* **100**, 468–500.

Zuniga, E.H. & Nall, B.T. (1983). Folding of yeast iso-1-AM cytochrome *c*. *Biochemistry.* **22**, 1430–1437.

Addendum

I. Publications in peer reviewed journals arising from the work described in this thesis:

1. The experiments described in Chapter 3, dealing with the determination of the structures of the F82Y, L85A and F82Y/L85A mutants of yeast iso-1 cytochrome c and the roles of Phe82 and Leu85 at the interactive face of this protein, have been published in:

   Lo, T.P., Guillemette, J.G., Louie, G.V., Smith, M. & Brayer, G.D. (1995). Structural studies of the roles of residues 82 and 85 at the interactive face of cytochrome c. *Biochemistry* **34**, 163–171.

2. The determination of the structures of the L85C, L85F, L85M and L94S mutant proteins and an interpretation of the structural and functional effects of these amino acid substitutions as described in Chapter 4 have been published in:

   Lo, T.P., Murphy, M.E.P., Guillemette, J.G., Smith, M. & Brayer, G.D. (1995). Replacements in a conserved leucine cluster in the hydrophobic heme pocket of cytochrome c. *Protein Science* **4**, 198–208.

3. In conjunction with the structural studies described in Chapters 3 and 4, experiments involving the analysis of the kinetics of electron transfer between yeast iso-1 cytochrome c mutant proteins and bovine cytochrome b_5 were performed. My contribution to these studies was the modeling of two complexes formed between wild-type yeast iso-1 cytochrome c and bovine cytochrome b_5 by computational techniques. The interpretation of the observed electron transfer kinetics using these models of the protein-protein complex has been described in:

Guillemette, J.G., Barker, P.D., Eltis, L.D., Lo, T.P., Smith, M., Brayer, G.D. & Mauk, A.G. (1994). Analysis of the bimolecular reduction of ferricytochrome *c* by ferrocytochrome b_5 through mutagenesis and molecular modeling. *Biochimie* **76**, 592–604.

4. The studies described in Chapter 5 regarding the structural and functional analyses of the F82I, F82L and F82M mutants of yeast iso-1 cytochrome *c* have been prepared for publication and submitted as:

Lo, T.P. & Brayer, G.D. (1995). Structural analysis of the replacement of the invariant phenylalanine 82 in cytochrome *c* by aliphatic residues. *Biochemistry, submitted.*

5. The studies presented in Chapter 6 regarding the elucidation of the structures of yeast iso-1 cytochrome *c* proteins having multiple site mutations at Arg38, Asn52 and Phe82 and the analysis of the effects of these mutations on reduction potential and protein stability have been published in:

Lo, T.P., Komar-Panicucci, S., Sherman, F., McLendon, G. & Brayer, G.D. (1995). The structural and functional effects of multiple mutations at distal sites in cytochrome *c. Biochemistry, in press.*

II. Publications arising from collaborative work on related topics:

These studies dealt with an analysis of cytochrome b_5 and mapping antibody sites with synthetic peptides. As such, these results deal with topics that fall outside the scope of the present work and therefore are not discussed herein.

1. In this study, the structure of a triple mutant of cytochrome b_5 was determined using molecular replacement methods (Section 2.4.3.2). These analyses revealed the manner in which the addition of a negative charge adjacent to the heme moiety results in a decrease in heme reduction potential for this protein.

Funk, W.D., Lo, T.P., Mauk, M.R., Brayer, G.D., MacGillivray, R.T.A. & Mauk, A.G. (1990). Mutagenic, electrochemical, and crystallographic investigation of the cytochrome b_5 oxidation-reduction equilibrium: Involvement of asparagine-57, serine-64, and heme propionate-7. *Biochemistry* **29**, 5500–5508.

2. This work determined the exposed surface areas of cytochrome c and the correlation of the surface exposure of short stretches of polypeptide chain with the antigenicity of the corresponding peptides from a peptide library.

Schwab, C., Twardek, A., Lo, T.P., Brayer, G.D. & Bosshard, H.R. (1993). Mapping antibody binding sites on cytochrome c with synthetic peptides: are results representative of the antigenic structure of proteins? *Protein Science* **2**, 175–182.